

CONVECTIVE INSTABILITY IN A LAYER OF
RADIATING FLUID

by

JOHN CHARLES GILLE

B.S., Yale College
(1956)

B.A., Cambridge University
(1958)

WITHDRAWN
MASS. INST. OF
TECH.
FROM
MIT LIBRARIES
LINDGREN

SUBMITTED IN PARTIAL FULFILLMENT

OF THE REQUIREMENTS FOR THE

DEGREE OF DOCTOR OF

PHILOSOPHY

at the

MASSACHUSETTS INSTITUTE OF TECHNOLOGY

June, 1964

Signature of Author

Department of Geology and Geophysics, March 2, 1964

Certified by

Thesis Supervisor

Accepted by

Chairman, Departmental Committee on Graduate Students

ABSTRACT

Title: Convective Instability in a Layer of Radiating Fluid

Author: John C. Gille

Submitted to the Department of Geology and Geophysics on February 28, 1964 in partial fulfillment of the requirements for the degree of Ph.D.

The Rayleigh theory of convective instability applies to a medium in which heat is diffusively transferred. Recent work is reviewed which predicts added stabilization in a medium capable of both diffusive and gray radiative transfer.

A thermal and interferometric experimental apparatus capable of verifying these predictions is described. After calculating the radiative properties of ammonia and the physical properties of air and ammonia, it is shown that the temperature distribution and heat flux can be calculated for a medium in which the absorption coefficient is frequency dependent (non-gray), as is the case for ammonia. Experimental observations of radiative-diffusive temperature distributions, obtained for the first time with the interferometer, show striking agreement with calculated values. The change of heat flux with optical depth (gray medium) or pressure (non-gray medium) are calculated for the first time. The observed ammonia results agree satisfactorily with the calculated values.

The radiative stabilization is divided into one part due to the concentration of the gradient near the boundary, and another due to radiative dissipation of perturbations. The former is calculated by techniques due to Chandrasekhar, the latter is shown closely equivalent to the results of a dimensional argument which predicts stabilizations of one plus the ratio of radiative to diffusive dissipation times. Non-gray radiative and diffusive dissipation times are calculated, put into the dimensional statement, and the total stabilization calculated as the product of gradient and dissipative stabilization.

Experimentally the Rayleigh numbers were changed by changing χ and ν through the pressure dependence of the density. The measurement of critical Rayleigh numbers in air by locating the change of effective conductivity gave a mean value for air $Ra_c = 1786 \pm 16$. This is the first accurate determination of Ra_c in a gas. Comparison with measured Rayleigh numbers in ammonia gave observed stabilizations which agree well with those calculated.

The findings are summarized and future problems suggested. The radiative data is thought to have wide applicability in physical problems.

Thesis Supervisor: Richard M. Goody

Title: Professor of Meteorology, Harvard University

ACKNOWLEDGEMENTS

It is a pleasure to acknowledge my great debt to Professor R. M. Goody of Harvard for suggesting this problem, for many helpful discussions and criticisms, and for his continued interest. Professor Raymond Hide suggested several apparatus improvements, and was invariably encouraging. I have also had stimulating discussions with Professors W. V. R. Malkus of U.C.L.A. and E. A. Spiegel of N.Y.U. on theoretical aspects of the problem. To the many others who contributed suggestions and the stimulus of discussion I should like to express my appreciation.

Special thanks, however, are due to Mr. Joachim Joseph for helping with many of the heat flux measurements, Mrs. Haydee Ern for assistance with the numerical computations, and to Mrs. Joyce Bradley for her patience and skill in typing the final draft.

The financial support of the N.S.F. is gratefully acknowledged.

Finally, to my wife Ellen I would like to formally express my deep appreciation for her assistance in writing equations and proofreading during the final few weeks, but mainly for her understanding and encouragement over a considerable period.

CONTENTS

ACKNOWLEDGEMENTS	iii
TABLE OF CONTENTS	iv
LIST OF TABLES	vii
LIST OF FIGURES	ix
CHAPTER 1. THE NATURE AND HISTORY OF THE PROBLEM	1
1.1 The Problem of Rayleigh Convection and Radiative Transfer	1
1.2 Convection in Naturally Occurring Radiating Layers	2
1.3 Scope of the Present Investigation	4
1.4 Organization of the Thesis	5
1.5 An Historical Survey	6
1.6 Convective Onset in a Gray Absorbing Medium	10
CHAPTER 2. APPARATUS	20
2.1 Introduction	20
2.2 Description of the Thermal Apparatus	20
2.3 Treatment of Gases	29
2.4 Corrections to Heat Flux Measurements	29
2.5 Derivation of Formula Relating \bar{S} and Radiative and Conductive Fluxes	31
2.6 Calculation of Emissivity and Nylon Conductivity	33
2.7 A Description of the Apparatus for Interferometric Temperature Measurement	38
2.8 Interferometer Adjustments	47
2.9 Experimental Procedures	50
2.10 Data Reduction	51

2.11	Theory of the Interferometer Measurement	52
2.12	Gas Imperfection Corrections for Interferometer Measurements	56
CHAPTER 3. RADIATIVE PROPERTIES OF AMMONIA		60
3.1	Introduction	60
3.2	Description of the Quantities Desired	60
3.3	Spectroscopic Constants for Vibration-Rotation Bands of Ammonia at 300°K	65
3.4	Pressure Effects	70
3.5	Treatment of the Pure Rotation Spectrum	76
3.6	The Weak Line Correction Band in NH ₃	79
3.7	Calculation of E_p	83
3.8	Calculation of ϵ and ϵ'	83
CHAPTER 4. THE PHYSICAL PROPERTIES OF AIR AND AMMONIA		90
4.1	Introduction	90
4.2	The Physical Properties of Air	90
4.3	The Physical Properties of Ammonia	93
4.4	Accuracy of Physical Properties of Air and Ammonia	98
4.5	Refractive Indices	103
CHAPTER 5. THE INITIAL STATIC STATE		105
5.1	Introduction	105
5.2	Calculation of Temperature Distribution for Mixed Radiation and Diffusion	106
5.3	Radiative-Diffusive Flux Calculations	132
5.4	Measurement of the Temperature Distribution	142
5.5	Measurement of Static State Heat Flux	160

CHAPTER 6. THE ONSET OF CONVECTION	165
6.1 Introduction	165
6.2 The Problem of Convective Onset	165
6.3 Calculation of S_{β}	171
6.4 Calculation of S_H	177
6.5 Measurement of the Critical Rayleigh Number	205
6.6 Reduction of Data to Get Critical Rayleigh Numbers	208
6.7 Radiative Stabilization	215
CHAPTER 7. CONCLUSIONS	223
7.1 Introduction	223
7.2 Results of this Work	223
7.3 Suggestions for Future Research	229
BIBLIOGRAPHY	235
BIOGRAPHY	239

LIST OF TABLES

1-1	Comparison of Radiative Parameters in Nature and the Laboratory	3
2-1	Data for Calculating Emissivity and Nylon Conductivity	34
2-2	$B(\theta)/\theta$ for Several Values of θ	57
2-3	Virial Coefficient Data for Ammonia	58
2-4	Calculation of $\frac{\rho_o}{\rho_s}$ for Ammonia	58
2-5	Calculation of $\left(\frac{1}{\rho} \frac{\partial \rho}{\partial \theta}\right)_o$ for Ammonia	59
3-1	Observed Fundamentals of Gaseous NH_3	65
3-2	Source of NH_3 Range Parameters	68
3-3	Range Parameters for NH_3	70
3-4	Relative Effectiveness of Ammonia and Nitrogen in Line Broadening	72
3-5	Total Broadening Pressures in Port's Experiments	75
3-6	Calculated and Observed Values of E_p	84
3-7	ξ as a Function of Pressure and Distance	86
3-8	ξ' as a Function of Pressure and Distance	87
4-1	Physical Properties of Air	93
4-2	Virial Coefficient Data for Ammonia	96
4-3	Calculated Specific Heats of Ammonia	96
4-4	Conductivity of Ammonia	98
4-5	$\frac{g\alpha}{K\nu} \rho c_p \left(\frac{p_o}{p}\right)^2$ for Several Pressures of Ammonia	101

5-1	$\frac{-(\theta - \bar{\theta} - \zeta \Delta \theta)}{\Delta \theta}$ in pure NH_3	129
5-2	Experimental Conditions for Temperature Distribution Measurements	148
5-3	Data and Results of Run 2	151
5-4	Data and Results of Run 1	153
5-5	Data and Results of Run 3	153
5-6	Data for Calculations of $\bar{S}(0)$ for Ammonia	161
6-1	Exact and Dimensional Argument Calculations of Ra_c / γ	186
6-2	$\tilde{k}(p, n)$ for Several Values of p and n	201
6-3	$t_D / t_R(p, n)$ for Several Values of p and n	201
6-4	Experimental Conditions for Heat Flux Measurements	209
6-5	Measured Critical Rayleigh Numbers in Air	213
6-6	Measured Critical Rayleigh Numbers in Ammonia	217
6-7	Stabilization in Ammonia	218

LIST OF FIGURES

1-1	Critical Rayleigh Numbers versus λ	17
2-1	The Convection Cell in the Pressure Vessel	21
2-2	\bar{S} versus p_{air}	32
2-3	Interferometer Arrangement (Top View)	39
2-4	Convection Cell Optical Details (Side View)	41
2-5	A Portion of a Densitometer Scan Record	45
3-1	A Low Resolution Absorption Spectrum of Ammonia	63
3-2	Ammonia Emissivities Measured by Port	71
3-3	Calculated and Observed Values of E_p	85
3-4	Perturbation Emissivity, $\xi(r)$ as a Function of r for Several Pressures	88
3-5	Derivative of Perturbation Emissivity, $\xi'(r)$, as a Function of r for Several Pressures	89
4-1	Conductivity of Air and Ammonia	99
4-2	$\frac{g\alpha}{K\nu} \rho c_p \left(\frac{p_0}{p}\right)^2$ versus θ for Air and Ammonia	102
5-1	The Effect of Boundary Conditions on Temperature Profiles in a Gray Medium	121
5-2	Comparison of Gray and Non-Gray Temperature Profiles	123
5-3	$-100 \frac{(\theta - \bar{\theta} - \zeta \Delta \theta)}{\Delta \theta}$ Calculated for Pure Ammonia. $h=1.987$ cm.	131

5-4	$-100 \frac{(\theta - \bar{\theta} - \zeta \Delta \theta)}{\theta}$	Calculated for Pure Ammonia. $h=5.048$ cm	133
5-5	A, B, and C	versus Pressure	134
5-6	Effective Conductivity	in a Gray Absorbing Gas	137
5-7	Calculated $\frac{\Delta F(p)}{F(0)}$	for Pure Ammonia. $h=1.987$ cm	145
5-8	Calculated $\frac{\Delta F(p)}{F(0)}$	for Pure Ammonia. $h=5.048$ cm	146
5-9	Photographs of Interferometer Fringes		154
5-10	Measured Temperature Profiles	in Air and Ammonia	155
5-11	Measured Heat Flux in Pure Ammonia	as a Function of Pressure	161a
6-1	$S(x)$	as a Function of x	198
6-2	$\tilde{k}(\ell)$	as a Function of $n = \ell^{-1}$	202
6-3	$\frac{t_D}{t_R}$	(n) as a Function of n	203
6-4	Characteristic Time Constants	in Ammonia	204
6-5	\bar{S}	as a Function of Rayleigh Number for Dry Air	212
6-6	\bar{S}	as a Function of Rayleigh Number for Ammonia	216

PREFACE

Since this thesis contains some review material and other relevant material which the author chose to include for convenience, it seems desirable to state clearly what the author's contribution is.

He is responsible for the design, construction and operation of the apparatus described in Chapter 2. It was his decision to use ammonia, and his method of using the spectroscopic data and theory to calculate the several emissivities and the comparison with Port in Chapter 3. He also devised the numerical integrals to obtain $\tilde{k}(n)$ in 6.4.5. The necessity for very accurate physical properties and their temperature dependences were recognized by him, and the calculation of ammonia properties in 4.3 is his.

The working out of the theory of interferometric temperature measurement in 2.11, showing the refraction is not important (2.8), and the necessity and calculation of the corrections to the equations for deviations from the perfect gas laws (2.12) were first done by the author.

One of the prime results of the thesis is the measurement of the radiative-diffusive temperature profile with an accuracy of 0.02°C . This measurement and its data reduction (5.4) is due to the author.

Another major result is the measurement of the critical Rayleigh number in air (6.6.1). A third is the measurement of the critical Rayleigh number in ammonia (6.6.2) and thus the stabilization(6.7). These are due to the author.

Theoretically, the several calculations of the stabilization due to the gradient (6.3) are the author's work, as is the suggestion of separating the calculation of the stabilization due to gradient and dissipation (6.2). In addition, in (6.4) he altered Spiegel's dimensional argument, showed the existence of another term in the non-gray temperature perturbation equations, and provided the interpretation of \hat{q} .

These are not exclusive, of course. Suggestions of others have been incorporated in these sections, and he has contributed in other areas.

The total impact of his work in this thesis is to verify Goody's theory of radiative stabilization for the specific case of narrow layers of ammonia.

CHAPTER 1

THE NATURE AND HISTORY OF THE PROBLEM

1.1 The Problem of Rayleigh Convection and Radiative Transfer

The convection problem named for Rayleigh concerns thermally driven motions in a thermally conducting, viscous fluid between two flat, infinite, horizontal surfaces maintained at uniform temperatures with a temperature difference between them. The temperature difference creates density differences which can become unstable in the gravitational field and initiate motions within the fluid if the temperature difference is in the right direction and exceeds a certain finite amount.

This can be expressed by saying that the Rayleigh number, Ra , a dimensionless combination of the temperature difference, fluid properties, and layer thickness, must exceed a certain value, $Ra(a)$, which depends on a , the dimensionless horizontal wave number of the disturbance. On increasing Ra , the first observed motion will be of that a for which $Ra(a)$ is a minimum, Ra_c .

Goody[1956] treated the problem of Rayleigh convection in which the temperature equation had terms for both diffusion and gray (frequency independent) radiative transfer. He solved for the two extremes of optically very thin and very thick layers, and extrapolated to the region of intermediate thickness for several ratios of radiative to diffusive conductivity. Radiation was found to have a stabilizing effect (i.e., raising Ra_c) in all situations. In concluding that paper he suggested that it might be possible to investigate this problem in the laboratory with a substance like water vapor.

This work is then concerned with the extension of the theory to the prediction and measurement of stabilization due to radiation in the laboratory.

1.2 Convection in Naturally Occurring Radiating Layers

Thermal convection is a common and widely occurring phenomenon. It is known or thought to occur in the interiors, oceans, and atmospheres of planets, and in the bodies of stars. Certainly in the latter two radiative transfer is important.

The inclusion of radiative transfer introduces two new dimensionless quantities, which are \mathcal{K} , the ratio of radiative to diffusive conductivity, and τ , the optical depth of a layer. In Table 1-1 some typical values of length scales, \mathcal{K} , and τ are given for the sun, earth's atmosphere, and present laboratory investigation. The table further contains $t_R(1/\ell)$, the time for radiative dissipation of a sinusoidal temperature disturbance of wave number ℓ^{-1} . This can be compared with the time scales of hydrodynamic motions to give an indication of the importance of radiative transfer on fluid motions. Also included are $t_R(\infty)$, the minimum radiative dissipation time, and the expected critical Rayleigh number, Ra_c , over the critical Rayleigh number for diffusion alone, $Ra_c(\text{diff})$. This last is the measure of radiative stabilization, or increase of stabilization over that of the standard Rayleigh problem. Data on the sun are from Goody [1956] and Spiegel [1960], that on the atmosphere from Goody [1964].

Table 1-1
COMPARISON OF RADIATIVE PARAMETERS IN NATURE
AND THE LABORATORY

<u>Quantity</u>	<u>Sun</u>	<u>Earth's Atmosphere</u>	<u>Laboratory</u>
Length(l)	500 km	10 km	2 - 5 cm.
χ	10^{12}	9.3×10^7	6.3 - 25
τ	1.1	0.2	0.05 - 0.1
$t_R(1/l)$	2.4×10^2 sec.	1.4×10^7 sec.	7 - 10 sec.
$t_R(\infty)$	2 sec.	1.2×10^3 sec.	1 sec.
$\frac{Ra_c}{Ra_c(\text{diff})}$	10^{12}	5.2×10^5	0 - 2.1

It should be remarked that t_R is a strong function of length scale, as are χ and $Ra_c/Ra_c(\text{diff})$ for the atmosphere and the laboratory, where τ is a weak function of length. In the sun χ is a constant and τ is linear in length, because the sun is much more nearly a gray medium.

The quantity $Ra_c/Ra_c(\text{diff})$ is the one with which this investigation will deal primarily. In the atmosphere, as Goody remarks, the Rayleigh number can be many orders of magnitude larger than the stabilization of 10^5 , so that the radiative effect on the onset of convection is not immediately applicable. However, it is in itself an interesting and challenging problem that can be expected to offer insight into the actual

structure of the atmosphere. In addition, Malkus [1954b] has a theory of turbulence based on the eigenmodes of the stability problem. For an understanding at very large Rayleigh numbers in this view, an understanding of the stability problem with radiation is necessary. Moreover, the growth rates and spectrum of the eddy sizes may be expected to be strongly influenced by radiative transfer.

In an astrophysical context, Spiegel [1960] remarks that the degree of instability must in some way determine the importance of the convective zones in certain stellar classes. The theory thus has applicability not so much in indicating stability or instability (although he does this for a B0 star), but in measuring the degree of instability. The same remarks on the modification of the turbulent field by radiation that applied to the planetary atmosphere applies in astrophysics also.

As listed in Table 1-1, the maximum stabilization predicted in the laboratory is 2.1, not large compared to natural stabilizations because of scale differences, but large enough to encourage an experimental attempt to demonstrate the effect and compare it with theory.

1.3 Scope of the Present Investigation

This investigation will attempt to predict and measure the Rayleigh number in a radiating fluid at which convection begins. This is composed of several problems, which are:

- 1) Extension of the theory to a non-gray medium.
- 2) Extension of the theory to a variable gradient between rigid boundaries.

- 3) Obtaining complete radiative and physical data for the radiating material and for a non-radiating material to be a control.
- 4) Solution of the zeroth order field (the steady state) in the radiating and non-radiating media. This means not only temperature distribution, but heat fluxes as well.
- 5) Measurement with as great accuracy as possible of the initial static state to verify the validity of the solutions of (4).
- 6) Measurement of the critical Rayleigh number in a non-radiating and a radiating medium under similar conditions, and comparison of these measurements.

For this investigation air has been chosen for the non-radiating fluid and ammonia for the radiating fluid.

The choice of ammonia over water vapor was dictated by two considerations. The first is that it appears to have a higher emissivity and effective absorption coefficient in laboratory conditions than water vapor. The second reason is that it is not subject to the vapor pressure limitations at room temperature that water vapor is.

The spectra are similar in that both ^{molecules} have ^{large dipole moments and} small moments of inertia, which give them extensive rotation bands. The latter fact makes them effective in transferring appreciable amounts of energy.

1.4 Organization of the Thesis

The remainder of Chapter 1 will be devoted to a survey of the history of theoretical and experimental investigations of convection and a mathematical look at the most pertinent theoretical papers, those of Goody [1956] and Spiegel [1960].

The apparatus for making thermal and interferometric measurements are

described in Chapter 2, with the theory of interferometric measurements.

The radiative properties of ammonia in forms applicable later are calculated in Chapter 3 from spectroscopic and total emissivity data.

The physical properties of air and ammonia and their temperature variations are calculated in Chapter 4.

The equations for the static state distribution of temperature and heat flux in a non-gray gas are derived, solved, and compared with experiment in Chapter 5.

The problem of predicting radiative stabilization is broken into the two problems of determining gradient stabilization and heating rate stabilization in Chapter 6. The gradient stabilization, S_{β} , is calculated by a technique formulated by Chandrasekhar, and the heating rate stabilization S_H is shown to be given by a dimensional argument. The ratio of diffusive to radiative time constants is calculated and inserted to give numerical values for S_H . The taking and reduction of the data for air and ammonia that leads to the determination of critical Rayleigh numbers is then described. The results for air are discussed, and the comparison with ammonia results give observed stabilizations. These are compared with $S_{\beta} \cdot S_H$ and found to give good agreement.

In Chapter 7 the overall results of the investigation are presented and some future problems suggested.

1.5 An Historical Survey

1.5.1 A History of Theoretical Development

The problem was first discussed by Rayleigh [1916] to explain experiments by Benard [1901]. Pellew and Southwell [1940] completed theoretical work on the onset problem with constant coefficients by

demonstrating the principle of exchange of stabilities and finding a variational principle for evaluating the critical Rayleigh number. The exchange of stabilities says that if we insert a time dependence for our solution in the equations of motion of form $e^{(\sigma_r + i\sigma_i)t}$, for $\sigma_r \geq 0$, it can be shown that $\sigma_i = 0$. This means that no instability that grows can be oscillatory, and that we can solve for the conditions of instability by putting $\sigma_r = \sigma_i = 0$.

Doing this leads to a sixth order differential equation involving Ra , the Rayleigh number (see below), as a parameter. It is an eigenvalue equation, in which only certain values of Ra are allowed. The first allowed value, Ra_c , is the critical Rayleigh number; for $Ra < Ra_c$ there is no fluid motion even though an adverse density gradient may exist, while for $Ra > Ra_c$ motion is allowed. An exposition of the stability theory and its modern formulation is given by Chandrasekhar [1961], who also summarizes the experimental findings.

The theoretical inclusion of radiative transfer was first performed by Goody [1956], who considered a medium in which absorption is independent of frequency -- what is termed a gray medium. He turned the integral form of the equation for radiative heating into differential forms for two limiting cases -- those of optically thick and optically thin layers -- which he used to extend the Pellew and Southwell treatment. He also solved the equations for radiative flux by means of the Eddington approximation, in closed form to obtain the actual gradient β , relative to the mean gradient $\bar{\beta}$. The ratio $\beta/\bar{\beta}$ is a coefficient in the equations which provides additional stabilization. Even with this non-constant coefficient

Goody found a variational principle for free boundaries. From critical Rayleigh numbers for the two limiting cases he was able to extrapolate to cover the region of intermediate opacity.

A complement was provided by the work of Spiegel [1958, 1960], who started with the three-dimensional integral form for the equation of radiative heating in a gray medium, integrated out the horizontal integrals, and arrived at an integral over fluid depth, depending on the horizontal wave number, for the heating rate. He was able to show that if $\beta = \bar{\beta}$ (applicable to the stellar interiors he was considering), then the exchange of stabilities holds. He also found a variational principle for general $\beta/\bar{\beta}$ for rigid boundary conditions, but solved for $\beta = \bar{\beta}$ and two trial functions for the temperature θ . These showed good agreement with Goody's results (allowing for different boundary conditions), except for one region where the difference was ascribed to the effect of the gradient.

The work of Goody and Spiegel will be outlined in mathematical detail below.

1.5.2 Experimental Investigations of Convection

The experiments on convection in the 1930's were aimed for the most part at discovering whether there was a critical point or not, i.e., a critical Rayleigh number below which convection did not occur even if an adverse density gradient existed. In this class is the work of Schmidt and Milverton [1935] and the corroborating work of Schmidt and Saunders [1938]. More recently have been careful experiments by Malkus [1954a] and those of Silveston [1958], which are cited by Chandrasekhar [1961]. In Silveston's article there is an extensive bibliography of experimental

convective work. The last two investigators have worked with liquids in making accurate determinations of the critical Rayleigh number, which was found to agree very closely with the theoretical value of 1708.

In the case of gases, no such accurate determination has been made. Chandra [1938] looked for the cessation of motion in air, as indicated by a tracer of cigarette smoke, when the apparatus was allowed to cool off through the critical Rayleigh number. He used layer thicknesses from 4 to 16 mm. , and a graphical and tabular presentation of his data suggests errors of perhaps 25 percent. He is not explicit as to his values for the properties of air. The presence of the cigarette smoke also exerts some effect, which he made no attempt to assess.

Schmidt and Saunders [1938] used an optical method that showed by changes in optical density the onset of convection. This indicated a value which they state as Ra_c just under 2000 . Again, they do not state what values of the properties they have used.

Benard and Avsec [1938] did experiments on air with tobacco smoke as a tracer and observed the onset of convection in layers between 1 and 5 cm. thick. Their results lie nearly exactly in the middle, between the free-free and rigid-rigid boundary theoretical results, which is perhaps due to the use of a poorly conducting glass plate as the upper boundary of the convecting region.

Sutton [1951] reports unpublished work of Dassanayake on CO_2 , in which he used much the same apparatus and method as Chandra [1938]. This indicated a mean value for Ra_c observed of $0.978 Ra_c$ theoretical, with an r.m.s. deviation of 7 percent. He did not state his physical parameters.

The most recent previous observations seem to be those of De Graaf and Van der Held [1953], which used both the previous methods and a third, the change in the heat transfer with convective onset.

Using the optical method, they corroborated Schmidt and Saunders [1938] values of $Ra_c \sim 2000$. Their smoke measurements also indicated a value of $Ra_c = 2000$. Their heat transfer measurements indicated a change at $Ra_c \sim 1480$. They do not give their values for the air properties either.

Thus, the Rayleigh theory for liquids had been established in detail, but only in its broad outlines for gases. Aside from experimental difficulties is the possibility that uncertainties in the values of the physical properties of gases, especially conductivity and viscosity, made precise assignment of Rayleigh numbers impossible.

1.6 Convective Onset in a Gray Absorbing Medium

This is a brief outline of the treatments of Goody[1956] and Spiegel [1960]. The following symbols will be used in all subsequent sections;

η = viscosity

ν = kinematic viscosity

g = gravitational acceleration

x, y, z = rectangular coordinates (z vertical)

u, v, w = velocities in rectangular coordinates

$$\nabla^2 = \frac{\partial^2}{\partial x^2} + \frac{\partial^2}{\partial y^2} + \frac{\partial^2}{\partial z^2} = \nabla_1^2 + \frac{\partial^2}{\partial z^2}$$

θ = temperature

θ_0 = temperature in the static state

$\theta' = \theta - \theta_0$ = temperature fluctuation from the initial static state

H = rate of radiative heating/vol.

H_0 = rate of radiative heating in the static state/vol.

$H' = H - H_0$ = fluctuations of radiative heating from the static state/vol.

K = thermal conductivity

$\chi = K/\rho c_p$ = thermometric diffusivity

ρ = fluid density/vol.

$c_{p,v}$ = specific heats per unit mass

k = absorption coefficient (gray)

The linearized equation governing heat transfer by fluid motion in a steady state was given by Pellew and Southwell [1940]

$$-\nu \nabla^2 \omega = \alpha g \nabla_1^2 \theta' \quad (1.1)$$

Although they made use of the fact that without radiative transfer, the temperature gradient is almost constant, the same result can be obtained if β is allowed to vary with z .

The steady state temperature distribution is given by

$$\omega/\beta = \frac{H}{\rho c_p} + \frac{K}{\rho c_p} \nabla^2 \theta \quad (1.2)$$

when the fluid is in motion, and

$$0 = \frac{H_0}{\rho c_p} + \frac{K}{\rho c_p} \nabla^2 \theta_0 \quad (1.3)$$

in the initial static state.

Temperature is assumed constant over the upper and lower boundaries, and therefore H_0 and θ_0 are functions of z only. The vector flux of radiative energy in the initial static state will also be in the z direction, and a function only of z . If F_z is this flux, then

$$H_0 = - \frac{dF_z}{dz} \quad (1.4)$$

and (1.3) may be integrated to

$$F_z = K\beta = F_T \text{ (const.)}$$

Combining (1.2) and (1.3),

$$\omega\beta = \frac{H'}{\rho c_p} + K \frac{\nabla^2 \theta'}{\rho c_p} \quad (1.5)$$

Following Pellew and Southwell, assume that w and θ' are separable functions of x , y , and z , and that

$$\nabla_{xy}^2 w = - \frac{a^2}{h^2} w \quad (1.6)$$

where h is the distance between the upper and lower surfaces and a is a characteristic number. Also let

$$\zeta = \left(\frac{z}{h} - \frac{1}{2} \right), \quad \frac{\partial^2}{\partial \zeta^2} = D^2$$

so that

$$\nabla^2 w = \frac{1}{h^2} (D^2 - a^2) w \quad (1.7)$$

Eliminating θ' between (1.1) and (1.5) with the aid of (1.7) leads to

$$\frac{a^2}{h^2} \omega \beta = - \frac{\nabla_1^2 H'}{\rho c_p} + \frac{\kappa \nu}{\alpha g} \frac{(D^2 - a^2)^3}{\rho c_p h^6} \omega \quad (1.8)$$

Still paralleling the conventional (non-radiative) Rayleigh problem, we will look for values of the Rayleigh number Ra

$$Ra = - \frac{g \alpha \bar{\beta} h^4 \rho c_p}{\kappa \nu} \quad (1.9)$$

at which there is marginal stability. In general, Ra will be a function of a^2 , and the least stable mode will correspond to the value of a^2 for which Ra is a minimum.

The crux of the problem is the evaluation of $\nabla_1^2 H'$. This Goody [1956] did by taking limiting forms of the equation of transfer

$$\frac{dI}{d\bar{s}} = k [B - I(\bar{s})] \quad (1.10)$$

The radiative heating rate is

$$H = - \int \frac{dI}{d\bar{s}} d\omega \quad (1.11)$$

where the integral is over a solid angle of 4π . Since the Planck function is isotropic,

$$H = - 4\pi k B + k \int I(\bar{s}) d\omega \quad (1.12)$$

in which the first term represents local cooling by heat emission and the second absorption from other regions of the fluid and the boundaries. The mean free path of the radiation is of the order k^{-1} , and if this is much greater than the cell dimension, h/a , the radiation will not show much divergence over a distance comparable to the cell dimension, and the variability of H will be due to the variability of B . Hence

$$\nabla_1^2 H' = -4\pi k \nabla_1^2 B' \quad (1.13)$$

This is the transparent approximation, $h^2 k^2 \ll a$.

Linearizing the Planck function,

$$\frac{\partial B}{\partial x} = \frac{4\sigma}{\pi} \Theta^3 \frac{\partial \Theta}{\partial x} \doteq Q \frac{\partial \Theta}{\partial x} \quad (1.14)$$

or, by (1.1),

$$\nabla_1^2 H' \doteq -4\pi k Q \nabla_1^2 \Theta' = \frac{4\pi k Q \nu}{\alpha g} \nabla^4 \omega \quad (1.15)$$

Conversely, for large k (1.10) may be formally solved to yield

$$I(\bar{s}) = e^{-ks} \int_q^s k e^{k\sigma} B(\sigma) d\sigma \quad (1.16)$$

where q remains to be determined from the boundary conditions. These will have an appreciable effect only for distances less than k^{-1} from the boundary. Away from the boundary Goody neglects boundary contributions and after some manipulation finds

$$\nabla_1^2 H' = \frac{4\pi Q \nu}{3k\alpha g} \nabla^6 \omega \quad (1.17)$$

This is the opaque approximation, $k^2 h^2 \gg a^2$.

If the quantity χ is defined as the ratio of the Eddington radiative conductivity to the diffusive conductivity,

$$\chi = \frac{4\pi Q}{3kK}$$

equation (1.8) can now be rewritten

$$Ra \frac{\beta}{\bar{\beta}} = - \frac{(D^2 - a^2)^2}{a^2} \left[(D^2 - a^2) - 3k^2 h^2 \chi \right] w, \quad (1.18)$$

$k^2 h^2 \ll a^2$

$$= - \frac{(D^2 - a^2)^3}{a^2} (1 + \chi) w, \quad K^2 h^2 \gg a^2 \quad (1.19)$$

where the first corresponds to an optically thin layer, the second to an optically thick one.

The form of (1.18) and (1.19) illustrates the fact that radiation not only affects Ra by altering the transfer of energy, but also by changing the initial mean temperature field, β .

This he calculated from the equation of transfer and the Milne-Eddington approximation for black boundaries.

If the right side of (1.18) or (1.19) is considered as an operator Q on w , it may be shown that for free boundaries, $w = D^2 w = \theta' = 0$, a variational principle is applicable. Consider the expression

$$Ra' = \frac{\int_{-1/2}^{1/2} w' Q(w') ds}{\int_{-1/2}^{1/2} w' \frac{\beta}{\bar{\beta}} w' ds} \quad (1.20)$$

in which w' is a trial function which satisfies the boundary conditions. If w' contains an adjustable parameter, the value of Ra' , minimized with respect to this parameter, will be the best value of Ra_c obtainable with this form of trial function and cannot be less than Ra_c . Its value lies in the fact that if we guess a function w' that differs from the true function w by a small quantity ϵ , the value of Ra_c' that we calculate differs from the true value of Ra_c by terms of order ϵ^2 .

Goody made this calculation for $w' = \sin n\pi(\zeta + 1/2)$, the solution of the conventional problem, and found R' lowest for $n = 1$. The resulting expression must now be minimized with respect to cell size, a . It is found that $a^2 = \pi^2/2$ in the opaque case (as in the conventional case), and $\pi^2/2 \leq a^2 \leq \pi^2$ in the transparent case, indicating a tendency for cell size to decrease in more transparent situations.

Values of Ra_c computed in this way are shown in Fig. 1-1, taken from Goody. The dashed lines are an interpolation over the range where neither approximation is valid. The chain lines do not concern us here.

Spiegel obtained rigorous results for general k by the use of the operator

$$\mathcal{O}(\bar{r} - \bar{r}') = \frac{k e^{-k(\bar{r} - \bar{r}')}}{4\pi(\bar{r} - \bar{r}')^2} - \mathcal{S}(\bar{r} - \bar{r}') \quad (1.21)$$

One can then write

$$H'(\bar{r}, t) = 4\pi k \mathcal{O} \int \Theta'(\bar{r}', t) \mathcal{O}(\bar{r} - \bar{r}') d\bar{r}' \quad (1.22)$$

where the integral is over the whole fluid, which is infinite.

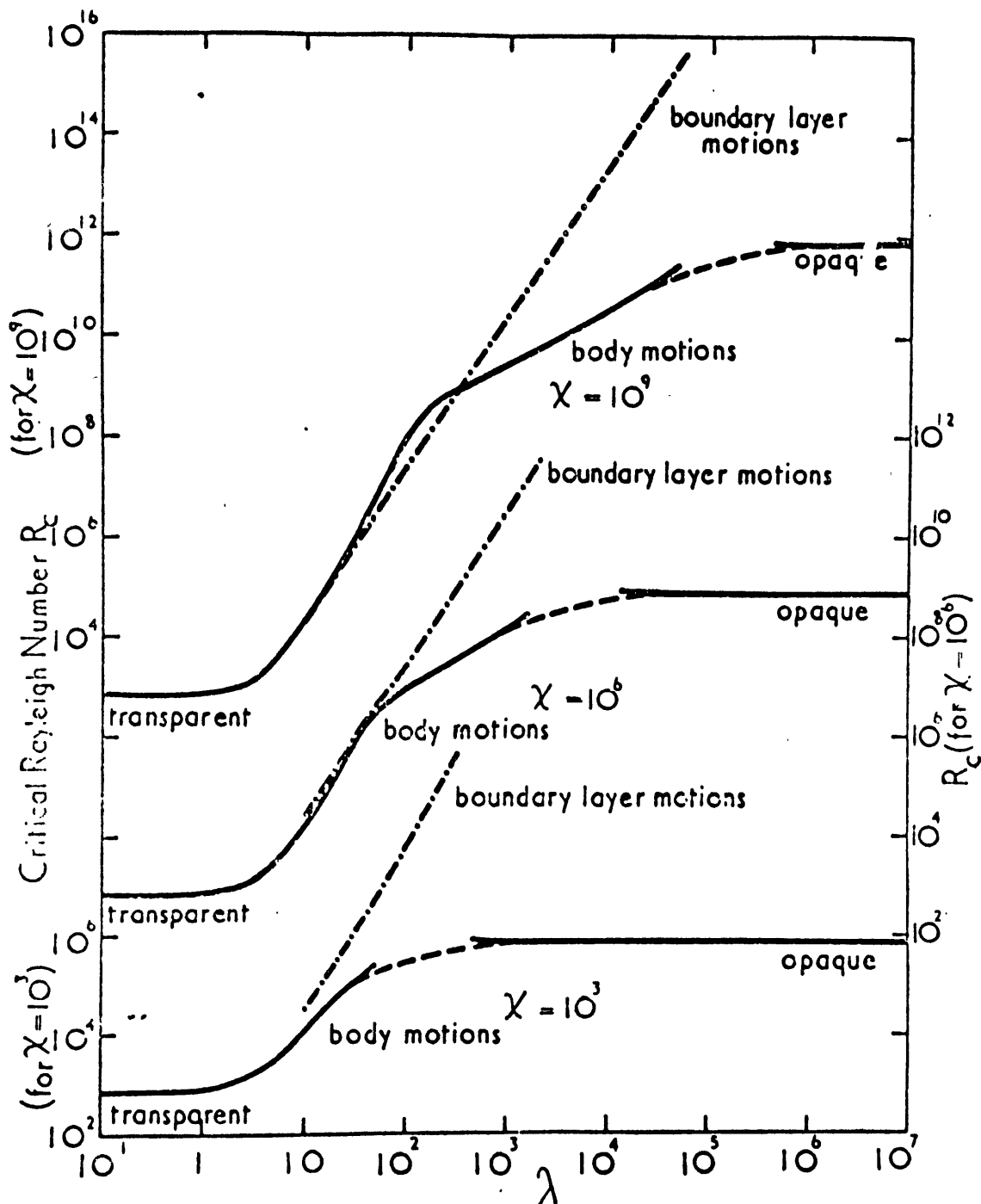


Fig. 1-1. CRITICAL RAYLEIGH NUMBERS VS. λ [from Goody, 1956]

The solid lines are calculated from (1.20); the dashed lines are a graphical interpolation. The chained lines are irrelevant here.

The abscissa is $\lambda = kh(3 + 3\chi)^{1/2}$.

Inserting a horizontal variation of temperature as in the diffusive problem, non-dimensionalizing distances, and performing several ingenious transformations, he can write the heat equation

$$\beta \omega = \frac{K}{c_p \rho h^2} (D^2 - a^2) \theta + \frac{4\pi k Q}{c_p \rho} \int \mathcal{J}(\zeta - \zeta') \theta(\zeta') d\zeta' \quad (1.23)$$

where

$$\mathcal{J}(\zeta) = \frac{\tau}{2} \int_{-\infty}^{\infty} \frac{e^{-a|s|}}{\sqrt{s^2 - 1}} ds - \delta(\zeta) \quad (1.24)$$

and

$$\tau = kh \quad (1.25)$$

is the optical depth of the whole layer.

The problem for which he finally got answers was that with $\beta = \bar{\beta}$, $K = 0$, which are reasonable simplifications for the stellar interiors he was considering. He also found a variational method for this case

$$Ra = \frac{3\tau^2 \chi \int_{-1/2}^{1/2} d\zeta \int_{-1/2}^{1/2} d\zeta' \mathcal{F}(\zeta) \mathcal{F}(\zeta') \mathcal{J}(\zeta - \zeta')}{a^2 \int_{-1/2}^{1/2} \mathcal{F}(\zeta) \omega(\zeta) d\zeta} \quad (1.26)$$

where

$$\mathcal{F} = (D^2 - a^2)^{-2} \omega \propto \theta \quad (1.27)$$

$$\mathcal{F}(\frac{1}{2}) = \mathcal{F}(-\frac{1}{2}) = 0$$

Because of computation difficulties, Spiegel used two trial functions with no variational parameters that satisfied the boundary

conditions but had much different first derivatives. These turned out to yield rather similar results for $\tau < 1$ (transparent), while for $\tau > 1$ (opaque), the solution to the standard diffusion problem

$$\tilde{F}_1 = \cos \pi \zeta$$

gave the lowest value. The Rayleigh numbers given by (1.26) are not immediately comparable with those calculated by Goody for mixed radiation and diffusion, but when this and different boundary conditions are taken into account, the results are in good agreement [Goody, 1964] except for a region near $\lambda = 10^2$ where Goody's results show a kink attributable to variable β , which provides some extra stabilization.

CHAPTER 2

APPARATUS

2.1 Introduction





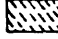
The apparatus was designed for two different types of measurement: the determination of heat flux across the gas layer, and the measurement of the temperature at several points within the fluid. This latter could also be styled a gradient measurement. The techniques used are quite different, and could be called respectively thermal and optical or interferometric. The thermal apparatus, the process of making measurements, and the necessary corrections will be discussed initially, followed by a description of the interferometer, with its measuring and data reduction procedures. Finally, since the theory of this type of measurement is not so well known, it will be given, along with corrections necessary to the simple theory.

2.2 Description of the Thermal Apparatus

The purpose of the apparatus in the convective onset measurements is to maintain a uniform heat flux and measure the temperature drops, while maintaining the conditions within the cell constant.

The thermal apparatus (see Fig. 2-1) was maintained inside a removable plexiglass cylinder with 10 in. I.D. and 1/2 in. walls. Within this, heat was supplied and removed from the two ends by water circulating through 1/4 in. copper tube, wound in a double flat spiral and soldered on the backs of brass plates 1/2 in. thick and 10 in. in diameter. The coils were then covered with a low melting point alloy to make solid pieces about 1 in. thick, 10 in. in diameter, weighing about 8300 grams (18-1/2 pounds) each.

KEY TO MATERIALS

-  ALUMINUM
-  NYLON
-  BRASS
-  PHENOLIC
-  GLASS OR PLEXIGLASS

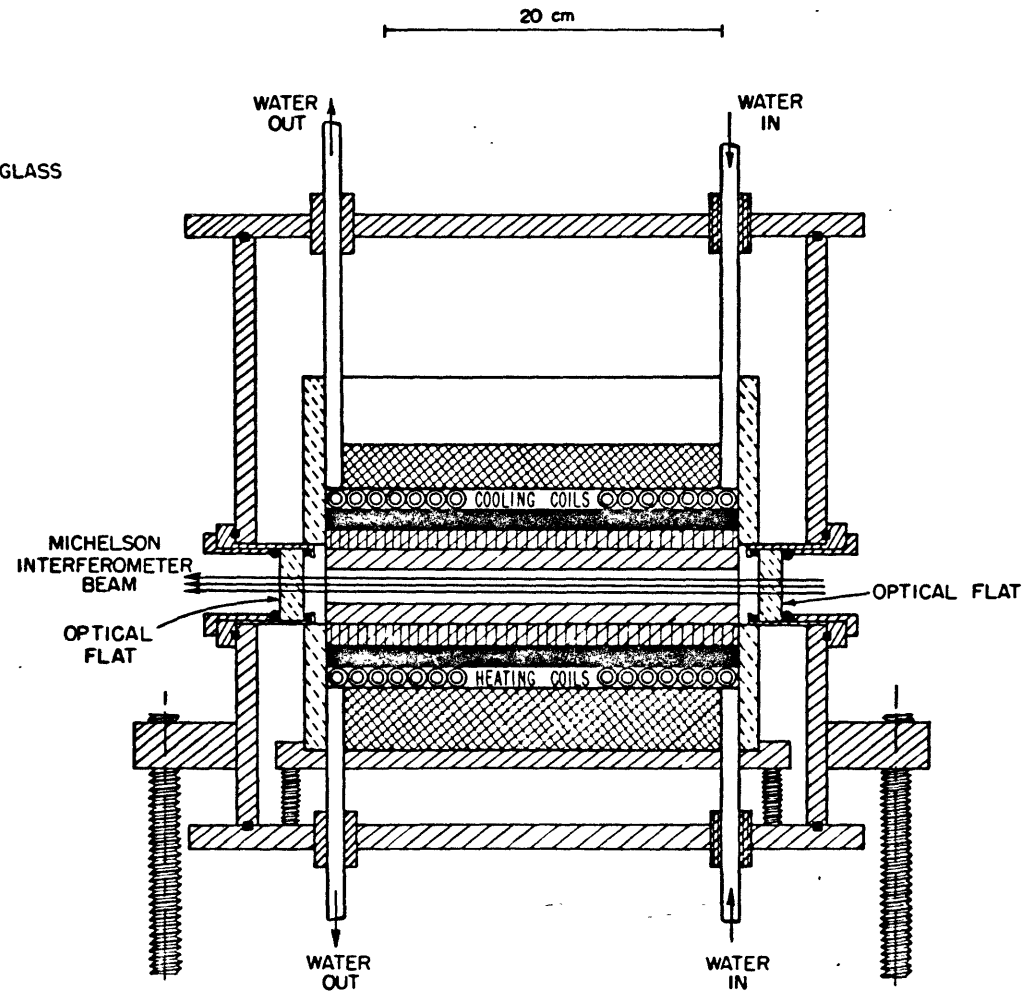


Fig. 2-1. THE CONVECTION CELL IN THE PRESSURE VESSEL

The insulating discs were two pieces of nylon, machined flat to a few thousandths of an inch, $5/8$ in. thick by 10 in. diameter. The nominal conductivity according to the manufacturer was 6×10^{-4} cal/cm.sec. deg. , and $\rho = 1.14 \text{ gm/cm}^3$, $c = 0.32 \text{ cal/gm}$.

The aluminum plates were of the purest commercial grade of aluminum, flat on the face to about 0.001 in., $1/2$ in. thick by 10 in. diameter. The rear was tapped to take 5 $6/32$ thermocouple mounting screws, each hole being about $3/8$ in. deep, and grooves about 0.05 in. deep carried the leads to the edge.

Before installation, the surfaces were chemically cleaned and plated to give a smoother and brighter surface. Unfortunately, over a year elapsed between this step and the first determination of emissivity, by which time the plates had become somewhat cloudy, and had been in contact with glycerine and kerosene. Small amounts of this clinging to the plates in spite of cleanings would increase the emissivity considerably. A high reflectivity was desired to increase the radiative effects on the gradient.

The exact diameter of the plates was 25.337 ± 0.025 cm., giving an area of $504.2 \pm 1.0 \text{ cm}^2$. Both aluminum plates weighed 1644 ± 25 grams.

The plates were separated by three spacers, located equidistantly from each other and near the outer wall, with the following dimensions:

<u>Spacer</u>	<u>Actual Height</u>	<u>Diameter</u>
5 cm.	$5.048 \pm 0.006 \text{ cm.}$	0.635 cm.
2 cm.	$1.987 \pm 0.002 \text{ cm.}$	0.635 cm.

The total area of the spacers is thus 0.95 cm^2 . Giving the phenolic a conductivity about 10 times that of air (i.e., 6×10^{-4} cal./cm.sec.deg.) would indicate 2 percent of the flux between the plates is carried by the spacers. However, they are located at the walls, where this effect appears as more leakage along the walls. The large area of the plates gives us an effective guard ring area for our measurements at the center. Preliminary measurements (see below) indicate that over the circle within the inside half of the radius, the temperature is constant to within 0.01° C . Conductive fluxes through the spacers and walls thus cause no distortion of the lines of heat flow in the central region, although they may cause an unpredictable distortion near the outer walls, which will affect the interferometer measurements.

On the outside of the brass plates a phenolic disc, 1 in. thick, is placed as an insulator. The whole apparatus rests upon an aluminum ring, which stands about 1-1/2 in. above the bottom of the outer tank on three iron stove bolts. The plexiglass cylinder is slid around the series of discs mentioned above, which are stacked to form two sandwiches with the aluminum discs to the center on either side of the gas layer, nylon next, and brass and phenolic on the outside. It has windows opened at either end of a diameter to allow a light beam through.

The outer tank is composed of a cylinder about 14 in. in diameter, with 3/8 in. walls, and two end pieces about 15 in. in diameter and 1/4 in. thick. An alloy of aluminum with a high silicon content to minimize corrosion by NH_3 was used. The purpose of this tank was to keep the ammonia confined, and to allow pressure regulation, both of which

require a gastight apparatus. O-ring seals were installed in the top and bottom of the cylinder, and at the two side windows. These were cut at two ends of a diameter at a height such that the holes in the inner cell could be aligned with them. Water lead-throughs were constructed to screw into the top and bottom plates. For the ingoing water they were constructed of nylon to avoid any influence of tank temperature change on the ingoing water. The outgoing lead is aluminum to allow the water temperature (very nearly the plate temperature) to control to some extent the tank top and bottom temperatures and create an interior temperature whose mean is the mean of the between-plate temperatures.

(not shown)
The thermocouple leads_a are brought out through packing glands in the cylinder lid.

(not shown)
In the lid_a are also lead-throughs for the manometer hose, a fitting to the vacuum pump, and a gas inlet.

The manometer is a mercury column, mounted on a ruled mirror. The vacuum pump is a conventional fore-pump, fitted with a vented exhaust to avoid dissolving gases in the pump oil.

During the taking of heat flux data, the holes for the light beam were closed over with cardboard to avoid large-scale motion through the inter-plate region, and the whole was enclosed to reduce the effects of short-term room temperature variations.

Heating and cooling were accomplished by circulating water from temperature-controlled baths through insulated hose at a rate of about .3 liter/minute. The baths themselves were ceramic tanks holding a few gallons of water which were vigorously stirred. Cold water from the city water supply circulated through cooling coils in the tanks.

The heating was supplied by krike heaters controlled by a mercury expansion switch which actuated a solid state switching device, which in turn controlled a relay. The manufacturer claimed 0.01° C temperature control or better. Temperatures were measured in the apparatus, and showed steadiness (due in part to the large thermal inertia) of 0.005° C over several hours. Slow changes were observed which could be traced to the influence of diurnal variations, and long-term changes due to deposits forming in the tubes and slowing the water flow.

The temperature sensors were copper-constantan (Cu-Cs) thermocouples, no. 24 gauge wire, mounted in the center of the heated and cooled plates, and in the center of the aluminum disc. In all cases the junction was formed and soldered lightly, and then soldered into a mounting screw of the same material as the plate in which it was to go, i.e., a thermocouple was soldered in an aluminum screw with aluminum solder for mounting in an aluminum plate. The holes in which the thermocouples were to go were tapped to receive the screw. Screw mounting was utilized to facilitate the change of thermocouples and provide good thermal contact. The thermocouples were thus in electrical contact with their plates at the junction.

The leads from the thermocouple in the brass plates were brought out through holes in the center of the copper tube spiral and in the center of the insulator. These provided no special problem.

The leads from the thermocouples in the aluminum plates were brought out through channels in the aluminum just deep enough to contain them and up the inside wall of the plexiglass cylinder. It was necessary to make

certain that there was no electrical contact between the wire and the plates; for this purpose the wires were coated with glyptol and the inside of the channel painted with Duco cement. A probe, run through the channel, showed no electric contact to the plate. This channel was on the side of the aluminum plate next to the insulating disc, allowing any disturbance in temperature caused by the channel to smooth out before reaching the other face.

In the construction and calibration of the thermocouples, the important point was that at the same temperature they should all read the same e.m.f. within 0.01°C ($0.4\ \mu\text{v.}$). From manufacturing standards, it is known that the probable error of absolute temperature measurement is 0.44 percent = 0.11°C at 25°C , [Finch, 1962], which a rough check confirmed. For absolute temperature measurements the N.B.S. [1955a] tabulated values were used to convert e.m.f.'s to temperatures; the temperature differences were converted with thermoelectric powers derived from the tables. The probable error here is again 0.44 percent in $\Delta\Theta$ used to get the Rayleigh number, but zero to first order for the ratio of temperature differences.

Thirteen thermocouples were made and soldered into fittings, of which eleven were standardized. All were made from one roll of wire, including the copper wires from the ice point.

The cold junction was always immersed in a tube of kerosene, which was inserted about 8 in. into a Dewar filled with a mixture of finely crushed ice and water. The use of tap water in the ice and atmospheric pressure variations are known to cause errors not greater than 0.001°C [Finch, 1962], which were neglected.

To avoid errors due to stray e.m.f.'s in the switches, leads, and potentiometer during comparison, the thermocouple leads were shorted with no. 18 copper wire, the potentiometer set to zero and the galvanometer zero position noted. Galvanometer deflections were noted from this point.

All thermocouples were required to have an e.m.f. $< 0.2 \mu\text{v}$ ($= 0.005^\circ \text{C}$) when both junctions were inserted in the same ice bath. The hot junctions in fittings were then put in separate glass tubes sealed at the bottoms, about 6 mm. in diameter, filled to a depth of 6 in. with kerosene, and immersed to a depth of 6 in. into a temperature-controlled bath.

The bath was run at three temperatures, nominally 23.4°C , 22.1°C , and 28.1°C , and all thermocouples were found to give readings within $0.4 \mu\text{v} = 0.01^\circ \text{C}$ of each other at these three temperatures. The readings corresponded within the errors of thermometer temperature measurements to the absolute N.B.S. tabulated values as well.

The thermocouples were then mounted in the brass and aluminum plates. In the preliminary stages, four thermocouples were put in each aluminum plate, one in the center and one halfway to the edge on three perpendicular radii. This was done to test the uniformity of each plate. When the apparatus was assembled with the aluminum plates touching, the whole well insulated from the outside, and hot and cold water circulated through the end plates, both plates were isothermal within 0.01°C . There was a slight difference in the temperatures of the two aluminum plates that implied a thermal contact resistance between them equivalent to 0.003 in. of air.

This is not unreasonable, since the aluminum plates were flat to 0.001 ± 0.001 in. and 0.001 ± 0.0005 in. respectively. These values were found by putting the plates on a plane table and going over them with a surface gauge.

This difference was not due to thermocouple differences, since if the water was turned off and the mass allowed to come to equilibrium, all the center temperatures were within 0.01° C. (Radial temperatures agreed with these.)

When spacers were inserted between the plates, temperatures within a plate were found to be equal to within 0.01° C. Once this was established, further measurements at the radial thermocouples were discontinued.

Several times since, all heating and cooling has been turned off, the aluminum plates put together, and the apparatus allowed to become isothermal. The thermocouples continue to read to within 0.01° C in this case.

In these readings and all that follow, the constantan lead from the apparatus went to the ice junction, from which a copper wire came to the same terminal board as the direct copper lead from the apparatus. This terminal board was immersed in oil to limit temperature differences between terminal strips. From the terminal board leads went to a shorting switch, also immersed in oil, which could measure either a dead short or the thermocouple voltage directly. The leads from the shorting switch went through a selector switch and reversing switch to a Leeds and Northrup potentiometer, capable of reading to $0.1 \mu\text{v}$, with a galvanometer as a null instrument.

2.3 Treatment of Gases

The gases used in this investigation were air and ammonia. Since the properties of these gases are affected by water vapor, it is necessary to have them as dry as possible. The air was dried by passing it slowly through a tube of Drierite (Na_2SO_4). The process of manufacture of ammonia involves several condensations and evaporations at temperatures near -70°C , which should remove H_2O . Refrigeration grade NH_3 is stated to contain less than 0.01 percent H_2O . Condensing 4 cc of NH_3 revealed no H_2O crystals. Since this is pure enough for our purposes, no further efforts were made to dry the tank ammonia.

2.4 Corrections to Heat Flux Measurements

If the spacers are removed and the aluminum plates put face-to-face in contact, the ratio of temperature drops

$$\frac{\Delta \Theta_{\text{I}}}{\Delta \Theta_{\text{II}}} = \frac{\Theta_0 - \Theta_1}{\Theta_2 - \Theta_3} \quad (2.1)$$

(where Θ_0 measures temperature in the lower brass plate,
 Θ_1 measures temperature in the lower aluminum plate,
 Θ_2 measures temperature in the upper aluminum plate,
 Θ_3 measures temperature in the upper brass plate,)

is found to be 0.850 ± 0.026 . This is presumably due to different contact resistance and boundary conditions on the nylon discs, as well as thermal differences and inhomogeneities. A measure of the latter is obtained by assembling one sandwich of brass heating plate, insulating disc, and

aluminum plate, shiny side toward the insulating plate. If one applies a sudden step function temperature disturbance to the heating plate, and observes the response of the aluminum plate temperature, one has a measure of the time constant of the insulating disc, which is inversely proportional to the conductivity, if all other factors are constant.

Getting time constants, τ , graphically, the values obtained are

$$\tau_1 = 49.9 \pm 1 \text{ minutes}$$

$$\tau_2 = 56.6 \pm 1 \text{ minutes}$$

which have a ratio $\tau_1/\tau_2 = 0.882 \pm 0.031$, within the limits of the more accurately determined conductivity ratios.

To correct for the difference between the plates, the quantity

$$S = \frac{\Delta\theta_I + 0.85 \Delta\theta_{II}}{\theta_2 - \theta_3} \quad (2.2)$$

was calculated for each point.

There were eight experimental situations, arising from the permutations of the three factors; gas (air or ammonia), plate separation (5 or 2 cm.), and temperature difference (2° and 6° roughly). In each situation there was a further separation into those with heating below (but not convecting) yielding values of S^+ , and those with heating above, leading to S^- . Since the Rayleigh number for the onset of convection, Ra_c , could be roughly determined by eye from plots of S^+ vs. Ra , only S^+ corresponding to $Ra \leq 0.8 Ra_c$ were included as definitely non-convecting. The means of S^+ and S^- in the i^{th} situation, \bar{S}_i^+ and \bar{S}_i^- were

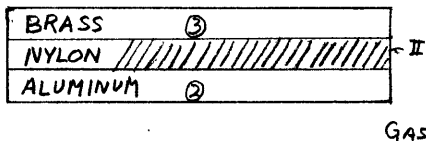
found, and combined to give \bar{S}_i . The \bar{S}_i^- were always slightly larger than \bar{S}_i by an average of 2.3 percent. (The maximum was 6.3 percent.) This presumably is due to heat leakage, and provides an estimate of the ratio of leakage heat to impressed heat flux.

The factors \bar{S}_i/\bar{S}_i^- and \bar{S}_i/\bar{S}_i^+ were then used to convert individual S_i^- and S_i^+ respectively to \bar{S}_i , which were plotted against pressure. For air (Fig. 2-2), there is no pressure dependence expected or observed, the temperature differences do not matter, and only the layer thickness has importance. From the mean values at 2 and 5 cm., \bar{S}_2 and \bar{S}_5 , the conductivity of the nylon discs and the emissivity of the aluminum surfaces will be calculated in 2.5.

For ammonia, the heat flux F_T is a function of pressure (see Fig. 5-11), due to its interaction with the radiation field. This effect will be explored in Chapter 5.

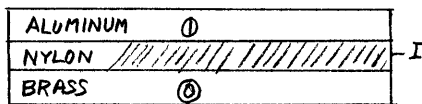
2.5 Derivation of Formula Relating \bar{S} and Radiative and Conductive Fluxes

Defining quantities with a subscript I as referring to conditions between thermocouples 0 and 1, II referring to those between thermocouples 2 and 3, and g referring to those between thermocouples 1 and 2,



K = thermal conductivity

$\Delta \Theta$ = temperature difference



h = thickness

$\mathcal{R} = \frac{F_R}{\Delta \Theta_g}$ = radiative flux/temperature difference.

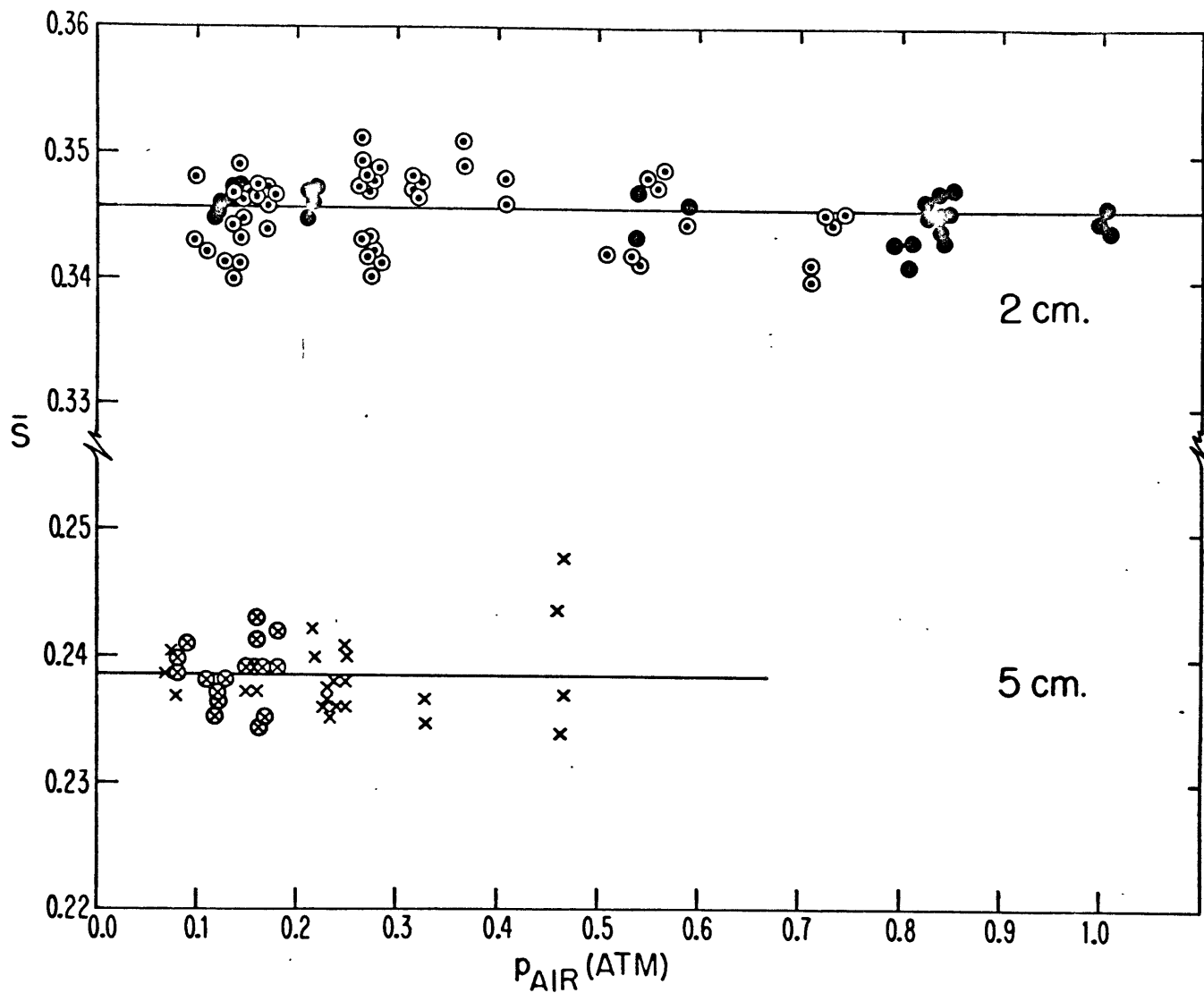


Fig. 2-2. \bar{S} vs. P_{AIR}

● plate spacing 1.987 cm. x plate spacing 5.048 cm.
 Ringed points are for upward fluxes.

With the assumption of constant heat flux, when the two aluminum plates are in contact:

$$\Delta\theta_I \frac{k_I}{h_I} = \Delta\theta_{II} \frac{k_{II}}{h_{II}} \quad (2.3)$$

it is observed that

$$\frac{\Delta\theta_I}{\Delta\theta_{II}} = 0.85 = \frac{\frac{k_{II}}{h_{II}}}{\frac{k_I}{h_I}} \quad (2.4)$$

or

$$\begin{aligned} \Delta\theta_I \frac{k_I}{h_I} + \Delta\theta_{II} \frac{k_{II}}{h_{II}} &= (\Delta\theta_I + 0.85\Delta\theta_{II}) \frac{k_I}{h_I} \\ &= 2\Delta\theta_g \left[\frac{k_g}{h_g} + \mathcal{R} \right] \end{aligned} \quad (2.5)$$

and

$$\left(\frac{\Delta\theta_I + 0.85\Delta\theta_{II}}{\Delta\theta_g} \right) \frac{1}{2} \frac{k_I}{h_I} = \frac{k_g}{h_g} + \mathcal{R} \quad (2.6)$$

or,

$$S_{hg} = f \left(\frac{k_g}{h_g} + \mathcal{R} \right) \quad (2.7)$$

2.6 Calculation of Emissivity and Nylon Conductivity

For two h's K and \bar{S} are known, allowing one to solve for \mathcal{R} and f . However, $\mathcal{R} \propto \theta^3$, and $K = K(\theta)$, so these must be

corrected for the various temperatures at which the results were obtained. The following table is constructed.

Table 2-1

DATA FOR CALCULATING EMISSIVITY AND NYLON CONDUCTIVITY

<u>h(cm)</u>	<u>\bar{S}_h</u>	<u>Θ_m (°K)</u>	<u>No. of cases</u>	<u><math>\frac{K}{cm. sec. deg.}</math> (ergs x 10³)</u>	<u>K/K(25)</u>	<u>$(T/298.16)^3$</u>
5.048 ± 0.006		296.91	13	2.601	0.9960	0.9874
	0.2385 ± 0.0005	297.89	23	2.609	<u>0.9989</u> 0.9979	<u>0.9991</u> 0.9949
1.987 ± 0.002		301.66	43	2.637	1.0096	1.0355
	0.3454 ± 0.0003	298.84	39	2.616	<u>1.0016</u> 1.0058	<u>1.0019</u> 1.0195

These conductivities are based on $K(25^\circ C) = 2.612 \times 10^3$ erg/cm.sec.deg.

Solving the above equations,

$$1/f = 7.852 \pm 0.063 \times 10^3 \text{ erg/cm.sec. } ^\circ C$$

$$R = 1.363 \pm 0.018 \times 10^3 \text{ erg/cm.sec. } ^\circ C .$$

This does not include the uncertainty in the value of air conductivity, which may be as large as 4 percent according to N.B.S. circular 564. [1955b]

Defining

$$\frac{dB}{d\Theta} = Q = \frac{4\sigma\Theta^3}{\pi} \quad (2.8)$$

and taking the value $\pi Q = 6.0108 \times 10^3$ erg/cm.sec. at 25° C yields

$$\frac{Q}{\pi Q} = 0.2268 \pm 0.0030 .$$

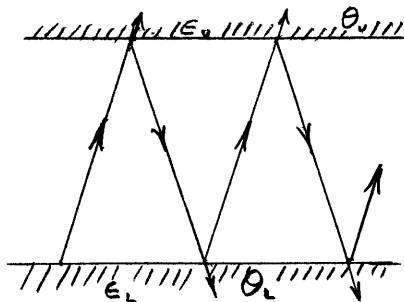
The values [Handbook of Chemistry and Physics, 38th ed., hereafter referred to as HCP]

$$0^\circ \text{ C} = 273.16^\circ \text{ K}$$

$$\sigma = 5.672 \times 10^{-5} \text{ erg/cm.}^2 \text{ sec. deg.}^4$$

were adopted.

By making the assumptions of isotropic emissivities and absorptivities, and infinite horizontal extent, we write for the emissive intensity from



the lower boundary $\epsilon_L B(\Theta_L)$.

Then $\epsilon_u \epsilon_L B(\Theta_L)$ is absorbed

at the upper surface with no

reflection, $\epsilon_u \epsilon_L (1 - \epsilon_u)(1 - \epsilon_L) B(\Theta_L)$

after 2 reflections, and

$\epsilon_U \epsilon_L (1 - \epsilon_U)^n (1 - \epsilon_L)^n B(\theta_L)$ after $2n$ reflections, or summing

$$\epsilon_U I^+ = \frac{\epsilon_U \epsilon_L B(\theta_L)}{1 - (1 - \epsilon_U)(1 - \epsilon_L)} \quad (2.9)$$

Similarly,

$$\epsilon_L I^- = \frac{\epsilon_U \epsilon_L B(\theta_U)}{1 - (1 - \epsilon_U)(1 - \epsilon_L)} \quad (2.10)$$

Denoting upward flux as [Goody, 1956]

$$F = \int \mu I d\omega = \int_0^\pi \int_0^{2\pi} I \cos \psi \sin \psi d\psi d\phi$$

where ψ is the angle from the z axis, the net, ^{absorbed} flux is

$$\pi (\epsilon_U I^+ - \epsilon_L I^-) = \frac{\pi \epsilon_U \epsilon_L [B(\theta_L) - B(\theta_U)]}{1 - (1 - \epsilon_U)(1 - \epsilon_L)} \quad (2.11)$$

If

$$\theta_m = \frac{1}{2} (\theta_L + \theta_U) \quad (2.12)$$

we approximate in our scheme

$$B(\theta_L) - B(\theta_U) = (\theta_L - \theta_U) Q(\theta_m) \quad (2.13)$$

and

$$Q = \frac{F}{\Delta\theta} = \frac{\epsilon_U \epsilon_L}{\epsilon_U + \epsilon_L - \epsilon_U \epsilon_L} \pi Q(\theta_m) \quad (2.14)$$

$$\frac{\epsilon_U \epsilon_L}{1 - (1 - \epsilon_U)(1 - \epsilon_L)} = \frac{Q}{\pi Q} \quad (2.15)$$

if we further assume $\epsilon_u = \epsilon_L$,

$$\frac{R}{\pi Q} = \frac{\epsilon}{2 - \epsilon} \quad (2.16)$$

Making use of the value of $R/\pi Q$ above, we find

$$\epsilon = 0.3697 \pm 0.0048 .$$

The value of the emissivity depends markedly on the conditions of the plate surfaces. An alteration with time might be expected in that case. The value obtained above, $\epsilon = 0.370 \pm 0.005$, should be assigned to the central date of the measurements on which ^{it} is based, or June 1, 1962.

A re-measure, on August 4-6, 1963, using a different pair of spacers ($h = 0.9271$ and 1.987 cm) gave $\epsilon = 0.417 \pm 0.010$.

From measurements made in October, 1961, before the temperature-controlled baths were installed, measurements on which the same procedure may be used gave (for spacers $h = 1.987$ and 1.52 cm) $\epsilon = 0.421 \pm 0.085$.

The greater uncertainty is due to the less accurate definitions of \bar{S}_h and the less well-conditioned matrix to be solved for R and $1/f$.

This also indicates that the difference in ϵ may be due to the use of different spacers. The change is in the anticipated direction, since as h is increased, the aspect ratio is decreased and more radiation goes out of the sides of our finite system. This appears in the measurement as a greater drop in heat flux with distance, which the equations attribute to the conductive flux, and remove from the radiative flux.

2.7 A Description of the Apparatus for Interferometric Temperature Measurement

The temperature distribution in two gases between two flat, isothermal plates as a function of the distance from the plates has been measured by measuring the optical path lengths at different distances from the plates, and relating this to density and thus to temperature. This is a quantitative use of a principle used qualitatively by Kennard [1940] and semiquantitatively by Croft [1958].

The difference in optical path lengths is measured with a Michelson interferometer, in one arm of which is the gas cell. See Fig. 2-3.

2.7.1 The Interferometer

The whole critical optical assembly is mounted on a rigid table 30 x 44 x 8 in. thick, constructed of 1/4 in. thick aluminum in a honeycomb structure, glued together with epoxy. This was cantilevered out from the base of a pillar which rested on a pile driven well down below the building. These precautions were necessary to obtain fringes free from vibration in the presence of building vibration and nearby heavy road and subway traffic.

The two end mirrors are front surface mirrors of aluminum deposited on a quartz flat, 2 in. in diameter x 1/2 in. thick, flat to 0.1λ for the sodium D doublet. They are mounted on heavy brass stands, with complete freedom of adjustment.

The beam splitter is a piece of optical glass, 3 in. in diameter x 5/8 in. thick, upon which a half-reflecting coating has been deposited. This is also flat on both sides to 0.1λ and highly parallel.

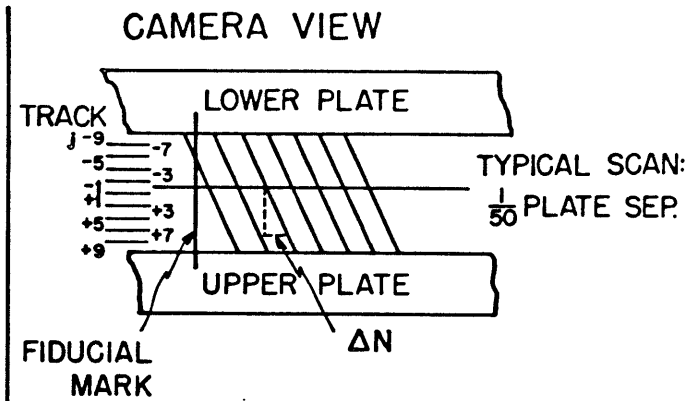
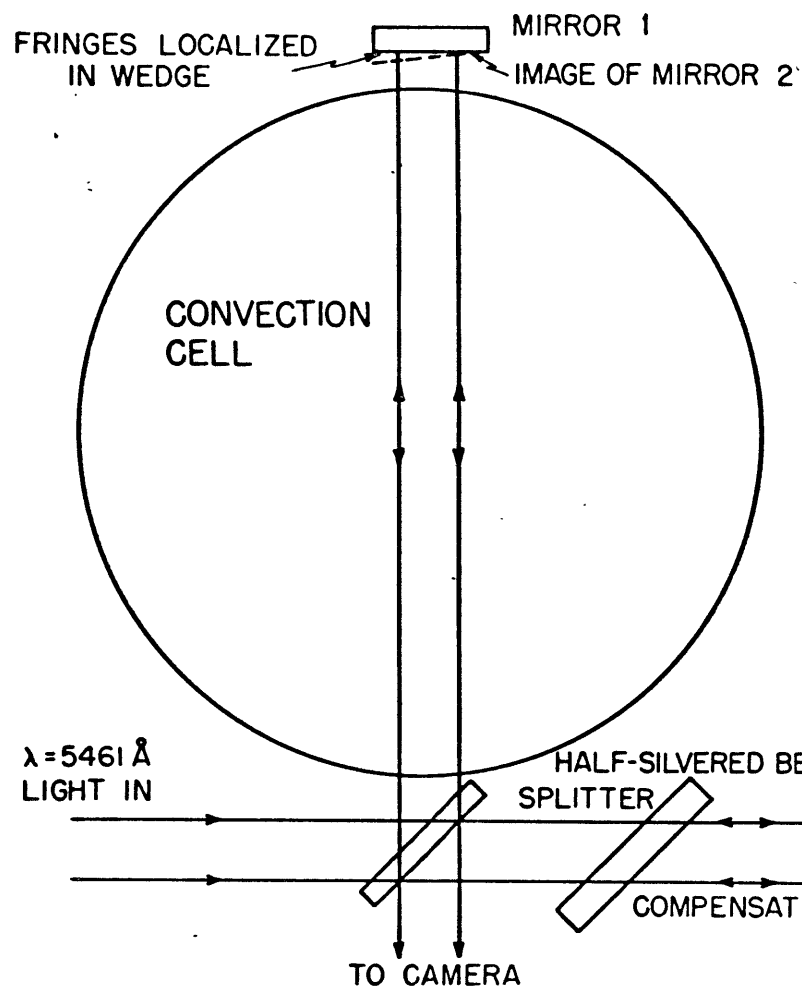


Fig. 2-3. INTERFEROMETER ARRANGEMENT (TOP VIEW)

The compensating plate is identical to the beam splitter except that it has no reflecting coating.

The windows are 2-1/4 in. diameter x 1/2 in. thick, also flat to 0.1λ and highly parallel. The windows are mounted in tubes that insert into the pressure tank and minimize the dead space beyond the heated plates to 0.68 cm. (See Fig. 2-4.)

The length of the arms was about 44 cm.

2.7.2 Light Source

The light source was a G.E. A-H-11 bulb in a housing with a low quality lens that provided some parallelism. The light was rendered parallel for the present purposes by passing it through a mask with the same aperture as the plate spacing (2 cm), located 4 meters from the beam splitter, or 5 meters from the lens of the camera.

A Wratten 77A filter was used to remove all but the $5461 \overset{\circ}{\text{A}}$ line of mercury.

2.7.3 Image System

The Michelson interferometer was adjusted to give thin wedge fringes, which are localized near the reflecting surfaces. A Burke and James view camera with a 4 x 5 in. back and a Schneider-Kreuznach Symmar lens, 1:5.6, 210 mm. focal length, was focussed on the reflection in the rear mirror of the rear edge of the convecting region in order to provide sharp top and bottom boundaries to the convecting region. The fringes were as distinct here as at the mirror surface.

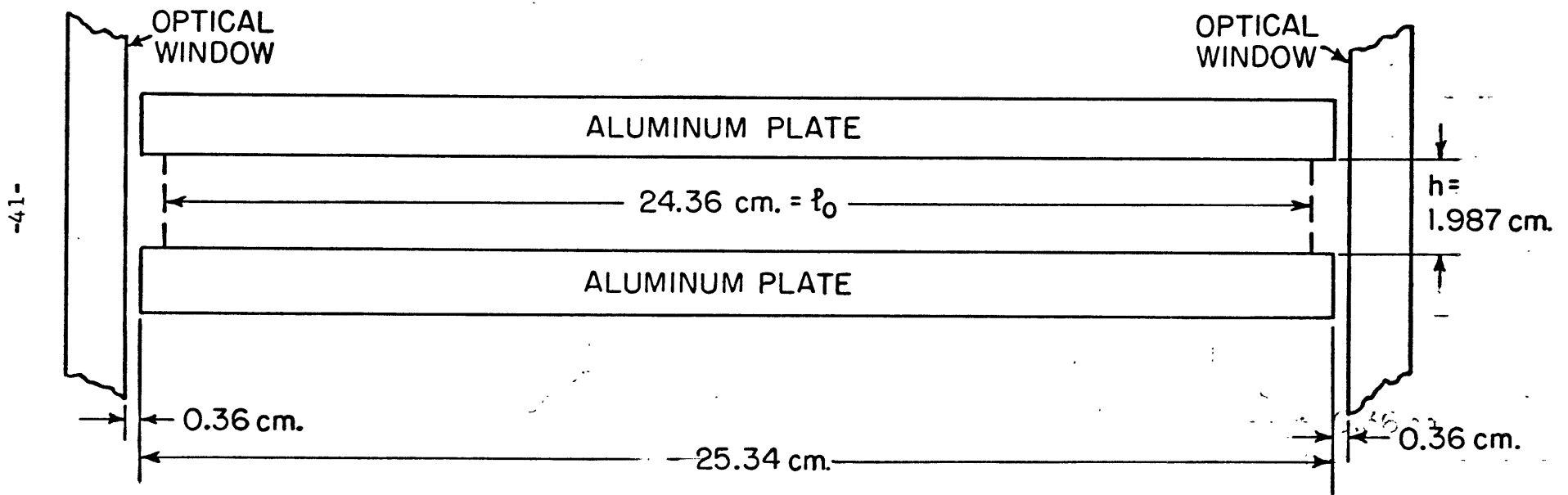


FIG. 2-4. Detail of Interferometer. (side view)

To provide a vertical reference mark in the image, a thin wire with a plumb bob on the end was hung in the plane of focus, in the arm not traversing the cell.

For focussing, a ground glass could be used. Pilot pictures to check the photographic arrangement were made with a Polaroid back and type 42 film, and later with a Polaroid film back and type 52 film. These films were used because they were within a factor of 3-5 in speed for the 5461 \AA line of the Kodak metallographic plate which was used for the actual measurements.

At this point the conditions which led to this type of data acquisition should be mentioned. The attempt was made to measure to 0.01° C , which meant for this situation 0.01 fringe displacement. The difficulties of maintaining very accurate temperature differences and pressures between the plates for extended periods, the possibility of instability with the cell or turbulence in the room path, and the vibrational shudder and thermal drift of the apparatus demanded a short time for recording the physical situation. Practical considerations (and the example of others) suggested photography over any electronic systems. The availability of a densitometer and Brown type recorder with variable speed drive meant that the photographic records of dark and light lines could be converted into a quantitative record of light intensity versus distance, with a variable magnification in length scale. As finally used, the marks indicating passage of the film carriage by 1 mm. were 15.2 cm. apart on the records, a magnification of 152 , which made possible measurement to 0.01 's of a fringe. Glass plates were necessitated by the demand for dimensional stability.

2.7.4 Film

Kodak Metallographic Plates were used with good results. They were chosen because of their speed in the green region, high contrast, and high resolution of 115 lines/mm. Since the fringes were approximately 1.3 mm. wide, a resolution of 0.007 fringe was possible. The use of High Resolution Plates could have reduced this by an order of magnitude, but their speed is prohibitively slow, and there are other sources of difficulty which make their use pointless.

The plates were developed according to instructions for highest contrast, in D-19 for 8 minutes, stopped in stop bath S-5 for 1 minute, and fixed in Kodak Rapid Fix for 5 minutes, all at 20° C. After washing for one-half hour in running water, they were treated for 30 seconds with Kodak Photo-Flo to prevent streaks and spots and dried overnight.

2.7.5 Densitometer Techniques

All profiles were taken with $h = 1.987$ cm. (A size limitation is imposed by the aperture of the optics.) The size of the photographic images was about 1.10 cm. high by 2 cm. wide, which was magnified by the optical system on the densitometer to allow easy adjustment with the naked eye. The densitometer aperture slit was set to be a few thousandths of a cm. wide, and the projection of the vertical reference mark aligned with it. This assured that the tracks across the plate would be perpendicular to the vertical reference, or through a horizontal layer of gas. The occurrence of the fiducial mark at the same carriage displacement (as deduced from marks automatically placed on the record at each mm. of

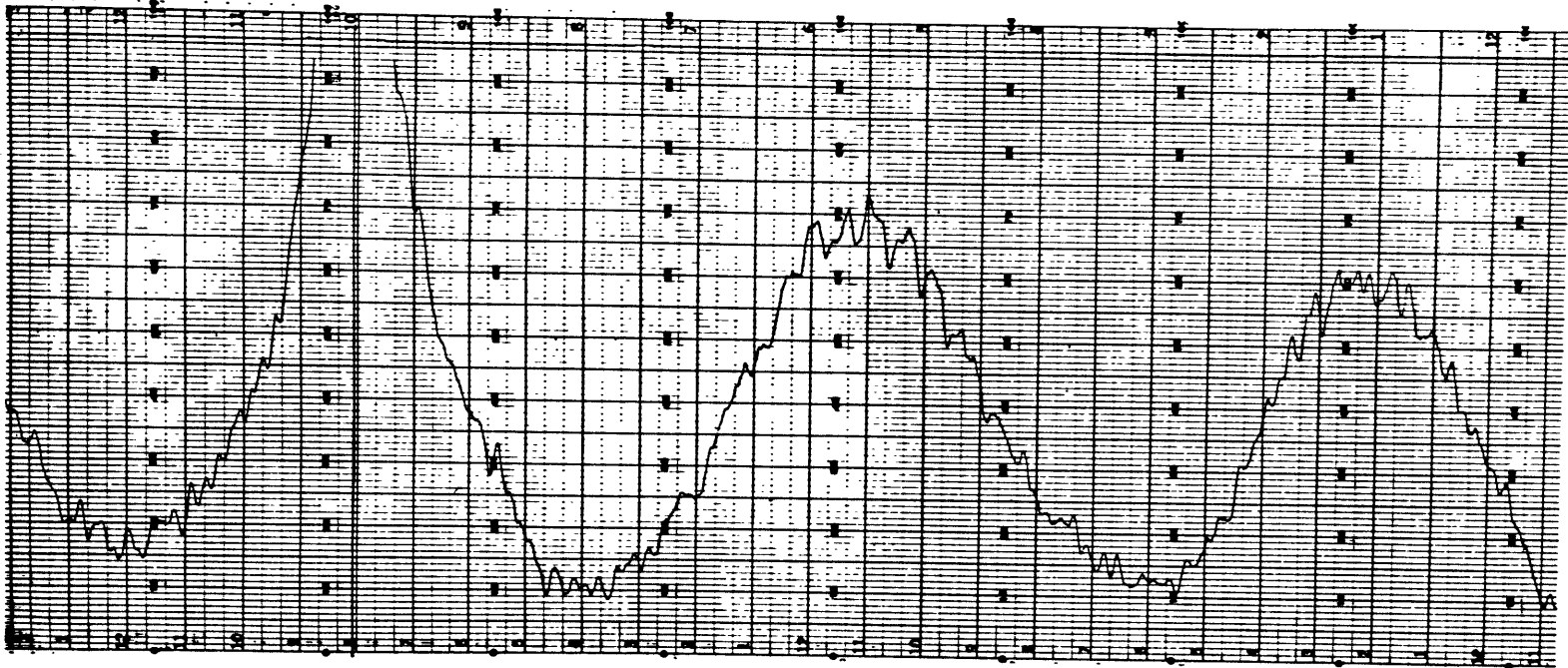
carriage displacement) proved that the track was accurately horizontal.

The slit height was now set equal to about 0.025 cm. By means of a micrometer mounted to measure the densitometer carriage position, the locations of the top and bottom of the image were found. The image was then divided into ten tracks, and the center of the densitometer slit set to coincide with the center of the first track. The carriage was turned manually to one side of the image, the amplifier adjusted, and the motor started to drive the plate uniformly across past the densitometer slit. The recorder drive was also begun. When the first track had been run, the carriage was returned manually to the start, the correct setting of the track verified with the micrometer, and the next track set, and so forth until all ten tracks had been scanned. A portion of a scan record which includes the fiducial mark is shown in Fig. 2-5.

2.7.6 Record Measurement

The following designation will be adopted. Imagine the space between the plates divided into 20 regions by 19 lines and two boundaries. A j value ranging from -10 at the bottom to 0 in the center and $+10$ at the top is assigned to each boundary and line. Then even j 's correspond to lines dividing the region into tenths and odd j 's correspond to the centers of each tenth, the lines along which the plate was tracked.

For measurement, the paper record corresponding to $j = -1$ was chosen as a reference, a line was drawn through the center of the fiducial mark on the record, and its distance from the carriage displacement mark



FIDUCIAL
MARK

Fig. 2-5. A PORTION OF A DENSITOMETER SCAN RECORD

(automatically recorded for every mm. of densitometer carriage displacement) noted. The spacing of ten of these carriage displacement marks on the recorder record was also measured, as an indication of relative speeds of carriage and recorder drives. This was never found to vary by more than one part in a thousand. The recorded track corresponding to $j = +1$ was then superposed on $j = -1$, and a line was put through the record of the fiducial mark at the same distance from the carriage displacement mark as on the $j = -1$ track. This distance was never more than one or two mm. from what one would have measured as the center of the fiducial mark record.

Now the $j = +1$ record was slid over the $j = -1$ record and the two fringes closest to the fiducial line were superposed as closely as possible by eye. The displacement of the fiducial line of $j = +1$ relative to $j = -1$ was measured. This was then done for all the other pairs of corresponding fringes, and the displacements averaged. In effect, what one is doing is performing a visual cross-correlation between a record of the form

$$y_{-1} = A \sin 2\pi x/L \quad (2.17)$$

with a record of the form

$$y_{+1} = A \sin 2\pi \left(\frac{x}{L} + \delta_{+1} \right) \quad (2.18)$$

in order to obtain δ_{+1} . This was done for all records for that plate,

giving a $\delta_j \pm \sigma_{\delta_j}$ for each track (j odd) relative to $j = -1$. Note that if δ changes by more than L , only the fractional portion is measured: the integral portion is known exactly.

A little thought will convince one that the quantity δ_j/L is the number of fringes displaced between the $j = -1$ level and the j level, $N_j - N_{-1}$. L is thus needed to convert the measured δ_j 's to N 's.

Taking the best sinusoidal curve on the $j = -1$ track as a reference and putting a reference mark through its center, the successive maxima of the $j = +1$ record are overlaid on it, and the reference line transferred to the $j = +1$ record. When this has been completed for all $j = +1$ maxima, a series of approximately equally spaced marks is the result. The distance between each pair of adjacent lines is measured: these are measures of L . The mean and standard deviation are taken. The same is done for $j = +9$. No significant variation across the space was found for these values of L , which differed by less than 2 percent, and were between 20-24 cm. for different plates. This introduces an uncertainty into $N_j - N_{-1}$, but since this quantity can be written $n_{j,-1} + \delta_{j,-1} / L$ where $n_{j,-1}$ is an integer known from inspection of the plate, the uncertainty only applies to the measured portion $\delta_{j,-1}/L$. The uncertainty then is a constant, ± 0.01 fringe, since $-0.5 < \delta_{j,-1}/L \leq 0.5$.

2.8 Interferometer Adjustments

The cell was first placed so that the rear mirror could be seen through the beam splitter and cell. The aluminum plate was then made horizontal by leveling a highly polished steel plate and going over the

aluminum plates with a surface gauge and indicator. In this way the plates were made horizontal from side to side, to 0.001 radian, and from back to front to 0.004 radian. No difference could be detected between upper and lower plates.

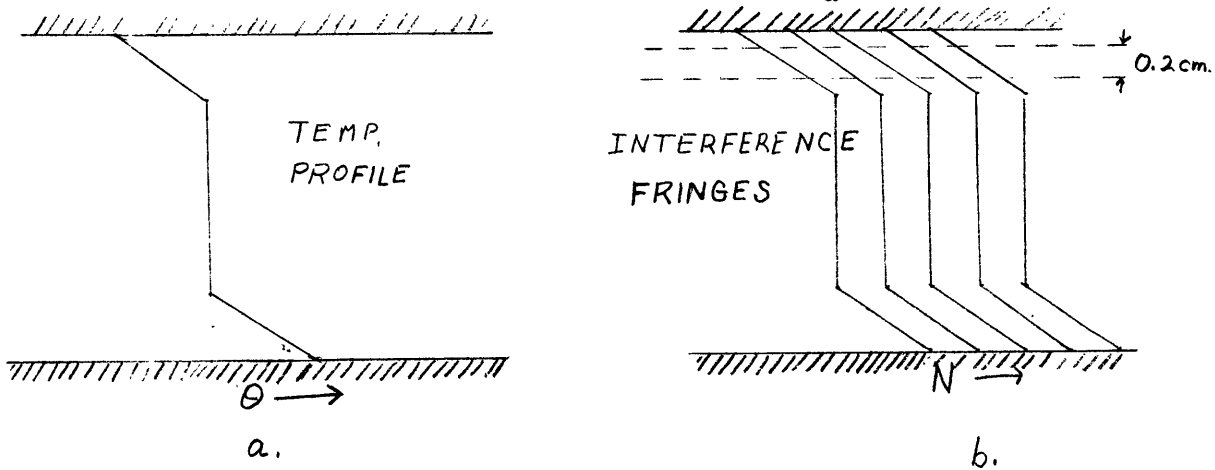
The rear mirror was next aligned by trial and error, to be perpendicular to the plane of the plates. This was necessary so that a ray of light parallel to the plates would traverse the same horizontal layer through the gas after the reflection as before.

The side mirror was then adjusted to give circular fringes, and moved until the central region filled the entire field of view. The two mirrors were then at nearly equal distances from the beam splitting surface. When the side mirror was tilted slightly, a thin wedge was formed which produced straight parallel fringes. The compensating plate could be rotated a few degrees to remove any last curvature from the fringes.

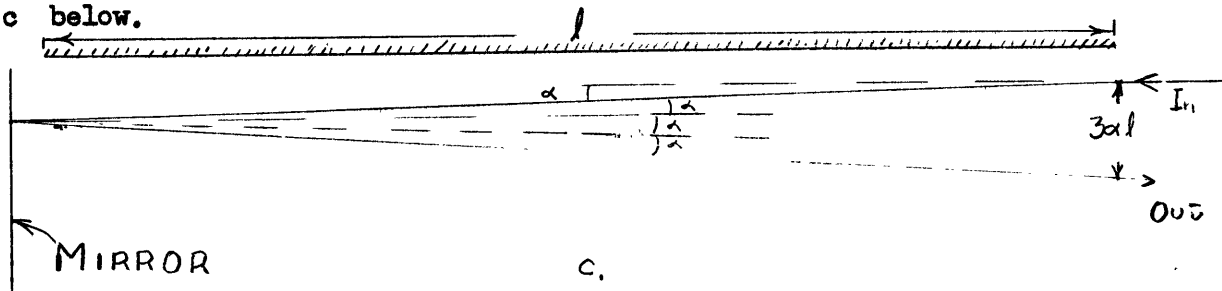
In order for the measurements to be valid, the temperature measured at the center of a layer must be representative of that layer. For this to be so, any light beam which falls in track j on the plate should have spent its entire path through the fluid between levels $j-1$ and $j+1$, so that it has not gone up or down more than 0.2 cm. in 50 cm. through the fluid, an angular deviation of 0.004. Since the whole space must be illuminated, an aperture 2 cm. high must be located 5 meters from the camera lens, or about 4 meters from the beam splitter. The light source was adjusted to the proper height by trial and error, by minimizing dark and reflecting regions at upper and lower boundaries.

The apertures of the system were drawn in the image space of the camera lens, and it was graphically verified that the light forming the image on track j had spent all or virtually all of its travel within the $j+1$ to $j-1$ space.

It was necessary to show that the steep gradients near the boundary for the case of ammonia would not displace the image so much as to make the method inaccurate. Consider an extreme case, in which the temperature profile is as shown in a. below, and in which N changes by 1 between two adjacent tracks. (See b below.) The path difference = λ , which over 0.2 cm. corresponds to an angle $\alpha = \frac{\lambda}{d} = 2.5 \times 10^{-4}$ radians.



The downward displacement is given by $l \alpha$ in the first traversal of the fluid, and would be $2 l \alpha$ for double that distance, were it not for the fact that it returns through the gas after reflection, which again bends the beam αl . The total displacement is thus $3 \alpha l$, as shown in c below.



$$\text{Total displacement} = 3 \cdot 2.5 \cdot 10^{-4} \cdot 25 \text{ cm.} = 1.9 \cdot 10^{-2} \text{ cm.}$$

Since one track is 0.2 cm. wide, this corresponds to a maximum of about 0.1 track width, which is about 0.01 of the plate separation. Since a scanning section is about 0.02 plate separation, this is not a large deflection. Because the temperature distribution is very nearly anti-symmetric about the center, the gradient is nearly symmetric. Thus, taking the means of upper and lower halves of the fluid gives a good approximation to the profile that would be obtained if there were no vertical refractive displacement.

2.9 Experimental Procedures

In making measurements on a temperature profile, the temperature baths and plates were brought to a temperature difference of about 7° C, the hot plate at the top. This enables higher temperature differences and pressures to be used without convective instability. The gas being studied, air or ammonia, was admitted to the proper pressure and allowed to come to equilibrium for several hours.

After blowing new isothermal air into the window wells, three photographs were taken as quickly as possible. The exposure was about 3 seconds each; all photographs were taken in 45-60 seconds. The $\Delta \epsilon$ was measured before and after the pictures, as well as the pressure. Temperature differences never changed by $>0.002^{\circ}$ C. As soon as pressure and temperature had been measured, the tank was evacuated. During the photographs all rotating machinery was turned off to stop vibration. In about 15 minutes, when the manometer read p about 0, (<0.3 cm. Hg.), pressure and temperature were read again, three photographs were taken as before, and pressure and temperature were again read.

Identification of the plates was by tape on the plate holder, which was transferred to the plate itself prior to development.

Photographs taken in the sequence vacuum, gas, vacuum, indicated that there was no measurable change in the vacuum fringe system due to mechanical or thermal drifts over periods of one or two hours. The constancy of the visual pattern to the eye over 2 or 3 days supports the assertion that drift may be neglected between gas and vacuum photographs.

2.10 Data Reduction

After development, densitometer tracking, and measurement of records from the 6 plates, weighted means of the fringes with and without gas were obtained with their standard deviations. The vacuum case has no applied difference between the two plates and gives the reference state of the system, provided by the positioning of the optical elements. Thus, denoting $N_j^G - N_{-1}^G$ as the mean of the three measurements of $N_j - N_{-1}$ with the gas in the apparatus and $N_j^V - N_{-1}^V$ as the same quantity with the apparatus evacuated, the raw net change is

$$(N_j - N_{-1})^R = (N_j^G - N_{-1}^G) - (N_j^V - N_{-1}^V) \quad (2.19)$$

This must now be corrected for the slight pressure remaining in the evacuated tank, by multiplying by $p_o(p_o - p_{VAC})^{-1}$ where p_o is the pressure at which the gas photographs were made and p_{VAC} is the pressure remaining when the evacuated photograph was taken. This factor was always less than 1.006. Now

$$N_j - N_{-1} = \frac{P_0}{P_0 - P_{VAC}} (N_j - N_{-1})^R \quad (2.20)$$

These are the data with which the theory must deal.

2.11 Theory of the Interferometer Measurement

The following symbols will be used;

λ = wavelength of light at given conditions.

l = length over which differential conditions are applied. (Here the length over which the gradient is applied.)

n = index of refraction.

$c = n - 1$.

ρ = gas density.

p = pressure.

θ = temperature.

Subscripts:

S = standard temperature and pressure.

0 = conditions at $j = 0$ in the fluid.

m = conditions at $j = m$, the point being measured.

At $j = m$ there is the condition

$$N_m = \frac{l}{\lambda} n_m \quad (2.21)$$

where N_m is the order of interference at m while at $j = 0$

$$N_0 = \frac{l}{\lambda} n_0 \quad (2.22)$$

For gases, the relation

$$\frac{n_m - 1}{\rho_m} = \frac{n_0 - 1}{\rho_0} = \frac{n_s - 1}{\rho_s} = \frac{c_m}{\rho_m} = \frac{c_0}{\rho_0} = \frac{c_s}{\rho_s} \quad (2.23)$$

gives

$$N_m - N_0 = \frac{l}{\lambda_{VAC}} (n_0 - 1) \left(\frac{\rho_m}{\rho_0} - 1 \right) \quad (2.24)$$

$$= \frac{l}{\lambda_{VAC}} c_s \frac{\rho_0}{\rho_s} \left(\frac{\rho_m}{\rho_0} - 1 \right) \quad (2.25)$$

where, since c is about 4×10^{-4} , $\lambda_m = \lambda_0 = \lambda_s = \lambda_{VAC}$ very nearly.

Consider the case of a perfect gas where, since

$$P_m = P_0$$

$$\frac{\rho_m}{\rho_0} = \frac{\Theta_0}{\Theta_m} \quad (2.26)$$

or writing

$$\Theta_m = \Theta_0 + \Delta \Theta_m \quad (2.27)$$

$$N_m - N_0 = \frac{l}{\lambda_{VAC}} c_s \frac{\rho_0}{\rho_s} \frac{-\Delta \Theta_m}{\Theta_0 + \Delta \Theta_m} \quad (2.28)$$

Similarly,

$$N_{-m} - N_0 = \frac{l}{\lambda_{VAC}} \frac{c_s \rho_0}{\rho_s} \frac{-\Delta\Theta_{-m}}{\Theta_0 + \Delta\Theta_{-m}} \quad (2.29)$$

For a temperature distribution symmetric about the median plane

$$\Delta\Theta_m = -\Delta\Theta_{-m} \quad (2.30)$$

Therefore, taking the mean

$$\begin{aligned} \overline{N_m - N_0} &= \frac{(N_m - N_0) - (N_{-m} - N_0)}{2} \\ &= \frac{l}{\lambda_{VAC}} \frac{c_s \rho_0}{\rho_s} \frac{(-1)}{2} \left(\frac{\Delta\Theta_m}{\Theta_0 + \Delta\Theta_m} - \frac{\Delta\Theta_{-m}}{\Theta_0 + \Delta\Theta_{-m}} \right) \quad (2.31) \\ &= \frac{l}{\lambda_{VAC}} \frac{c_s \rho_0}{\rho_s} \frac{(-1)}{2} \frac{(\Delta\Theta_m - \Delta\Theta_{-m})}{\Theta_0} \end{aligned}$$

The (-1) occurs because a positive $N_m - N_0$ means greater optical density at m , which implies greater density and lower temperature, as here formulated, in which it has been assumed that the path traversing the cell is longer than the reference beam. If it is shorter, the sign is positive. The sign is not known, but the direction of the temperature gradient is, and may be corroborated with the direction in which the fringes move on evacuation. Fringes are measured as positive and the negative sign is omitted.

One could consider writing

$$\overline{N_m - N_0} = \frac{l}{\lambda_{VAC}} \frac{c_s \rho_0}{\rho_s} \overline{\Delta\Theta}_m \left(\frac{1}{\rho} \frac{\partial \rho}{\partial \Theta} \right)_0 \quad (2.32)$$

For a perfect gas

$$\left(\frac{1}{\rho} \frac{\partial \rho}{\partial \Theta} \right)_0 = - \frac{1}{\Theta_0} \quad (2.33)$$

or

$$\overline{N_m - N_0} = \frac{h}{\lambda_{VAC}} c_s \frac{\rho_0}{\rho_s} (-1) \frac{\overline{\Delta \Theta_m}}{\Theta_0} \quad (2.34)$$

The same result occurs upon inclusion of the correction for gas imperfection; that taking the mean of expressions for the upper and lower halves of the layer is identical to treating the density difference as being obtained from the first term of a Taylor expansion. The mean

$$\frac{1}{2} [(N_m - N_0) - (N_{-m} - N_0)] = \frac{1}{2} [(N_m - N_{-1}) - (N_{-m} - N_{-1})] \quad (2.35)$$

will be interpreted using (2.34). The quantities on the right-hand side of (2.35) are the ones measured.

The corrections necessitated by gas imperfections can be seen by writing the equation of state in the virial form:

$$\frac{pV}{R\Theta} = 1 + \frac{B(\Theta)}{V} = 1 + \frac{b_0 B^*(T^*)}{V} \quad (2.36)$$

Then

$$\frac{1}{V} = \rho = \frac{p}{R\Theta} \frac{1}{1 + \frac{pB}{R\Theta}} \quad (2.37)$$

Corrections for gas imperfections enter the calculations in two places:

$$1) \frac{\rho_0}{\rho_s} = \frac{p_0 \theta_s}{p_s \theta_0} \frac{1 + \frac{p_s B(\theta_s)}{R \theta_s}}{1 + \frac{p_0 B(\theta_0)}{R \theta_0}} \quad (2.38)$$

$$2) \left(\frac{1}{\rho} \frac{\partial \rho}{\partial \theta} \right)_0 = - \frac{1}{\theta_0} \left[1 - \frac{p_0 B(\theta_0)}{R \theta_0} + \frac{p_0}{R} \left(\frac{\partial B(\theta)}{\partial \theta} \right)_0 \right] \quad (2.39)$$

$$= - \frac{1}{\theta_0} \left[1 + \frac{p_0 \theta_0}{R} \frac{\partial}{\partial \theta} \left(\frac{B(\theta)}{\theta} \right)_0 \right]$$

By writing $1 + \frac{p B(\theta)}{R \theta} = 1 + B(\theta)$, the corrections were calculated from N.B.S. tabulated values for air and from virial coefficient data in Hirschfelder, Curtiss, and Bird [1954] for ammonia for the conditions at which the measurements were made.

2.12 Gas Imperfection Corrections for Interferometer Measurements

The corrections must be calculated for the following conditions:

Air	$p_0 = 76.05$ cm. Hg.	$\theta_0 = 298.07^\circ$ K.
Ammonia	$p_0 = 53.00$ cm. Hg.	$\theta_0 = 300.60^\circ$ K.
	$p_0 = 98.32$ cm. Hg.	$\theta_0 = 298.06^\circ$ K.

2.12.1 Air

ρ_0/ρ_s was interpolated from tables of $\rho(\theta)/\rho_s$ given by N.B.S. Circular 564 [1955b] at intervals of 10° C. This gives

$$\frac{\rho_0}{\rho_s} = 0.9163$$

From tabulated values of $B(\theta)$ at several θ , a table of $B(\theta)/\theta$ vs. θ was made, a graph drawn, and a slope picked off. The values are given in Table 2-2.

Table 2-2

$B(\theta)/\theta$ FOR SEVERAL VALUES OF θ
(FOR AIR)

$\theta(^{\circ}\text{K})$	$B(\theta)/\theta[\text{cc./deg.}]$
270	-0.05179
280	-0.04156
290	-0.03267
300	-0.02493
310	-0.01816
320	-0.01222

Drawing a tangent at 298.07°K ,

$$\frac{\partial}{\partial \theta} \frac{B(\theta)}{\theta} = 0.00075 \text{ cc.deg.}^{-2}$$
$$\frac{P_0 \theta_0}{R} \frac{d}{d\theta} \frac{B(\theta)}{\theta} = 0.002724$$

and

$$\left(\frac{1}{P} \frac{\partial P}{\partial \theta} \right)_0 = - \frac{1.00272}{\theta_0} \text{ deg.}^{-1}$$

2.12.2 Ammonia

From Hirshfelder, Curtiss, and Bird [1954]

$$B(\theta) = b_0 B^*(T^*, t^*)$$

where for ammonia

$$T^* = \theta/320$$

$$t^* = 1.00$$

and

$$b_0 = 22.12 \text{ cc./mole}$$

The following data are given or easily calculable.

Table 2-3

VIRIAL COEFFICIENT DATA FOR AMMONIA

T^*	B^*	$\frac{dB^*}{dT^*}$
0.85	-18.40	80.20
0.90	-14.92	57.79
0.95	-12.42	43.04

Table 2-4 follows immediately.

Table 2-4

CALCULATION OF $\frac{p_0}{p_s}$ FOR AMMONIA

$p(\text{cm. Hg.})$	$\theta_0(^{\circ}\text{K})$	$\frac{p_0 \theta_s}{p_s \theta_0}$	$\frac{pb_0 b^*(T^*)}{R\theta} = B$	$1+B$	$\frac{1+B_s}{1+B_0}$	$\frac{p_0}{p_s}$
76.00	273.16	1.0000	-0.0178	0.9822	1.0000	1.0000
53.00	300.60	0.6336	-0.0080	0.9920	0.9901	0.6273
98.32	298.06	1.1853	-0.0154	0.9846	0.9976	1.1825

Similarly, one can calculate the following.

Table 2-5

CALCULATION OF $\left(\frac{1}{p} \frac{\partial p}{\partial \theta}\right)_0$ FOR AMMONIA

$p(\text{cm. Hg.})$	$\frac{B^*}{\theta}$ $\frac{\text{deg.}^{-1}}$	$\frac{dB^*}{dT^*}$	$\frac{dB^*}{d\theta}$ $\frac{\text{deg.}^{-1}}$	$\frac{-B^*}{\theta} + \frac{dB^*}{d\theta}$ $\frac{\text{deg.}^{-1}}$	$\frac{\theta \frac{dB^*}{d\theta}}{R(\text{atm}^{-1})}$	$\frac{p_0 \theta \frac{dB^*}{d\theta}}{R}$	$\left(\frac{1}{p} \frac{\partial p}{\partial \theta}\right)_0$ $\frac{\text{deg.}^{-1}}$
53.00	-0.0426	45.0	0.141	0.184	0.04960	0.0346	$\frac{1.0346}{\theta_0}$
98.32	-0.0443	47.5	0.148	0.192	0.05176	0.0670	$\frac{1.0670}{\theta_0}$

CHAPTER 3

RADIATIVE PROPERTIES OF AMMONIA

3.1 Introduction

In this treatment of radiative effects in a gas, use is made of the functions $\bar{\epsilon}(r)$ and $\bar{\epsilon}'(r)$, which might be called the perturbation emissivity and its spatial derivative. Unfortunately, these functions are not those usually measured. From the data typically taken by spectroscopists, such as line positions, widths and numbers, and from calculations of relative strengths, it is possible to calculate $\bar{\epsilon}(r)$ and $\bar{\epsilon}'(r)$. A useful check is provided by comparing calculations of ordinary emissivity with measurements made by heat transfer engineers. So that $\bar{\epsilon}(r)$ and $\bar{\epsilon}'(r)$ are available when required, the calculations will be described here and results presented.

3.2 Description of the Quantities Desired

It will be seen in Chapters 5 and 6 that the theory can be stated in terms of the quantities

$$\bar{\epsilon}(r, \theta, p) = \frac{\int_0^{\infty} \frac{dB_{\nu}}{d\theta} (1 - e^{-k_{\nu} r}) d\nu}{\int_0^{\infty} \frac{dB_{\nu}}{d\theta} d\nu} \quad (3.1)$$

and

$$\bar{\epsilon}'(r, \theta, p) = \frac{\int_0^{\infty} k_{\nu} e^{-k_{\nu} r} \frac{dB_{\nu}}{d\theta} d\nu}{\int_0^{\infty} \frac{dB_{\nu}}{d\theta} d\nu} \quad (3.2)$$

where

B_ν = Planck function at frequency ν (erg/cm.² sec. sterad cm.⁻¹).

k_ν = monochromatic volume coefficient of absorption at frequency ν
(cm.⁻¹),

r = distance (cm.),

θ = temperature (deg. K),

p = pressure (atmospheres).

\mathcal{E} may be described as a modified emissivity, by analogy to the emissivity

$$E(r, \theta, p) = \frac{\int_0^\infty B_\nu (1 - e^{-k_\nu r}) d\nu}{\int_0^\infty B_\nu d\nu} \quad (3.3)$$

It might be remarked that \mathcal{E} and E should be rather similar, since $\frac{dB_\nu}{d\theta}$ and B_ν are similar [Elsasser, 1942]. \mathcal{E}' is the distance derivative of the modified emissivity. As remarked, \mathcal{E} and \mathcal{E}' are functions of r , θ , and p . The r dependence enters only in the exponential. The Planck function B_ν is a function of temperature. It will be evaluated at 300° K. The absorption coefficient is strongly dependent on density, and therefore on pressure. It is also in general dependent on temperature, but this dependence seems very slight in this case. Dowding [1939] showed that the energy radiated by ammonia at 645° K was predicted by using the Planck function for 645° K and the same absorption coefficients measured at 300° K.

Clearly, since

$$\int_0^\infty B_\nu d\nu = \frac{\sigma}{\pi} \theta^4 = B \quad (3.4)$$

$$\int_0^{\infty} \frac{dB_{\nu}}{d\theta} d\nu = \frac{4\sigma}{\pi} \Theta^3 = Q \quad (3.5)$$

The problem of evaluating the numerator of (3.1) and (3.2) directly is very difficult, if not impossible, because of the rapid variation of k_{ν} with ν . (See Fig. 3-1.) From a line peak to an adjacent trough, factors of 10^4 are not uncommon. Therefore a procedure which is analogous to that employed for meteorological problems will be followed [see Goody, 1964]. Since $\frac{dB_{\nu}}{d\theta}$ is a smooth, slowly varying function of ν , the spectrum may be broken up into a series of regions of mean $\frac{dB_{\nu}}{d\theta}$, and

$$\mathcal{E} = \frac{1}{Q} \sum_i \left(\frac{dB_{\nu}}{d\theta} \right)_i (1 - \bar{T}_i) \Delta\nu_i \quad (3.6)$$

$$E = \frac{1}{B} \sum_i \bar{B}_{\nu_i} (1 - \bar{T}_i) \Delta\nu_i \quad (3.7)$$

where the mean transmission is

$$\bar{T}_i = \int_{\Delta\nu_i} e^{-k_{\nu} r} d\nu \quad (3.8)$$

\mathcal{E} can be obtained by a differentiation of (3.6). A band model may then be used to describe the integral over frequency in (3.8). The use of band models is fully described by Goody [1964], and in the context of combustion engineering, by Penner [1961].

The band model chosen was that of a random distribution of lines with equal intensities. Since the choice of intensity distribution makes

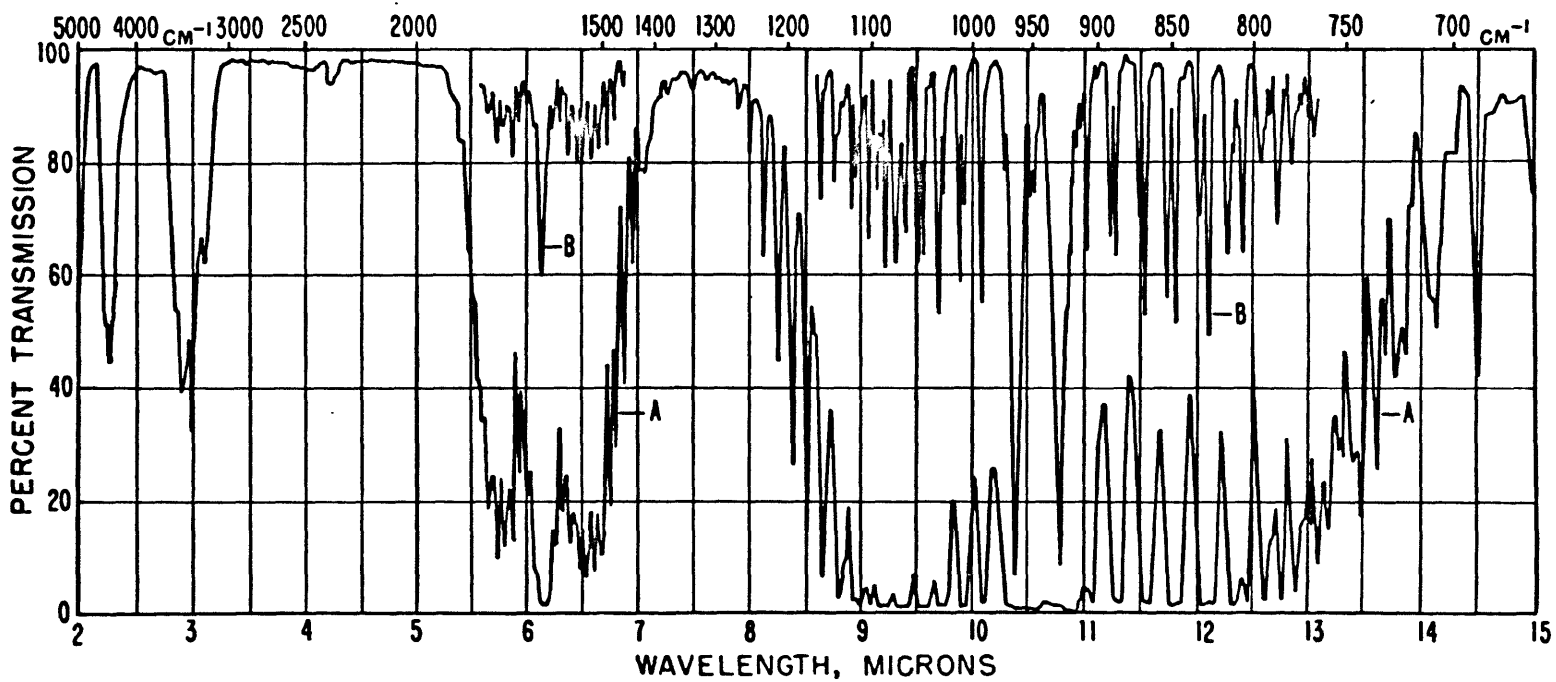


Fig. 3-1. A LOW RESOLUTION ABSORPTION SPECTRUM OF NH_3 [from Pierson, Fletcher and Gantz, 1956]

Curve A, $P_{\text{NH}_3} = 700 \text{ mm.Hg}$; Curve B, $P_{\text{NH}_3} = 45 \text{ mm.Hg}$; Cell length = 10 cm.

little difference in the random model [Penner, 1961], the latter restriction is not important. In addition, our method of correction to observed values reduces still further any differences. This model has certain advantages of simplicity.

Then, let

α = Lorentz line width (cm.^{-1}),

δ = mean line spacing (cm.^{-1}) = $\Delta\nu/N$,

N = number of lines in the range,

S = line intensity ($\text{cm. atmos.})^{-1}$ (cm.^{-1}),

$\Delta\nu$ = frequency width of the range (cm.^{-1}),

r = distance (cm.),

p = gas pressure (atmospheres),

$y = \alpha/\delta$,

$u = \frac{Srp}{2\pi\alpha}$.

The mean transmission for the i^{th} range can then be shown to be [Goody, 1964; Penner, 1961]

$$\bar{T}_i = e^{-2\pi y_i L(u_i)} \quad (3.9)$$

where

$$L(u) = ue^{-u} [I_0(u) + I_1(u)] \quad (3.10)$$

is the Ladenberg and Reiche function [Elsasser, 1942], which has been tabulated by Kaplan and Eggers [1956]. Finally we have

$$E(r, \theta, \rho) = \frac{1}{Q} \sum_i \left(\frac{dB_\nu}{d\theta} \right)_i (1 - e^{-2\pi y_i L(\omega_i)}) \Delta \nu_i \quad (3.11)$$

$$E(r, \theta, \rho) = \frac{1}{B} \sum_i \overline{B_{\nu_i}} (1 - e^{-2\pi y_i L(\omega_i)}) \Delta \nu_i \quad (3.12)$$

3.3 Spectroscopic Constants for Vibration-Rotation Bands of Ammonia at 300° K

Comparing a curve of black body intensity, B_ν , and its temperature derivative, $\frac{dB_\nu}{d\theta}$, vs. ν , [see, for example, Elsasser, 1942] with Table 3-1 indicates that the only bands that will matter are ν_2 and ν_4 .

Table 3-1

OBSERVED FUNDAMENTALS OF GASEOUS NH_3^*

<u>Mode</u>	<u>Frequency</u> <u>(cm.^{-1})</u>	<u>Remarks</u>
ν_1	3335.9 3337.9	Strong
ν_2	931.58 968.08	Strong
ν_3	3414	⊥
ν_4	1627.5	⊥ Very strong

*[after Herzberg, 1952]

Herzberg's Table 73 indicates that overtone and combination bands, with the exception of $2\nu_2 - \nu_2$, are not important in the spectral region of interest.

Figure 3-1 gives an indication of the complexity of the ammonia spectrum, the interpretation of which lies beyond the scope of this thesis. An introduction to the extensive literature is given by Herzberg [1952], and more recent work of Benedict, Plyler, and Tidwell [1958], and Garing, Nielson, and Rao [1959].

A few brief points should be made. Ammonia is a symmetric top molecule whose rotation is described by the quantum numbers J , the total angular momentum, and K , the angular momentum about the symmetry axis. Clearly, $|K| \leq J$. The relative strengths of lines in a given type of vibrational transition depend on J , K , and a number of other factors which can be calculated once and for all. This has been done for NH_3 by Benedict et al. [1958] up to $J = 16$.

Vibrational transitions are classified according to whether the change of dipole moment is parallel (\parallel) to the symmetry axis or perpendicular (\perp) to it. Rotational changes may occur simultaneously with vibrational changes, leading to the branches P, Q, R according to whether $\Delta J = -1, 0, +1$.

The molecule is in the form of a squat pyramid with the three H atoms at the corners of its triangular base. The N atom is either above or below the plane of the hydrogens, but since the two configurations are not identical, the molecular state is described by symmetric and anti-symmetric wave functions, which have large energy splittings for parallel

vibrational states. The energy difference between the ν_2 transitions $1^a - 0^s$ and $1^s - 0^a$ (superscript s refers to symmetric, a to anti-symmetric states) is about 38 cm.^{-1} , leading to two very similar spectra displaced by 38 cm.^{-1} from each other.

The intense ν_2 band, near the peak of the black body curve, was divided into 7 ranges: the anti-symmetric Q branch (aQ), the symmetric Q branch (sQ), the region between (I), the strong and weak portions of the P branch (P(s) and P(w)), and the strong and weak portions of the R branch (R(s) and R(w)). The division into strong and weak portions was somewhat arbitrary. The $2\nu_2^s - \nu_2^a$ transition was treated in two parts -- the P and Q branches (2aP, 2aQ) were lumped together, and the R branch (2aR) was lumped with the P(w), which it overlaps. The $2\nu_2^a - \nu_2^s$ falls in the center of the intense ν_2 band, which is much stronger, and its strength is neglected. The ν_4 band is treated as a single region. Sources of band parameters are given in Table 3-2. The relative range strengths were obtained by adding relative strengths of the individual lines [from Benedict, et al.] included in the range.

The intensities used were those listed in Table 3-2, obtained by calculating

$$A_i = K_i A \frac{\nu}{\nu} \quad (3.13)$$

where the relative strength of the i^{th} range is K_i and the integrated intensity of the band is A .

Table 3-2
SOURCES OF NH₃ RANGE PARAMETERS *

Range	$\Delta\nu(\text{cm.}^{-1})^*$	$\frac{\nu}{\bar{\nu}}$	Relative Range Strengths (BPT)	N
aQ	910-945 GNR Obs.	0.976	0.196	52 GNR Obs.
I	945-952 GNR Obs.	0.998	0.013	11 GNR Obs.
sQ	952-970 GNR Obs.	1.011	0.196	45 GNR Obs.
P(s)	785-910 GNR Obs.	0.892	0.19843	59 GNR Obs.
	(Includes aP(6,K) and sP(7,K), less P(0,0) in I.)			
P(w)	648-785 GNR Obs.	0.746	0.02232	141 GNR Obs.
	(Includes J" = 14 (final rotation number), the same limit as that to which BPT calculate relative strengths.)			
R(s)	970-1123 GNR Obs.	1.101	0.37850	51 GNR Obs.
	(Includes aR(9,K) and sR(8,K), less R(1,0) in I.)			
R(w)	1123-1265 GNR Obs.	1.257	0.03500	70 GNR Obs.
	(Includes lines to J" = 15. This is slightly more than calculated by BPT, but the lines here tend to overlap, giving fewer but stronger lines.)			
ν_4	1324-1940 Formula BPT, J"=16.	1.0	1.00000	549 Counting lines in BPT with strength > 2×10^{-6} of total band.
2aQ	648-603 GNR Obs.		0.392	194 Line count of BPT
2aP	603-325 Same as P of ν_2		0.226	calc. for band, P and Q branches.
2aR	In with P(w) of ν_2		0.382	Lines measured with those of P(w).

*Abbreviations used: BPT - Benedict, Plyler, and Tidwell [1958]
GNR - Garing, Nielson, and Rao [1959]

For complete consistency, the values obtained by calculating relative intensities should be used, i.e., the relative strength of the i^{th} range is proportional to $\frac{\nu_i}{D}$. Letting

$$Z = \sum \frac{\nu_i}{D} K_i$$

the intensity of the i^{th} range may be written

$$A_i = \frac{A}{Z} \frac{\nu_i}{D} K_i \quad (3.14)$$

The values calculated from (3.14) differ by only a few percent from those calculated with (3.13), and when the correction is considered, the final results will be unaltered by using values of A_i from (3.13).

The integrated intensities in the ranges are [McKean and Schatz, 1956]

$$A_{\nu_2} = 600 \text{ cm.}^{-1} (\text{atmos. cm.})^{-1}$$

$$A_{\nu_4} = 110 \text{ cm.}^{-1} (\text{atmos. cm.})^{-1}$$

and from these,

$$\begin{aligned} A_{2\nu_2}^s - \nu_2^a &= \frac{1}{2} A_{\nu_2} e^{-\frac{2\pi h \nu_2}{k_B \theta}} \\ &= 3.07 \text{ cm.}^{-1} (\text{atmos cm.})^{-1} \end{aligned}$$

Table 3-3

RANGE PARAMETERS FOR NH₃

Range	Spectral Range [cm. ⁻¹]	$\Delta \nu$ [cm. ⁻¹]	Range Intensity A=NS ₁ [cm. ⁻¹] (atmos.cm) ⁻¹	N	S ₁ [cm. ⁻¹] (atmos.cm) ⁻¹	$\delta = \frac{\Delta \nu}{N}$ [cm. ⁻¹]
aQ	910 - 945	35	114.8	52	2.207	0.67
I	945 - 952	7	7.8	11	0.708	0.64
sQ	952 - 970	18	118.9	45	2.642	0.40
P(s)	785 - 910	125	106.2	59	1.800	2.12
p(w) 2aR } }	648 - 785	137	11.3	141	0.081	0.97
R(s)	970 -1123	153	224.11	51	4.394	3.00
R(w)	1123-1265	142	26.40	70	0.377	2.03
ν_4	1324-1940	616	110	549	0.200	1.12
2 _a Q 2 _a P } }	325 - 647	322	1.90	194	0.010	1.66

3.4 Pressure Effects

3.4.1 Pressure Broadening of NH₃

E has been measured by Port [1940] for mixtures of ammonia and nitrogen at a total pressure of one atmosphere with constant r . These results are presented by Hottel [1954], from whom Fig. 3-2 is taken.

To duplicate the results of Port, the amount of line broadening due to nitrogen must be separated from that due to the ammonia self-broadening. One expects the latter to be considerably larger, due to the permanent dipole moment of ammonia, which suggests a larger collision radius with other dipoles and resonance broadening according to Anderson's [1949] theory.

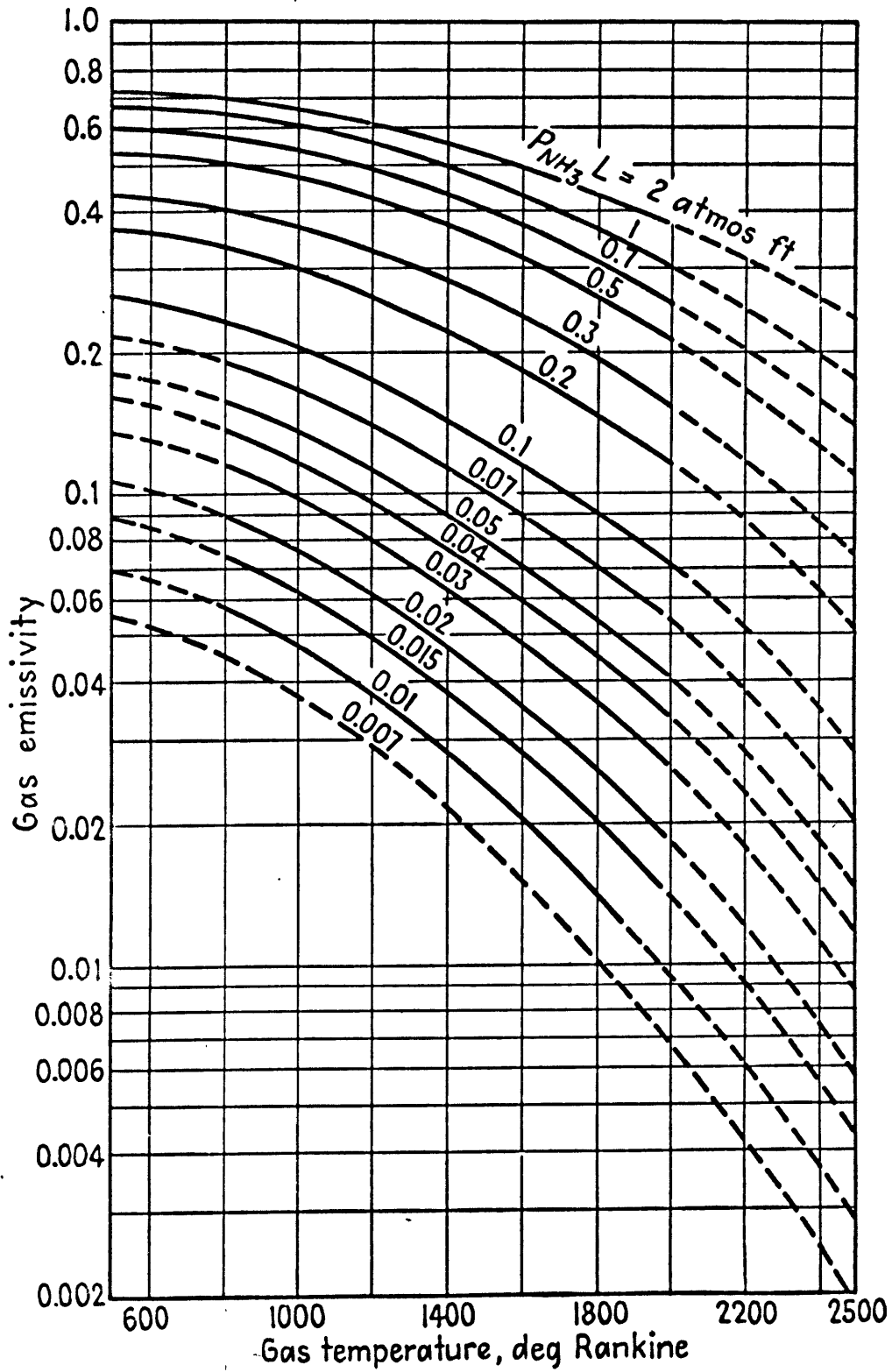


Fig. 3-2. AMMONIA EMISSIVITIES MEASURED BY PORT
[from Hottel, 1954]

The expression for the line width is given in a convenient form by Hirschfelder, Curtiss, and Bird [1954]

$$\alpha_{ab} = \frac{1}{2} \sqrt{\frac{3}{k_B \Theta}} \left[\rho_a \frac{(\sigma_{aa})^2}{\sqrt{m_a}} + \rho_b \frac{(\sigma_{ab})^2}{\sqrt{m_b}} \right] \quad (3.15)$$

where α is the half width in the Lorentz expression for the line shape $k_\nu \propto \frac{\alpha}{(\nu - \nu_0)^2 + \alpha^2}$, caused by collisions between emitting atoms of species a, and perturbing atoms of species a or b. Here m is the mass of the species denoted by the subscript and k_B is the Boltzman constant. The collision radii are σ_{aa} for self-broadening and σ_{ab} for broadening by b.

The figures in Table 3-4 are for the $J = 3, K = 3$ line in the microwave region, taken from Hirschfelder, Curtiss, and Bird [1954].

Table 3-4

RELATIVE EFFECTIVENESS OF AMMONIA AND NITROGEN
IN LINE BROADENING

Gas	$\sigma(\text{\AA})$	m	$\frac{\sigma^2}{\sqrt{m}}$
NH ₃	13.8	17.03	46.2
N ₂	5.54	28.00	5.80

Thus

$$\frac{\alpha_{\text{NH}_3}}{\alpha_{\text{N}_2}} = \frac{46.2}{5.80} = 7.97 \quad ,$$

or ammonia is eight times as effective per unit pressure broadening itself as nitrogen is, for the 3,3 line.

The broadening for a particular J,K value depends directly on $K/\sqrt{J^2 + J}$ [Bleaney and Penrose, 1948]. Thus the lines with highest K value will be most broadened, and the greatest broadening increases with J. The values of the collision radii for different states listed by Hirschfelder, Curtiss, and Bird [1954] for self-broadening of ammonia in the microwave region range from 8.8 Å (J = 5, K = 1) to 14.1 Å (5,5) and (6,6) and 15.2 Å (6,4), but the (3,3) line is the only one for which broadening by nonpolar gases is given. Their collision diameters are close to kinetic theory values, as one might expect, and those values might be used for other transitions, but this added complexity will provide no useful information since accurate quantitative data for the application of these microwave values to the infra-red spectrum is lacking.

We might also expect that the ratio $\frac{\alpha_{\text{NH}_3}}{\alpha_{\text{N}_2}}$ would show less variation than either of the parameters separately -- α_{N_2} an easily perturbed state presumably showing an increase in both α_{NH_3} and α_{N_2} , and conversely.

The above formula yields $\alpha_{\text{NH}_3} = 0.515 \text{ cm.}^{-1}$ for an atmosphere of pure ammonia, while $\alpha_{\text{N}_2} = 0.065 \text{ cm.}^{-1}$ for a small amount of ammonia broadened by 1 atmosphere of nitrogen, when collisions between ammonia molecules could be assumed to be extremely rare.

This compares favorably with the values measured in the infra-red combination band $\nu_2 + \nu_3$. Benedict, Plyler, and Tidwell [1958] find values of line width from 0.16 - 0.59 cm.^{-1} for lines of differing J,K in pure ammonia. For four lines measured by three different methods, they

get an average of 0.42 cm.^{-1} , while for the same rotation lines the microwave average is 0.52 cm.^{-1} . This follows a general trend for the vibration-rotation lines to be 20 - 25 percent narrower than microwave lines. This can be explained on the basis of Anderson's [1949] theory and the existence of ground states split by less than 1 cm.^{-1} while the upper vibration states are widely separated (c.f., 37 cm.^{-1} for the ν_2 band). This prevents simultaneous dipole changes of colliding molecules and the upper states. Another factor contributing to the different average widths is the fact that the narrow $K = 0$ transitions are very narrow, and are forbidden in the microwave region.

The value $\alpha_{\text{NH}_3} = 0.515$ will be used, however, since the microwave values are more accurate, and to weight the broader lines that will have a greater effect at higher pressures, where they will show considerable broadening and influence a wider portion of the spectrum.

From Port's [1940] data the pressure of NH_3 , p_{NH_3} , and the total broadening pressure given (because of (3.16)) by

$$p_T = p_{\text{NH}_3} + \frac{p_N}{8} \quad (3.17)$$

and the ratio of p_{NH_3}/p_T can be calculated. These are presented in Table 3-5.

3.4.2 Inclusion of Pressure in the Mean Transmission

The transmission, as remarked above, is defined as

$$\bar{T} = 1 - e^{-2\pi y L(u)} \quad (3.18)$$

Table 3-5

TOTAL BROADENING PRESSURES IN PORT'S EXPERIMENTS

p_L [ft., atm.]	p_L [cm., atm.]	P_{NH_3} [atm.]	P_T [atm.]	$\frac{P_{NH_3}}{P_T}$
.007	.213	0.0043	0.129	0.0333
.01	.305	0.0061	0.131	0.0466
.015	.457	0.0092	0.134	0.0687
.02	.610	0.012	0.136	0.0882
.03	.914	0.018	0.141	0.128
.04	1.22	0.025	0.147	0.170
.05	1.52	0.031	0.153	0.203
.07	2.13	0.043	0.161	0.27
.1	3.05	0.061	0.18	0.34
.2	6.10	0.12	0.23	0.52
.3	9.14	0.18	0.28	0.64
.5	15.2	0.31	0.40	0.78
.7	21.3	0.43	0.50	0.86
1.0	30.5	0.61	0.66	0.92
1.63	49.7	1.00	1.00	1.00

where

$$y = \frac{R}{S} \quad (3.19)$$

$$v = \frac{S r p}{2 \pi \alpha} \quad (3.20)$$

The relationship between line width and pressure is accurately given by

$$\alpha(p) = \alpha_0 \frac{P_T}{P_0} \quad (3.21)$$

where α_0 is the line width at pressure p_0 and p_T is the total broadening pressure. In Section 3.4.1 we found $\alpha_0 = 0.515 \text{ cm.}^{-1}$ at $p_0 = 1$ atmosphere for ammonia, so that we have for ammonia, denoting

$$\alpha' = \frac{\alpha_0}{p_0} \quad (3.22)$$

$$\overline{T} = 1 - e^{-2\pi \frac{\alpha'}{\delta} p_T L(\nu)} \quad (3.23)$$

$$\nu = \frac{S r}{2\pi \alpha'} \frac{P_{NH_3}}{P_T} \quad ; \quad y = \frac{\alpha'}{\delta} P_T \quad (3.24)$$

3.5 Treatment of the Pure Rotation Spectrum

3.5.1 Relative Intensities of the Rotation Lines

An expression for the total intensity of the J^{th} rotation line in absorption is given by Gerhard and Dennison [1933] for the positive branch of an oblate axi-symmetric molecule,

$$I_J = -\frac{L}{\beta} \left[\frac{\sigma(1+\beta)}{\pi} \right]^{1/2} e^{-\sigma J^2} \left\{ \frac{1 - 2\sigma\beta J^2}{J(-\sigma\beta)^{1/2}} \int_0^{J(-\sigma\beta)^{1/2}} e^{\nu^2} d\nu - e^{-\sigma\beta J^2} \right\} \quad (3.25)$$

where

$$\beta = \frac{A}{c} - 1 \quad (3.26)$$

and

$$\sigma = \frac{h^2}{2k_B \Theta}$$

A and C are moments of inertia of the molecule

$$L = \frac{4\pi^2 \nu_J N \mu^2}{3c\hbar} \left(1 - e^{-\frac{2\pi h \nu_J}{k_B \Theta}}\right) \quad (3.27)$$

where ν_J = location of the "line" center,
 N = number of absorbing molecules.

The following values are available [Herzberg, 1952]:

$$A = 2.816 \times 10^{-40} \text{ gm. cm.}^2$$

$$C = 4.437 \times 10^{-40} \text{ gm. cm.}^2$$

$$\mu = 1.3 \times 10^{-18} \text{ c.g.s. e.s.u.} \\ \text{[Foley and Randall, 1941].}$$

Taking c , \hbar , k_B , and Avagadro's number from the HCP,

$$\beta = -0.3653, \quad (3.28)$$

$$\sigma = 0.04770. \quad (3.29)$$

L depends on temperature through N. It was evaluated at 300° K.

L also depends on the frequency of the J lines, which to our accuracy is [Herzberg, 1952]

$$2 \frac{h}{4\pi c A} \cdot J = 19.890 \text{ J cm.}^{-1} = \nu_J \quad (3.30)$$

Then

$$L = 346.80 \text{ J at } 300^\circ \text{ K.} \quad (3.31)$$

For values of J from 5-20, the quantity $I_J \left(1 - e^{-\frac{2\pi h \nu_J}{k_B \Theta}}\right)$ was calculated.

3.5.2 Widths of Rotation Lines

"Lines" of equal J are actually split into their K components, forming small bands. The measurements of the widths of rotation bands show considerable scatter, but all show an increase with J . The values taken are $\Delta\nu_J = 4 \text{ cm.}^{-1}$ for $J < 10$ [Wright and Randall, 1933; Slawsky and Dennison, 1939] and theoretical values from Hansler and Oetjen [1952], Foley and Randall [1941], and Hadni [1953] for $10 \leq J \leq 16$.

3.5.3 Number of Lines

Each J "line" is composed of $2J + 1$ lines, due to splitting of K components.

3.5.4 J-Line Parameters

From the intensities, line widths, and numbers of lines, with $\alpha_{\text{NH}_3} = 0.515 \text{ cm.}^{-1}$ as for all bands, \bar{S} and δ for the bands were found. From $\nu_J = 19.89J$ and $\Delta \nu_J$, the area under the black body curve was found by linear interpolation. At complete absorption, 3.35 percent of the black body curve would be absorbed.

3.5.5 Rotation Band Calculations

The values of E_p (emissivity under Port's conditions, i.e., ammonia broadened by nitrogen), $\bar{\epsilon}$ and $\bar{\epsilon}'$ were calculated for each J , and summed for several values of r on each curve. For E_p these were plotted, a smooth curve drawn through the points, and the values thus obtained added to the results calculated from the vibration-rotation bands.

For $\bar{\epsilon}$ and $\bar{\epsilon}'$ the sums of the rotation bands were expressed as a fraction of the sums of the vibration-rotation bands. These were found to be within 0.005 of a constant value over wide ranges of p and r . A mean percentage was taken and applied over these regions. The mean was of the order of 1-1/2 percent, and never more than 2.4 percent.

3.6 The Weak Line Correction Band in NH_3

Calculations based on the vibration-rotation bands and pure rotation bands are found to predict an E_p which is on the average about 8 percent below that observed.

There is evidence [Godson, 1955] that this band model underestimates the number of weak lines. This is exacerbated by the use of the number of observed lines on the ranges of the ν_2 band, leaving out those too weak to be observed.

Consider, therefore, the effect of a number of weak lines, randomly spaced with respect to other lines across the entire spectrum, and use the multiplicative property of transmission functions to write [Goody, 1964]

$$\hat{E} = 1 - T_w T = 1 - T_w (1 - E) \quad (3.32)$$

where \hat{E} = emissivity including weak lines,

E = emissivity omitting weak lines,

T = transmission function without the weak lines,

T_w = transmission function of the weak lines.

The transmission function for this random collection of lines can be written

$$T_w = e^{-\frac{I_0 \bar{w}}{\delta}} \doteq 1 - \frac{I_0 \bar{w}}{\delta} \quad (3.33)$$

since their total absorption is small. Here \bar{w} is the equivalent width of the lines.

Inserting (3.33) in (3.32)

$$\hat{E} = E + \frac{\bar{w}}{\delta} (1 - E) \quad (3.34)$$

or

$$\frac{\hat{E}}{E} = 1 + \frac{\bar{w}}{\delta} \frac{(1 - E)}{E} \quad (3.35)$$

and

$$\ln \frac{\hat{E}}{E} = \frac{\bar{w}}{\delta} \frac{(1 - E)}{E} \quad (3.36)$$

For \bar{w} the formula relating to any distribution of line shapes could be used. The Ladenberg-Reiche function (3.10) will again be used in the expression

$$\frac{\bar{w}}{\delta} = 2\pi y L(u) \quad (3.37)$$

corresponding to all lines have a mean intensity \bar{S} , and where, as above

$$y = \frac{2\pi\alpha'}{\delta} P_T \quad (3.22)$$

$$u = \frac{\bar{S} r}{2\pi\alpha'} \frac{P_{NH_3}}{P_T} \quad (3.23)$$

Then

$$\ln \frac{\hat{E}}{E} = 2\pi y L(u) \frac{(1-E)}{E} \quad (3.38)$$

There are two disposable parameters: \bar{S} and δ . From an inspection, the value $u = 1$ was put at $p_{\text{NH}_3} = 0.12$ atmos. This is equivalent to fixing \bar{S} , since

$$\frac{\bar{S} r}{2\pi \alpha'} \cdot \frac{p_{\text{NH}_3}}{p_T} = 1 \quad (3.39)$$

On substitution

$$\bar{S} = 0.1252 \quad (3.40)$$

Since the weakest band included was the $P(w) + 2aR$, with $\bar{S} = 0.0811$, this is merely adding more lines of about this strength. As this is near the limit of what can be measured with the spectrometers, the existence of these lines can be neither proved nor disproved. The exact location of $u = 1$ is not very important either. Putting $u = 1$ at $p_{\text{NH}_3} = 0.43$ would give $\bar{S} = 0.076$, but would not change the correction appreciably.

When $I = p_T L(u)(1-E)/E$ is plotted against $\Delta E/E_{\text{Obs.}} = (E_{\text{Obs.}} - E_{\text{Cal.}})/E_{\text{Obs.}}$ (since

$$\frac{\hat{E}'}{E} = 1 + \frac{\Delta E}{E} \quad (3.41)$$

$$\ln \frac{\hat{E}'}{E} = \frac{\Delta E}{E} \quad) \quad (3.42)$$

the points exhibit a great deal of scatter. A straight line was drawn through by eye, which was found to satisfy the relation

$$\ln \frac{\hat{E}}{E} = 0.23 I \quad (3.43)$$

Note that this implies

$$\frac{2\pi\alpha'}{\delta} = 0.23 \quad (3.44)$$

or

$$\delta = 14.06 \text{ cm.}^{-1} .$$

Since the black body curve has 99 percent of its energy below 2089 cm.^{-1} , this indicates that only about 149 lines are being added, or an increase of total intensity of 2.6 percent -- much less than the 20 percent uncertainty stated by McKean and Schatz [1956].

Using (3.44) in (3.43) gives

$$\frac{\hat{E}}{E} = 1 + 0.23 \frac{1-E}{E} \rho_T L(\nu) \quad (3.46)$$

or

$$\hat{E} = E \left[1 - 0.23 \rho_T L(\nu) \right] + 0.23 \rho_T L(\nu) \quad (3.47)$$

From the same argument and parameters, it follows that

$$\frac{\hat{E}}{E} = 1 + 0.23 \frac{1-E}{E} \rho_T L(\nu) \quad (3.48)$$

$$\frac{\partial \bar{E}_p}{\partial r} = \frac{\partial \bar{E}}{\partial r} \left[1 - 0.23 \rho_T L(u) \right] + 0.23 \rho_T (1 - \bar{E}) \frac{\partial L(u)}{\partial r} \quad (3.49)$$

3.7 Calculation of \bar{E}_p

All is now ready for the evaluation of \bar{E}_p .

$$\bar{E}_p(r, p) = \frac{1}{B} \sum_i B_i \left(1 - e^{-\frac{2\pi\alpha'}{\delta_i} \rho_T L(u_i)} \right) \Delta u_i + \bar{E}_{R_{OT}}(r, p) \quad (3.50)$$

$$u_i = \frac{\delta_i r}{2\pi\alpha'} \frac{P_{NH_3}}{\rho_T} \quad (3.24)$$

$$\hat{\bar{E}}_p = \bar{E}_p \left[1 - 0.23 \rho_T L(u) \right] + 0.23 \rho_T L(u) \quad (3.47)$$

In Port's experiment, the path length $r = 1.63$ feet was a constant. For each of Port's values of pL the pressures from Table 3-5 are inserted and the expression (3.47) evaluated. The results are presented with the circumflex dropped in Table 3-6 and Fig. 3-3. The accuracy is seen to be about ± 2 percent.

3.8 Calculation of \bar{E} and \bar{E}'

We have thus validated the method and parameters by comparison with experimental data related to that which will be used. The quantity $\bar{E}(r, p)$ can now be evaluated with the same band parameters and correction as we used above, and \bar{E}' , obtained by differentiating the expression for \bar{E} , can also be evaluated and corrected.

$$\bar{E}(r, p) = \sum_i \frac{Q_i}{Q} \left(1 - e^{-\frac{2\pi\alpha'}{\delta_i} \rho_{NH_3} L(u_i)} \right) \Delta u_i + \bar{E}_{R_{OT}}(r, p) \quad (3.51)$$

Table 3-6

CALCULATED AND OBSERVED VALUES OF E_p

P_{NH_3}	E_p (calc.)	E_p (obs.)	E_p before weak line correction
.0043	.0587	.055	.0570
.0061	.0728	.070	.0765
.0092	.0922	.087	.0887
.012	.1069	.105	.1025
.018	.1335	.13	.1273
.025	.1582	.16	.1501
.031	.1771	.19	.1677
.043	.2092	.22	.1970
.061	.2489	.26	.2333
.12	.3404	.37	.3161
.18	.4105	.43	.3801
.31	.5143	.53	.4718
.43	.5733	.60	.5217
.61	.6371	.68	.6315
1.00	.7215	.71	.6315

$$v_i = \frac{S_i r}{2\pi\alpha'} \quad (3.52)$$

(Since for an atmosphere of pure ammonia, $p_{NH_3} = p_T$.) By differentiating

$$\epsilon' = \sum_i \frac{Q_i}{Q} \Delta v_i \frac{2\pi\alpha'}{S_i} p_{NH_3} e^{-\frac{2\pi\alpha'}{S_i} p_{NH_3} L(v_i)} \frac{\partial L(v_i)}{\partial r} + \epsilon'_{ROT}(r, p) \quad (3.53)$$

$$\frac{\partial L(v)}{\partial r} = \frac{\partial L(v)}{\partial v} \frac{dv}{dr} = \frac{\partial L(v)}{\partial v} \frac{S_i}{2\pi\alpha'} \quad (3.54)$$

$$\epsilon' = \sum_i \frac{Q_i}{Q} \Delta v_i \frac{S_i}{S_i} p_{NH_3} \frac{\partial L(v)}{\partial v} e^{-\frac{2\pi\alpha'}{S_i} p_{NH_3} L(v_i)} + \epsilon'_{ROT}(r, p) \quad (3.55)$$

The values of ϵ and ϵ' are presented for a range of r and p in Tables 3-7 and 3-8 and graphically in Figs. 3-4 and 3-5, respectively, after being corrected according to (3.48) and (3.49) respectively (but with the circumflex dropped).

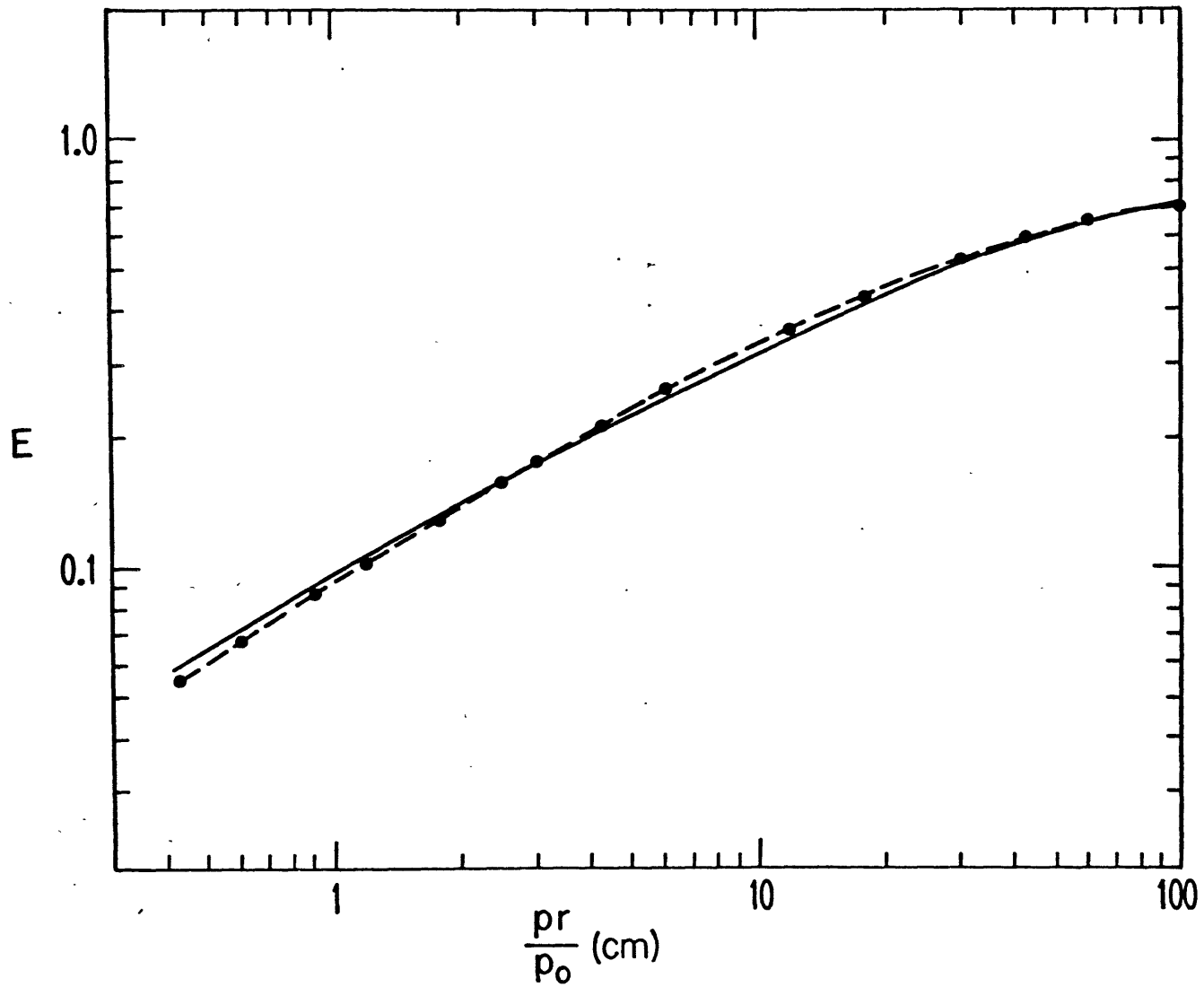


Fig. 3-3. COMPARISON OF CALCULATED AND OBSERVED VALUES OF E_p
 Points are from Fig. 3-2. Solid line is calculated.

Table 3-7

Σ AS A FUNCTION OF PRESSURE AND DISTANCE

r [cm.]	Pressure [atmospheres]								
	.1	.2	.4	.6	.8	1.0	1.2	1.4	1.6
0.001		.000015	.000285	.000419	.000512	.000640	.000747	.000764	.000229
0.003		.000366	.000802	.00120	.00160	.00201		.00227	.002634
0.010		.000809	.00184	.00277	.00368	.00454		.00730	.00854
0.030		.00323	.006456	.00974	.01278	.01590		.02157	.02459
0.055		.00577	.01145	.01696	.02230	.02756			
0.075		.00784	.01547	.02283	.02993	.03684			
0.10	.00525	.01053	.02068	.03342	.04264	.05150	.05615	.06423	.0724
0.17		.01720	.03326	.05815		.07521			
0.30	.01438	.02796	.05214	.07547	.09396	.1109	.1313	.1468	.1615
0.55		.04563	.08373	.1161		.1705			
0.75	.03045	.05736	.1032	.1414	.1754	.2029			
1.00	.03766	.06996	.1237	.1674	.2045	.2363	.2641	.2890	.3113
1.70	.05244	.09751	.1672	.2216	.2664	.3042			
3.00	.07600	.1364	.2258	.2928	.3466	.3906	.4294	.4575	.4846
5.50	.10679	.1850	.2983	.3794	.4409	.4820			
10.00	.14838	.2458	.3829	.4743	.5391	.5870	.6229	.6521	.6756
17.00	.18695	.3066	.4612	.5560	.6191	.6634			
30.00	.24211	.3846	.5513	.6421	.6977	.7351	.7623	.7837	.8019
55.00	.30793	.4725	.6357	.7164	.7637	.7960			
60.00	.31797	.4812	.6469	.7259	.7722	.8040			
80.00	.35217	.5213	.6823	.7557	.7992	.8298			
100.00	.37980	.5521	.7081	.7774	.8190	.8493	.8737	.8951	.9140

Table 3-8

ϵ' AS A FUNCTION OF PRESSURE AND DISTANCE

r [cm.]	Pressure [atmospheres]								
	.1	.2	.4	.6	.8	1.0	1.2	1.4	1.6
0.001		.1109	.2217	.3324	.4432	.5539	.6669	.7794	.8884
0.003		.1108	.2211	.3308	.4406	.5500	.6632	.7722	.8810
0.010		.1094	.2181	.3257	.4324	.5384	.6442	.7478	.8503
0.030		.1065	.2099	.3104	.4080	.5029	.5989	.6889	.7771
0.10	.05005	.09784	.1872	.2668	.3411	.4094	.4799	.5394	.5947
0.30	.04173	.07864	.1409	.1789	.2365	.2697	.2987	.3246	.3421
1.00	.02070	.04704	.07316	.0929	.1080	.1198	.1312	.1381	.1435
3.00	.01478	.02435	.03670	.0443	.0491	.0522	.0551	.0557	.0562
10.00	.00733	.01119	.0150	.0164	.0172	.0158	.0153	.0146	.0140
17.00	.00522	.00694							
30.00	.00337	.004532	.00489	.00434	.00394	.00368	.00391	.00331	.00326
55.00		.002534	.00236	.00202	.00180	.00169			
60.00	.00196	.002314	.00212	.00179	.00159	.00151			
80.00	.00153	.001719	.00148	.00124	.00114	.00111			
100.00	.00131	.001368	.00111	.00094	.000877	.000863	.000868	.000876	.000879

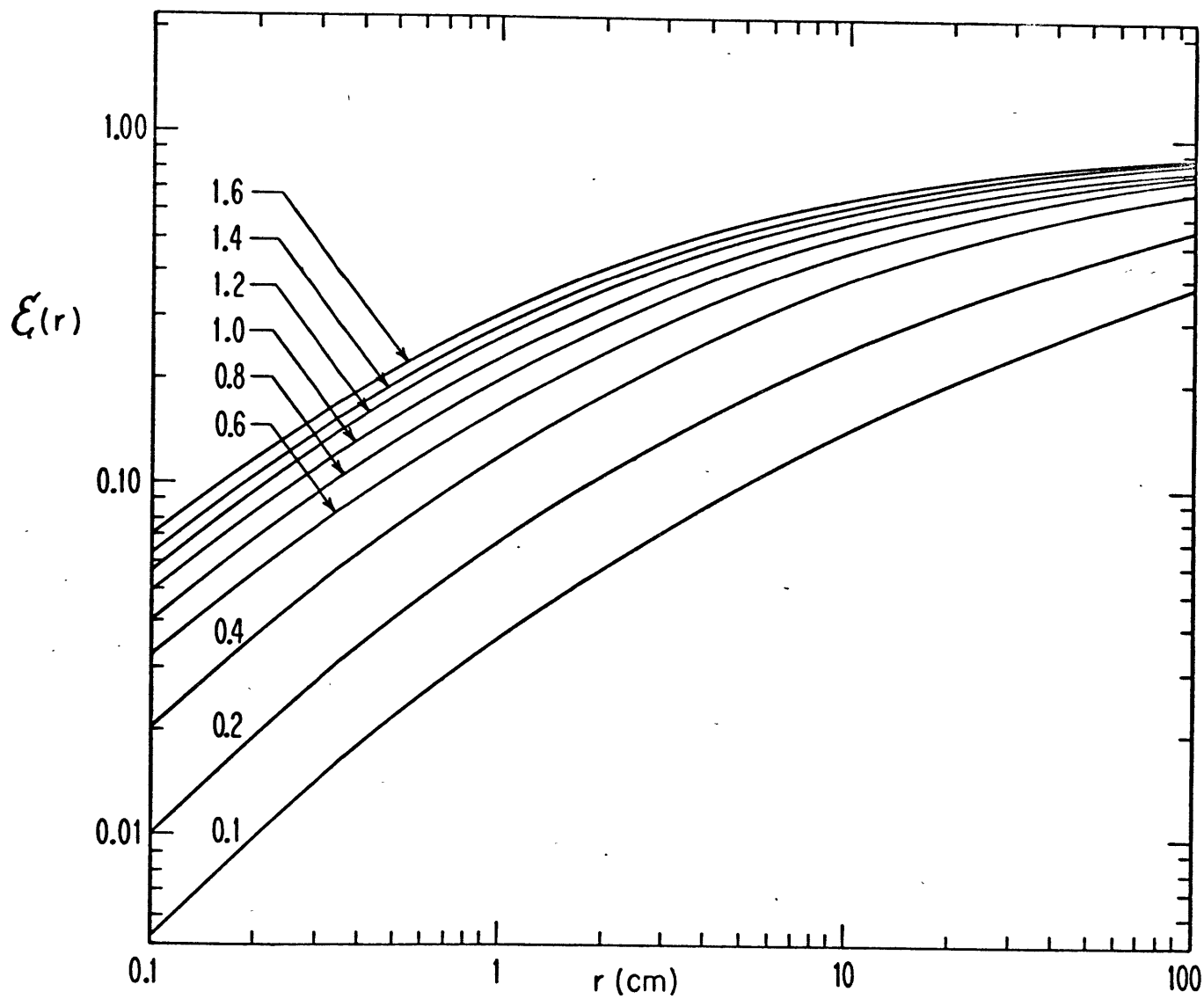


Fig. 3-4. PERTURBATION EMISSIVITY $\xi(r)$ AS A FUNCTION OF r

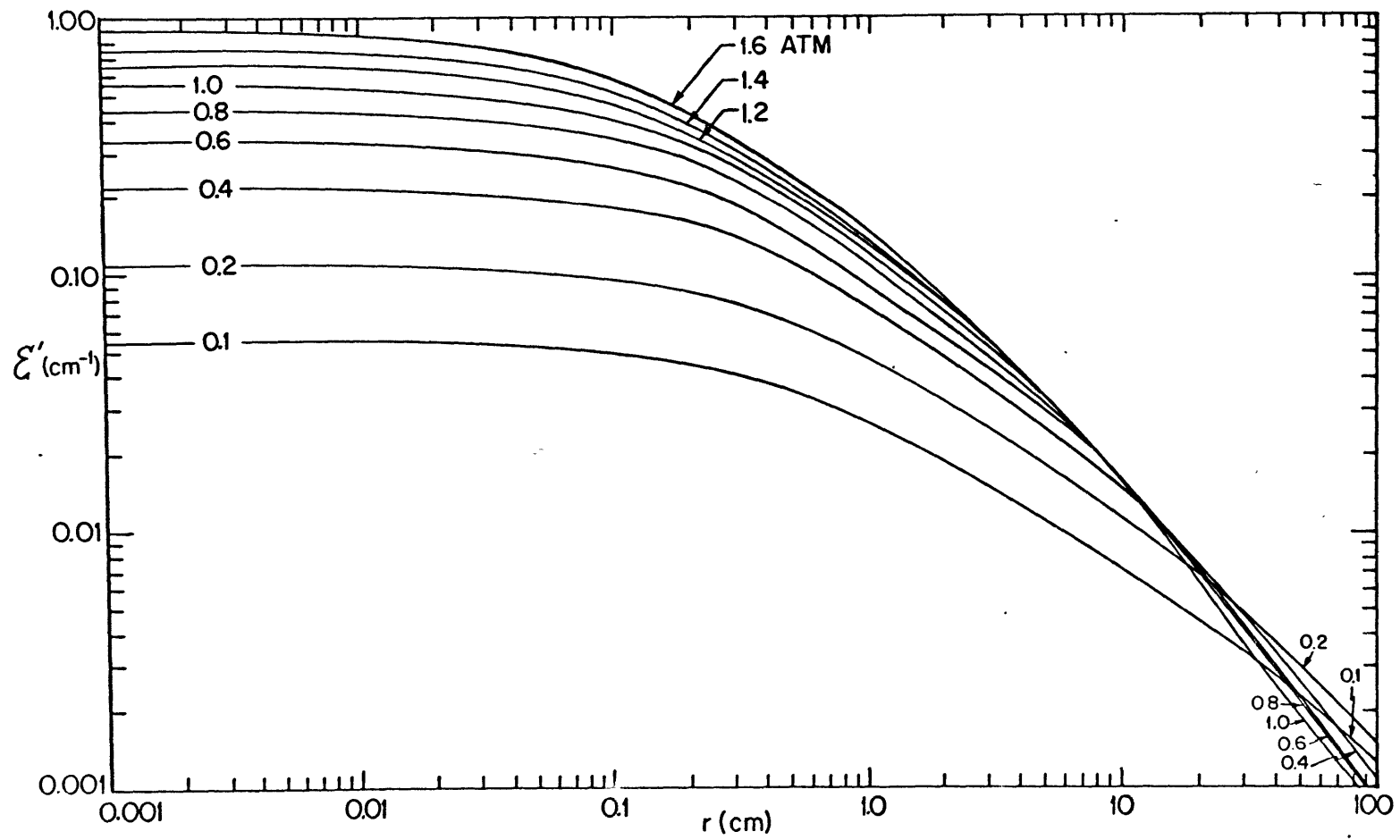


Fig. 3-5. DERIVATIVE OF PERTURBATION EMISSIVITY AS A FUNCTION OF r

CHAPTER 4

THE PHYSICAL PROPERTIES OF AIR AND AMMONIA

4.1 Introduction

Since so many of the physical properties of a fluid enter into the determination of the Rayleigh number, it is imperative that they be known with the highest accuracy possible. In addition, for the understanding of the steady state and the heat fluxes, it is necessary to have the conductivity. Many of these factors vary with temperature, and some with pressure, making it necessary to allow interpolation between known values. In this chapter the source and manipulation of data concerning the physical properties will be collected and presented in a usable form for our later purposes.

The indices of refraction will also be discussed.

4.2 The Physical Properties of Air

These data are taken from data tabulated in N.B.S. Circular 564 [1955]. The only quantities we need to interpret the experiments are $K(\theta)$ and $\frac{\partial \alpha}{\partial K_L}(\theta, p)$ (and the index of refraction).

The conductivity $K(\theta)$ should be independent of pressure, and all evidence suggests that this is so. This is given as K/K_0 as a function of θ , and a value for K_0 . Values of $K(\theta)$ are given in Table 4-1 and plotted later with $K(\theta, p)_{\text{NH}_3}$ in Fig. 4-1.

The properties of the fluid that enter into the Rayleigh number for a gas are highly temperature dependent. That is, considering

$$\alpha \propto \frac{1}{\Theta}$$

$$\eta, \kappa \propto \Theta^{1/2}$$

$$\rho \propto \frac{1}{\Theta}$$

or

$$\frac{\frac{\alpha}{\frac{\kappa}{\rho c_p} \frac{\eta}{\rho}}}{\frac{\eta}{\rho}} \propto \frac{1}{\Theta^4} \quad (4.1)$$

according to the simplest kinetic theory model. A 2 percent change of temperature across a layer can indicate an 8 percent change of Rayleigh number. This fact imposes a limit on the temperature difference if equations with constant coefficients are to be appropriate. The quantity

$$\frac{g\alpha}{K\nu} = \frac{g\alpha}{\kappa\eta} c_p \rho^2 = \frac{g\alpha c_p}{\kappa\eta} \rho_0^2 \left(\frac{\rho_0 \rho}{\rho' \rho_0}\right)^2 \left(\frac{\rho}{\rho_0}\right)^2 \quad (4.2)$$

for a gas has a strong pressure dependence which may be removed by writing

$$\frac{g\alpha c_p \rho^2}{\kappa\eta} \left(\frac{\rho_0}{\rho}\right)^2 = \frac{g\alpha c_p \rho_0^2}{\kappa\eta} \left(\frac{\rho_0 \rho}{\rho' \rho_0}\right)^2 \quad (4.3)$$

which depends only upon the temperature.

To obtain the Rayleigh number, one multiplies

$$d^3 \times \Delta\Theta \times \frac{g\alpha c_p \rho_0^2}{\kappa\eta} \frac{\rho_0^2}{\rho^2}(\Theta) \times \frac{\rho^2}{\rho_0^2} = \frac{g\alpha}{\kappa\nu} d^3 \Delta\Theta = Ra \quad (4.4)$$

where the first two quantities are set before a run begins, the third by the temperature and nature of the fluid, and the fourth by the pressure.

To calculate the quantity $\frac{g \alpha c_p \rho^2}{k \eta} \left(\frac{\rho_0}{\rho}\right)^2$ we combine

$$k = k_0 \frac{k(\theta)}{k_0}$$

$$\nu = \frac{\eta}{\rho} = \frac{\eta_0}{\rho_0} \frac{\frac{\eta}{\eta_0}(\theta)}{\frac{\rho}{\rho_0}(\theta, \rho)} = \frac{\frac{\eta}{\eta_0}(\theta)}{\rho \cdot \frac{1}{\rho} \cdot \frac{\rho}{\rho_0}(\theta, \rho)} \cdot \frac{\eta_0}{\rho_0}$$

From $\rho(\theta, \rho)$ we can get

$$\alpha(\theta, \rho) = -\frac{1}{\rho} \cdot \frac{\partial \rho}{\partial \theta} = \frac{1}{\rho} \frac{\rho_{\theta-10} - \rho_{\theta+10}}{20}$$

Combining these, we find

$$\frac{g \alpha c_p \rho^2}{k \eta} \left(\frac{\rho_0}{\rho}\right)^2 = \frac{g \rho_0^2 R}{k_0 \eta_0} \left[\frac{\alpha \frac{c_p}{R} \left(\frac{\rho}{\rho_0} \frac{1}{\rho}\right)^2}{\frac{k}{k_0} \frac{\eta}{\eta_0}} \right] \quad (4.5)$$

The quantity in brackets has a slight pressure dependence (< .3 per cent). It was calculated at pressures (in atmospheres) of 0.1, 0.4, 0.7, and 1.0, and a mean taken.

Using the values from N.B.S. 564,

$$k_0 = 5.770 \times 10^{-5} \text{ cal./cm. sec. deg.} = 2.414 \times 10^3 \text{ ergs/cm. sec. deg.,}$$

$$\eta_0 = 1.716 \times 10^{-4} \text{ gm./cm. sec.,}$$

$$\rho_0 = 1.29304 \times 10^{-3} \text{ gm./cm.}^3,$$

$$R = 0.0686042 \text{ cal./gm. deg., and}$$

$$g = 980.398 \text{ cm./sec.}^2 \text{ [HCP],}$$

it is found

$$\frac{g \rho_0^2 R}{k_0 \eta_0} = 1.13575 \times 10^4 \text{ cm.}^3$$

The values from (4.5) are presented in Table 4-1.

Table 4-1

PHYSICAL PROPERTIES OF AIR

Temp. [° K]	K/K ₀	K [erg / cm.sec.deg.]	$\alpha \frac{c_p}{R} \left(\frac{\rho_0}{\rho} \frac{1}{P} \right)^2$ [deg. ⁻¹ atm.]	$\frac{\eta}{\eta_0}$	$\frac{g \alpha c_p \rho^2}{K \eta} \left(\frac{P_0}{P} \right)^2$ [cm. ⁻³ deg. ⁻¹]
290	1.065	2.547	0.010738	1.048	110.301
300	1.087	2.624	0.009702	1.076	94.21
310	1.119	2.701	0.008794	1.103	80.92

The results of the last column are graphed in Fig. 4-2.

4.3 The Physical Properties of Ammonia

4.3.1 Method of Calculating Conductivity

To find the conductivity of ammonia, we make use of the kinetic theory relationship [Chapman and Cowling, 1952]

$$K(\theta, p) = f \eta(\theta) c_v(\theta, p) \quad (4.6)$$

The quantity f has been studied by Mason and Monchick [1962] and found to be an extremely slow function of temperature. In order to calculate f (it is not clear what data were used to get the f reported by Mason and Monchick, so we will make our own determination), we must have the values of $c_v(\theta, p)$.

4.3.2 Pressure and Temperature Dependence of c_p and c_v for NH_3

Kaye and Laby [1956] cite data from Spencer and Flannagan [1942] for the temperature dependence of c_p . This is a least squares fit of the form

$$c_p^o = a + b\theta + c\theta^2$$

(superscript o refers to zero pressure) to values of c_p^o from Thompson [1941] in which c_p^o was calculated from spectroscopic data for several temperatures between 291-1000° K. An experimental determination is reported in Osborne, Stimson, Sligh, and Crague [1924]. This seems to be an extremely carefully done experiment. They find their results can be fitted by the empirical relation

$$c_p(p, \theta) = 1.1255 + 0.00238\theta + \frac{76.8}{\theta} + \frac{5.45 p 10^8}{\theta^4} + \frac{p(6.5 + 3.8p) \cdot 10^{27}}{\theta^{12}} + \frac{2.37 p^6 10^{45}}{\theta^{20}} \quad (4.7)$$

over the range $-15^\circ C$ to $+150^\circ C$, and 0.5 - 20 atmospheres. In their expression, c_p is in joules/gm. $^\circ C$,
 p is in meters of mercury, and
 θ is $^\circ C + 273.1$.

This is fitted to the experimental data with an average error of 0.07 percent and a maximum error of 0.27 percent.

Since the two sets of data differ by only 1 percent, they confirm each other. The experimental data will be utilized because it is observed, and has the pressure dependence included in it, as well as because improved knowledge of vibrational constants might change the calculated specific

heat slightly. In addition, with a highly polar gas not too far from its critical temperature, calculations of thermodynamic quantities must be somewhat suspect.

Thus $c_p^0(\theta)$ and $c_p(\theta)$ have been found. Since $c_p^0 - c_v^0 = \frac{R}{M}$, one immediately has $c_v^0(\theta)$. To obtain $c_v(\theta)$, the difference of the following expressions [HCB]* is considered to first order in V^* .

$$\frac{c_v - c_v^0}{R} = - \frac{2(\beta_1^* + \beta_2^*)}{V^*} \quad (4.8)$$

$$\frac{c_p - c_p^0}{R} = - \frac{\beta_2^*}{V^*} \quad (4.9)$$

In the above,

$$B(\theta) = b_0 B^*(T^*, t^*)$$

$$\beta_1^* = T^* \frac{dB^*}{dT^*}$$

$$T^* = \theta/T_R$$

$$t^* = \mu^*/8^{1/2}$$

$$v = v^* b_0$$

$$c = C/M$$

The second virial coefficients which enter in terms involving $(1/V^*)^2$ are not tabulated in this region for polar gases. At the low densities in which we are interested, the C^*/V^{*2} terms are much smaller than the B^*/V^* terms, so we may suppose that one term will give the pressure correction with sufficient accuracy.

The following values are listed for ammonia [HCB]

* This designation will be used hereafter for Hirschfelder, Curtiss and Bird [1954].

$$\mu = 1.47 \times 10^{-18} \text{ e.s.u.}, \quad t^* = 1.0$$

$$T_R = 320^\circ \text{ K}$$

$$b_o = 22.12 \text{ cc/mole.}$$

The values of B^* and $B_1^* - B^*$ are tabulated for $t^* = 1.0$ [HCB], from which values of B_1^* are obtained. These are presented in Table 4-2.

Table 4-2

VIRIAL COEFFICIENT DATA FOR AMMONIA

T^*	B^*	$B_1^* - B^*$	B_1^*
0.75	- 30.4	163.2	132.8
0.80	- 23.2	116.3	93.1
0.85	- 18.4	86.6	68.2
0.90	- 14.92	66.93	52.01
0.95	- 12.42	53.31	40.89
1.00	- 10.54	43.54	33.00

B_1^* was graphed and a smooth line drawn through the points, which are shown with the calculated results in Table 4-3.

Table 4-3

CALCULATED SPECIFIC HEATS OF AMMONIA

θ [$^\circ \text{K}$]	T^*	B_1^*	$\frac{2b_o B_1^*}{MT}$	c_p^o [cal./gm.deg.]	c_p^o [cal./gm.deg.]	c_v^o [cal./gm.deg.]	c_v^o [cal./gm.deg.]
273	.8531	66.5	.0153	.4917	.5194	.3751	.3875
283	.8844	56.0	.0124	.4950	.5168	.3784	.3878
293	.9156	48.0	.0103	.4985	.5161	.3819	.3892
303	.9469	41.0	.0085	.5021	.5167	.3855	.3916

The values used in obtaining $2b_0/M$ were

$$\begin{aligned} M &= 17.031 \text{ gm./mole [HCP]} \\ 1 \text{ atm.} &= 1.01325 \times 10^6 \text{ dyne/cm.}^2 \text{ [HCP]} \\ J &= 4.1855 \times 10^7 \text{ erg/cal. [HCP]} \\ R &= 1.98646 \text{ cal./mole degree [HCP]} \\ \frac{2b_0}{M} &= 0.06288 \text{ cal./gm. atm.} \end{aligned}$$

The quantity c_p is linear in p from pressures of 0 to 1 atmosphere, according to (4.7). Values were calculated at intervals of 0.1 atmosphere at 293°K and 303°K , and the values graphed. From each of these values the correction $\frac{1}{M} \left(R + 2 \frac{d B}{d \Theta} p \right) = \frac{R}{M} + 2 \frac{b_0 \mathcal{E}_1^*}{M \Theta} p$ was subtracted and the result plotted similarly in a graph of $c_v(\Theta, p)$.

4.3.3 The Conductivity of NH_3

To get the conductivity of NH_3 as a function of pressure, we make use of the relationship (4.6)

$$K(\Theta, p) = f \eta(\Theta) c_v(\Theta, p)$$

and the following values:

$$\begin{aligned} K(0^\circ\text{C}, 240 \text{ mm.Hg.}) &= 516 \times 10^{-7} \text{ cal./cm.sec.deg. [Franck, 1951]} \\ \eta(0^\circ\text{C}) &= 926 \times 10^{-7} \text{ gm./cm.sec. [Van Cleave and Maass, 1935]} \\ c_v(0^\circ\text{C}, 240 \text{ mm.Hg.}) &= 0.3791 \text{ erg/cm.sec.deg.} \end{aligned}$$

These values yield $f = 1.47$.

The experimental viscosities of Van Cleave and Maass [1935] were plotted, a curve passed through them, and Table 4-4 was constructed.

Table 4-4
CONDUCTIVITY OF AMMONIA

θ ° K	$\eta \times 10^{-7}$ gm/cm, sec.	c_v^0 ergs x 10 ⁷ cm, sec, deg.	K^0 ergs x 10 ³ cm, sec, deg.	c_v^1 ergs x 10 ⁷ cm, sec, deg.	K^1 ergs x 10 ³ sec, deg.
285	972.0	1.5877	2.267		
290	992.5	1.5943	2.326		
293	1005.0	1.5984	2.361	1.6290	2.407
298	1025.5	1.6060	2.421	1.6340	2.463
303	1046.0	1.6135	2.481	1.6390	2.520

The conductivities are plotted in Fig. 4-1. It will be noted that this predicts a 1.75 percent increase in conductivity for a pressure change from 0 - 1 atmosphere.

4.3.4 The Rayleigh Number in Ammonia

$$\frac{g\alpha}{\frac{K\nu}{\rho c_p}} = \frac{g\alpha(\rho, \theta)}{\frac{K(\rho, \theta)}{\rho(\rho, \theta) c_p(\rho, \theta)} \cdot \frac{\eta(\theta)}{\rho(\rho, \theta)}} \quad (4.10)$$

$$= \frac{g}{f} \rho_0^2 \frac{1}{\eta(\theta)^2} = \frac{c_p(\theta)}{c_v(\theta)} \alpha(\rho, \theta) \left[\frac{\rho}{\rho_0}(\rho, \theta) \right] \quad (4.11)$$

Thus $\rho(\theta, p)$, $\Delta \rho(\theta, p)$, and $\alpha(\theta, p)$ are needed. The virial form of the equation is again employed, as given by HCB:

$$\frac{P\nu}{R\theta} = 1 + \frac{b_2 B^*}{V} \quad (4.12)$$

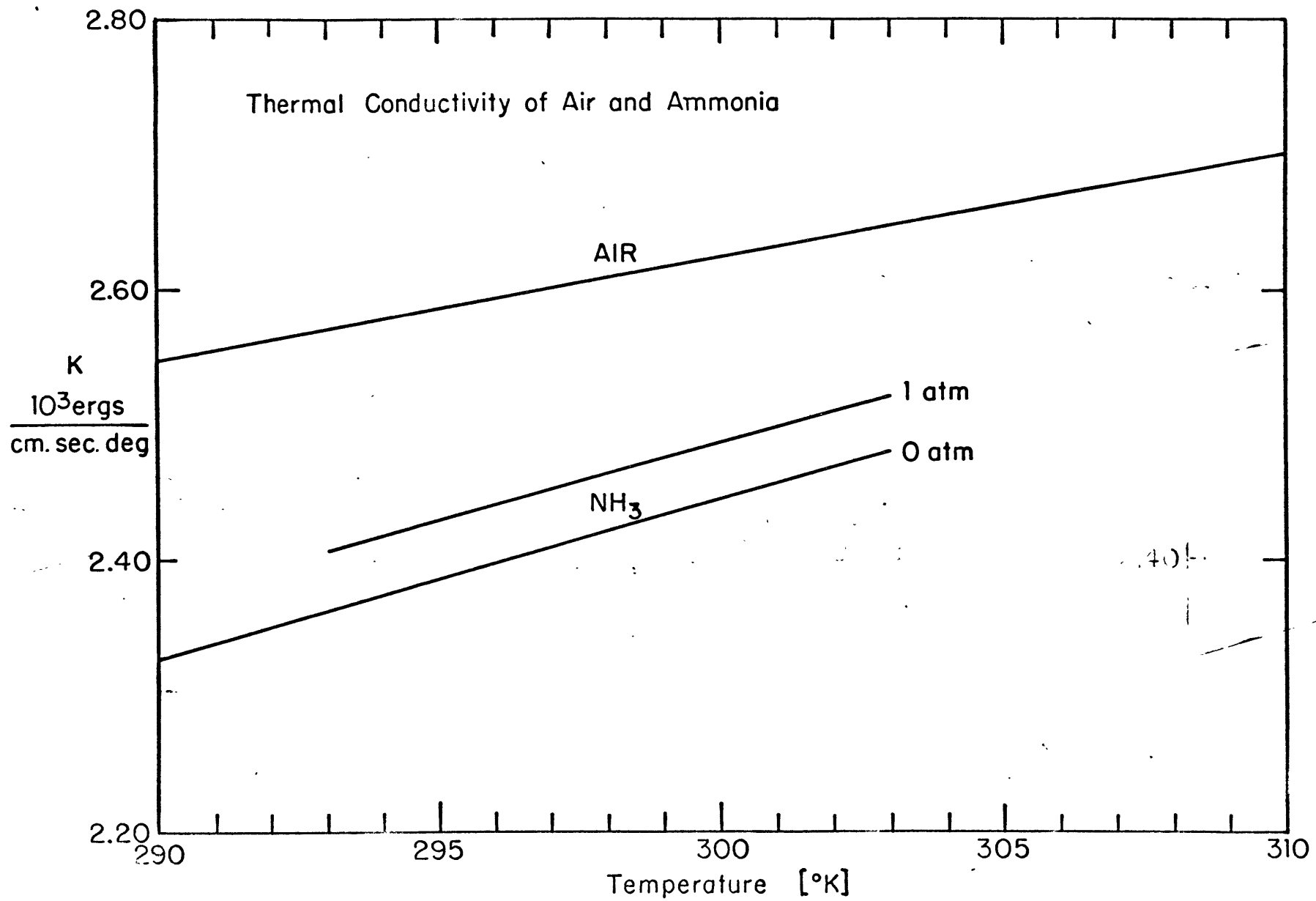


FIG. 4-1. Conductivity of Air and Ammonia

and on the right-hand side we can use the first approximation for V

$$\frac{1}{v} = \frac{p}{R\theta} \quad (4.13)$$

giving

$$p = \frac{pM}{R\theta} \frac{1}{1 + \frac{p b_0}{R\theta} B^*(\theta)} = \frac{pM}{R\theta} \left(1 - \frac{p b_0}{R\theta} B^*(\theta)\right) \quad (4.14)$$

We may also define

$$p_0 = p_0 \lim_{p \rightarrow 0} \frac{p}{p} = \frac{p_0 M}{R\theta} = \frac{M}{v_0} \quad (4.15)$$

Employing the same data for ammonia as in 4.3.2, B^* was graphed and read as a function of temperature and the correction term calculated.

This was combined with the first term to give p/p_0 . Then

$$\alpha(\theta) = -\frac{1}{p} \frac{\partial p}{\partial \theta} = \frac{\left(\frac{p}{p_0}\right)_{\theta-10} - \left(\frac{p}{p_0}\right)_{\theta+10}}{\left(\frac{p}{p_0}\right)_{\theta}} \quad (4.16)$$

was found. The specific heats from the previous section, c_p and c_v , are combined with these quantities to give $\frac{c_p(\theta)}{c_v(\theta)} \alpha(p, \theta) \left[\frac{p}{p_0}(p, \theta)\right]^2$ which are all the quantities which have pressure and temperature dependence.

For the density,

$$p_0 = \frac{M}{v_0} = \frac{17.031}{22.415} = 0.7598 \times 10^{-3} \frac{\text{gm.}}{\text{cc.}}$$

The viscosity was read from the graph of the data of Van Cleave and Maass [1935]. Putting all these together in the expression

$$\frac{g\alpha}{K\eta} \left(\frac{p}{p_0}\right)^2 = \frac{g\rho_0^2}{f} \frac{1}{\eta(\theta)^2} \left\{ \frac{c_p(p, \theta)}{c_v(p, \theta)} \alpha(p, \theta) \left[1 - \frac{p b_0}{R\theta} B^*(\theta)\right]^2 \right\} \quad (4.17)$$

the results in Table 4-5 are obtained. It can be seen from (4.17) that there is still a small pressure dependence of $\frac{g\alpha}{K\nu} \left(\frac{P_0}{P}\right)^2 (\theta, P)$, as seen in Table 4-5 and Fig. 4-2. For intermediate values of pressure, an interpolated value was used to compute Rayleigh numbers.

Table 4-5

$$\frac{g\alpha}{K\nu} \rho c_p \left(\frac{P}{P_0}\right)^2$$

θ [° K]	Pressure [atmospheres]					
	0	0.2	0.4	0.6	0.8	1.0
290	156.4	159.9	163.2	166.7	170.1	173.6
300	129.4	131.7	134.0	136.4	138.8	141.2
310	109.6	111.5	113.3	115.2	117.1	119.0

The results are graphed in Fig. 4-2.

4.4 Accuracy of Physical Properties of Air and Ammonia

The accuracy of the data for air is discussed in N.B.S. Circular 564. The two quantities which supply most of the uncertainty are the transport quantities η and K . The authors state that reliabilities are within 2 percent and 4 percent respectively, though this may be large. It is a fact that the two most recent determinations of air conductivity differ by over 3 percent at room temperature, giving an indication of the difficulty of the measurements, and the somewhat unsatisfactory state of the art.

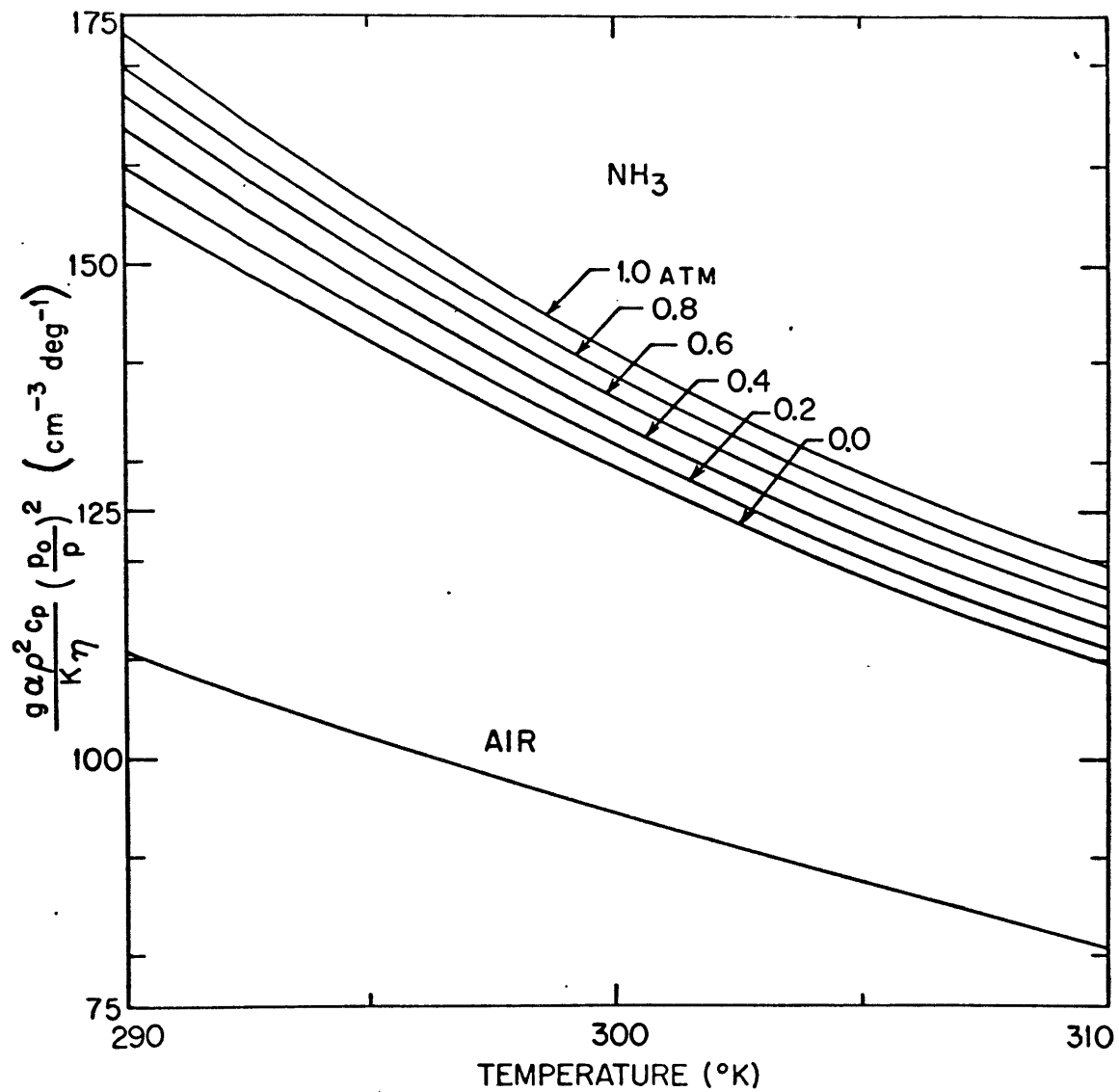


Fig. 4-2. $\frac{g\alpha}{K\nu} \rho c_p \left(\frac{P_0}{p}\right)^2$ VERSUS θ FOR AIR AND AMMONIA

The accuracy of the ammonia data is of the same order. The data used here for NH_3 viscosity is that favored by Krieger [1951], on which the transport data in H.C.B. is based. Other data for viscosity exist which differ from this by 2 percent (in a direction to increase the Rayleigh number). There is not so much data for conductivity, but the spread in values is at least 2 percent, and probably at least the same as the 4 percent for air.

The accuracy of ρ is seemingly quite a bit better, as is c_p for air. The values of c_p and c_v are not much better than 1 percent each, giving an accuracy for $\frac{\partial \alpha}{K \nu}$ for air of 3 percent and for ammonia of 4 percent.

4.5 Refractive Indices

4.5.1 Air

The value accepted internationally for the mercury 5462.26 \AA ^o (green) line is

$$(n-1) \times 10^6 = 277.901 \text{ at } 15^\circ \text{ C, } 760 \text{ mm.Hg. ,}$$

quoted by Landholt and Bornstein [1960].

4.5.2 Ammonia

Uncertainty in the experimental data for ammonia is more due to the method of reduction to S.T.P. than to the measurement of the refractive index. Friberg [1927] makes clear his method of reduction, and his value at 5462 \AA ^o was adopted.

$$(n-1) \times 10^6 = 384.42 \text{ .}$$

Measurements by Cuthbertson and Cuthbertson [1913], Klemm and Henkel [1933], and Frivold, Hassel, and Rustand [1937] either agree with this method or are not fully explicit as to the method of reduction.

CHAPTER 5

THE INITIAL STATIC STATE

5.1 Introduction

The initial static state refers to the state of the fluid when there is no motion. The quantities of interest in the present case are the temperature distribution within the fluid and the heat flux through the fluid.

There are two immediate reasons for understanding the static state: the first is that the temperature distribution in the static state enters the equations that tell when the fluid will become unstable (see Chapter 6); the second reason is that the heat flux and its variation with Rayleigh number must be known in the absence of convection to locate the changes caused by the onset of fluid motions.

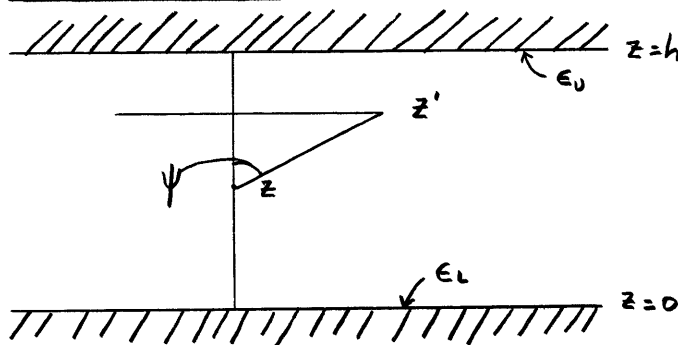
However, these problems of temperature distribution and flux are interesting of themselves, involving as they do solutions of the radiative-diffusive equations for heat balance in a non-gray medium. There is a further importance. In solving for this state, many of the approximations employed in meteorology will be used. Because of disturbances or practical difficulties in the atmosphere, it has been impossible to compare these approximations with nature. Such a comparison will be one result of this investigation of the static state.

In this chapter, the relevant equations of the mixed radiative-diffusive state will be presented and solved for gray and non-gray media. The formulation is extended to yield heat fluxes in gray and non-gray media.

The interferometric temperature measurements are presented and compared with theory. The flux variation with pressure is also compared with calculated values.

5.2 Calculation of Temperature Distribution for Mixed Radiation and Diffusion

5.2.1 General Equations



Consider the situation pictured above. The following symbols will be used:

I = intensity of radiation

$\mu = \cos \psi$

F_z = upward flux of radiation = $\int \mu I d w$

k = absorption coefficient

θ = temperature

β = temperature gradient = $\frac{d\theta}{dz}$

$\zeta = \frac{z}{h} - \frac{1}{2}$, non-dimensional height

H = radiative heating rate

K = thermal conductivity

ϵ = surface emissivity

- ν = subscript to indicate monochromatic value
- o = subscript to indicate zeroth order quantities
- +,- = superscripts to indicate upward and downward components respectively
- = average from top to bottom of the fluid.

For the case of temperature equilibrium, when a small element is neither gaining nor losing temperature,

$$H_o + K \nabla^2 \theta_o = 0 \quad (5.1)$$

Before motion begins, there are variations only in the z direction, so (5.1) may be written, using

$$H_o = - \frac{dF_z}{dz} \quad (5.2)$$

$$\frac{dF_z}{dz} - K \frac{d^2 \theta_o}{dz^2} = 0 \quad (5.3)$$

This may be integrated once to give

$$F_z(z) - K\beta(z) = F_T \quad (5.4)$$

where F_T is the total heat flux through the layer, a constant clearly independent of z .

Now formally

$$\beta(z) = \frac{F_z(z) - F_T}{K} \quad (5.5)$$

and taking an average

$$\frac{\beta(z)}{\bar{\beta}} = \frac{F_z(z) - F_T}{F_z - F_T} \quad (5.6)$$

This has three interesting special cases.

1. The radiation does not interact with the fluid, but traverses it without attenuation, so $F_z(z) = F_z$. In this case, $\beta/\bar{\beta} = 1$. This is the usual conductive case in a transparent gas, such as air, in which an appreciable radiative flux may pass through the gas without interaction or distortion of the linear temperature gradient. Henceforth, noninteracting gases will be neglected, since no radiative effects are produced. This will also be the case of an optically thin layer of a radiating gas, which might be termed the transparent limit.

2. $F_T \gg F_z$. This will occur in geometrically thin layers of conducting material, not necessarily optically thin. It could also occur at low temperatures. Here again, $\beta/\bar{\beta} = 1$. This limit will not concern us here, but might be termed the conductive limit.

3. $F_z(z) = K_R \beta(z)$, where K_R is a radiative conductivity, the Eddington conductivity, which holds when the radiation must diffuse across a layer several mean free paths wide. In this case

$$\beta(z) = \frac{F_T}{K + K_R} \quad (5.8)$$

$$\frac{\beta}{\bar{\beta}} = 1 \quad (5.9)$$

This might be called the opaque limit.

These limiting cases are features of the subsequent formulations, but the physical reasons for them have now been made plain.

From (5.3) - (5.6) it is clear that the radiative flux or radiative heating must be evaluated to find $\beta/\bar{\beta}$.

5.2.2 The Basic Equations of the Radiation Field

The monochromatic intensity I_{ν}^{+} at z with direction cosine μ may be expressed, with $\epsilon_{\mu} = \epsilon_{- \mu} = \epsilon$,

$$I_{\nu}^{+}(z, \mu) = \epsilon B_{\nu}(0) e^{-k_{\nu} z / \mu} + (1 - \epsilon) I_{\nu}^{-}(0) e^{-k_{\nu} z / \mu} + \int_0^z B_{\nu}(z') k_{\nu} e^{-k_{\nu}(z-z') / \mu} \frac{dz'}{\mu} \quad (5.10)$$

where B is the Planck function. Local thermodynamic equilibrium has been assumed.

The physical significance of the terms is clear. The first term on the right is the contribution of emission from the lower boundary, attenuated by the intervening material. The second term is the part of the downward intensity at the lower boundary which is reflected back upward, and attenuated by the intervening material. The third term is the contribution by material lying between the level z and the lower boundary.

Similarly

$$I_{\nu}^{-}(z, \mu) = \epsilon B_{\nu}(h) e^{-k_{\nu}(h-z) / \mu} + (1 - \epsilon) I_{\nu}^{+}(h) e^{-k_{\nu}(h-z) / \mu} + \int_z^h B_{\nu}(z') k_{\nu} e^{-k_{\nu}(z'-z) / \mu} \frac{dz'}{\mu} \quad (5.11)$$

Evaluating (5.10) at $z = h$ and (5.11) at $z = 0$ yields a coupled set of equations

$$I_{\nu}^{+}(h, \mu) = \epsilon B_{\nu}(0) e^{-k_{\nu} h / \mu} + (1 - \epsilon) e^{-k_{\nu} h / \mu} I_{\nu}^{-}(0, \mu) + \int_0^h k_{\nu} B_{\nu}(z') e^{-k_{\nu}(h-z') / \mu} \frac{dz'}{\mu} \quad (5.12)$$

$$I_{\nu}^{-}(0, \mu) = \epsilon B_{\nu}(h) e^{-k_{\nu} h / \mu} + (1 - \epsilon) e^{-k_{\nu} h / \mu} I_{\nu}^{+}(h, \mu) + \int_0^h k_{\nu} B_{\nu}(z') e^{-k_{\nu} z' / \mu} \frac{dz'}{\mu} \quad (5.13)$$

Equations (5.12) and (5.13) can be solved simultaneously to yield expressions for $I_{\nu}^{+}(h, \mu)$ and $I_{\nu}^{-}(0, \mu)$, which can be put into (5.10) and (5.11). After a partial integration these become

$$I_{\nu}^{+}(z, \mu) = B_{\nu}(z) - \int_0^z \frac{\partial B_{\nu}(z')}{\partial z'} e^{-k_{\nu}(z-z') / \mu} dz' + R_{\nu}^{+}(z) \quad (5.14)$$

where

$$R_{\nu}^{+}(z) = \frac{(1 - \epsilon) e^{-k_{\nu} z / \mu}}{1 - (1 - \epsilon)^2 e^{-2k_{\nu} h / \mu}} \left[\int_0^h \left(\frac{\partial B_{\nu}(z')}{\partial z'} - (1 - \epsilon) e^{-k_{\nu} h / \mu} \frac{\partial B_{\nu}(h-z')}{\partial z'} \right) e^{-k_{\nu} z' / \mu} dz' \right] \quad (5.15)$$

and

$$I_{\nu}^{-}(z, \mu) = B_{\nu}(z) + \int_z^h \frac{\partial B_{\nu}(z')}{\partial z'} e^{-k_{\nu}(z'-z) / \mu} dz' - R_{\nu}^{-}(z) \quad (5.16)$$

where

$$R_{\nu}^{-}(z) = \frac{(1 - \epsilon) e^{k_{\nu}(h-z) / \mu}}{1 - (1 - \epsilon)^2 e^{-2k_{\nu} h / \mu}} \left[\int_0^h \left(\frac{\partial B_{\nu}(z')}{\partial z'} - (1 - \epsilon) e^{-k_{\nu} h / \mu} \frac{\partial B_{\nu}(h-z')}{\partial z'} \right) e^{-k_{\nu}(h-z') / \mu} dz' \right] \quad (5.17)$$

Note that in the case of a symmetric gradient of B_ν ,

$$\frac{\partial B_\nu(z')}{\partial z'} = \frac{\partial B_\nu(h-z')}{\partial z'}$$

and

$$R_\nu^{+s}(z) = \frac{(1-\epsilon)e^{-k_\nu z/\mu}}{1+(1-\epsilon)e^{-k_\nu h/\mu}} \int_0^h \frac{\partial B_\nu(z')}{\partial z'} e^{-k_\nu z'/\mu} dz' \quad (5.18)$$

$$R_\nu^{-s}(z) = \frac{(1-\epsilon)e^{-k_\nu(h-z)/\mu}}{1+(1-\epsilon)e^{-k_\nu h/\mu}} \int_0^h \frac{\partial B_\nu(z')}{\partial z'} e^{-k_\nu z'/\mu} dz' = R_\nu^{+s}(h-z) \quad (5.19)$$

The flux is related to the intensity by

$$F_{z\nu}(\bar{z}) = \int_{-1}^{+1} 2\pi\mu I_\nu(\mu, \bar{z}) d\mu \quad (5.20)$$

where

$$I_\nu^\pm(\mu, \bar{z}) = I_\nu(\pm\mu, \bar{z}), \quad 1 \geq \mu > 0 \quad (5.21)$$

$$F_{z\nu} = F_\nu^+(\bar{z}) - F_\nu^-(\bar{z})$$

$$= \int_0^1 2\pi\mu I_\nu^+(\mu, \bar{z}) d\mu - \int_0^1 2\pi\mu I_\nu^-(\mu, \bar{z}) d\mu \quad (5.22)$$

The operator $\int_0^1 2\pi\mu d\mu$ applied to an isotropic quantity such as B_ν leads to πB_ν . Applied to exponential terms, it yields the exponential integrals. Following meteorological usage and the argument presented by Goody [1964, Ch. 2], the approximation

$$\int_0^{\infty} 2\pi\mu e^{-z/\mu} d\mu = \pi e^{-sz} \quad (5.23)$$

(where s is the diffusivity factor) is introduced. Good results have been obtained for $s = 1.667$ [Elsasser, 1942; Goody, 1964].

On application of the flux operator to (5.14) and (5.16)

$$F_{\nu}^{+}(z) = \pi B_{\nu}(z) - \int_0^z \frac{\partial \pi B_{\nu}(z')}{\partial z'} e^{-sk_{\nu}(z-z')} dz' + \tilde{R}_{\nu}^{+}(z) \quad (5.24)$$

$$F_{\nu}^{-}(z) = \pi B_{\nu}(z) + \int_z^h \frac{\partial \pi B_{\nu}(z')}{\partial z'} e^{-sk_{\nu}(z'-z)} dz' - \tilde{R}_{\nu}^{-}(z) \quad (5.25)$$

Since $(1-\epsilon)e^{-k_{\nu}h/\mu} < 1$ for $\epsilon > 0$, $k_{\nu} > 0$, the denominator of (5.15) may be expanded, integrated term by term, and re-collected, to yield

$$R_{\nu}^{+}(z) = \frac{(1-\epsilon)e^{-sk_{\nu}z}}{1-(1-\epsilon)^2 e^{-2sk_{\nu}h}} \int_0^h \left[\frac{\partial \pi B_{\nu}(z')}{\partial z'} - (1-\epsilon)e^{-sk_{\nu}h} \frac{\partial \pi B_{\nu}(h-z')}{\partial z'} \right] e^{-sk_{\nu}z'} dz' \quad (5.26)$$

Similarly,

$$\tilde{R}_{\nu}^{-}(z) = \frac{(1-\epsilon)e^{-sk_{\nu}(h-z)}}{1-(1-\epsilon)^2 e^{-2sk_{\nu}h}} \int_0^h \left[\frac{\partial \pi B_{\nu}(z')}{\partial z'} - (1-\epsilon)e^{-sk_{\nu}h} \frac{\partial \pi B_{\nu}(h-z')}{\partial z'} \right] e^{-sk_{\nu}(h-z')} dz' \quad (5.27)$$

These complete the expression of the radiative flux, which can be used in equations (5.3) - (5.6) to get $\beta/\bar{\beta}$.

5.2.3 The Radiative-Diffusive Equations

Introducing the linear approximation

$$dB_\nu = Q_\nu d\Theta \quad (5.28)$$

where

$$Q_\nu = \frac{dB_\nu}{d\Theta} \quad (5.29)$$

is justified for the small temperature differences here considered.

Combining (5.24), (5.25), and (5.21) with (5.28)

$$F_\nu(z) = -\pi Q_\nu \left\{ \int_0^z \beta(z') e^{-sk_\nu(z-z')} dz' + \int_z^h \beta(z') e^{-sk_\nu(z'-z)} dz' \right. \\ \left. - \frac{(1-\epsilon)e^{-sk_\nu z}}{1-(1-\epsilon)^2 e^{-2sk_\nu h}} \int_0^h \left[\beta(z') - (1-\epsilon)e^{-sk_\nu h} \beta(h-z') \right] e^{-sk_\nu z'} dz' \right. \\ \left. - \frac{(1-\epsilon)e^{-sk_\nu(h-z)}}{1-(1-\epsilon)^2 e^{-2sk_\nu h}} \int_0^h \left[\beta(z') - (1-\epsilon)e^{-sk_\nu h} \beta(h-z') \right] e^{-sk_\nu(h-z')} dz' \right\} \quad (5.30)$$

and with (5.2),

$$H_\nu(z) = \pi s \left\{ - \int_0^z \beta(z') k_\nu Q_\nu e^{-k_\nu s(z-z')} dz' - \int_z^h \beta(z') k_\nu Q_\nu e^{-k_\nu s(z'-z)} dz' \right. \\ \left. - \frac{(1-\epsilon)k_\nu e^{-sk_\nu z}}{1-(1-\epsilon)^2 e^{-2sk_\nu h}} \int_0^h \left[\beta(z') - (1-\epsilon)e^{-sk_\nu h} \beta(h-z') \right] e^{-sk_\nu z'} dz' \right. \\ \left. - \frac{(1-\epsilon)k_\nu e^{-sk_\nu(h-z)}}{1-(1-\epsilon)^2 e^{-2sk_\nu h}} \int_0^h \left[\beta(z') - (1-\epsilon)e^{-sk_\nu h} \beta(h-z') \right] e^{-sk_\nu(h-z')} dz' \right\} \quad (5.31)$$

To get the radiative heating due to all frequencies, it is

necessary to integrate over frequency

$$H_R = \int_0^{\infty} H_{\nu} d\nu \quad (5.32)$$

which may be done by making use of the function

$$\xi(x) = \frac{\int_0^{\infty} Q_{\nu} (1 - e^{-k_{\nu} x}) d\nu}{\int_0^{\infty} Q_{\nu} d\nu} \quad (5.33)$$

Writing

$$\int_0^{\infty} Q_{\nu} d\nu = Q \quad (5.34)$$

then

$$\xi'(x) = \frac{1}{Q} \int_0^{\infty} Q_{\nu} k_{\nu} e^{-k_{\nu} x} d\nu \quad (5.35)$$

and

$$\begin{aligned} H_R = \pi s Q \left\{ - \int_0^z \beta(z') \xi'[s(z-z')] dz' - \int_z^h \beta(z') \xi'[s(z'-z)] dz' \right. \\ \left. + (1-\epsilon) \left[\int_0^h \beta(z') \left(\xi'[s(z+z')] - \xi'[s(2h-z-z')] \right) \right. \right. \\ \left. \left. - (1-\epsilon) \beta(h-z') \left(\xi'[s(h+z+z')] - \xi'[s(3h-z-z')] \right) \right] \right. \\ \left. + (1-\epsilon)^2 \beta(z') \left(\xi'[s(2h+z+z')] - \xi'[s(4h-z-z')] \right) \dots dz' \right\} \quad (5.36) \end{aligned}$$

At this point, the assumption of a symmetric temperature gradient

$$\beta(z') = \beta(h-z') \quad (5.37)$$

will be made. This is in accord with the necessary assumptions that the emissivities of the plates are equal.

Putting (5.37) and (5.36) in (5.3) now gives the equation to be solved for $\beta(z')$ or $\theta(z')$.

5.2.4 Temperature Profile in a Gray Gas

Goody [1956] has gotten an expression for $\beta/\bar{\beta}$ in a gray gas with slightly different assumptions. That treatment will be presented and extended to general radiative boundary conditions, to provide an insight into the problem.

Starting with the equation of transfer

$$\mu \frac{d\bar{I}}{dz} = k(\beta - \bar{I}) \quad (5.38)$$

and making use of the Eddington approximation

$$I(\mu, z) = \bar{I}^+(z) \quad , \quad 0 < \mu \leq 1 \quad (5.39)$$

$$I(\mu, z) = \bar{I}^-(z) \quad , \quad -1 \leq \mu < 0.$$

and the definition of the flux

$$F_z = 2\pi \int_{-1}^1 \mu I d\mu \quad (5.20)$$

he obtains, on integrating (5.38) over a complete solid angle

$$\frac{dF_z}{dz} = 4\pi k\beta - 2\pi k(\bar{I}^+ + \bar{I}^-) \quad (5.40)$$

since B is isotropic.

Multiplying (5.38) by μ and integrating over a solid angle gives

$$\frac{2\pi}{3} \frac{d}{dz} (I^+ + I^-) = -k F_z \quad (5.41)$$

Eliminating I^+ and I^- between (5.40) and (5.41),

$$\frac{d^2 F_z}{dz^2} = 4\pi k \frac{dB}{dz} + 3k^2 F_z \quad (5.42)$$

Now using

$$F_z - KB = F_T \quad (5.4)$$

and

$$\frac{dB}{dz} = \frac{dB}{d\theta} \frac{d\theta}{dz} = Q\beta \quad (5.43)$$

$$\frac{d^2 F_z}{dz^2} - 4\pi k Q \left(\frac{F_z - F_T}{K} \right) - 3k^2 F_z = 0 \quad (5.44)$$

It might be noted parenthetically that a gray version of (5.30) derived with the use of the approximation (5.23) would satisfy an equation of the form

$$\frac{d^2 F_z}{dz^2} - 2\pi \sigma k Q \frac{(F_z - F_T)}{K} - s^2 k^2 F_z = 0 \quad (5.45)$$

Putting

$$\begin{aligned} \zeta &= \frac{z}{h} - \frac{1}{2} \\ \mathcal{F} &= \frac{4\pi Q}{3kK} \\ \lambda^2 &= 3k^2 h^2 (1 + \mathcal{F}) \end{aligned}$$

(5.44) becomes

$$\frac{d^2 F_z}{dz^2} - \lambda^2 F_z = -3k^2 h^2 \mathcal{X} F_T \quad (5.46)$$

It is now necessary to determine the boundary conditions. For a general partially-absorbing upper and lower boundary, the condition at $z = h$ is

$$I^-(h) = \epsilon_U B(h) + (1 - \epsilon_U) I^+(h) \quad (5.47a)$$

and at $z = 0$

$$I^+(0) = \epsilon_L B(0) + (1 - \epsilon_L) I^-(0) \quad (5.47b)$$

where ϵ_U , ϵ_L are the emissivities of the upper and lower plates, respectively.

Since

$$F_z = \pi (I^+ - I^-) \quad (5.48)$$

(5.47) may be simplified by writing

$$F_z(h) = \pi \epsilon_U [I^+(h) - B(h)] \quad (5.49)$$

Equation (5.40) becomes

$$\begin{aligned} \left(\frac{dF_z}{dz} \right)_h &= 4\pi k B(h) - 2\pi k [(2 - \epsilon_U) I^+(h) + \epsilon_U B(h)] \\ &= 2\pi k (2 - \epsilon_U) [B(h) - I^+(h)] \end{aligned} \quad (5.50)$$

$$\left(\frac{dF_z}{dz} \right)_h = -2k \left(\frac{2 - \epsilon_U}{\epsilon_U} \right) F_z(h) \quad (5.51)$$

Similarly,

$$\left(\frac{dF_z}{dz}\right)_0 = 2k \left(\frac{2-\epsilon_L}{\epsilon_L}\right) F_z(0) \quad (5.52)$$

Obviously these do not apply if ϵ_U or $\epsilon_L = 0$ (mirror boundaries). In that case

$$I^+(h) = I^-(h) \quad , \quad I^+(0) = I^-(0) \quad (5.53)$$

$$F_z(h) = F_z(0) = 0 \quad (5.54)$$

The general solution for (5.46) is

$$F_\zeta = A \sinh \lambda \zeta + B \cosh \lambda \zeta + \frac{\chi F_T}{1+\chi} \quad (5.55)$$

Writing $\frac{2-\epsilon}{\epsilon} = m$ and applying the boundary conditions (5.51) and (5.52),

$$\lambda A \cosh \frac{\lambda}{2} + \lambda B \sinh \frac{\lambda}{2} = -2khm_U \left(A \sinh \frac{\lambda}{2} + B \cosh \frac{\lambda}{2} + \frac{\chi F_T}{1+\chi} \right) \quad (5.56)$$

$$\lambda A \cosh \frac{\lambda}{2} - \lambda B \sinh \frac{\lambda}{2} = 2khm_L \left(-A \sinh \frac{\lambda}{2} + B \cosh \frac{\lambda}{2} + \frac{\chi F_T}{1+\chi} \right)$$

These may be solved in a straightforward manner to yield

$$A = \frac{-\frac{F_T}{1+\chi} \chi \left[\frac{\lambda}{2kh} \left(\frac{1}{m_L} - \frac{1}{m_U} \right) \sinh \frac{\lambda}{2} \right]}{2 \left[1 + \left(\frac{\lambda}{2kh} \right)^2 \frac{1}{m_L} \frac{1}{m_U} \right] \sinh \frac{\lambda}{2} \cosh \frac{\lambda}{2} + \frac{\lambda}{2kh} \left(\frac{1}{m_L} + \frac{1}{m_U} \right) \left(\sinh^2 \frac{\lambda}{2} + \cosh^2 \frac{\lambda}{2} \right)} \quad (5.57)$$

$$B = \frac{-\frac{F_T}{1+\chi} \chi \left[2 \sinh \frac{\lambda}{2} + \frac{\lambda}{2kh} \left(\frac{1}{m_L} + \frac{1}{m_U} \right) \cosh \frac{\lambda}{2} \right]}{2 \left[1 + \left(\frac{\lambda}{2kh} \right)^2 \frac{1}{m_L} \frac{1}{m_U} \right] \sinh \frac{\lambda}{2} \cosh \frac{\lambda}{2} + \frac{\lambda}{2kh} \left(\frac{1}{m_L} + \frac{1}{m_U} \right) \left(\sinh^2 \frac{\lambda}{2} + \cosh^2 \frac{\lambda}{2} \right)} \quad (5.58)$$

Now

$$\begin{aligned} \bar{F}_\zeta &= \int_{-\frac{1}{2}}^{\frac{1}{2}} \left(A \sinh \lambda \zeta + B \cosh \lambda \zeta + \frac{\mathcal{X} F_T}{1+\mathcal{X}} \right) d\zeta \\ &= \frac{2B}{\lambda} \sinh \frac{\lambda}{2} + \frac{\mathcal{X} F_T}{1+\mathcal{X}} \end{aligned} \quad (5.59)$$

By

$$\frac{\beta}{\bar{\beta}} = \frac{F_z - F_T}{\bar{F}_z - F_T} \quad (5.6)$$

or

$$\frac{\beta}{\bar{\beta}} = \frac{A \sinh \lambda \zeta + B \cosh \lambda \zeta - \frac{F_T}{1+\mathcal{X}}}{\frac{2B}{\lambda} \sinh \frac{\lambda}{2} - \frac{F_T}{1+\mathcal{X}}} \quad (5.60)$$

$$\begin{aligned} \frac{\beta}{\bar{\beta}} &= \left\{ \mathcal{X} \left[\frac{\lambda}{2kh} \left(\frac{1}{m_L} - \frac{1}{m_U} \right) \sinh \frac{\lambda}{2} \right] \sinh \lambda \zeta + \right. \\ &+ \mathcal{X} \left[2 \sinh \frac{\lambda}{2} + \frac{\lambda}{2kh} \left(\frac{1}{m_L} + \frac{1}{m_U} \right) \cosh \frac{\lambda}{2} \right] \cosh \lambda \zeta + 2 \left[1 + \left(\frac{\lambda}{2kh} \right)^2 \frac{1}{m_L m_U} \right] \sinh \frac{\lambda}{2} \cosh \frac{\lambda}{2} + \\ &+ \frac{\lambda}{2kh} \left(\frac{1}{m_L} + \frac{1}{m_U} \right) \left(\sinh^2 \frac{\lambda}{2} + \cosh^2 \frac{\lambda}{2} \right) \left. \right\} \left\{ \frac{2\mathcal{X}}{\lambda} \sinh \frac{\lambda}{2} \left[2 \sinh \frac{\lambda}{2} + \frac{\lambda}{2kh} \left(\frac{1}{m_L} + \frac{1}{m_U} \right) \cosh \frac{\lambda}{2} \right] + \right. \\ &+ 2 \left[1 + \left(\frac{\lambda}{2kh} \right)^2 \frac{1}{m_L m_U} \right] \sinh \frac{\lambda}{2} \cosh \frac{\lambda}{2} + \frac{\lambda}{2kh} \left(\frac{1}{m_L} + \frac{1}{m_U} \right) \left(\sinh^2 \frac{\lambda}{2} + \cosh^2 \frac{\lambda}{2} \right) \left. \right\}^{-1} \end{aligned} \quad (5.61)$$

Since (5.61) is too unwieldy for clarity, the following special cases will be explored:

1. $m_L = m_U = m$

In this case, $A = 0$ by (5.57), and the profile is symmetric.

After some simplification

$$\frac{\beta}{\bar{\beta}} = \frac{\mathcal{X} \cosh \lambda \zeta + \cosh \frac{\lambda}{2} + \frac{\lambda}{2khm} \sinh \frac{\lambda}{2}}{\frac{2\mathcal{X}}{\lambda} \sinh \frac{\lambda}{2} + \cosh \frac{\lambda}{2} + \frac{\lambda}{2khm} \sinh \frac{\lambda}{2}} \quad (5.62)$$

For the special case $m = 1$, or black boundaries, this is

$$\frac{\beta}{\bar{\beta}} = \frac{\mathcal{X} \cosh \lambda \zeta + \cosh \frac{\lambda}{2} + \frac{\lambda}{2kh} \sinh \frac{\lambda}{2}}{\frac{2\mathcal{X}}{\lambda} \sinh \frac{\lambda}{2} + \cosh \frac{\lambda}{2} + \frac{\lambda}{2kh} \sinh \frac{\lambda}{2}} \quad (5.63)$$

This is the answer obtained by Goody [1956].

For $m = 0$, or mirror boundaries,

$$\frac{\beta}{\bar{\beta}} = \frac{\mathcal{X} \cosh \lambda \zeta + \cosh \frac{\lambda}{2}}{\frac{2\mathcal{X}}{\lambda} \sinh \frac{\lambda}{2} + \cosh \frac{\lambda}{2}} \quad (5.64)$$

2. $m_L = 1, m_U = 0$

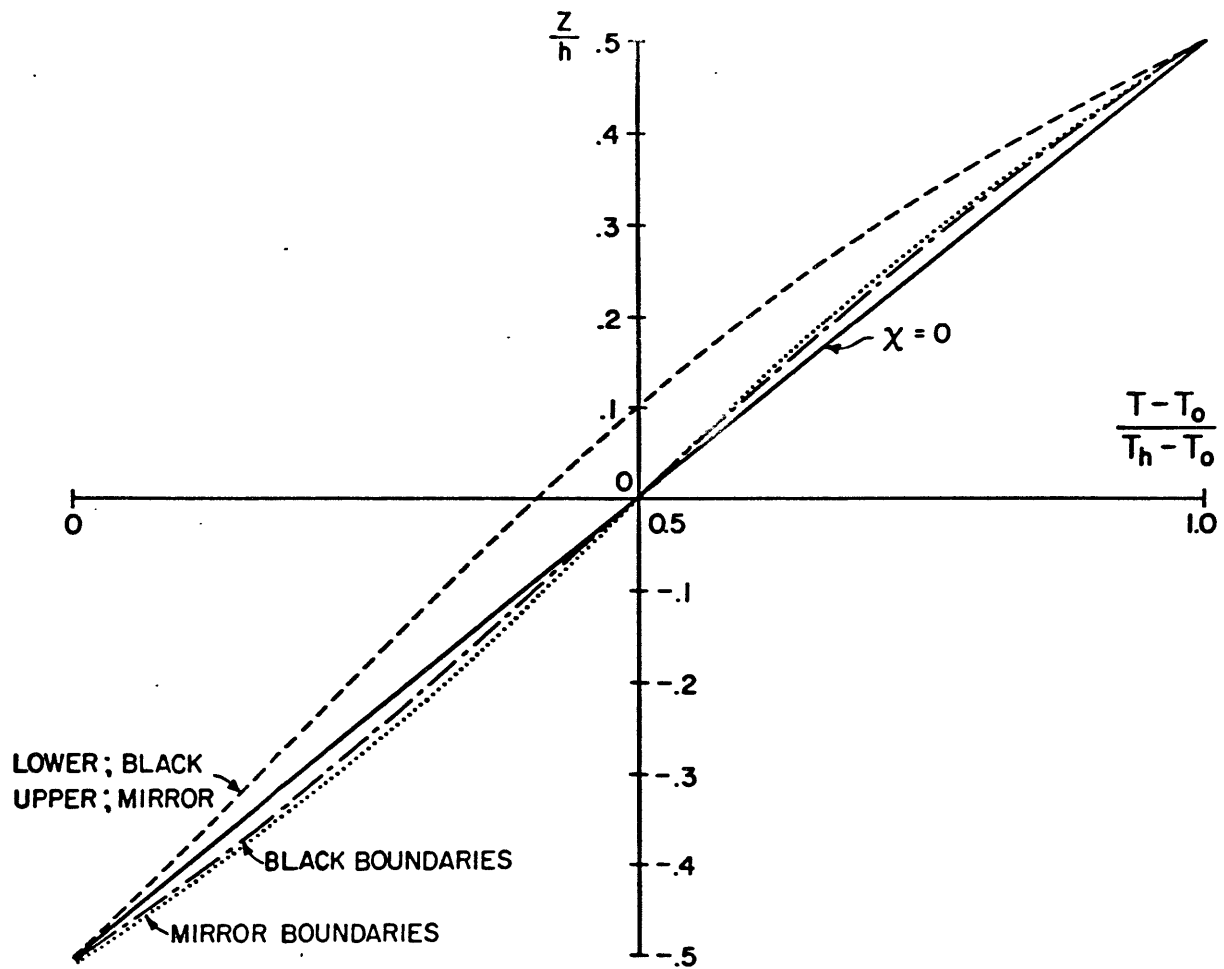
This is the case of maximum radiative profile asymmetry -- a black lower boundary and reflecting upper one. Now (5.61) becomes

$$\frac{\beta}{\bar{\beta}} = \left[\frac{\mathcal{X} \lambda}{2kh} \sinh \frac{\lambda}{2} \sinh \lambda \zeta + \mathcal{X} \left(2 \sinh \frac{\lambda}{2} + \frac{\lambda}{2kh} \cosh \frac{\lambda}{2} \right) \cosh \lambda \zeta + 2 \sinh \frac{\lambda}{2} \cosh \frac{\lambda}{2} + \frac{\lambda}{2kh} \left(\sinh^2 \frac{\lambda}{2} + \cosh^2 \frac{\lambda}{2} \right) \right] \left[\frac{2\mathcal{X}}{\lambda} \sinh \frac{\lambda}{2} \times \right. \quad (5.65)$$

$$\left. \times \left(2 \sinh \frac{\lambda}{2} + \frac{\lambda}{2kh} \cosh \frac{\lambda}{2} \right) + 2 \sinh \frac{\lambda}{2} \cosh \frac{\lambda}{2} + \frac{\lambda}{2kh} \left(\sinh^2 \frac{\lambda}{2} + \cosh^2 \frac{\lambda}{2} \right) \right]^{-1}$$

The temperature profiles $\Theta(\zeta) = \frac{\int_0^\zeta \beta(\zeta) d\zeta}{\Delta \Theta}$ are presented in

Fig. 5-1 for certain parameters that might be applied to NH_3 . From



TEMPERATURE PROFILES FOR A 2 cm LAYER OF NH_3 IN DIFFUSIVE RADIATIVE EQUILIBRIUM UNDER DIFFERENT BOUNDARY CONDITIONS
 $k = 0.27 \text{ cm}^{-1}$; $\chi = 5.46$; $\lambda = 2.38$

Fig. 5-1. THE EFFECT OF BOUNDARY CONDITIONS ON TEMPERATURE PROFILE IN A GRAY MEDIUM

the equations and curves it is clear that the mirror boundaries will distort the symmetric gradient more than black boundaries will. It was this that dictated the choice of radiative boundary conditions. It is interesting to see how much the profile is changed by the asymmetric boundary conditions.

The values used for the gray model of ammonia that is plotted were

$$\begin{aligned}k &= 0.27 \text{ cm.}^{-1} \\d &= 2 \text{ cm.} \\ \theta &= 300^\circ \text{ K} \\ K/\rho c_p &= 0.32 \text{ cm.}^2/\text{sec.}\end{aligned}$$

Straightforward substitution leads to

$$\begin{aligned}\mathcal{X} &= 5.46 \\ \lambda &= 2.38\end{aligned}$$

Comparing the results of this calculation with those to be described later for $p = 1.294 \text{ atm. NH}_3$ taking account of the non-grayness (Fig. 5-2), one sees immediately that the gray model does not have as sharp a boundary layer, that the maximum deviation occurs slightly further toward the center, and that the gray model has larger effects toward the center. These are consistent with the picture of the strong lines of a non-gray gas having a larger short-range effect but a weaker long-range effect than a gray gas with the same total emissivity.

Because of the crudeness of the estimate of k in this calculation, which was done for design purposes, no comparison with observations will be made.

$h = 1.987 \text{ cm}$

— Non Gray Calculation

$\rho_{\text{NH}_3} = 1.294 \text{ atm.}, \epsilon = 0.417$

- - - Gray Calculation

$k = 0.27 \text{ cm}^{-1}$

$\epsilon = 0$

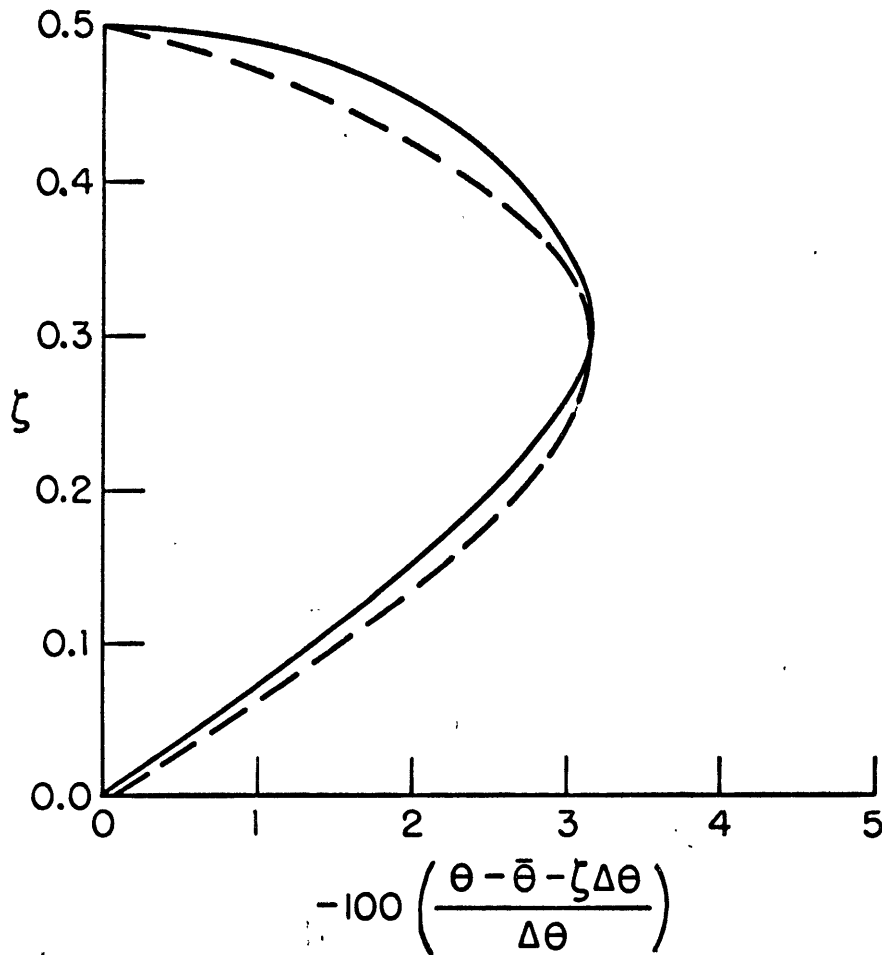


FIG. 5-2. Comparison of Gray and Non-Gray Temperature Profile.
Abcissa is % deviation from a linear gradient.

Physically what seems to be happening in the radiative-diffusive case with symmetric boundaries is that near the warm boundary a parcel of gas is not only losing heat by diffusion, but also by radiation to the rest of the gas, which lowers its temperature below what it would be with diffusion alone. The converse happens at the cold boundary. Near the center, the radiative gains and losses are more nearly in balance, and the profile does not display so much curvature.

The effect of the boundaries can be understood if it is remembered that the gas parcel can absorb directly from a black boundary and thereby gain heat by radiation, while for a mirror boundary the parcel "sees" mainly colder regions, thus maximizing the radiative heat losses.

5.2.5 Matrix Calculation of the Temperature Gradient

The first numerical method of solving (5.3) with (5.36) in it was to divide the region between the plates into a finite number of thin, isothermal layers and write difference equations in the n unknown θ_j 's. Consider a series of levels, $j = 0, \pm 1, \pm 2, \dots, \pm n$ (n even) (as in Chapter 2), where $j = 0$ is the center, and $j = \pm n$ are the boundaries. The levels of odd j correspond to the centers of the layers defined by the even n 's. The derivatives $\frac{d\theta}{dz}(j)$ and $\frac{d^2\theta}{dz^2}(j)$ for odd j were expressed in terms of the θ_j 's. For $\epsilon = 1$ (black boundaries), (5.3) with (5.36) was written in a form equivalent to

$$0 = \frac{\theta_{j+2} - 2\theta_j + \theta_{j-2}}{\left(\frac{h}{2n}\right)^2} + \frac{\pi s Q}{K} \sum_{f=0}^{n-j-1} \epsilon' \left(s f \frac{h}{n} \right) \frac{[\theta_{j+2(f+1)} - \theta_{j+2f}] \frac{h}{n}}{\frac{h}{n}} + \frac{\pi s Q}{K} \sum_{f=0}^{j-(n-1)} \epsilon' \left(s f \frac{h}{n} \right) \frac{[\theta_{j-2f} - \theta_{j-2(f+1)}] \frac{h}{n}}{\frac{h}{n}} \quad (5.66)$$

where the sums run to the region next to the boundary. For each of the n values of j at which θ_j was sought, linear equations could then be written relating $\Delta \theta_j = \theta_j - \bar{\theta}$ to all other $(n-1)\Delta \theta_j$'s, i.e., an $n \times n$ matrix for the $\Delta \theta_j$'s was obtained. Making use of (5.37) in the form

$$\Delta \theta_j = - \Delta \theta_{-j} \quad (5.67)$$

the matrix could be reduced to $n/2 \times n/2$. The diffusion term for $j = n - 1$ must be modified to allow for the shorter distance to the wall. The terms involving diffusion from the wall provide non-zero terms on the l.h.s. of (5.66).

For the case $\epsilon = 0$ (mirror boundaries) (see equation (5.36)), (5.67) was altered to allow an iterated sum over a distance equal to the plate spacing. This allowed for perfect reflection at the walls by extending the sums from $f = 0$ to $f = n$. The intervals were counted from each j level to the boundary, then back into the fluid. The quantity $\Sigma'(sh) = \Sigma'(n sh/n)$ in the first term not evaluated was not negligible, but because of the form of the terms in the sums, differences of form $\Sigma'(fsh) - \Sigma'(sh(f+1))$, $f > 10$ are needed, which cannot be obtained with high accuracy. Therefore, because the flux divergence is small at path lengths beyond this, the remainder $\Sigma(sh)$ was distributed equally over the n intervals. Equation (5.66) is then written

$$0 = \frac{\theta_{j+2} - 2\theta_j + \theta_{j-2}}{\left(\frac{h}{2n}\right)^2} + \frac{\pi s Q}{K} \sum_{f=0}^{10} \frac{\theta_{j+2(f+1)} - \theta_{j+2f}}{\frac{h}{n}} \cdot \frac{h}{n} \left[\Sigma'\left(sf \frac{h}{n}\right) + \frac{\Sigma'(sh)}{n} \right] \\ + \frac{\pi s Q}{K} \sum_{f=0}^{10} \left[\frac{\theta_{j-2f} - \theta_{j-2(f+1)}}{\frac{h}{n}} \right] \cdot \frac{h}{n} \left[\Sigma'\left(sf \frac{h}{n}\right) + \frac{\Sigma'(sh)}{n} \right] \quad (5.68)$$

The systems of equations (5.66) and (5.68) were solved for some preliminary estimates of situations at convective onset and yielded results in good agreement with the results of the following section. These cases used $n = 10$ at 2 cm.; and $n = 20$ at 5 cm. However, it would have necessitated more work to show that an adequate number of points had been chosen. In addition, the isothermal layer hypothesis is clearly in error, especially at the boundaries. Practically, solutions demanded solving matrices larger than those necessitated by the following method.

5.2.6 Calculation of the Temperature Gradients by Power Series Expansion

This method was suggested by Prof. R. M. Goody of Harvard University.

One would like to solve for $\beta(z)$ or $\theta(z)$ from (5.3)

$$H_R + K \frac{d\beta(z)}{dz} = H_R + K \frac{d^2\theta}{dz^2} = 0 \quad (5.3)$$

where H is given by (5.36) (with the insertion of (5.37))

$$H_R = \pi s Q \left\{ - \int_0^z \beta(z') \Xi'[s(z-z')] dz' - \int_z^h \beta(z') \Xi'[s(z'-z)] dz' + \right. \\ \left. + (1-\epsilon) \left[\int_0^h \beta(z') \left(\Xi'[s(\frac{z'}{2}+z)] - \Xi'[s(2h-z-z')] - \dots \right) dz' \right] \right\} \quad (5.36)$$

Since, as seen above, the temperature dependence of Ξ' is small, this is a linear integral equation of the non-dimensional variable ζ , since β is symmetric about the center,

$$\frac{\beta(z)}{\bar{\beta}} = A + B\zeta^2 + C\zeta^4 + \dots \quad (5.69)$$

It follows

$$\frac{d\beta}{dz} = \frac{\bar{\beta}}{h} (2B\zeta + 4C\zeta^3 + \dots) \quad (5.70)$$

while from (5.69) by integration

$$1 = A + \frac{B}{12} + \frac{C}{80} + \dots \quad (5.71)$$

Then substituting (5.69) in (5.36), one obtains integrals of the type

$$\begin{aligned} & A \int_0^h \xi' [\text{sh}(\zeta - \zeta')] d\zeta' \\ & B \int_0^h \zeta^2 \xi' [\text{sh}(\zeta - \zeta')] d\zeta' \\ & C \int_0^h \zeta^4 \xi' [\text{sh}(\zeta - \zeta')] d\zeta' \end{aligned} \quad (5.72)$$

Equation (5.71) gives one relationship between the coefficients.

(N - 1) equations are needed to fit N coefficients; these are obtained by evaluating (5.3) at N - 1 places between $\zeta = 0$ and $\zeta = 0.5$.

By symmetry, the heating at $\zeta = 0$ is 0, which is assured by the expansion. In this investigation, (5.36) was evaluated at $\zeta = 0.3$ and 0.5 for the three coefficient curves.

The form in which H was evaluated was

$$\begin{aligned} H_R = \pi Q \bar{\beta} h \left\{ & - \int_0^{\zeta} \frac{\beta(\zeta')}{\bar{\beta}} \xi' [\text{sh}(\zeta - \zeta')] d\zeta' - \int_{\zeta}^h \frac{\beta(\zeta')}{\bar{\beta}} \xi' [\text{sh}(\zeta' - \zeta)] d\zeta' + \right. \\ & + (1-\epsilon) \int_0^h \frac{\beta(\zeta')}{\bar{\beta}} \left(\xi' [\text{sh}(1+\zeta-\zeta')] - \xi' [\text{sh}(1-\zeta+\zeta')] \right) d\zeta' - \\ & - (1-\epsilon)^2 \int_0^h \frac{\beta(\zeta')}{\bar{\beta}} \left(\xi' [\text{sh}(2+\zeta-\zeta')] - \xi' [\text{sh}(2-\zeta+\zeta')] \right) d\zeta' + \quad (5.73) \\ & + (1-\epsilon)^3 \int_0^h \frac{\beta(\zeta')}{\bar{\beta}} \left(\xi' [\text{sh}(3+\zeta-\zeta')] - \xi' [\text{sh}(3-\zeta+\zeta')] \right) d\zeta' - \\ & \left. - (1-\epsilon)^4 \int_0^h \frac{\beta(\zeta')}{\bar{\beta}} \left(\xi' [\text{sh}(4+\zeta-\zeta')] - \xi' [\text{sh}(4-\zeta+\zeta')] \right) d\zeta' \right\} \end{aligned}$$

Values of ξ' were taken from the graphs and tables of Chapter 3 for the pressure at which the profile was to be found. The first two terms in (5.73) were evaluated at intervals of 0.05 in ξ , and Simpson's rule employed to form the integral. The second pair of terms was evaluated at $\xi = \pm 0.5$, ± 0.25 , 0, and the integral formed by the 7-32-12-32-7 rule. The evaluation of the third, fourth, and fifth terms was based on the approximate identity

$$\frac{\xi'[\text{sh}(n+\xi-\xi')] - \xi'[\text{sh}(n+\xi'-\xi)]}{2\text{sh}(\xi-\xi')} \doteq \xi''(\text{sh}n) \quad (5.74)$$

Now

$$\int_{-1/2}^{1/2} (A + B\xi^2 + C\xi^4)(1-\epsilon)^n \cdot 2\xi''(\text{sh}n) \cdot \text{sh}(\xi-\xi') d\xi' = \quad (5.75)$$

$$= (1-\epsilon)^n 2\text{sh}\xi''(\text{sh}n) \int (A + \frac{B}{12} + \frac{C}{80})$$

The last term provides less than one percent of the value of the coefficients of A, B, and C,

$$\frac{H_R(\xi)}{\pi s Q \sqrt{\beta} h} = a_R(\xi)A + b_R(\xi)B + c_R(\xi)C \quad (5.76)$$

To this must be added the diffusive heat

$$H_o = -K \frac{d\beta(z)}{dz} = -\frac{K\sqrt{\beta}}{h} (2B\xi + 4C\xi^3) \quad (5.77)$$

$$\frac{H_o(\xi)h}{K\sqrt{\beta}} = b_D(\xi)B + c_D(\xi)C$$

Multiplying (5.77) by $\frac{K}{h^2 \pi Q}$ and adding to (5.76) results in

$$H(\zeta) = 0 = a(\zeta)A + b(\zeta)B + c(\zeta)C \quad (5.78)$$

As mentioned, when this is done for $N - 1$ values of ζ and the relation (5.71) included, enough information is available to determine N coefficients.

In the case $d = 5.048$ cm., $p_{\text{NH}_3} = 304$ cm.Hg. = 0.4 atm., $\epsilon = 0.352$ (a preliminary estimate of plate emissivity), a strong deviation from linear gradient and sharpest boundary layer of interest for this work was expected. To see how much effect the number of coefficients had, a four-coefficient expansion for $\beta/\bar{\beta}$ was made, and evaluated at $\zeta = 0.5$, 0.35, and 0.2. The results are compared with a three-coefficient expansion (described above) in Table 5-1.

Table 5-1
 $\frac{\bar{\theta} + \zeta \Delta \theta - \theta}{\Delta \theta}$ IN PURE NH_3
 $h = 5.048$ cm., $p_{\text{NH}_3} = 0.4$ atm., $\epsilon = 0.352$

ζ	Three Coefficients	Four Coefficients
0.0	0.0000	0.0000
0.1	0.0226	0.0260
0.2	0.0432	0.0469
0.3	0.0565	0.0565
0.4	0.0498	0.0480
0.5	0.0000	0.0000

The numbers in Table 5-1 are deviations from the linear gradient, divided by the total temperature drop. Since $\Delta\Theta$ is about 7° , the maximum difference is about $2.6 \times 10^{-2} \text{ }^\circ\text{C}$, which is close to the limit of accuracy of the measuring apparatus described in Chapter 2. This leads to the conclusion that a three-coefficient calculation is sufficiently accurate.

5.2.6 Temperature Profile Calculations

In Fig. 5-3 the quantity $-\left(\frac{\Theta - \bar{\Theta} - \zeta\Delta\Theta}{\Delta\Theta}\right)$ for pure ammonia at several pressures (in atmospheres) is plotted against ζ for $h = 1.987$ cm. This quantity $-\left(\frac{\Theta - \bar{\Theta} - \zeta\Delta\Theta}{\Delta\Theta}\right)$ is the fractional deviation of the temperature from the linear gradient. The linear gradient, the limiting case for an optically thin layer, is then the vertical axis of the diagram.

In addition, for $p = 0.6$ atmospheres, the effect of a change of ϵ is shown by the broken and the dashed lines. The profile is thus seen to be rather insensitive to the plate emissivity.

It is immediately apparent that these deviations are not nearly linear without pressure. This is due to two causes:

1. For a gray atmosphere at small values of k , the deviations are proportional to k . However, as k is increased, the more complicated phenomena of (5.62) remove the linearity.
2. Although the Planck mean (see Chapter 3) is linear in pressure, at r of the order of a centimeter and above Σ' becomes noticeably nonlinear in pressure.

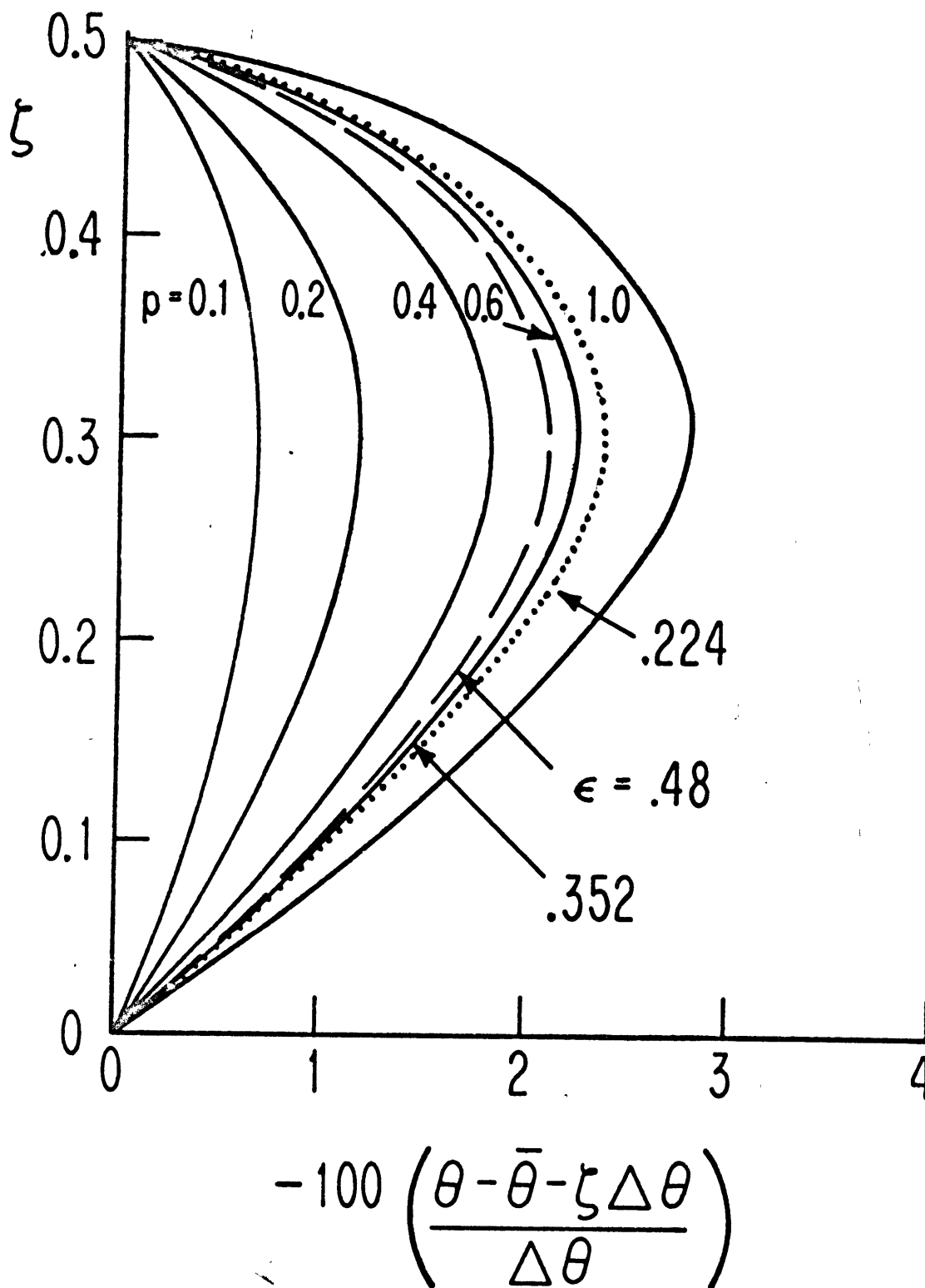


Fig. 5-3. $-100 \left(\frac{\theta - \bar{\theta} - \zeta \Delta \theta}{\Delta \theta} \right)$ CALCULATED FOR PURE NH_3 ; $h = 1.987$ cm.

Pressure in atmospheres as marked on the curves. $\epsilon = 0.352$.
 For $p = 0.6$ atmospheres, the effect of changing plate emissivity is shown.

From both, it would be expected that at lower pressures or smaller h , the deviations would be linear in pressure.

In Fig. 5-4, $-\left(\frac{\theta - \bar{\theta} - \zeta \Delta \theta}{\Delta \theta}\right)$ is plotted against ζ for $h = 5.048$ cm.

In Fig. 5-5, the coefficients A , B , and C are plotted against pressure for $h = 1.987$ centimeters. As the pressure increases, A first drops below 1.0, then reaches a minimum and begins to return. B climbs to a maximum and begins to recede toward zero, and C also shows signs of bending back to zero. This is fully in accord with what was seen in Sec. 5.1, where as the medium became opaque the profile again became linear. The fact that C is still increasing after A and B have passed their minimum and maximum respectively indicates a concentration of the gradient in the boundary layer and is an indication that higher powers of ζ should be included in the expansion at this point. A plot for $h = 5.048$ cm. shows the same type of behavior.

5.3 Radiative-Diffusive Flux Calculation

5.3.1 Gray Theory

Consider that in (5.4)

$$F_z(z) - K\beta(z) = F_T \quad (5.4)$$

$F_z(z)$ and $\beta(z)$ depend on the radiative parameters and so, in general, must F_T . This possibility may be easily explored for the case of a gray gas with the results of 5.2.4. Consider only the case of symmetric boundaries to radiation $m_U = m_L = m$.

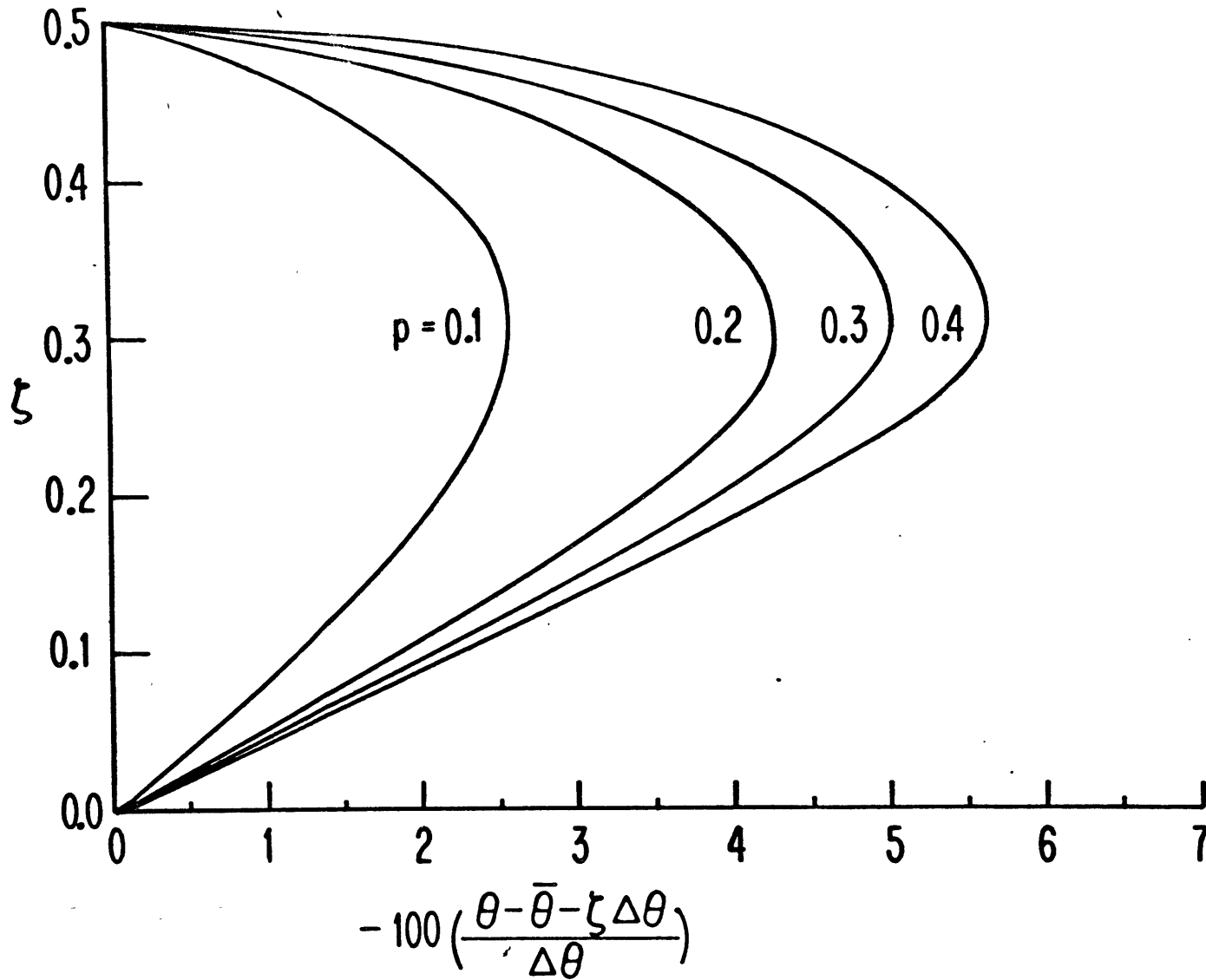
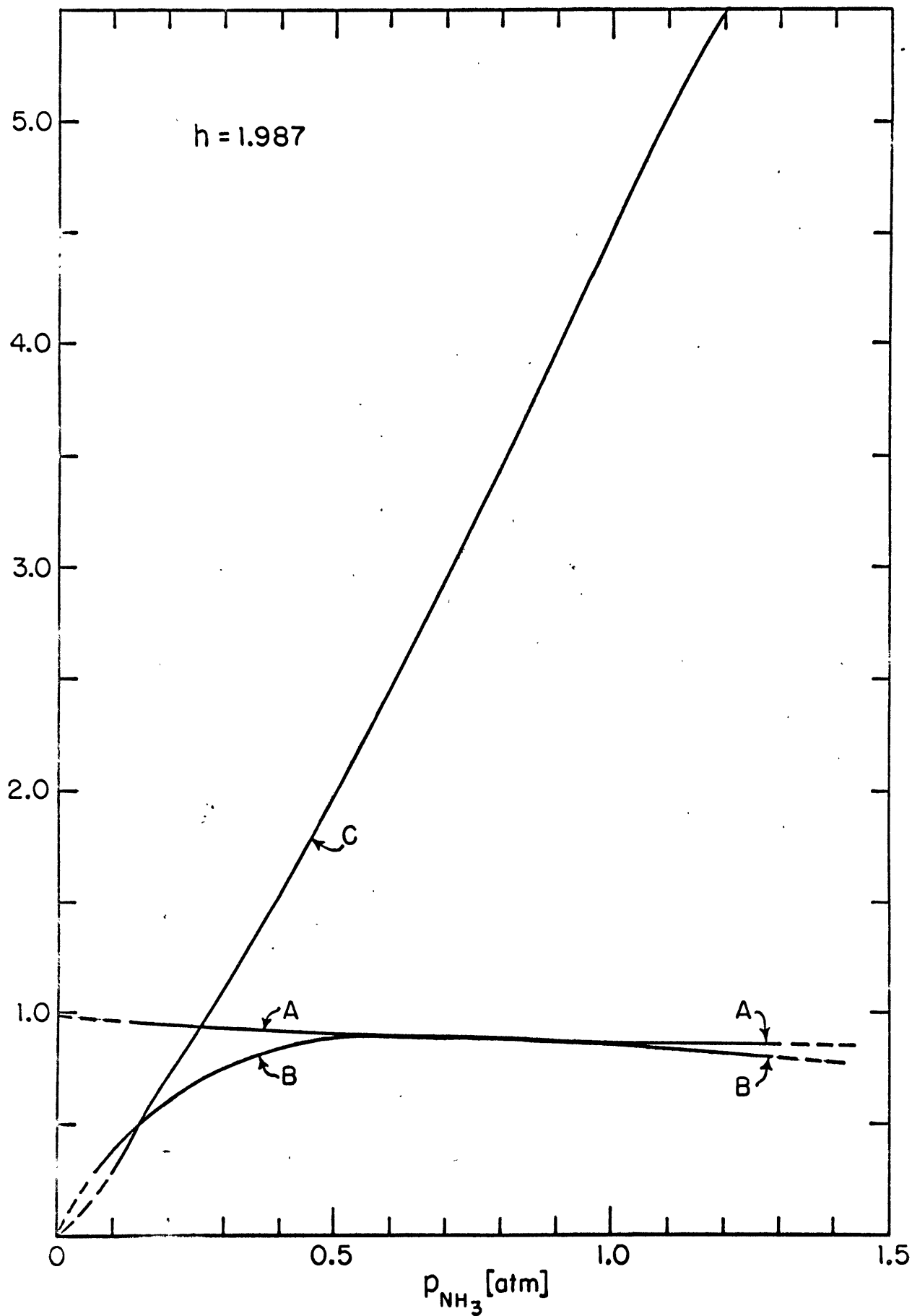


Fig. 5-4. $-100 \left(\frac{\theta - \bar{\theta} - z \Delta \theta}{\Delta \theta} \right)$ CALCULATED FOR PURE NH_3 : $h = 5.048$ cm.
 Pressure in atmospheres as marked on the curves. $\epsilon = 0.352$.



.. 5-5. A, B, and C versus pressure.

These are the coefficient in the expression $\frac{\beta}{\beta} = A + B\zeta^2 + C\zeta^4$

$$F_z = F_R = B \cosh \lambda \xi + \frac{\mathcal{X} F_T}{1 + \mathcal{X}} \quad (5.55)$$

where F_R denotes the radiation heat flux.

With the use of (5.58)

$$F_z = F_T \left[\frac{\mathcal{X}}{1 + \mathcal{X}} \left(1 - \frac{\cosh \lambda \xi}{\cosh \frac{\lambda}{2} + \frac{\lambda}{2khm} \sinh \frac{\lambda}{2}} \right) \right] \quad (5.79)$$

Letting $F_D =$ diffusive flux

$$F_D = -K\beta = -K\beta \frac{\mathcal{X} \cosh \lambda \xi + \cosh \frac{\lambda}{2} + \frac{\lambda}{2khm} \sinh \frac{\lambda}{2}}{\frac{2\mathcal{X}}{\lambda} \sinh \frac{\lambda}{2} + \cosh \frac{\lambda}{2} + \frac{\lambda}{2khm} \sinh \frac{\lambda}{2}} \quad (5.80)$$

or

$$\frac{F_T}{-K\beta} = \frac{\frac{\mathcal{X} \cosh \lambda \xi + \cosh \frac{\lambda}{2} + \frac{\lambda}{2khm} \sinh \frac{\lambda}{2}}{\frac{2\mathcal{X}}{\lambda} \sinh \frac{\lambda}{2} + \cosh \frac{\lambda}{2} + \frac{\lambda}{2khm} \sinh \frac{\lambda}{2}}}{1 - \frac{\mathcal{X}}{1 + \mathcal{X}} \frac{\cosh \frac{\lambda}{2} - \cosh \lambda \xi + \frac{\lambda}{2khm} \sinh \frac{\lambda}{2}}{\cosh \frac{\lambda}{2} + \frac{\lambda}{2khm} \sinh \frac{\lambda}{2}}} \quad (5.82)$$

$$= \frac{(1 + \mathcal{X}) \left(\cosh \frac{\lambda}{2} + \frac{\lambda}{2khm} \sinh \frac{\lambda}{2} \right)}{\frac{2\mathcal{X}}{\lambda} \sinh \frac{\lambda}{2} + \cosh \frac{\lambda}{2} + \frac{\lambda}{2khm} \sinh \frac{\lambda}{2}} \quad (5.83)$$

$$= \frac{1 - \mathcal{X}^{-1}}{\left(\frac{\lambda}{2} \coth \frac{\lambda}{2} + \frac{\lambda^2}{4khm} \right)^{-1} + \mathcal{X}^{-1}} \quad (5.84)$$

which of course does not depend upon ξ , but depends markedly on m .
 Imagining that corresponding to F_T there is an effective conductivity,

$$F_T = - K_{\text{eff}} \bar{\beta}$$

$$\frac{K_{\text{eff}}}{K} = \frac{1 + \chi^{-1}}{\left(\frac{\lambda}{2} \coth \frac{\lambda}{2} + \frac{\lambda^2}{4khm}\right)^{-1} + \chi^{-1}} \quad (5.85)$$

The present apparatus always measures a $K(\text{eff})$, not K , due to the radiative flux. Let (5.85) therefore be normalized with respect to the $K_{\text{eff}}(0)$, the effective conductivity at zero pressure. (In this and later contexts, zero pressure means that the opacity is zero, but the molecular mean free path is much less than h .) It is easy to show that

$$\lim_{kh \rightarrow 0} \frac{K_{\text{eff}}}{K} = \frac{K_{\text{eff}}(0)}{K} = 1 + \frac{\pi h Q}{m K} \quad (5.86)$$

so that

$$\frac{K_{\text{eff}}}{K_{\text{eff}}(0)} = \frac{1}{1 + \frac{\pi h Q}{m K}} \frac{1 + \chi^{-1}}{\left[\frac{\lambda}{2} \coth \frac{\lambda}{2} + \frac{3kh}{4m}(1 + \chi)\right]^{-1} + \chi^{-1}} \quad (5.87)$$

This expression was first derived by Goody [1963], based on a different approach. This has been plotted in Fig. 5-6 for several values of ϵ , with $d = 1.987$ cm., K for NH_3 , and all temperatures set at 25° C.

The phenomena presented in Fig. 5-6 can be understood in the following ways. The radiative flux between the plates depends on the emissivities of the surfaces and the attenuation of the gas. As the optical density

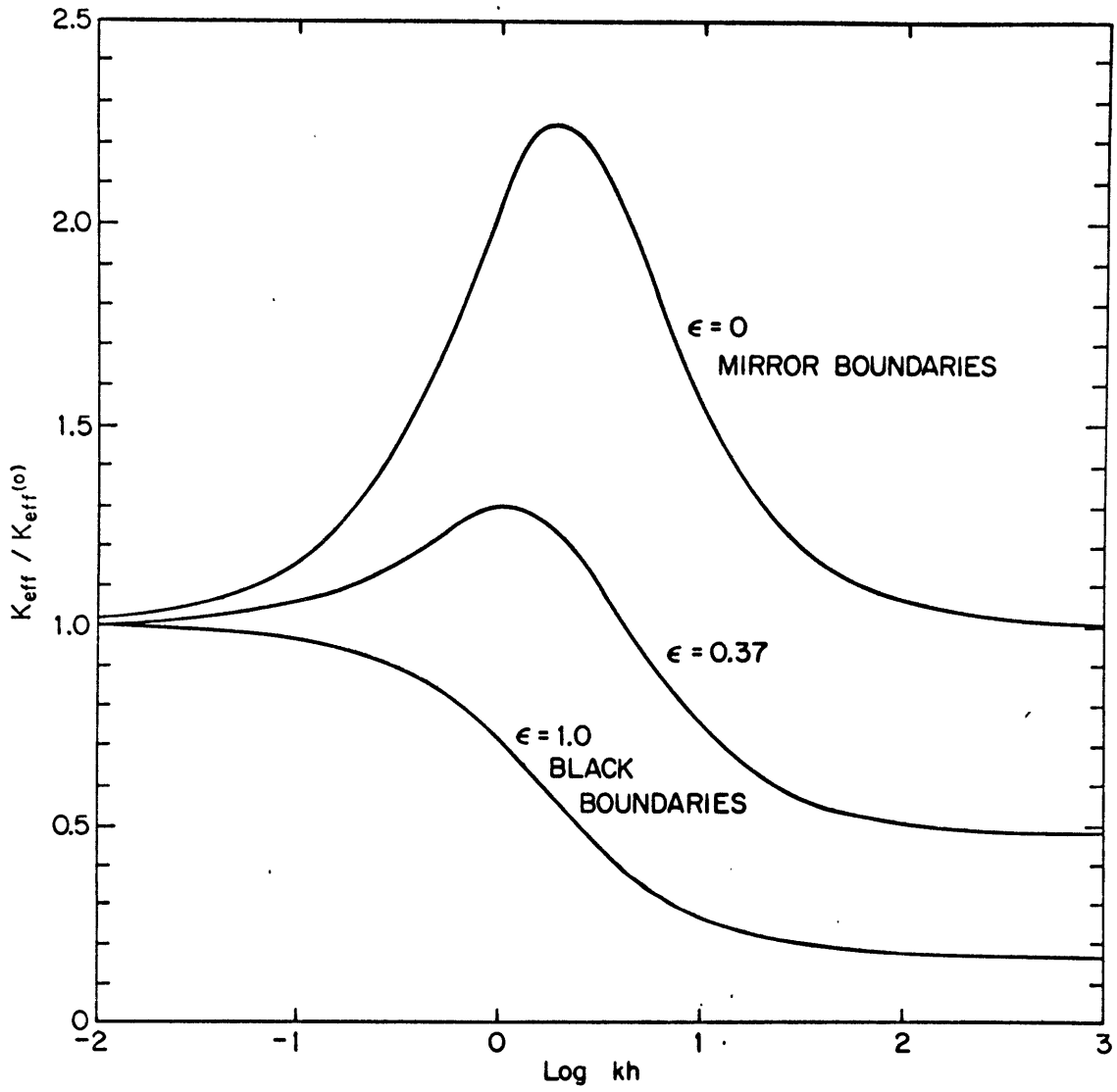


Fig. 5-6. EFFECTIVE CONDUCTIVITY IN A GRAY ABSORBING GAS

increases, the direct flux from plate to plate is decreased and finally stopped altogether. The diffusive flux from the surface depends on the local gradients. As the optical density is increased, as noted before, the gradient at the wall increases, indicating an increased diffusive flux. Beyond a certain point, increases in optical density decrease the gradient and the diffusive flux returns to its original value. The initial increase, then decrease, in total heat flux is the result of the interplay of these forces. Another way of seeing the phenomenon is to consider two mirror boundaries. For very low gas pressures there is no radiative transfer between the two plates, and the total flux is the conductive one, $K_{\text{eff}} = K$. With increasing optical density, the heat will be transmitted within the gas more easily from parcel to parcel. The initial increase is therefore to be expected.

It is a curious feature of this presentation that as k is increased indefinitely, the ratio of radiative to diffusive conductivity,

$\chi = \frac{4\pi Q}{3Kk}$, goes to zero, so that the limiting conductivity is the molecular one.

5.3.2 Evaluation of the Non-Gray Flux

5.3.2.1 Derivation of the Equations

With a hueristic journey through the lucid uplands of gray gas phenomena behind, one descends once more into the non-gray murk. It is now desired to evaluate

$$F_z(z) - K\bar{\beta} \frac{\beta(z)}{\beta} = F_T \quad (5.4)$$

for a non-gray gas. $F_{z\nu}(z)$ and $\beta/\bar{\beta}$ are given by (5.30) and (5.69)

respectively

$$\begin{aligned}
 F_{z\nu}(z) = & -\pi Q \left[\int_0^z \beta(z') e^{-sk_\nu(z-z')} dz' + \int_z^h \beta(z') e^{-sk_\nu(z'-z)} dz' + \right. \\
 & + \frac{(1-\epsilon) e^{-sk_\nu z}}{1+(1-\epsilon) e^{-sk_\nu h}} \int_0^h \beta(z') e^{-sk_\nu(h-z')} dz' - \\
 & \left. - \frac{(1-\epsilon) e^{-sk_\nu(h-z)}}{1+(1-\epsilon) e^{-sk_\nu h}} \int_0^h \beta(z') e^{-sk_\nu z'} dz' \right] \quad (5.30)
 \end{aligned}$$

$$\frac{\beta(z)}{\bar{\beta}} = A + B \zeta^2 + C \zeta^4 \quad (5.69)$$

The values of A, B, and C are known as a result of the operations described in 5.2.5.

As in the case of the gray fluid, the flux could be evaluated at a specific or general point within the fluid. Because of the fact that there are two processes, acting in opposite directions and leading to near cancellation, a system of averaging across the fluid was adopted for greater accuracy.

The following computational scheme was suggested by Professor R. M. Goody of Harvard University.

$$\begin{aligned}
 \bar{F} &= \frac{1}{h} \int_0^h F dz = \frac{1}{h} \int_0^h F_z dz - K \frac{1}{h} \int_0^h \beta(z) dz \\
 &= \frac{1}{h} \int_0^h F_z dz - K \frac{\Theta(h) - \Theta(0)}{h} \quad (5.88)
 \end{aligned}$$

Because of the symmetric profile, the third and fourth integral in (5.30) are the same. Equation (5.30) may be written as

$$\frac{F_v}{\pi} = - \int_0^z Q_v \beta(z') e^{-sk_v(z-z')} dz' - \int_z^h Q_v \beta(z') e^{-sk_v(z'-z)} dz' + \left[e^{-sk_v z'} + e^{-sk_v(h-z')} \right] \frac{(1-\epsilon)}{1+(1-\epsilon)e^{-sk_v h}} \int_0^h Q_v \beta(z') e^{-sk_v z'} dz'$$

Integrating from 0 to h with respect to z

$$\frac{h \bar{F}_v}{\pi} = - \frac{2Q_v}{sk_v} [\Theta(h) - \Theta(0)] + \int_0^h \frac{1}{sk_v} Q_v \beta(z') \left[e^{-sk_v(h-z')} + e^{-sk_v z'} \right] dz' + \frac{2(1-\epsilon)(1-e^{-sk_v h})}{sk_v [1+(1-\epsilon)e^{-sk_v h}]} \left[\int_0^h Q_v \beta(z') e^{-sk_v z'} dz' \right] \quad (5.89)$$

$$\frac{hs \bar{F}_v}{\pi} = - \frac{2Q_v}{k_v} [\Theta(h) - \Theta(0)] + \frac{2(1-\epsilon)}{k_v [1+(1-\epsilon)e^{-sk_v h}]} \int_0^h Q_v \beta(z') e^{-sk_v z'} dz' \quad (5.90)$$

After integrating (5.89) over frequency, the new function

$$\begin{aligned} \tilde{\Xi}(x) &= \int_0^x \Xi(x) dx = \frac{1}{Q} \int_0^\infty \int_0^x Q_v (1 - e^{-k_v x}) dv dx \\ &= x + \frac{1}{Q} \int_0^\infty \frac{Q_v}{k_v} e^{-k_v x} dv - \frac{1}{Q} \int_0^\infty \frac{Q_v}{k_v} dv \end{aligned} \quad (5.91)$$

is substituted in the form

$$\frac{1}{Q} \int_0^{\infty} \frac{Q_\nu}{k_\nu} e^{-sk_\nu z'} d\nu = \tilde{\zeta}(sz') - sz' + \frac{1}{Q} \int_0^{\infty} \frac{Q_\nu}{k_\nu} d\nu \quad (5.92)$$

into the curly brackets of (5.90), where it is found that the third term on the right-hand side of (5.92) exactly cancels the first term on the right-hand side of (5.90), giving

$$\begin{aligned} \frac{sh\bar{F}}{\pi Q} &= 2(2-\epsilon) \int_0^h \beta(z') \left\{ \left[\hat{\zeta}(sz') - sz' \right] - (1-\epsilon) \left[\tilde{\zeta}(s(z+h)) - s(z'+h) \right] + \right. \\ &\quad \left. + (1-\epsilon)^2 \left[\tilde{\zeta}(s(z'+2h)) - s(z'+2h) \right] \cdot \cdot \cdot \right\} dz' \end{aligned} \quad (5.93)$$

Because of the symmetry of $\beta(z')$,

$$\begin{aligned} \int z' \beta(z') dz' &= \frac{1}{2} \int [z' + (h-z')] \beta(z') dz' \\ &= \frac{h}{2} [\Theta(h) - \Theta(0)] \end{aligned} \quad (5.94)$$

and recalling

$$\begin{aligned} \frac{1}{2-\epsilon} &= \sum_{n=0}^{\infty} (-1)^n (1-\epsilon)^n \\ \frac{(1-\epsilon)}{2-\epsilon} &= \sum_{n=0}^{\infty} (-1)^{n+1} (1-\epsilon)^n \end{aligned}$$

$$\begin{aligned} -2(2-\epsilon) \sum_{n=0}^{\infty} \int_0^h \beta(z') s z' (-1)^n (1-\epsilon)^n &= -2s \int_0^h z' \beta(z') dz' \\ &= -sh [\Theta(h) - \Theta(0)] \end{aligned} \quad (5.95)$$

$$+ 2(2-\epsilon) \sum_{n=0}^{\infty} \int_0^h \beta(z') n sh (-1)^{n+1} (1-\epsilon)^n = \frac{2(1-\epsilon)sh}{2-\epsilon} [\Theta(h) - \Theta(0)] \quad (5.96)$$

and finally

$$\frac{sh \bar{F}}{\pi Q} = 2(2-\epsilon) \int_0^h \beta(z') \left[\tilde{\Sigma}(sz') - (1-\epsilon) \tilde{\Sigma}(s(z'+h)) + \right. \\ \left. + (1-\epsilon)^2 \tilde{\Sigma}(s(z'+2h)) - \dots \right] dz' - \frac{\epsilon}{2-\epsilon} [\Theta(h) - \Theta(0)] sh \quad (5.97)$$

The second term on the right is simply the radiative flux in the absence of intervening material, while the integral contains all the changes caused by the change of optical depth. The integral's convergence is assured by the alternation of sign and the supposition that beyond a certain distance x , $\tilde{\Sigma}(sx)$ varies linearly with x . This latter is another way of stating that beyond a certain point all the radiation that matters is included and that the emissivity has reached a constant limiting value (by definition ≤ 1.0). The convergence, however, is slow for small ϵ .

It is possible to take care of the portion beyond which the function $\tilde{\Sigma}(sx)$ becomes linear in x . Evaluating $\tilde{\Sigma}$ out to the n^{th} term, where it becomes linear, the remainder of the terms in the square brackets in (5.97) may be written

$$Q_n = (-1)^{n+1} \left[(1-\epsilon)^{n+1} (\tilde{\Sigma}_n + \epsilon sh \tilde{\Sigma}_n) - (1-\epsilon)^{n+2} (\tilde{\Sigma}_n + 2sh \tilde{\Sigma}_n) + \dots \right] \quad (5.98)$$

$$= (-1)^{n+1} (1-\epsilon)^{n+1} \left[\frac{\tilde{\Sigma}_n}{2-\epsilon} + \frac{\epsilon_n sh}{(2-\epsilon)^2} \right] \quad (5.99)$$

by again using the relationships (5.94). This correction term may be fairly large, but so long as the linear hypothesis is obeyed, it is an

analytical solution. In practice, the second term in the bracket of (5.99) should be much less than the first, a situation always obeyed for $n \geq 6$.

5.3.2.2 Computation of the Non-Gray Flux

The values of $\tilde{\Sigma}$

$$\tilde{\Sigma}(x) = \int_0^x \tilde{\Sigma}(s) ds$$

were obtained from the data for Σ of Chapter 3 by integration using the trapezoidal rule, and plotted. Values were subsequently picked off the plots for use in the formula (5.97). Consider now

$$\Delta \bar{F} = \frac{\pi Q 2(2-\epsilon) \bar{\beta}}{sh} \int_0^h \frac{\beta(z')}{\beta} \left[\tilde{\Sigma}(sz') - (1-\epsilon) \tilde{\Sigma}(s(z'+h)) + \dots \right] dz' \quad (5.100)$$

By changing to coordinates of ζ , integrals of the type

$$I_n = \int_{-\frac{1}{2}}^{\frac{1}{2}} (A + B \zeta^2 + C \zeta^4) \tilde{\Sigma} \left[sh \left(\zeta + \frac{1}{2} + n \right) \right] d\zeta \quad (5.101)$$

are evaluated and summed in

$$\Delta F_n = \frac{\pi Q 2(2-\epsilon) \bar{\beta}}{sh} \left[\sum_{l=0}^n (1-\epsilon)^l I_l + \mathcal{R}_n \right] \quad (5.102)$$

The integrals I_n were found by evaluating the integrand at $\zeta = 0$, ± 0.25 , ± 0.50 and summed using the 7-32-12-32-7 rule. This was done for values of n up to and including 10. Values of ΔF_n were found for values of $n \leq 10$ with (5.102) and compared to verify convergence.

5.3.2.3 Results of Calculations of Flux Changes

With ΔF calculated as some number times $\bar{\beta}$, it is an easy matter to write

$$F_D = -K\bar{\beta}$$

$$F_R = \frac{-\epsilon}{2-\epsilon} \pi Q h \bar{\beta}$$

At $p = 0$, $\Delta F = 0$, and

$$F_T(0) = -\bar{\beta} \left[\frac{\epsilon}{2-\epsilon} \pi Q h + K \right] \quad (5.103)$$

At a pressure p ,

$$\Delta F(p) \doteq -\frac{\pi Q 2(2-\epsilon)}{s} \bar{\beta} \left[\sum_{i=0}^n (1+\epsilon)^i I_i(p) + R_n(p) \right] \quad (5.104)$$

and

$$\frac{\Delta F(p)}{F_T(0)} \doteq \frac{\frac{\pi Q 2(2-\epsilon)}{s} \left[\sum_{i=0}^n (1-\epsilon)^i I_i(p) + R_n(p) \right]}{\frac{\epsilon}{2-\epsilon} \pi Q h + K} \quad (5.105)$$

The results of the calculations at $h = 1.987$ cm. for several values of pressure are given in Fig. 5-7 and similar results for $h = 5.048$ cm. in Fig. 5-8. In both cases the results have been calculated at three emissivities; the central one ($\epsilon = 0.37$) is the one calculated from measurements in Chapter 2. The outer two illustrate the effect of altered emissivity. The effect is quite large. As noted in 5.2, this change of ϵ has very little effect on $\beta/\bar{\beta}$, and it was found that the change of β

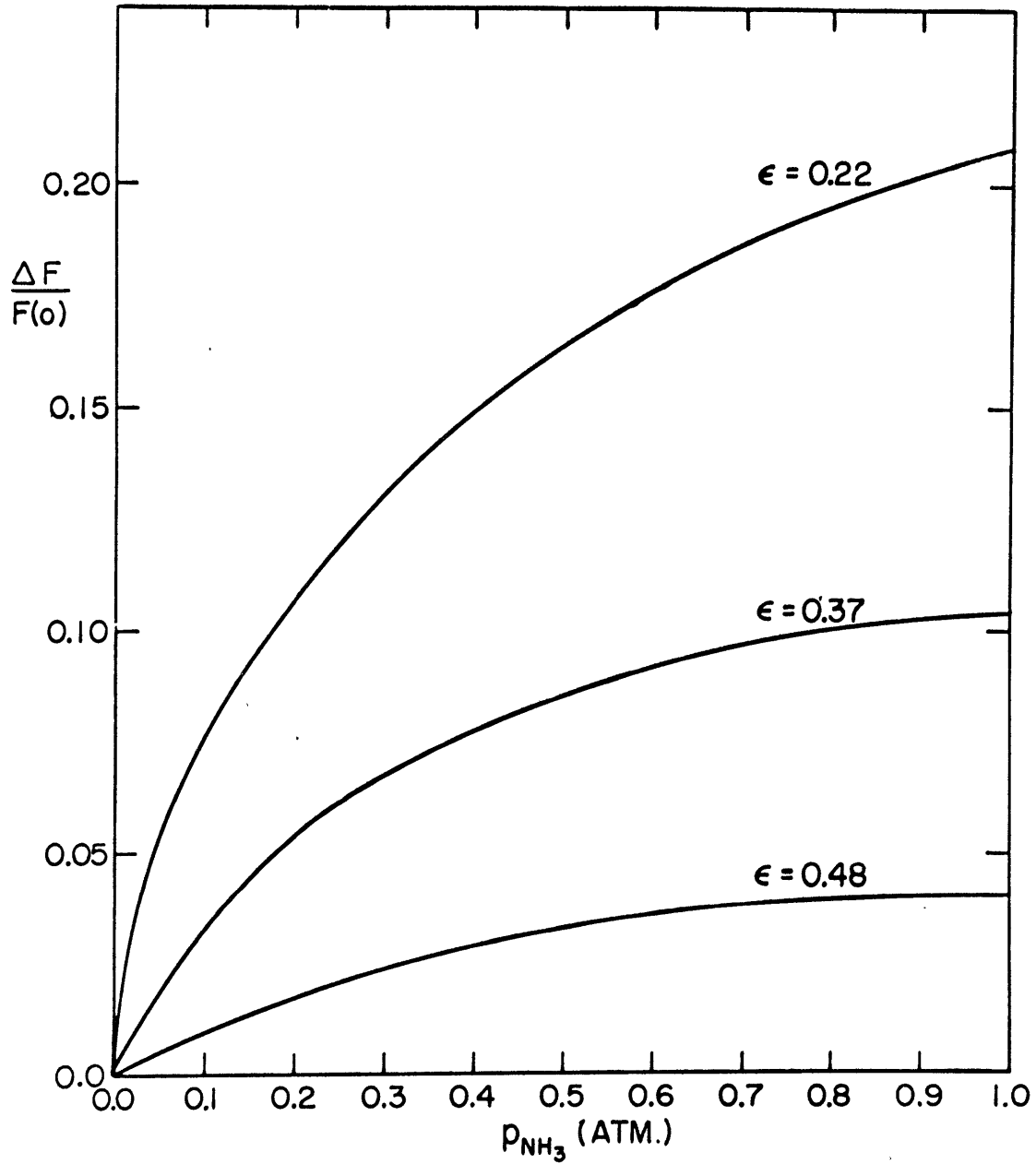


Fig. 5-7. CALCULATED $\frac{\Delta F}{F(0)}$ FOR PURE AMMONIA, $h = 1.987$ cm.

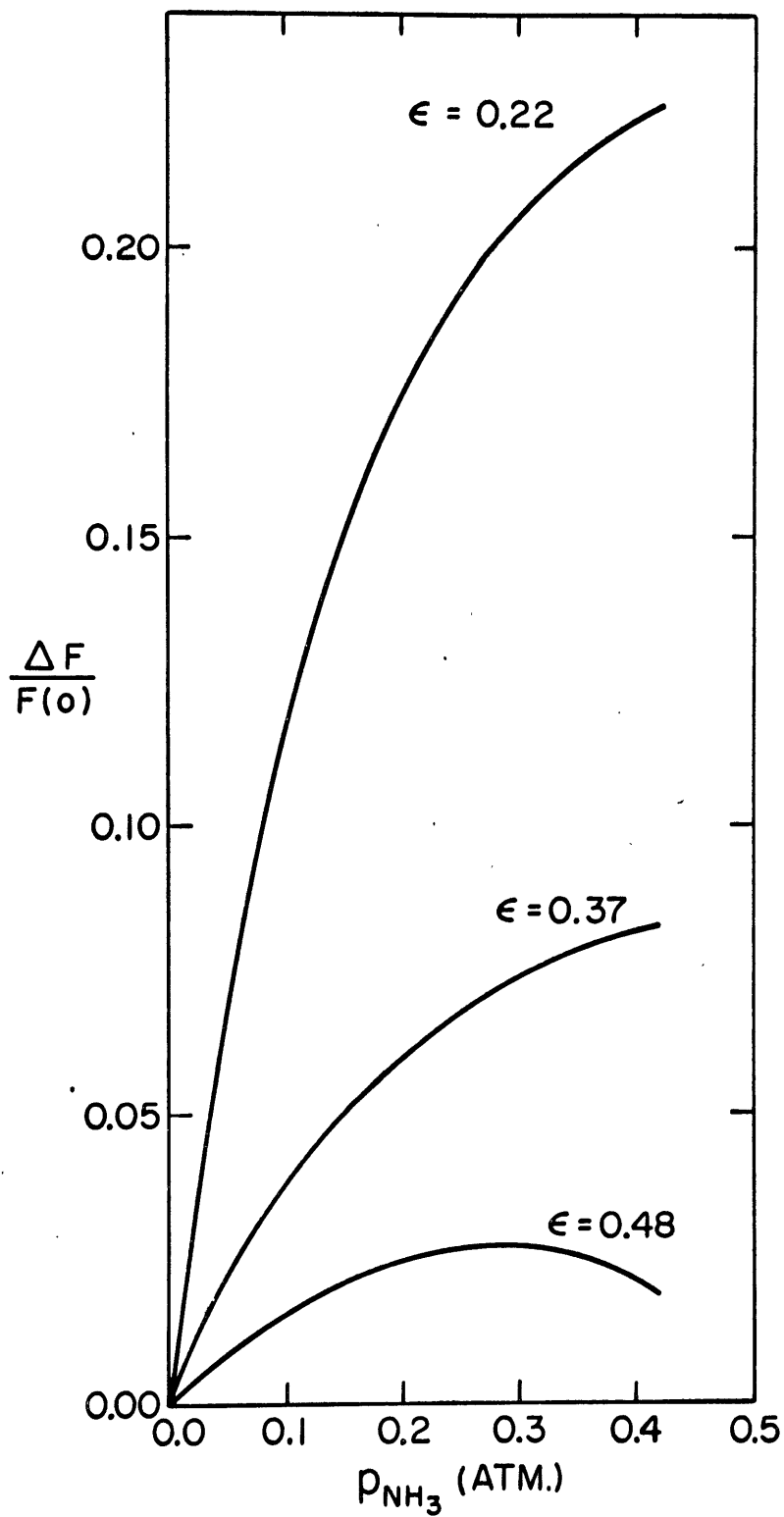


Fig. 5-8. CALCULATED $\frac{\Delta F}{F(0)}$ FOR PURE AMMONIA, $h = 5.048$ cm.

with ϵ produced no change in the integrals. The real effect of emissivity is outside the integrals.

The lines in Figs. 5-7 and 5-8 are drawn smoothly through points that have some scatter. This seems to be due to the nature of the approximations in the radiative data and the sensitivity of the slowly converging sum to these data. By putting in one mean intensity per range, each range has its maximum effect in a rather narrower distance interval than it would with a smoother distribution of line intensities.

5.4 Measurement of the Temperature Distribution

5.4.1 Conditions

Because of the experimental complexity of the measurements of temperature distribution and the slightly different conditions necessary for their maximum accuracy from those of the best heat flux measurements, the two were not made simultaneously. Also, because of limitations of optics sizes, a profile across the whole fluid could be made only at a separation of 1.987 cm.

In order to have a clearly measurable effect, it is desirable to use longer optical paths, which here means higher pressures. Since any effects which distort the temperature are linear in temperature difference, $\Delta\Theta$, it is desirable to use a large value of this also. However, large pressures and temperature differences indicate a large Rayleigh number if the heating is below, and dynamical instability. Since the radiative-diffusive balance holds no matter which way the heat flux is directed, it is clearly better to heat the upper plate.

As the profile cannot be measured at the onset of convection, what is done is to show that in two well-explored cases, the observed profiles can be calculated very exactly. With confidence in the techniques, the profiles are then calculated for conditions at which the onset of convective instability is measured.

Because of the labor of taking and reducing the data, only three runs were taken, one on air as a check in a non-radiative situation, and two in ammonia at different pressures. Each run consisted of taking six photographic plates -- three of the system with gas in it, and three with the system evacuated to give an instrument zero.

The experimental conditions are given in Table 5-2.

Table 5-2
EXPERIMENTAL CONDITIONS FOR TEMPERATURE
DISTRIBUTION MEASUREMENTS

<u>Quantity</u>	<u>Run 1</u>	<u>Run 2</u>	<u>Run 3</u>
Date	Aug. 23, 1963	Sept. 6, 1963	Sept. 16, 1963
Gas	Ammonia	Air	Ammonia
λ_{VAC}	5461 Å	5461 Å	5461 Å
p	53.00 cm.Hg. 0.697 atm.	76.05 cm. Hg. 1.0007 atm.	98.33 cm.Hg. 1.294 atm.
$\Delta\theta$	7.26° C	6.85° C	6.79° C
c_s	3.8442×10^{-4}	2.932×10^{-4}	3.8442×10^{-4}
ρ_o/ρ_s	0.6273	0.9163	1.1825
$(\frac{1}{\rho} \frac{\partial \rho}{\partial \theta})_o$	$1.03457/\theta_o$	$1.00272/\theta_o$	$1.06677/\theta_o$
θ_o	300.60° K	298.07° K	298.06° K

The formula, as derived in Chapter 2, is (2.32)

$$|N_j - N_o| = \frac{2 l_o}{\lambda_{VAC}} c_s \frac{\rho_o}{\rho_s} (\theta_j - \theta_o) \left(\frac{1}{\rho} \frac{\partial \rho}{\partial \theta} \right)_o \quad (5.106)$$

where the expression

$$2 l_o = l$$

has been inserted to enable calculation of the effective length. Because this is a Michelson interferometer, the space is traversed twice, leading to the factor 2 .

The bars indicating means of upper and lower halves have been suppressed, but means will be understood in this chapter.

The expressions $\theta_{10} - \theta_{-10}$ and $\Delta \theta$ will be used interchangeably.

$N_j - N_o$ is measured for $j = 0, 1, 3, 5, 7$, and 9; $\Delta \theta_o = 0$ (the equation is the trivial one $0 = 0$ in this case), $\left(\frac{1}{\rho} \frac{\partial \rho}{\partial \theta} \right)_o$, $\frac{\rho_o}{\rho_s}$, λ_{VAC} and c_s are known, but l_o is uncertain because of the dead space between the plates and the windows, disturbances of temperature within the gas by the walls, and the fact that the edge of the plates may be slightly different in temperature from the center. Thus an effective l_o must be found. Taking means of the fringe measurements of the lower and upper halves forces

$$N_j - N_o = -(N_{-j} - N_o)$$

so that $N_j - N_o$ is an odd function of j . Fitting

$$N_j - N_o = aj + b j^3$$

gives

$$b = (1.72 \pm 37) \times 10^{-5}$$

i.e., b is not statistically significant. Refitting

$$N_j - N_0 = aj$$

gives

$$a = 0.27048 \pm 0.00082$$

and

$$N_{10} - N_0 = 2.7048 \pm 0.0082$$

Using the values from Table 5-2, after straightforward substitution in (5.106), gives

$$l_0 = 23.86 \pm 0.07 \text{ cm.}$$

Note that this is five percent shorter than the physical length of the aluminum plates.

Equation (5.106) can also be put in the form

$$\frac{\theta_j - \theta_0}{\theta_{10} - \theta_{-10}} = \left| \frac{N_j - N_0}{2 \cdot N_{10} - N_0} \right| \quad (5.107)$$

or 1 fringe = 1.27° C .

The normalized linear temperature would be $\frac{(\theta_j - \theta_0)_L}{2(\theta_{10} - \theta_{-10})} = j/20$.

Subtracting the measured temperature from the linear temperature, normalizing, and using the fact that $\bar{\theta} = \theta_0$

$$\frac{\bar{\theta} + \frac{j}{20} \Delta\theta - \theta}{\Delta\theta} = \frac{1}{2} \left(\frac{j}{10} - \frac{N_j - N_0}{N_{10} - N_0} \right) \quad (5.108)$$

The measured data and results of Run 2 are presented in Table 5-3.

Table 5-3
DATA AND RESULTS OF RUN 2 (AIR)

j (1)	$N_j - N_0$ (2)	$\frac{\theta_j - \theta_0}{\Delta \theta}$ (3)	$\frac{-(\theta_j - \bar{\theta} - \frac{j}{20} \Delta \theta)}{\Delta \theta}$ (4)	$\frac{-(\theta_j - \bar{\theta} - \frac{j}{20} \Delta \theta)}{\Delta \theta}$ (5)
10	2.7048	0.5000	0.0000	0.0105
9	2.432 ± 0.018	0.4496	0.0004 ± 0.0033	0.0096
7	1.908 ± 0.015	0.3527	-0.0027 ± 0.0027	0.0046
5	1.340 ± 0.014	0.2477	0.0023 ± 0.0025	0.0074
3	0.804 ± 0.010	0.1486	0.0014 ± 0.0018	0.0044
1	0.274 ± 0.009	0.0506	-0.0006 ± 0.0016	0.0004

The second column in Table 5-3 gives the measured fringe displacements with their standard deviations. The third column gives the fringe displacement at each j relative to the total displacement from center to boundary. The near-linearity is very clear. The fourth column contains the difference between the measured temperature and the linear temperature with its standard deviation. All of the measured points lie within one standard deviation on the linear gradient.

This serves as a validation of the instrument and procedure. The numbers in column (5) are those that would obtain if $l_0 = 24.36$ were used.

The $N_j - N_0$ for NH_3 can be well fit by a curve of the form

$$N_j - N_0 = aj + b j^3$$

The extrapolation of these values to $N_{10} - N_0$ yields values of l_0 that are larger than those for air, but these curves contain only j^3 terms, while the theoretical curves contain ζ (i.e., j^5) terms. To fit a curve which had a j^5 term would almost certainly lead to a coefficient of no statistical significance. Since the effect of these terms would be felt most strongly in the boundary (0.05 h), a value of $N_{10} - N_9$ has been taken from the calculated curves and added to $N_9 - N_0$ to give $N_{10} - N_0$. Substitution of these values in (5.107) with the numerical values of Table 5-2 gives determinations of $l_0 = 24.31 \pm 0.24$ cm. for Run 1, and $l_0 = 24.38 \pm 0.12$ cm. for Run. 3 Using the weighted mean value $l_0 = 24.36$ cm., the data and results for ammonia are given in Tables 5-4 and 5-5.

Straightforward substitution of the above values in (5.106) yields

$$\theta_j - \theta_0 = 1.349 |N_j - N_0|$$

or 1 fringe = 1.35° C in Run 1.

For ammonia at $p = 98.33$ cm.Hg., putting the data of Table 5-2 into (5.106) yields

$$\theta_j - \theta_0 = 0.6882 |N_j - N_0|$$

or 1 fringe = 0.69° C in Run 3.

The explanation of the column contents in Tables 5-4 and 5-5 is the same as that for Table 5-3.

Photographs of fringes in the different cases are shown in Fig. 5-9.

The interferometer temperature results are presented in Fig. 5-10, where the deviations from the linear gradient as a fraction of total

Table 5-4
 DATA AND RESULTS OF RUN 1
 Ammonia, p = 53.00 cm.Hg.

j (1)	$N_j - N_0$ (2)	$\frac{N_j - N_0}{2(N_{10} - N_0)}$ (3)	$-\frac{(\theta - \bar{\theta} - \frac{j}{20} \Delta\theta)}{\Delta\theta}$ (4)
10	2.682	0.4990	0.0010
9	2.330 ± 0.026	0.4335	0.0165 ± 0.0048
7	1.758 ± 0.016	0.3271	0.0229 ± 0.0030
5	1.215 ± 0.009	0.2260	0.0240 ± 0.0017
3	0.707 ± 0.009	0.1315	0.0185 ± 0.0017
1	0.234 ± 0.004	0.0435	0.0065 ± 0.0007

Table 5-5
 DATA AND RESULTS OF RUN 3
 Ammonia, p = 98.33 cm.Hg.

j (1)	$N_j - N_0$ (2)	$\frac{\theta_j - \theta_0}{\Delta\theta}$ (3)	$-\frac{(\theta - \bar{\theta} - \frac{j}{20} \Delta\theta)}{\Delta\theta}$ (4)
10	4.933	0.5004	-0.0004
9	4.240 ± 0.023	0.4301	0.0199 ± 0.0023
7	3.168 ± 0.015	0.3214	0.0286 ± 0.0015
5	2.175 ± 0.013	0.2206	0.0294 ± 0.0013
3	1.276 ± 0.017	0.1294	0.0206 ± 0.0017
1	0.417 ± 0.020	0.0423	0.0077 ± 0.0020

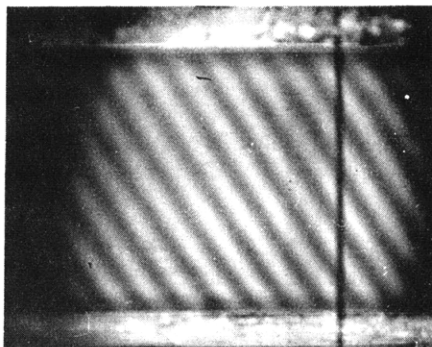
Figure 5-9
(following page)

PHOTOGRAPHS OF INTERFEROMETER FRINGE

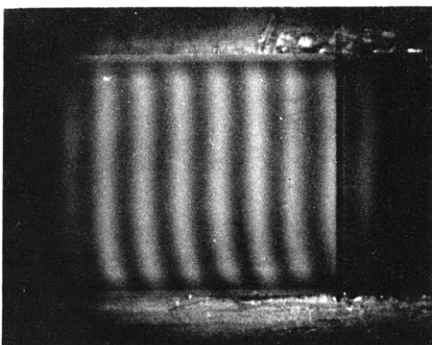
The experimental conditions are as follow:

- | | | |
|------------|-------------------|-------------------------------|
| a. Air | p = 76.05 cm. Hg. | $\Delta\theta = 6.85^\circ$ C |
| b. Ammonia | p = 53.00 cm. Hg. | $\Delta\theta = 7.26^\circ$ C |
| c. Ammonia | p = 98.33 cm. Hg. | $\Delta\theta = 6.79^\circ$ C |

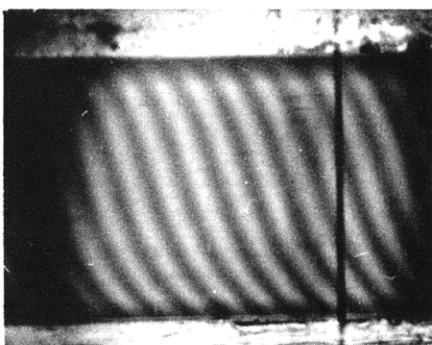
FIDUCIAL
MARK
I



a.



b.



c.

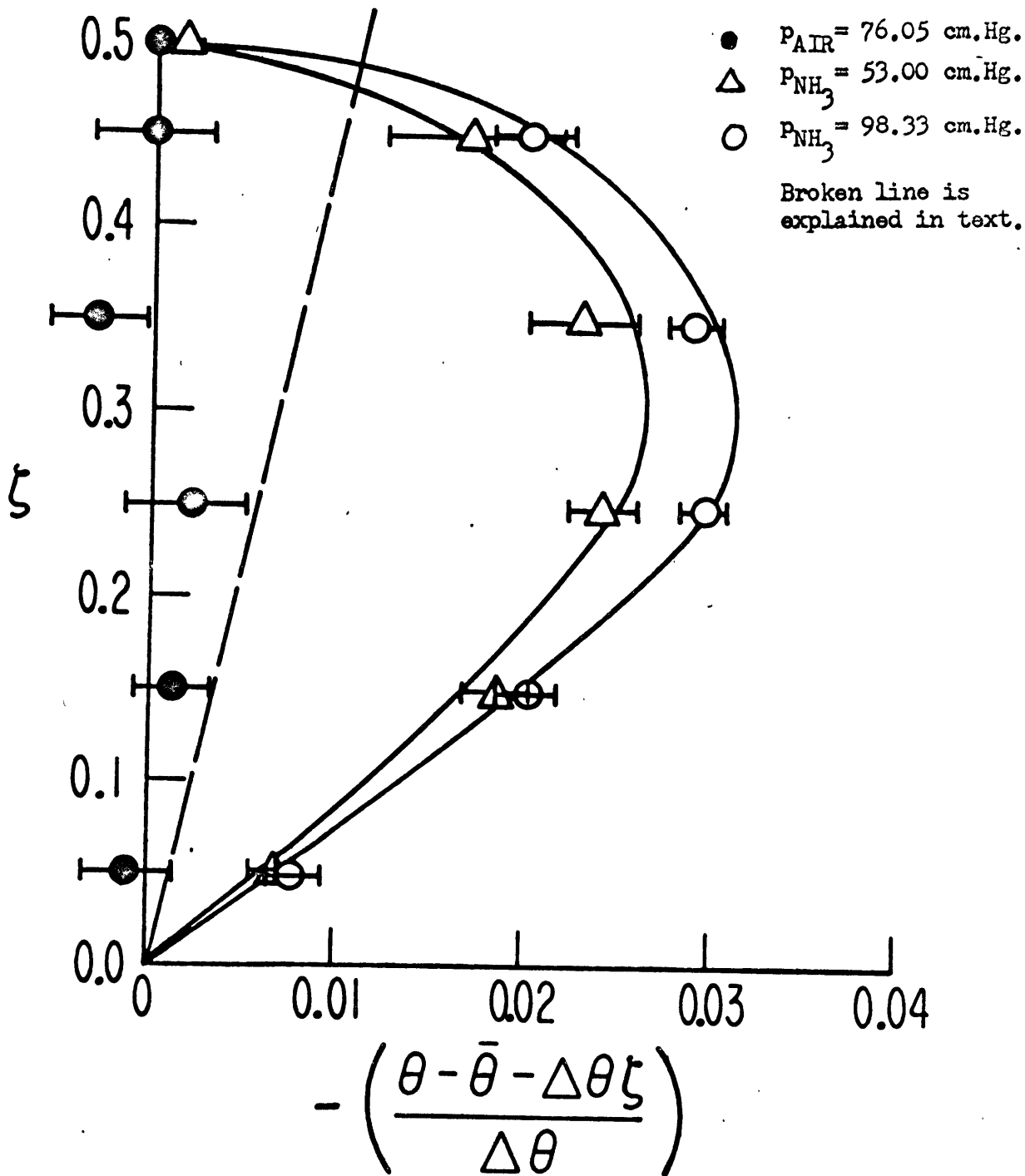


Fig. 5-10. MEASURED TEMPERATURE PROFILES IN AIR AND AMMONIA

Plate spacing 1.987 cm., $\Delta\theta \doteq +7^\circ \text{ C.}$ The full lines are computed. The points are measured and the horizontal lines indicate probable errors. $l_0(\text{NH}_3) = 24.36 \text{ cm.}$ $l_0(\text{air}) = 23.86 \text{ cm.}$ $\epsilon = 0.417.$

temperature drop, $\frac{\bar{\theta} + \frac{j}{20} \Delta\theta - \theta}{\Delta\theta}$, is plotted as a function of $\zeta = j/20$. The results for air are presented for $l_0 = 23.86$ cm., and grouped around the line of zero deviation. They would cluster around the broken line if $l_0 = 24.36$ cm. were used for the air results.

The ammonia results are presented using $l_0 = 24.36$ cm., and can be seen to agree strikingly with the theoretical curves calculated for these particular cases by the methods of 5.2, and using $\epsilon = 0.417$.

5.4.3 Precision of the Temperature Measurements

5.4.3.1 Relative Precision

The relative temperature distribution is given in this system by

$$\frac{\theta_j - \theta_0}{\theta_{10} - \theta_0} = \frac{1}{2} \frac{N_j - N_0}{N_{10} - N_0} \quad (5.108)$$

$$\frac{\theta_j - \theta_0}{\theta_{10} - \theta_0} = \frac{N_j - N_0}{N_{10} - N_0} \quad (5.109)$$

The quantity $\theta_{10} - \theta_0 = \frac{1}{2} \Delta\theta$ was measured to $0.01^\circ\text{C}/7^\circ\text{C}$, about 0.15 percent. $N_j - N_0$ was measured to between $0.015 - 0.020$ fringe, from $0.28 - 0.37$ percent of the total fringe change. The accuracy with which $\theta_j - \theta_0$ is known then clearly depends on how well $N_{10} - N_0$ is known.

For air, a straight line of the form

$$N_j - N_0 = \hat{a} j$$

was fitted to obtain $\hat{a} = 0.27048 \pm 0.0082$. This of course makes

$$N_{10} - N_0 = 2.7048 \pm 0.0082$$

an uncertainty of 0.3 percent.

This scheme assumes that l_0 is independent of j . One way of interpreting the uncertainty of $N_{10} - N_0$ is as an uncertainty of l_0 . The results obtained here, that with the best l_0 the deviations from the linear gradient are random and of the order of 0.02°C , would indicate that an l_0 independent of j is a very reasonable assumption.

The procedure for ammonia has been described above. It is more open to question but essentially is the same procedure used with air, except that the measured $N_9 - N_0$ was used with the theoretical $\frac{\bar{\theta} + \frac{9}{20} \Delta\theta - \theta}{\Delta\theta}$ to give $N_{10} - N_0$.

The reasons why $N_{10} - N_0$ cannot be measured directly are:

1. Reflection from the plates at the boundaries blurs the fringes.
2. Refraction in the boundary layers makes it unclear what mean layer is being sampled.
3. Because the edge is asymmetric with respect to the line $j = \pm 10$, the value measured there is actually an average through the region that should be assigned to a position in that region, not on its boundary.
4. The fringes are highly tilted, reducing the contrast between peak and trough on the densitometer trace (due to the finite size of the sampled area) and making any uncertainty of mean height of the traversing light very important.

5. Because of the finite height of the scan, it is impossible to get a reading which corresponds to the edge in any case.

Thus, for relative precision, if there is a way of obtaining the $N_{10} - N_0$ with the $\theta_{10} - \theta_0$, or indeed measuring both temperature and fringes at any two points with accuracy, this procedure will measure deviations to 0.25 percent as a limit. The limiting value when $N_{10} - N_0$ is not known with unlimited accuracy will be of course lower. Equivalent to measuring $N_{10} - N_0$ is measuring interferometrically or adequately guaranteeing l_0 . Then different states in the same fluid under similar conditions can be compared and their difference will have this precision.

5.4.3.2 Absolute Precision

A measure of the absolute precision might be obtained from the variations of l_0 between different cases. Collecting the previous results,

$$l_0 \text{ (Run 1)} = 24.31 \text{ cm.}$$

$$l_0 \text{ (Run 2)} = 23.86 \text{ cm.}$$

$$l_0 \text{ (Run 3)} = 24.38 \text{ cm.}$$

$$l_0 \text{ (mean)} = 24.18 \text{ cm.}$$

The maximum deviation from this is 1.36 percent. For a temperature difference of about 7° C , such as obtained here, this would amount to 0.10° C , or 0.0068 in the plots of $\frac{\bar{\theta} + \zeta \Delta \theta - \theta}{\Delta \theta}$ at $\zeta = 0.5$. This kind of change is equivalent to turning the gradient line, still a straight line, until the end is displaced by $\pm 0.10^\circ \text{ C}$

on a plot of θ vs. ζ , or by 0.0068 on a plot of $\frac{\bar{\theta} + \zeta \Delta\theta - \theta}{\Delta\theta}$ vs. ζ .

This is a reflection of the fact that l_0 cannot be controlled completely with this apparatus, and that $\frac{\rho_0}{\rho_s}, \left(\frac{1}{\rho} \frac{\partial \rho}{\partial \theta}\right)_0$, and c_s are not known with great enough absolute accuracy. Comparison of different states of the same fluid is much more accurate than the same state in different fluids.

Instrumental difficulties, such as turbulence in the portion of the interferometer arm exterior to the tank, vibration, or drift in interferometer dimensions apparently were not serious for these measurements. The three $N_j = N_0$ plates in a given situation were generally within 0.02 fringe of each other and showed no systematic trends relative to one another.

5.4.4 Commentary on the Temperature Profile Measurements

Interferometric techniques have been used by Kennard [1941] and Croft [1958] previously, but only to 0.1°C and 0.2°C respectively. Both recognized the need to apply end corrections. Kennard guessed several forms for his. Croft measured an end correction and read his temperatures to 0.2°C , but since he plotted on a very condensed scale, no accurate numbers are presented.

Thus, in this experiment the techniques have been applied with a precision five times that previously recorded, or 0.02°C . The apparent difficulties of knowing l_0 , or what is equivalent, $N_{10} = N_0$, are rather serious and indicate that special precautions must be taken; i.e., physical dimensions cannot be used without making certain that they are applicable by calibrating the interferometer with a known profile. To

this accuracy also, the refractive indices and equations of state are not well enough known for different fluids, indicating that a separate "calibration" is necessary for each one.

The results presented in this section indicated that the temperature profiles existing in the fluid can be calculated with the techniques of Sec. 5.2, and thus these techniques can be applied to the cases of interest in Chapter 6 at the onset of convection.

Of great interest is the fact that this is the first laboratory demonstration of the validity of some of the techniques used in studies of atmospheric radiation -- use of an emissivity or transmission function for different bands to treat the non-grayness of the atmosphere, and the use of the diffusivity factor to treat the angular integral of intensity. These cannot be tested in the atmosphere because of non-static conditions. Here, if only in the case of small length scales, they have received their first confirmation.

5.5 Measurements of Static state Heat Flux

5.5.1 Heat Flux in Air

The process of converting the measured temperature differences $\Delta\theta_{12}$, $\Delta\theta_{34}$, and $\Delta\theta$ to \bar{S} has been detailed in Chapter 2. These, for nonconvecting cases, were plotted against pressure in Fig. 2-2. Since no pressure dependence is expected and no statistically significant pressure dependence is observed, the mean is the simple mean. The values are those used in Chapter 2 to solve for ϵ and $1/f$.

5.5.2 Heat Flux in Ammonia

The values of nonconvecting \bar{S} are plotted against pressure for ammonia in Fig. 5-11. In this case it is quite apparent that a pressure dependence exists, a fact which is also clear on the raw $\Delta\Theta$'s and was noticed in the first ammonia runs. Also shown on the axis are the intercepts, $\bar{S}_2(0) = 0.3312$ and $\bar{S}_5(0) = 0.2284$, which were obtained by fitting the curves in Figs. 5-7 and 5-8 for $\epsilon = 0.37$ (adjusted to the proper scale) to the data. Ideally, these should be calculable from $1/f$, ϵ , and K_{NH_3} . This proved to give results in slight disagreement with the data, and instead the best values of the intercepts were used to calculate a K_{fit} . The temperature corrections were first made according to the data in Table 5-6 (assuming the same temperature dependence for K_{fit} as for K_{NH_3}).

Table 5-6

DATA FOR CALCULATION OF $\bar{S}(0)$ FOR AMMONIA

Plate Separation [cm.]	$^{\circ}K$	No. of Cases	$K(\Theta)$ $\frac{\text{erg} \times 10^3}{\text{cm. sec. deg.}}$	$\frac{K(\Theta)}{K(25^{\circ})}$	$\frac{(\Theta+273.16)^3}{(298.16)^3}$
5.048 ± 0.006	296.99	34	2.411	0.9960	0.9883
	297.99	37	2.420	$\frac{0.9995}{0.9978}$	$\frac{0.9983}{0.9935}$
1.987 ± 0.002	301.21	118	2.448	1.0113	1.0309
	298.81	48	2.428	$\frac{1.0028}{1.0088}$	$\frac{1.0066}{1.0239}$

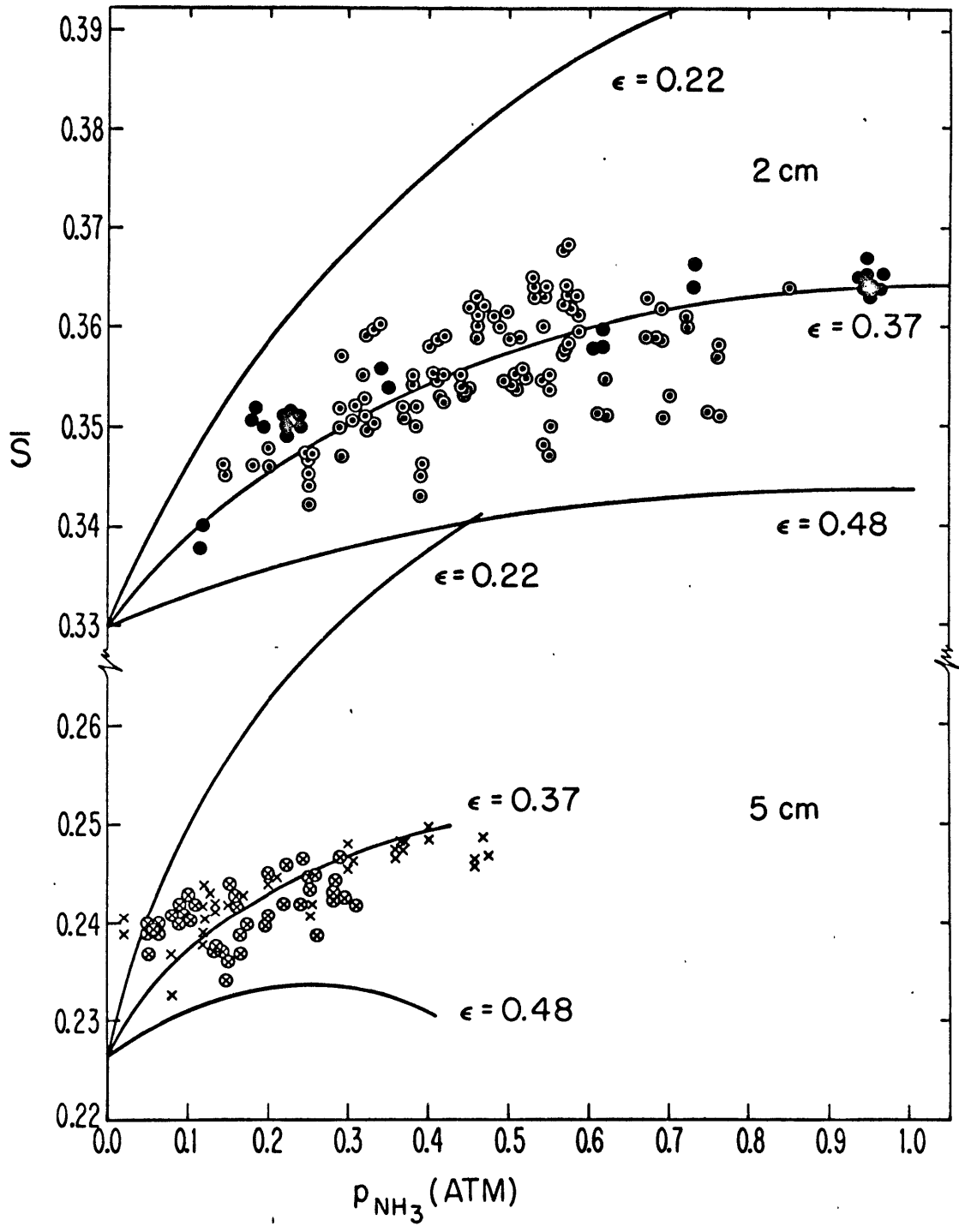


Fig. 5-11. MEASURED HEAT FLUX IN PURE AMMONIA AS A FUNCTION OF PRESSURE

● h = 1.987 cm. x h = 5.048 cm.

Ringed points are for upward fluxes. Lines are theoretical curves from Figs. 5-7 and 5-8.

Using the constants of Chapter 2 and the relationship

$$\bar{S} = f \left(\frac{K}{h} + Q \right) \quad (5.110)$$

the K_{fit} are now calculated to be

$$K_{fit} (2 \text{ cm.}) = 2.400 \times 10^3 \frac{\text{erg}}{\text{cm. sec. deg.}} \quad (-0.867 \text{ pct. from } 2.421 \times 10^3) \quad [\text{Ch.4}]$$

$$K_{fit} (5 \text{ cm.}) = 2.232 \times 10^3 \frac{\text{erg}}{\text{cm. sec. deg.}} \quad (-7.81 \text{ pct. from } 2.421 \times 10^3) \quad [\text{Ch.4}]$$

The value for $h = 1.987$ cm. is well within the uncertainty of measurement. The discrepancy at $h = 5.048$ cm. merely means that at 5 cm. the apparatus does not function well as a device to measure absolute conductivities, that there are leakages and edge effects that now become important. (Even here, since a detailed analysis shows that these intercepts depend on K_{NH_3}/K_{air} and each of the conductivities may be off by 4 percent, 6 percent of the difference could be inaccurate data.)

Also on Fig. 5-11 the calculated fluxes are plotted as the solid lines on the same scales. The agreement is reasonable. The integrals of 5.3 have enabled the calculation of the change in heat transfer caused by the changes wrought in the radiation field due to the interaction with the infra-red active material. This calculation certainly gives changes of the right sign and magnitude. While not as striking as the temperature profile measurements, the agreement must be regarded as satisfactory and some corroboration of meteorological procedures for obtaining fluxes.

5.6.3 Commentary on Heat Flux Measurements and Calculations

With the agreement between the calculated heat flux and measurements, justification is found for predicting the heat flux at the onset of convection. Data was at hand from beyond the onset point, derived from situations in which heating was applied above, but the nature of the interpolation now has a theoretical guide, making possible a more confident location of the onset point.

This appears to be the first measurement of the pressure effect on heat flux. It is surprising that it has not been observed before by those making measurements of gas conductivity for infra-red active gases -- especially NH_3 , CO_2 , CO , H_2O , and H_2S , which have rather large emissivities. The answer is probably that due to the use of small dimensions, low pressures, and thin tubes with concentric wires for modern gas-conductivity measurements rather than this sort of Lee's disc apparatus, the effects were quite small.

This effect could be of importance for heat transfer in industrial apparatus, especially those with non-black boundaries, although dynamic effects would certainly have to be taken into account.

The effect itself is perhaps worthy of some study to verify the effect of h , ϵ , and pressure. In particular, one would like to find the transition region in which increasing the pressure causes an increase, then a decrease of K_{eff} . It also seems possible that a series of measurements like this might be inverted to give direct information of $\xi(\kappa)$ for gases and mixtures. This could be useful for gases whose spectral characteristics are not as well explored as ammonia.

As for the temperature profiles, there is interest in the fact that this is the first verification of the approximations used in atmospheric radiation calculations for fluxes. Again, this means the use of emissivities and related functions to take care of the integrations over frequency and the diffusivity factor for the integration over zenith angle. Experimental underpinning, at least for small scales, has now appeared.

While it is true that temperature and flux calculations were based on solid physical principles and empirical observations, it is nonetheless comforting that they hold so well in a closely defined laboratory system.

CHAPTER 6

THE ONSET OF CONVECTION

6.1 Introduction

The difficulties of doing an exact non-gray treatment of convection are shown. Since the physical principles are believed well understood, the stabilization is divided into the part due to the non-constant gradient, S_{β} , and the part due to the radiative dissipation of temperature perturbations, S_H . A method of Chandrasekhar is used to calculate S_{β} . A dimensional argument shows how S_H may be calculated if the radiative dissipation time is known. This is expressed and calculated for ammonia. The measurement of the critical Rayleigh number and data reduction is then described. The results of the measurements of critical Rayleigh number and radiative stabilizations are presented and discussed.

6.2 The Problem of Convective Onset

In Goody's [1956] treatment of convective onset in a radiating fluid, as noted in Chapter 1, there were two causes of stabilization: the more rapid dissipation of temperature fluctuations by radiation and diffusion than by diffusion alone, and the concentration of the gradient into the boundary layers in the initial static state. The same features were appearing in Spiegel's [1960] treatment, but by considering only $\beta = \bar{\beta}$, he eliminated the gradient stabilization. These two causes of stabilization are expected for the non-gray case also.

One might expect that the same type of use of emissivities as in Chapter 5 could be used to express H' , the rate of perturbation temperature change. What is actually needed is the perturbation rate of temperature change as a function of wave number

$$a^2 = a_x^2 + a_y^2$$

for a temperature disturbance of the form

$$\Theta(x, y, z) = \Theta(\zeta) e^{i(a_x \xi + a_y \eta)} \quad (6.1)$$

For a gray medium and this form of temperature disturbance, Spiegel [1960] showed that

$$\rho c_p H' = 4\pi k Q \int_{F'} \Theta(F) \left[\frac{e^{-k|\bar{r}-\bar{r}'|}}{4\pi|\bar{r}-\bar{r}'|^2} \delta(\bar{r}-\bar{r}') \right] dV(F') \quad (6.2)$$

$$H'(\zeta) = \frac{4\pi k Q}{\rho c_p} \frac{kh}{2} \int_{-1/2}^{1/2} \left\{ \int_{\sqrt{1+\frac{(kh)^2}{a^2}}}^{\infty} \frac{e^{-a|\zeta-\zeta'|/s}}{\sqrt{s^2-1}} ds - \delta(\zeta-\zeta') \right\} \Theta(\zeta') d\zeta' \quad (6.3)$$

He remarks that the integral over s is an incomplete special Hankel function of zeroth order.

The ingenious process by which Spiegel went from (6.1) and (6.2) to (6.3) unfortunately does not seem to be immediately convertible to the non-gray case in forms like those seen previously. Much of his analysis can be altered to a general non-gray form, but more work needs to be done to allow a non-gray solution making use of perturbation emissivities.

Another approach would seem to be through machine methods, which make possible the calculation of numerical kernels

$$K_N(p, a^2, \zeta - \zeta')$$

which could be used in the form

$$H'(\zeta_j) \propto \sum_i K_N(p, a^2, \zeta_j - \zeta'_i) \Theta(\zeta_i) \propto \sum_i K_N(p, a^2, |\zeta_j - \zeta'_i|) (D^2 - a^2)^2 \omega_i(\zeta'_i)$$

to solve for the critical Rayleigh number. The K_N would presumably be calculated from the $\xi'(r, p)$ and $\xi(r, p)$ of Chapter 3.

The complexity of Spiegel's calculations, even with a closed form for the kernel in (6.3), and the consequent inability to do very much mathematically with the results lead one to look for another approach. Spiegel provides a valuable suggestion with his dimensional argument, which will be taken up later.

Consider the equations of the classic Rayleigh problem [see Pellew and Southwell, 1940] after the assumptions of exchange of stabilities, horizontal periodicities, and non-dimensionalization:

$$(D^2 - a^2)^2 w = - \frac{g \alpha h^2}{\nu} a^2 \Theta = F \quad (6.4)$$

$$\underline{H} \Theta = \beta w \quad (6.5)$$

with boundary conditions $w = Dw = F = 0$, $\zeta = \pm 1/2$, where \underline{H} is a linear operator, relating the temperature rate of change at any point to the temperature throughout the fluid. Equation (6.5) may be written

$$\begin{aligned} \underline{\underline{H}} F &= \underline{\underline{H}} (D^2 - a^2)^2 W = - \frac{g \alpha h^2 \bar{\beta} a^2}{\nu} \frac{\beta}{\beta} w \\ &= Ra \frac{a^2 K}{h^2 \rho c_p} \frac{\beta}{\beta} w \end{aligned} \quad (6.6)$$

This is the form for the generalized heating in the eigenvalue problem governing convective instability.

Bisshopp[1960] has shown the existence of several stationary principles for a system of equations like (6.5) and (6.6), which may be written

$$\begin{aligned} (D^2 - a^2)^2 W &= F \\ \underline{\underline{H}} F &= Ra \frac{a^2 K}{h^2 \rho c_p} \frac{\beta}{\beta} w \end{aligned} \quad (6.7)$$

$(D^2 - a^2)^2$ is self-adjoint [Ince, 1944]. $\underline{\underline{H}}$ is also self-adjoint for diffusion, $(D^2 - a^2)$ [Ince, 1944], and for radiation [Spiegel, 1958].

Bisshopp has shown that a set of adjoint equations may be written immediately, which here are

$$\begin{aligned} (D^2 - a^2)^2 \tilde{W} &= \frac{\beta}{\beta} \tilde{F} \\ \underline{\underline{H}} \tilde{F} &= Ra \frac{a^2 K}{h^2 \rho c_p} \tilde{w} \end{aligned} \quad (6.8)$$

with boundary conditions $\tilde{w} = D\tilde{w} = \tilde{F} = 0$ at $\zeta = \pm 1/2$. One can then prove that for

$$Ra = \frac{h^2 \rho c_p}{K} \frac{\int_{-1/2}^{1/2} \tilde{F} \underline{\underline{H}} (D^2 - a^2)^2 w d\zeta}{a^2 \int_{-1/2}^{1/2} \tilde{F} \frac{\beta}{\beta} w d\zeta} \quad (6.9)$$

$$Ra = \frac{h^2 \rho c_p}{K} \frac{\int_{-1/2}^{1/2} w \frac{H}{F} (D^2 - a^2)^2 \tilde{F} d\zeta}{a^2 \int_{-1/2}^{1/2} \frac{\beta}{\tilde{F}} w d\zeta} \quad (6.10)$$

Ra is stationary when (6.7) and (6.8) are satisfied. The forms (6.9) and (6.10) are equivalent. Note that the perturbation smoothing stabilization is in the numerator and the gradient stabilization in the denominator.

A standard way [Chandrasekhar, 1961] of solving equations of this sort is, because of the boundary conditions on F , to write

$$F = \sum_{n=1}^{\infty} A_n \cos[(2n+1)\pi \zeta] \quad (6.11)$$

The first equation of (6.7) becomes

$$(D^2 - a^2)^2 w = \sum_{n=1}^{\infty} A_n \cos[(2n+1)\pi \zeta] \quad (6.12)$$

which can be solved, because of the linearity, to give

$$w = \sum_{m=1}^{\infty} A_m w_m(\zeta) \quad (6.13)$$

where w_m is a solution of

$$(D^2 - a^2)^2 w_m = \cos[(2m+1)\pi \zeta] \quad (6.14)$$

satisfying $w_m = Dw_m = 0$, $\zeta = \pm 1/2$.

Substituting (6.11) and (6.13) in the second of (6.7) gives

$$\sum_m \underline{H} A_m \cos[(2m+1)\pi\zeta] = \frac{Ra a^2 K}{h^2 \rho c_p} \frac{\beta}{\beta} \sum_m A_m w_m(\zeta) \quad (6.15)$$

Chandrasekhar multiplies by $\cos(2n+1)\pi\zeta$, and integrates to get

$$\begin{aligned} A_m \int \cos[(2n+1)\pi\zeta] \underline{H} \cos[(2m+1)\pi\zeta] \\ = \frac{Ra a^2 K}{h^2 \rho c_p} \sum A_m \left(n \left| \frac{\beta}{\beta} \right| m\right) \end{aligned} \quad (6.16)$$

where

$$\int_{-1/2}^{1/2} \cos[(2n+1)\pi\zeta] \frac{\beta}{\beta} w_m(\zeta) d\zeta = \left(n \left| \frac{\beta}{\beta} \right| m\right)$$

This gives a secular determinant in the A_m 's, which can be solved for Ra . Very often the calculation is extended to no more than one term, however. This indicates

$$Ra = \frac{h^2 \rho c_p}{K} \frac{\frac{1}{2} \int_{-1/2}^{1/2} \cos(\pi\zeta) \underline{H} \cos(\pi\zeta) d\zeta}{a^2 \int_{-1/2}^{1/2} \cos(\pi\zeta) \frac{\beta}{\beta}(\zeta) w_0(\zeta) d\zeta} \quad (6.17)$$

which is just what (6.9) would give if the substitution

$$\tilde{F}_0 = \cos \pi \zeta \quad (6.18)$$

suggested by the boundary conditions is made. (A term of the form $\cos \pi \zeta$ exists in this formulation for diffusion. See Reid and Harris, [1958].)

To the accuracy of this computation, there is no difference between the formulation for constant or non-constant gradients, aside from the factor

in the denominator. This suggests that to the accuracy he finally used, Spiegel could have retained non-constant gradients.

This also points out that Chandrasekhar's [1961] matrix formulation is a systematic way of exploiting the stationary formulation embodied in (6.9). This equation can now be written

$$\frac{Ra_c}{Ra_c(\text{diff})} = S_{+} S_{\beta} \quad (6.19)$$

where

$$S_{\beta} = \frac{\int_{-1/2}^{1/2} \tilde{F} w d\zeta}{\int_{-1/2}^{1/2} \tilde{F} \frac{\beta}{\beta}(\zeta) w d\zeta} \quad (6.20)$$

contains the effects of the gradient stabilization and boundary conditions but not the heat transfer mechanism, while

$$S_{+} = \frac{\frac{h^2 \rho c_p}{Ka^2} \int_{-1/2}^{1/2} \tilde{F} \underline{H} (D^2 - a^2)^2 w d\zeta}{Ra_c(\text{diff}) \int_{-1/2}^{1/2} \tilde{F} w d\zeta} \quad (6.21)$$

gives the stabilization due to the change in heat transfer mechanism for a fluid with a constant gradient.

6.3 Calculation of S_{β}

To evaluate S_{β} (for rigid boundaries)

$$S_{\beta} = \frac{\int_{-1/2}^{1/2} \tilde{F} w d\zeta}{\int_{-1/2}^{1/2} \tilde{F} \frac{\beta}{\beta} w d\zeta} = \frac{\sum_m \sum_n \int_{-1/2}^{1/2} \cos[(2n+1)\pi\zeta] w_m(\zeta) d\zeta}{\sum_m \sum_n \int_{-1/2}^{1/2} \cos[(2n+1)\pi\zeta] \frac{\beta}{\beta}(\zeta) w_m(\zeta) d\zeta} \quad (6.22)$$

with, as before,

$$\frac{\beta}{\beta} = A + B \zeta^2 + C \zeta^4 \quad (6.23)$$

gives

$$S_{\beta} = \frac{\sum_m \sum_n (n|m)}{\sum_m \sum_n [A(n|m) + B(n|\zeta^2|m) + C(n|\zeta^4|m)]} \quad (6.24)$$

where

$$(n|\zeta^s|m) = \int_{-\frac{1}{2}}^{\frac{1}{2}} \cos[(2n+1)\pi\zeta] \zeta^s w_m(\zeta) d\zeta$$

Chandrasekhar gives

$$w_m(\zeta) = P_m \cosh(a\zeta) + Q_m \zeta \sinh(a\zeta) + \frac{\cos[(2m+1)\pi\zeta]}{[(2m+1)^2\pi^2 + a^2]^2}$$

$$P_m = (-1)^{m+1} \frac{(2m+1)\pi \gamma_{2m+1}^2}{a + \sinh a} \sinh \frac{a}{2}$$

$$Q_m = (-1)^m \frac{2(2m+1)\pi \gamma_{2m+1}^2}{a + \sinh a} \cosh \frac{a}{2} \quad (6.25)$$

$$(n|m) = \frac{1}{2} \gamma_{2m+1}^2 \delta_{mn} - 8a (-1)^{m+n} \frac{(2n+1)(2m+1)\pi^2 \gamma_{2n+1}^2 \gamma_{2m+1}^2}{1} \frac{\cosh^2 \frac{a}{2}}{\sinh a}$$

$$\gamma_{2m+1}^2 = \frac{1}{(2m+1)^2 \pi^2 + a^2}$$

One finds

$$(n|\zeta^2|m) = \left[\frac{1}{24} - \frac{1}{4(2n+1)^2\pi^2} \right] \gamma_{2m+1}^2 \delta_{mn} - (-1)^{n+m} \frac{(2m+1)(2n+1)\pi^2 \gamma_{2m+1}^2 \gamma_{2n+1}^2}{a + \sinh a}$$

$$\times \left\{ 6a \cosh^2 \frac{a}{2} - 4a \sinh^2 \frac{a}{2} - 8 [3a^2 - (2n+1)^2\pi^2] \gamma_{2n+1}^2 \right. \quad (6.26)$$

$$\left. + 192a [a^2 - (2n+1)^2\pi^2] \cosh^2 \frac{a}{2} \gamma_n^2 \right\} + (1 - \delta_{mn}) (-1)^{m+n} \frac{1}{4(m+n)^2\pi^2} + \frac{1}{4(m-n)^2\pi^2}$$

$$\begin{aligned}
 (n|\zeta^4|m) &= \left[\frac{1}{160} - \frac{1}{8(2n+1)^2\pi^2} + \frac{3}{4(2n+1)^4\pi^4} \right] \gamma_{2n+1}^2 \delta_{mn} - \\
 &\quad - (-1)^{m+n} \frac{(2m+1)(2n+1)\pi^2 \gamma_{2n+1}^2 \gamma_{2m+1}^2}{a + \sinh a} \left\{ \frac{5}{2} a \cosh^2 \frac{a}{2} - 2a \sinh^2 \frac{a}{2} - \right. \\
 &\quad \left. - 4[3a^2 - (2n+1)^2\pi^2] \gamma_{2n+1} \sinh \frac{a}{2} \cosh \frac{a}{2} + 48\gamma_{2n+1}^2 [a^2 - (2n+1)^2\pi^2] \right\} \times \quad (6.27) \\
 &\quad \times \left[5 \cosh^2 \frac{a}{2} - 2 \sinh^2 \frac{a}{2} \right] - 192a \left[5a^4 - 10a^2(2n+1)^2\pi^2 + (2n+1)^4\pi^4 \right] \gamma_{2n+1}^3 + \\
 &\quad + 960a \left[3a^4 - 10a^2(2n+1)^2\pi^2 + 3(2n+1)^4\pi^4 \right] \gamma_{2n+1}^4 \cosh^2 \frac{a}{2} \left. \right\} \\
 &\quad + (1 - \delta_{mn}) \int_{-1/2}^{1/2} \zeta^4 \cos[(2m+1)\pi\zeta] \cos[(2n+1)\pi\zeta] d\zeta
 \end{aligned}$$

Taking $n = 0$, $m = 0$, which corresponds to using the trial function $F = \cos \pi \zeta$, $\tilde{F} = \cos \pi \zeta$, and setting $a = \pi$ yields

$$(n|m) = 0.4551$$

$$(n|\zeta^2|m) = 0.00579$$

$$(n|\zeta^4|m) = -0.000381$$

or

$$S_{\beta} = \frac{1}{A + B \cdot 0.01272 + C \cdot (-0.000837)} \quad (6.28)$$

(The same values, for the constant gradient case, yield $Ra_c = 1715$, as opposed to the accurate value of 1708.)

As an interesting sidelight, several other measures of a more approximate nature have been suggested for the stabilization caused by the non-constant gradient.

Spiegel [1962] made the suggestion that the stabilization would be inversely proportional to the Potential Energy stored in the gravitational field, i.e., since

$$\rho(\zeta) \propto \frac{1}{\theta(\zeta)} = \frac{1}{\bar{\theta}(1 + \frac{\Delta\theta}{\bar{\theta}})} = \frac{1}{\bar{\theta}} \left[1 - \frac{\Delta\theta(\zeta)}{\bar{\theta}} \right] \quad (6.29)$$

$$\theta(\zeta) = \bar{\theta} + \Delta\theta(\zeta) \quad (6.30)$$

$$S_{\beta}(\text{P.E.}) \propto g \int_{-1/2}^{1/2} \rho \zeta d\zeta \approx g \int_{-1/2}^{1/2} [\bar{\theta} - \Delta\theta(\zeta)] \zeta d\zeta \quad (6.31)$$

Because of the symmetry,

$$\Delta\theta(\zeta) = -\Delta\theta(-\zeta) \quad (6.32)$$

so the integral need only be done over half of the fluid and for $\Delta\theta \zeta$. (The portion $\propto g\bar{\theta}$ is constant for all distributions and does not effect the relative stabilization of two gradients.) Then

$$S_{\beta}(\text{P.E.}) \propto \int_0^{1/2} \Delta\theta(\zeta) \zeta d\zeta \quad (6.33)$$

From (6.23)

$$\Theta(\xi) = \bar{\rho} \left(A\xi + \frac{B}{3}\xi^3 + \frac{C}{5}\xi^5 + \dots \right) \quad (6.34)$$

$$S_{\beta}(\text{P.E.}) = A + \frac{B}{20} + \frac{3C}{460} \quad (6.35)$$

For a linear gradient, $A = 1$, $B = C = 0$, and the stabilization of a nonlinear over a linear gradient is

$$S_{\beta}(\text{P.E.}) = \frac{1}{A + \frac{B}{20} + \frac{3C}{460}} \quad (6.36)$$

It was also thought that, since the dimensional argument is phrased in terms of Buoyancy Forces, the relative buoyancy forces would provide a measure of relative stabilization. In this argument an integral of the form

$$S_{\beta}(\text{B.F.}) \propto \int \rho'(\xi) d\xi \quad (6.37)$$

where an element of density ρ' is seen as being acted upon by the mean density $\bar{\rho}$; if $\rho' < 0$, the element experiences a buoyancy force upward, and vice-versa. The integral of this quantity gives a measure of these forces, i.e.,

$$S_{\beta}(\text{B.F.}) \propto \int_0^{1/2} \left(A\xi + \frac{B\xi^3}{3} + \frac{C\xi^5}{5} \right) d\xi \quad (6.38)$$

Calculating as before

$$S_{\beta}(\text{B.F.}) = \frac{1}{A + \frac{B}{24} + \frac{C}{240}} \quad (6.39)$$

To discover which of these corresponds best to the case of Free Boundaries, consider the equation

$$R' = \frac{\int_{-1/2}^{1/2} w' Q(w') d\zeta}{\int_{-1/2}^{1/2} w' \frac{\beta}{\bar{\beta}} w' d\zeta} \quad (6.40)$$

obtained by Goody [1956] as a variational statement for obtaining the Rayleigh number. Here w' satisfies

$$w' = D^2 w' = D^4 w' = 0 \quad \text{at } \zeta = \pm 1/2$$

and Q is one of the operators he obtained. (See Chapter 1.) Evaluating this with functions which are solutions for w' when $\beta/\bar{\beta} = 1$ will give an expression for the amount of stabilization of the initial gradient.

Thus, using $w' = \cos \pi \zeta$, it is desired to evaluate

$$I = \int_{-1/2}^{1/2} (A + B \zeta^2 + C \zeta^4) \cos^2(\pi \zeta) d\zeta \quad (6.41)$$

With tables, paper, energy, and no subtlety this becomes

$$I = A\left(\frac{1}{2}\right) + B\left(\frac{1}{24} - \frac{1}{4\pi^2}\right) + C\left(\frac{1}{160} - \frac{1}{8}\pi^2 + \frac{3}{4}\pi^4\right) \quad (6.42)$$

Again, comparing this with the linear gradient case yields

$$S_{\beta}(F,\beta) = \frac{1}{A + B\left(\frac{1}{12} - \frac{1}{2}\pi^2\right) + C\left(\frac{1}{80} - \frac{1}{4}\pi^2 + \frac{3}{4}\pi^4\right)} \quad (6.43)$$

Since this has no a 's in it, it is not affected by the minimization with respect to a , and thus the presence of $\beta/\bar{\beta} \neq 1$ does not influence cell size or cause a shift of the curve of Ra vs. a , but merely shifts its location upward or downward.

Thus, the stabilization due to the distortion of the zero order field in the following approximations may be compared:

$$\begin{aligned}
 S_{\beta}(\text{P.E.}) &= \left[\int \zeta \theta d\zeta \right]^{-1} \Rightarrow (A+B(0.05000)+C(0.005357))^{-1} \\
 S_{\beta}(\text{B.F.}) &= \left[\int \theta d\zeta \right]^{-1} \Rightarrow (A+B(0.04167)+C(0.004167))^{-1} \\
 S_{\beta}(\text{F.F.}) &= \left[\int w \frac{\beta}{2} w \right]^{-1} \Rightarrow (A+B(0.03267)+C(0.002569))^{-1} \\
 S_{\beta}(6.28) &= (A+B(0.01272)+C(-0.000837))^{-1}
 \end{aligned}$$

Thus the stabilization is least for rigid-rigid boundaries, presumably because they are already highly stabilized by the boundaries. In the rigid boundary case, because the minimization has not been carried out, the results can only be regarded as good approximations.

In the calculations of Chapter 5, the coefficient B was always less than 1, and C is always of order 10 or less. Then, to a first approximation good to one or two percent,

$$S_{\beta}(\text{R.R.}) = S_{\beta} = A^{-1} \quad (6.44)$$

6.4 Calculation of S_H

The chart on the following page gives an idea of what problems have been done and what will be done in this section.

As indicated on the chart, Spiegel's [1960] dimensional argument will be extended to a mixed radiative-diffusive case and shown to correspond very closely to an extension of Spiegel's exact calculation, and the limiting cases considered by Goody. A simplification is then intro-

CONVECTION

Medium Gray Non-Gray

Radiation Only

Theory

Exact	Spiegel [1960]	None. Shown difficult in Sec. 6.1.
Dimensional Argument	Spiegel [1960]	Could be done using techniques of this section.

Radiation and Diffusion

Exact	Goody [1956] limiting cases. Easy extension from Spiegel [1960] in this section.	None. Same difficulties as for radiation alone.
Dimensional Argument	Extension from Spiegel [1960] in this section.	Will be assumed to be same as for dimensional argument for gray case.

Goody [1956] also allowed for non-constant gradients; this has been discussed in Sec. 6.3 and will not be mentioned here.

duced to avoid the minimization with respect to a . Since the dimensional argument agrees closely with the expressions obtained by analytic calculations, it will be assumed valid for the non-gray medium.

6.4.1 A Dimensional Argument for S_H

This argument is an elaboration of one presented by Spiegel [1958].

The stability parameter in convective problems, the Rayleigh number, may be regarded as a ratio between buoyancy forces driving the fluid and viscous forces damping the motion. The condition for instability becomes

$$\text{buoyancy forces} \geq C \text{ viscous forces ,}$$

where C is some constant of order unity, or

$$g \delta \rho l^3 > C \eta l^2 \frac{dw}{dx} \quad (6.45)$$

for a perturbed cubical fluid element of dimension l , where $\delta \rho$ = the density difference from the surroundings and the other symbols have their usual meanings (see Chapter 1).

If $\delta \rho$ is due to temperature changes (as it is in thermal convection)

$$\delta \rho = -\rho \alpha \delta \theta \quad (6.46)$$

to first order. Now

$$\delta \theta \approx \beta L = \beta w t \quad (6.47)$$

where

$$L \approx w t \quad (6.48)$$

is the distance the element has come from the point where it received its buoyancy at a typical velocity w , in a typical time t .

Combining (6.45) and (6.48)

$$- \frac{g \alpha \beta l}{\gamma} \frac{w}{\frac{dw}{dx}} t \geq C \quad (6.49)$$

Letting

$$\frac{dw}{dx} \approx \frac{w}{l} \quad (6.50)$$

and writing

$$l = \frac{h}{p} \quad (6.51)$$

equation (6.49) becomes

$$-\frac{g \alpha \beta h^2}{\nu} \tau \geq C_p^2 \quad (6.52)$$

Because of (6.47), one might expect the time scale to be set by the dominant temperature-dissipating mechanism.

6.4.1.2 Diffusive Temperature Dissipation

In this case the time of decay of a temperature perturbation of dimension l' is

$$t_D = \frac{l'^2}{K} \rho c_p \quad (6.53)$$

Identifying $l' = l$, and using (6.53) in (6.52) yields

$$-\frac{g \alpha \beta h^4}{K \nu} \rho c_p = Ra \geq C_p^4 \quad (6.54)$$

This argument does not tell the size of C or p . The solution of the sixth order equation is very nearly [Chandrasekhar, 1961]

$$Ra(a) = \frac{(a^2 + \pi^2)^3}{a^2} G \quad (6.55)$$

where a is the characteristic number defined in 6.1 relating horizontal size to vertical spacing, and where

$$G = 1 \quad (\text{free boundaries})$$

$$= \left[1 - \frac{8\pi^2 a}{(a^2 + \pi^2)^2} \frac{1 + \cosh a}{a + \sinh a} \right]^{-1} \quad (\text{rigid boundaries}) \quad (6.56)$$

to a good approximation. When $Ra(a)$ is minimized with respect to a , the minimum value is Ra_c .

Comparing (6.54) and (6.55) gives

$$C_p^4 = \frac{(a^2 + \pi^2)^3}{a^2} G \quad (6.57)$$

6.4.1.2 Radiative Temperature Dissipation in a Gray Medium

Spiegel [1957] finds the time constant for the dissipation of a temperature perturbation of three-dimensional wave number n in a gray medium with zero conductivity to be

$$\frac{1}{t_R(n)} = \frac{1}{t_R(\infty)} \left(1 - \frac{k}{n} \cot^{-1} \frac{k}{n} \right) = N(n) \quad (6.58)$$

where

$$\frac{1}{t_R(\infty)} = \frac{16\sigma k \Theta^3}{\rho c_p} = \frac{4\pi k Q}{\rho c_p} \quad (6.59)$$

is an inverse time for an infinitely small perturbation to be dissipated.

Putting (6.58) in (6.52) results in

$$-\frac{g\alpha\beta h^2 t_R(\infty)}{\nu} \geq C_p^2 \left(1 - \frac{k}{n} \cot^{-1} \frac{k}{n}\right)$$

which by using the definitions

$$\mathcal{X} = \frac{4\pi Q}{3kK}$$

$$\tau = kh$$

$$q^2 = n^2 h^2 = k^2 (a^2 + \pi^2)$$

may be written

$$\frac{Ra}{\mathcal{X}} = C_p^2 3\tau^2 \left(1 - \frac{\tau}{q} \cot^{-1} \frac{\tau}{q}\right) \quad (6.60)$$

The solution to the complete equations obtained by Spiegel [1960] is

$$\begin{aligned} \frac{Ra(a)}{\mathcal{X}} = & \frac{(a^2 + \pi^2)^2}{a^2} \Gamma 3\tau^2 \left\{ 1 - \frac{\tau}{q} \cot^{-1} \frac{\tau}{q} + \frac{\tau}{q^2} \left(1 - \frac{\tau \sqrt{\tau^2 + a^2}}{\tau^2 + q^2} \right) - \right. \\ & \left. - \frac{q^2 + \pi^2}{2\pi q^3} \tau \ln \left[\frac{(q \sqrt{\tau^2 + a^2} + \pi \tau)}{(q \sqrt{\tau^2 + a^2} - \pi \tau)} \right] \left(\frac{q - \pi}{q + \pi} \right) \right\} + \pi \frac{\tau}{a} U(a, \tau) \cot^{-1} \frac{\tau}{a} \quad (6.61) \end{aligned}$$

or, neglecting all but the leading terms, in comparing (6.60) and (6.61)

$$C_p^2 = \frac{(a^2 + \pi^2)^2}{a^2} \Gamma \quad (6.62)$$

Comparing (6.57) with (6.62) yields

$$p = (a^2 + \pi^2)^{1/2} = q \quad (6.63)$$

$$C = \left(\frac{a^2 + \pi^2}{a^2} \right) G \quad (6.64)$$

6.4.1.3 Combined Gray Radiative and Diffusive Temperature Dissipation

If there are two parallel competitive processes occurring, a reasonable combined dissipation time t_C will be given by

$$\frac{1}{t_C} = \frac{1}{t_D} + \frac{1}{t_R} \quad (6.65)$$

which may be combined with (6.52), (6.63), and (6.64) to give

$$Ra = \frac{-g\alpha\beta h^4 \rho c_p}{K_v} \geq C p^4 \left(1 + \frac{t_D}{t_R} \right) \quad (6.66)$$

$$= \frac{(a^2 + \pi^2)^3}{a^2} G \left[1 + 3 \mathcal{F} \frac{\tilde{c}^2}{q^2} \left(1 - \frac{\tilde{c}}{q} \cot^{-1} \frac{\tilde{c}}{q} \right) \right] \quad (6.67)$$

6.4.2 The Extension of Spiegel's Exact Solution

This should be compared with the extension of Spiegel's [1960] exact calculation for radiation alone to the case of both radiation and diffusion.

Spiegel's equation (53) is equivalent to (6.9) (with of course $F = \tilde{F}$), with

$$\underline{H} = \mathcal{R} = \frac{1}{t_R(\infty)} \int_{-1/2}^{1/2} K(1\zeta - \zeta'1) d\zeta' \quad (6.68)$$

To extend his formulation to mixed radiation and diffusion, put

$$\underline{H} = \frac{K}{h^2 \rho c_p} (D^2 - a^2) + \frac{1}{t_R(\infty)} \int_{-1/2}^{1/2} K(1\zeta - \zeta'1) d\zeta' \quad (6.69)$$

in (6.9), giving

$$\begin{aligned} Ra &= \frac{h^2 \rho c_p}{K} \frac{\int_{-1/2}^{1/2} F(\zeta) d\zeta \left[\frac{K}{h^2 \rho c_p} (D^2 - a^2) + \frac{1}{t_R(\infty)} \int_{-1/2}^{1/2} K(1\zeta - \zeta'1) d\zeta' \right] F(\zeta')}{\alpha^2 \int_{-1/2}^{1/2} F(\zeta) w(\zeta) d\zeta} \\ &= \frac{\int_{-1/2}^{1/2} F(\zeta) d\zeta \left[(D^2 - a^2)^3 w(\zeta) + 3\mathcal{J} \tau^2 \int_{-1/2}^{1/2} K(1\zeta - \zeta'1) (D^2 - a^2)^2 w(\zeta') d\zeta' \right]}{\alpha^2 \int_{-1/2}^{1/2} F(\zeta) w(\zeta) d\zeta} \quad (6.70) \end{aligned}$$

To get results from this, one should put in trial functions containing a variable parameter for $F(\zeta)$, satisfying the boundary conditions, into (6.70), evaluate, and minimize with respect to the parameter and a , to give $Ra_c(\mathcal{J}, \tau)$ when $a = a_c(\mathcal{J}, \tau)$.

This is rather difficult for rigid boundaries even for diffusion, and was avoided by Spiegel for radiation alone. He chose two dissimilar functions satisfying the boundary conditions:

$$F_1 = \cos \pi \zeta$$

$$F_2 = 1 + \cos 2\pi \zeta$$

and found that they gave similar results for $\tau \leq 1$, while the usual diffusive solution F_1 gave lower results for $\tau > 1$. Assuming F_1 as the form for the trial function will give results that are never far off, then. Inserting this in (6.70) gives

$$Ra = \frac{(a^2 + \pi^2)^3}{a^2} G \left\{ 1 + \frac{3\tau^2}{a^2 + \pi^2} \left(1 - \frac{\tau}{q} \cot^{-1} \frac{\tau}{q} + \frac{\tau}{q} \left(1 - \frac{\tau \sqrt{\tau^2 + a^2}}{\tau^2 + q^2} \right) - \frac{q^2 + \pi^2}{2\pi q^2} \tau \ln \left[\frac{(q \sqrt{\tau^2 + a^2} + \pi \tau)}{q \sqrt{\tau^2 + a^2} - \pi \tau} \right] \left(\frac{q - \pi}{q + \pi} \right) + \pi \frac{\tau}{a} U(a, \tau) \cot^{-1} \frac{\tau}{a} \right\} \quad (6.71)$$

where $q = a^2 + \pi^2$ and

$$U(a, \tau) = \int_{-1}^1 \frac{\left[\frac{a}{\sin b(1-x)} \right] e^{-a/\sin b(1-x)}}{\left\{ \left[\frac{a}{\sin b(1-x)} \right]^2 + \pi^2 \right\}} dx, \quad b = \frac{1}{2} \cot^{-1} \frac{\tau}{a}$$

Clearly the leading terms agree with those of the dimensional argument.

The next task is to avoid minimizing with respect to a , and to use the fact that Ra_c and a_c are known when there is no radiation.

6.4.3 The Choice of Optimum \hat{q}

Spiegel's [1960] Table 2 gives $3\tau^2 \lambda_{crit}$, which is equal to Ra_c / \mathcal{F} , for radiation alone. In the dimensional argument for radiation alone

$$\frac{Ra_c}{\mathcal{F}} = \frac{(a^2 + \pi^2)^3}{a^2} G \frac{3\tau^2}{q^2} \left(1 - \frac{\tau}{q} \cot^{-1} \frac{\tau}{q} \right) \quad (6.72)$$

An excellent fit is obtained if one sets

$$\frac{(a^2 + \pi^2)^3}{a^2} G = \left[\frac{(a^2 + \pi^2)^3 G}{a^2} \right]_{\min} = Ra_c(\text{diff}) \quad (6.73)$$

Plotting Ra_c/\mathcal{F} from Spiegel, and

$$\frac{Ra_c}{\mathcal{F}} = Ra_c(\text{diff}) \mathfrak{B} \left(\frac{\tau}{\hat{q}} \right)^2 \left(1 - \frac{\tau}{\hat{q}} \cot^{-1} \frac{\tau}{\hat{q}} \right) \quad (6.74)$$

against τ leads to nearly identical results for $\hat{q} = 5.0$. The results are compared in Table 6-1. (This form of comparison was suggested by Goody [1963].)

Table 6-1

EXACT AND DIMENSIONAL ARGUMENT CALCULATIONS OF Ra_c/\mathcal{F}

$\hat{q} = 5.0$

τ	$Ra_c/\mathcal{F}(\text{Exact})$	$Ra_c/\mathcal{F}(6.74)$
0	0	0
0.1	2.01	1.99
0.5	44.90	43.70
1	155	149
π	749	739
5	1081	1100
10	1440	1488
1000	1716	1708

The dimensional argument gives for the critical Rayleigh number in the constant gradient case

$$Ra_c = Ra_c(\text{diff}) \left[1 + 3\pi \left(\frac{\tau}{\hat{q}} \right)^2 \left(1 - \frac{\tau}{\hat{q}} \cot^{-1} \frac{\tau}{\hat{q}} \right) \right] \quad (6.75)$$

with

$$\hat{q} = 5.0 \quad (6.76)$$

This proves of great benefit for application to the non-gray case. First, since q is independent of τ , the difficult specification of τ in a non-gray medium does not matter. Secondly, since

$$\hat{q} = h(\ell^{-1}) = h \cdot n$$

then

$$\ell^{-1} = n$$

is the wave number which governs the radiative dissipation. If $\frac{t_D}{t_R}(n)$ can be calculated for a non-gray gas, by (6.75), (6.66), (6.67), and (6.21), the radiative stabilization will be given by

$$S_H = 1 + \frac{t_D}{t_R} \left(\frac{5.0}{h} \right) \quad (6.77)$$

6.4.4. The Radiative Time Constant

The argument to be used closely follows that given by Spiegel [1957] for a gray gas. Consider the equation of transfer

$$\int_0^\infty d\nu \frac{dI(\bar{s})}{ds} = - \int_0^\infty k_\nu [I_\nu(\bar{s}) - B_\nu(\bar{s})] d\nu \quad (6.78)$$

in an infinite medium which is assumed to be in thermodynamic equilibrium.

From the definition of the heating rate,

$$-H = - \int_0^{\infty} h_{\nu} d\nu = \int_0^{\infty} d\nu \int_{4\pi} \frac{dI_{\nu}}{ds} d\omega \quad (6.79)$$

and by integrating over 4π steradians, one obtains (noting the isotropic nature of B)

$$-H = \int_0^{\infty} d\nu \int_{4\pi} \frac{dI_{\nu}}{ds} d\omega = - \int_0^{\infty} d\nu k_{\nu} \left[\int_{4\pi} I_{\nu}(\bar{s}) d\omega - 4\pi k B_{\nu}(\bar{s}) \right] \quad (6.80)$$

$$H = 4\pi \int_0^{\infty} d\nu k_{\nu} \left[\bar{I}_{\nu}(\bar{s}) - B_{\nu}(\bar{s}) \right]$$

where use has been made of the definition of average intensity [Chandrasekhar, 1960]

$$\bar{I}(\bar{s}) = \frac{1}{4\pi} \int_{4\pi} I(\bar{s}) d\omega \quad (6.81)$$

If we write for the optical separation of the point of interest \bar{s} , and an arbitrary field point $\bar{s} + \bar{r}$,

$$\tilde{I}_{\nu}(\bar{s}, \bar{s} + \bar{r}, t) = \int_0^{\bar{r}} k_{\nu}(\bar{s} + \bar{r}') d\bar{r}' = \int_0^{\bar{r}} k_{\nu}(\bar{s} + \frac{\bar{r}'}{\bar{r}} \bar{r}) d\bar{r}' \quad (6.82)$$

or, more briefly,

$$\tilde{I}_{\nu}(\bar{r}) = \bar{r} \int_0^1 k_{\nu}(\bar{s} + \alpha \bar{r}) d\alpha \quad (6.83)$$

Spiegel writes for the mean intensity

$$\bar{I}(\bar{s}) = \int_0^{\infty} d\nu \int_0^{\infty} \frac{k_\nu B_\nu (\bar{s} + \bar{r}) e^{-\tau_\nu(\bar{r})}}{4\pi r^2} dV(\bar{r}) \quad (6.84)$$

(The transit time of light has been neglected.) Then, if the heating rate at \bar{s} is $H(\bar{s})$,

$$\begin{aligned} H(\bar{s}) &= \rho c_p \frac{\partial \theta(\bar{s})}{\partial t} \\ &= 4\pi \int_0^{\infty} d\nu k_\nu \left[\int_0^{\infty} \frac{k_\nu B_\nu (\bar{s} + \bar{r}) e^{-\tau_\nu(\bar{r})}}{4\pi r^2} dV(\bar{r}) - B_\nu(\bar{s}) \right] \end{aligned} \quad (6.85)$$

In a state of radiative equilibrium, $H(\bar{s}) = 0$.

We are interested in the lifetime of a temperature perturbation $\theta'(s^-, t)$, and write for the temperature

$$\theta(\bar{s}, t) = \theta_0(\bar{s}) + \theta'(\bar{s}, t) \quad (6.86)$$

where $\theta' \ll \theta_0$. It is assumed that any quantity, f , may be expanded in a Taylor series about its steady state value f_0 ,

$$f(\bar{s}, t) = f_0(\bar{s}) + f'_0 \theta'(\bar{s}, t)$$

It is also assumed that the medium is homogeneous, so $k_\nu(\bar{s})$ depends only on $\theta(\bar{s})$.

Now expanding (6.85) and neglecting terms of order θ'^2

$$\begin{aligned}
 \frac{\partial \theta'}{\partial t} = & \frac{4\pi}{\rho_0 c_p} \left(1 - \frac{\rho' c_p'}{\rho_0 c_{p_0}} \right) \int_0^\infty d\nu k_\nu \left[\int \frac{k_\nu B_\nu(\bar{r} + \bar{s}) e^{-k_\nu r}}{4\pi r^2} dV(\bar{r}) - B_\nu(\bar{s}) \right] + \\
 & + \int_0^\infty d\nu k_\nu \left[\int \frac{k_\nu B_\nu'(\bar{s} + \bar{r}) e^{-k_\nu r}}{4\pi r^2} dV(\bar{r}) - B_\nu'(\bar{s}) \right] \textcircled{1} + \\
 & + \int_0^\infty d\nu k_\nu \left[\int \frac{k_\nu' \theta'(\bar{r} + \bar{s}) B_\nu e^{-k_\nu r}}{4\pi r^2} dV(\bar{r}) - \right. \\
 & \left. - \int_0^\infty \frac{k_\nu r B(\bar{r} + \bar{s}) e^{-k_\nu r} \int_0^1 k_\nu' \theta'(\bar{s} + \alpha \bar{r}) d\alpha}{4\pi r^2} dV(\bar{r}) \right] \textcircled{2} + \\
 & + \int_0^\infty d\nu k_\nu' \theta' \left[\int \frac{k_\nu B_\nu(\bar{s} + \bar{r}) e^{-k_\nu r}}{4\pi r^2} dV(\bar{r}) - B_\nu(\bar{s}) \right] \textcircled{3} \}
 \end{aligned} \tag{6.87}$$

The first integral is identically zero, since

$$\int_0^\infty d\nu k_\nu \left[\int \frac{k_\nu B_\nu(\bar{s} + \bar{r}) e^{-k_\nu r}}{4\pi r^2} dV(\bar{r}) - B_\nu(\bar{s}) \right] \equiv 0 \tag{6.88}$$

is the zeroth order solution of the equation of radiative equilibrium.

This shows why the effects of fluctuations of density and heat capacity vanish to first order.

The physical meaning of the remaining terms is quite clear. The first two labeled $\textcircled{1}$ give the effect on the temperature perturbation of the change in the source function -- the first in the local absorption of distant emission, the second the change in local emission. These have analogs in Spiegel's treatment. The remaining four terms contain the effects of a perturbation in the absorption coefficient -- the first the effect of distant emissivities, the second the effect on intervening attenuation, while the third and fourth contain the effect of change on the local coefficient on absorption and emission. The first two

labeled (2) appear in Spiegel's [1958] treatment, where they cancel each other. The proof here is identical to his and will be omitted.

The quantity

$$Q_3 = \int_0^{\infty} k_{\nu}' \Theta'(\bar{s}) \left[\int_0^{\infty} \frac{k_{\nu} B_{\nu}(\bar{s} + \bar{r}) e^{-k_{\nu} r}}{4\pi r^2} dV(\bar{r}) - B_{\nu}(\bar{s}) \right] d\nu \quad (6.89)$$

vanishes identically in the gray case, since in that case the terms within the brackets vanish for radiative equilibrium. Because of the similarity of B_{ν} and B_{ν}' , the terms in the brackets labeled (3) will be similar to those in the brackets labeled (1). A condition for neglecting Q_3 relative to the terms labeled (1) is

$$\int_0^{\infty} k_{\nu} B_{\nu}' d\nu \gg \int_0^{\infty} k_{\nu}' B_{\nu} d\nu$$

The inference $k_{\nu}' = 0$ was drawn from the data in Chapter 3 and assumed in the calculations. The quantity Q_3 will then be set equal to zero here.

For a material for which $k' \neq 0$, this term would have to be considered.

Now (6.87) becomes

$$\frac{\partial \Theta}{\partial t}(\bar{s}, t) = \frac{4\pi}{c_p} \int_0^{\infty} k_{\nu} \frac{\partial B_{\nu}}{\partial \theta} d\nu \left[\int_0^{\infty} \frac{k_{\nu} \Theta'(\bar{s} + \bar{r}) e^{-k_{\nu} r}}{4\pi r^2} dV(\bar{r}) - \Theta'(\bar{s}) \right] \quad (6.90)$$

Define

$$\Phi(\bar{n}) = \frac{1}{(2\pi)^{3/2}} \int_{-\infty}^{\infty} e^{i\bar{n} \cdot \bar{r}} \Theta'(\bar{r}, t) dV(\bar{r}) \quad (6.91)$$

a Fourier transform, and apply it to (6.90). This produces

$$\frac{\partial}{\partial t} \bar{\Phi}(\bar{n}, t) = \frac{4\pi}{\rho_0 c_p} \bar{\Phi}(\bar{n}, t) \int_0^\infty k_\nu \frac{\partial B_\nu}{\partial \theta} d\nu \left[\int \frac{k_\nu e^{-k_\nu r} e^{i\bar{n} \cdot \bar{r}}}{4\pi r^2} dV(\bar{r}) - 1 \right] \quad (6.92)$$

The solution to this differential equation is

$$\bar{\Phi}(\bar{n}, t) = \bar{\Phi}(\bar{n}, 0) e^{-N(\bar{n})t} \quad (6.93)$$

where

$$N(\bar{n}) = \frac{4\pi}{\rho_0 c_p} \int_0^\infty k_\nu \frac{\partial B_\nu}{\partial \theta} d\nu \left[1 - \int_r \frac{k_\nu e^{-k_\nu r} e^{i\bar{n} \cdot \bar{r}}}{4\pi r^2} dV(\bar{r}) \right] \quad (6.94)$$

is an inverse time for dissipation of a temperature disturbance of wave number \bar{n} . Any temperature perturbation can be made up of such components by (6.91), and the temperature disturbance at any later time is given by

$$\Theta'(r, t) = \frac{1}{(2\pi)^{3/2}} \int_{-\infty}^{\infty} e^{-i\bar{n} \cdot \bar{r}} \bar{\Phi}(\bar{n}, t) dV(\bar{n}) \quad (6.95)$$

The integral in (6.94) may be evaluated by writing

$$\bar{n} \cdot \bar{r} = nr \cos \Theta = nr\mu \quad (6.96)$$

$$dV(\bar{r}) = 2\pi r^2 \mu d\mu dr$$

and thus

$$N(n) = \frac{4\pi}{\rho_0 c_p} \int_0^\infty k_\nu \frac{\partial B_\nu}{\partial \theta} d\nu \left[1 - \int_0^\infty dr \int_{-1}^1 k_\nu e^{-k_\nu r} e^{inr\mu} d\mu \right] \quad (6.97)$$

After performing the integral over μ , the next integral may be performed over r , giving

$$N(n) = \frac{4\pi}{\rho c_p} \int_0^{\infty} d\nu k_\nu \frac{\partial B_\nu}{\partial \theta} \left[1 - \frac{k_\nu}{n} \cot^{-1} \frac{k_\nu}{n} \right] \quad (6.98)$$

Because of the sensitivity of this function to the exact values of k_ν and the wide range of variation of k_ν with ν in the case of molecular vibration-rotation bands ($10^4:1$ is not unusual), this appears to be useful only in the case of gray absorption, when it becomes

$$N_G(n) = \frac{4\pi k}{\rho c_p} \frac{\partial B}{\partial \theta} \left(1 - \frac{k}{n} \cot^{-1} \frac{k}{n} \right) = \frac{1}{t_R} \quad (6.59)$$

This is Spiegel's dissipation time for radiation.

However, in two limiting forms interesting results are obtained.

If $\frac{k_\nu}{n} = k_\nu r \ll 1$, (6.59) becomes

$$N(n) = \frac{4\pi}{\rho c_p} \int_0^{\infty} k_\nu \frac{\partial B_\nu}{\partial \theta} d\nu = \frac{4\pi Q \bar{k}_p}{\rho c_p} \quad (6.99)$$

where

$$\bar{k}_p = \frac{1}{Q} \int k_\nu \frac{\partial B_\nu}{\partial \theta} d\nu \quad (6.100)$$

is nearly equal to the Planck mean. The Planck mean is defined with B_ν rather than $\frac{\partial B_\nu}{\partial \theta}$, but the similarity of B_ν and $\frac{\partial B_\nu}{\partial \theta}$ as functions of ν ensures that the two means will not be grossly different. The condition $k_\nu r \ll 1$ implies the linear portion of the emissivity vs. r curve, where no lines are completely absorbed in the centers -- the so-called weak-line region.

If $\frac{k_\nu}{n} = k_\nu r \gg 1$ (6.59) becomes

$$N(n) = \frac{4\pi}{\rho c_p} \int_0^\infty k_\nu \frac{n^2}{3k_\nu^2} \frac{\partial B_\nu}{\partial \theta} d\nu = \frac{4\pi Q n^2}{3\bar{k}_R \rho c_p} \quad (6.101)$$

where

$$\frac{1}{\bar{k}_R} = \frac{1}{Q} \int_0^\infty \frac{1}{k_\nu} \frac{\partial B_\nu}{\partial \theta} d\nu \quad (6.102)$$

is the Rosseland mean. This mean is important when the line center and wings are completely absorbed. The largest contributions to this mean come from windows between spectral bands having only weak continuum absorption. (For example, see Goody [1964].)

Returning to (6.97) and noting that

$$1 = \int_0^\infty k_\nu e^{-k_\nu r} dr = \int_0^\infty \frac{k_\nu e^{-k_\nu r}}{4\pi r^2} dV(\bar{r}) \quad (6.103)$$

means that after the integral over μ

$$N(n) = -\frac{4\pi}{\rho c_p} \int_0^\infty d\nu \frac{\partial B_\nu}{\partial \theta} \int_0^\infty k_\nu^2 e^{-k_\nu n} dr \left(\frac{\sin nr}{nr} - 1 \right) \quad (6.104)$$

The integral over frequency may now be done by introducing the perturbation emissivity of Chapter 3 [Townsend, 1958; Goody, 1964],

$$\Sigma(r, \theta, \rho) = \frac{\int_0^\infty d\nu \frac{\partial B_\nu}{\partial \theta} (1 - e^{-k_\nu r})}{\int_0^\infty \frac{\partial B_\nu}{\partial \theta} d\nu} \quad (6.105)$$

and differentiating successively. One finds

$$\frac{\partial \Sigma}{\partial r} = \Sigma'(r, \theta, \rho) = \frac{\int_0^{\infty} k_\nu d\nu \frac{\partial B_\nu}{\partial \theta} e^{-k_\nu r}}{\int_0^{\infty} \frac{\partial B_\nu}{\partial \theta} d\nu} \quad (6.106)$$

$$\frac{\partial^2 \Sigma}{\partial r^2} = \Sigma''(r, \theta, \rho) = -\frac{\int_0^{\infty} k_\nu^2 d\nu \frac{\partial B_\nu}{\partial \theta} e^{-k_\nu r}}{\int_0^{\infty} \frac{\partial B_\nu}{\partial \theta} d\nu} \quad (6.107)$$

Putting (6.107) in (6.104),

$$N(n) = \frac{4\pi Q}{\rho c_p} \int_0^{\infty} \Sigma'' \left(\frac{\sin nr}{nr} - 1 \right) dr \quad (6.108)$$

$$= \frac{4\pi Q}{\rho c_p} \int_0^{\infty} \Sigma'(r, \theta, \rho) \left(\frac{\sin nr}{nr} - \cos nr \right) \frac{dr}{r} \quad (6.109)$$

By analogy with (6.99), designate

$$\tilde{k}(n, \theta, \rho) = \int_0^{\infty} \Sigma'(r, \theta, \rho) \left(\frac{\sin nr}{nr} - \cos nr \right) \frac{dr}{r} \quad (6.110)$$

Now if the time for radiative dissipation of a disturbance of wave number

n is t_R , then

$$\frac{1}{t_R}(n) = N(n) = \frac{4\pi Q}{\rho c_p} \tilde{k}(n) \quad (6.111)$$

Applying the Fourier transformation process to the diffusion equation

$$\frac{\partial \theta}{\partial t} = \frac{K}{\rho c_p} \nabla^2 \theta \quad (6.112)$$

leads to the familiar result

$$t_D(n) = \frac{\rho c_p}{K \cdot n^2} \quad (6.113)$$

Combining (6.111) and (6.113) gives the desired expression

$$\frac{t_D}{t_R}(n) = \frac{4\pi Q}{k} \frac{k(n)}{n^2} \quad (6.114)$$

Limiting cases are

1. For $\frac{k_p}{n} \ll 1$, from (6.99)

$$1 + \frac{t_D}{t_R} = 1 + \frac{4\pi Q \tilde{k}_p'}{Kn^2} \quad (6.115)$$

For small enough disturbances for k_p' to be a valid representation of the emissivity, n^2 is so large that there is no stabilization.

2. For $\frac{k_p}{n} \gg 1$, from (6.101)

$$1 + \frac{t_D}{t_R} = 1 + \frac{4\pi Q}{3K\tilde{k}_R} = 1 + \mathcal{X}_R \quad (6.116)$$

where \mathcal{X}_R is based on the Rosseland mean. Measurements of \tilde{k}_R for NH_3 are not available; this would involve path lengths too long for this sort of experiment at any rate.

6.4.5 Calculation of $\tilde{k}(n)$ and $\frac{t_D}{t_R}(n)$

The nature of the integral

$$\tilde{k}(n, \theta, \rho) = \int_0^{\infty} \xi'(r, \theta, \rho) \left(\frac{\sin nr}{nr} - \cos nr \right) \frac{dr}{r} \quad (6.110)$$

is most easily seen if it is written

$$\begin{aligned} \tilde{k}(n, \theta, \rho) &= \int_0^{\infty} \frac{\partial \xi(r, \theta, \rho)}{\partial r} \left(\frac{\sin nr}{nr} - \cos nr \right) \frac{dr}{nr} \\ &= \int_0^{\infty} \left(\frac{\partial \xi(r, \theta, \rho)}{\partial r} \right)_{\frac{x}{n}} \left(\frac{\sin x}{x^2} - \frac{\cos x}{x} \right) dx \quad (6.117) \\ &= \int_0^{\infty} \left(\frac{\partial \xi(\rho)}{\partial r} \right)_{\frac{x}{n}} S(x) dx \end{aligned}$$

A graph of $\frac{\partial \xi(r, \theta, \rho)}{\partial r}$ vs. r for several values of pressure at $\theta = 300^\circ \text{ K}$ has been given in Chapter 3. Since ξ , ξ' , and \tilde{k} were all evaluated at $\theta = 300^\circ \text{ K}$ and are not strong functions of θ , the θ dependence will not be noted explicitly henceforth. $S(x)$ is graphed below in Fig. 6-1. The values of $S(x)$ were obtained between $x = 0$ and $x = 20$ at intervals of 0.01, and for $x = 20 - 100$ at intervals of 0.1, in less than a minute of I.B.M. 7094 time.

Errors considerably below one percent for the area of $S(x)$ were obtained using Simpson's rule with spacing of 0.05 over the excursions of the curve labeled 1, 2, and 3, and approximating excursions 4-11 by triangles with base equal to Δx between zeros of $S(x)$ and height equal to $\left| S(x) \right|_{\max}$ between the successive zeros. This calculational scheme agrees with the analytical result that

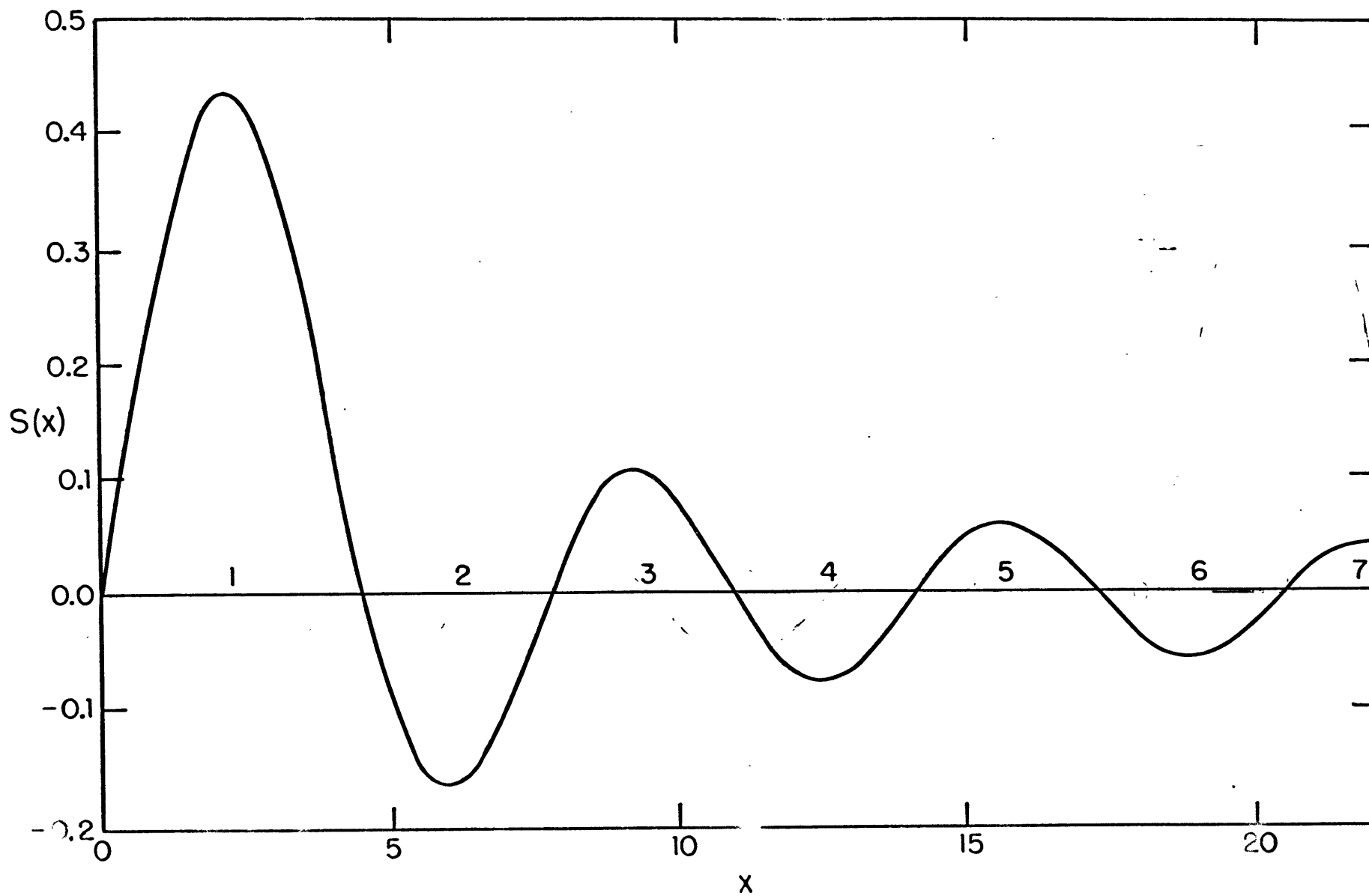


FIG. 6-1. $S(x)$ as a function of x .

$$\int_0^{\infty} 1 \cdot S(x) dx = 1 \quad (6.118)$$

which means

$$\lim_{n \rightarrow \infty} \tilde{k}(n, p) = \left[\frac{\partial \xi(r, p)}{\partial \theta} \right]_{r=0} = k_p'(p) \quad (6.119)$$

in agreement with the limiting formula.

To calculate $\tilde{k}(n, p)$ for a particular n , the x 's for the integral rule were written in a column. In the next column were placed values of $r = x/n$, and in the next six columns the values of $\xi'(r, p)_{r=x/n}$ for the six pressures. Finally the multiplying factors, written on a separate sheet, were aligned with the values of ξ' for one pressure and the multiplication was done cumulatively on a desk calculator.

Because $\xi'(r, p)$ falls off rapidly at large r , fewer terms are needed to get convergence to one percent as we take n small. The smallest value of n for which we can compute is $n = 0.1$, since $x \approx 10$ corresponds to $r \approx 100$, the largest value for which we can accurately compute $\xi'(r, p)$. To integrate over a smaller range of x would introduce larger quadrature errors than the one percent aimed for.

One effect of the rapid fall-off of $\xi'(r, p)$ is to make necessary more closely spaced values of x for Simpson's rule over the beginning of the first excursion. The small values of $S(x)$ are offset by large values of $\xi'(r, p)$. At $n = 0.1$, this had about a one percent effect.

Data at long enough path lengths does not exist to allow calculation to the Rosseland mean region.

The values obtained by these calculations are tabulated in Table 6-2 and graphed in Fig. 6-2.

Using these results and the data of Chapter 4, the quantity

$$\frac{t_D}{t_R}(n) = \frac{4\pi Q}{K} \frac{\tilde{k}(n)}{n^2} \quad (6.114)$$

was calculated at 25°C . It is presented in Fig. 6-3 and in Table 6-3. As a matter of interest, the radiative and the diffusive time constants and the combined time constant

$$\frac{1}{t_C} = \frac{1}{\frac{1}{t_D} + \frac{1}{t_R}} \quad (6.65)$$

have been plotted against $n = 1/\rho$ in Fig. 6-4.

In the last two graphs it is clear that at large wave numbers (i.e., small disturbances) the radiative effects will be small, while for small wave numbers the radiation will be much more effective than diffusion. The effects are of the same order near $n = 1$, or $r = 1 \text{ cm}$.

Table 6-2

$\tilde{k}(p,n)$ FOR SEVERAL VALUES OF p AND n

n [cm^{-1}]	Pressure [atmospheres]					
	0.1	0.2	0.4	0.6	0.8	1.0
1000	.0550	.1109	.2217	.3324	.4432	.5539
100	.0548	.1097	.2151	.3207	.4176	.5254
10	.0481	.0905	.1659	.2171	.3007	.3538
3.333	.0367	.0672	.1168	.1493	.1828	.2015
1.000	.0220	.0372	.0581	.0727	.0843	.0934
0.333	.0124	.0200	.0288	.0338	.0368	.0379
0.100	.0058	.0087	.0108	.0113	.0118	.0110

Table 6-3

$\frac{t_D}{t_R}(p,n)$ FOR SEVERAL VALUES OF p AND n

n [cm^{-1}]	Pressure [atmospheres]					
	0.1	0.2	0.4	0.6	0.8	1.0
1000	5.50×10^{-7}	1.10×10^{-6}	2.19×10^{-6}	3.27×10^{-6}	4.33×10^{-6}	5.42×10^{-6}
100	5.43×10^{-5}	1.09×10^{-4}	2.12×10^{-4}	3.15×10^{-4}	4.09×10^{-4}	5.14×10^{-4}
10	4.76×10^{-3}	8.95×10^{-3}	1.64×10^{-2}	2.13×10^{-2}	2.95×10^{-2}	3.46×10^{-2}
3.333	3.28×10^{-2}	5.99×10^{-2}	1.04×10^{-1}	1.33×10^{-1}	.161	.178
1.000	2.18×10^{-1}	3.68×10^{-1}	5.72×10^{-1}	.714	.825	.914
0.333	1.11	1.79	2.55	3.00	3.25	3.34
0.100	5.78	8.63	10.61	11.10	11.55	10.76

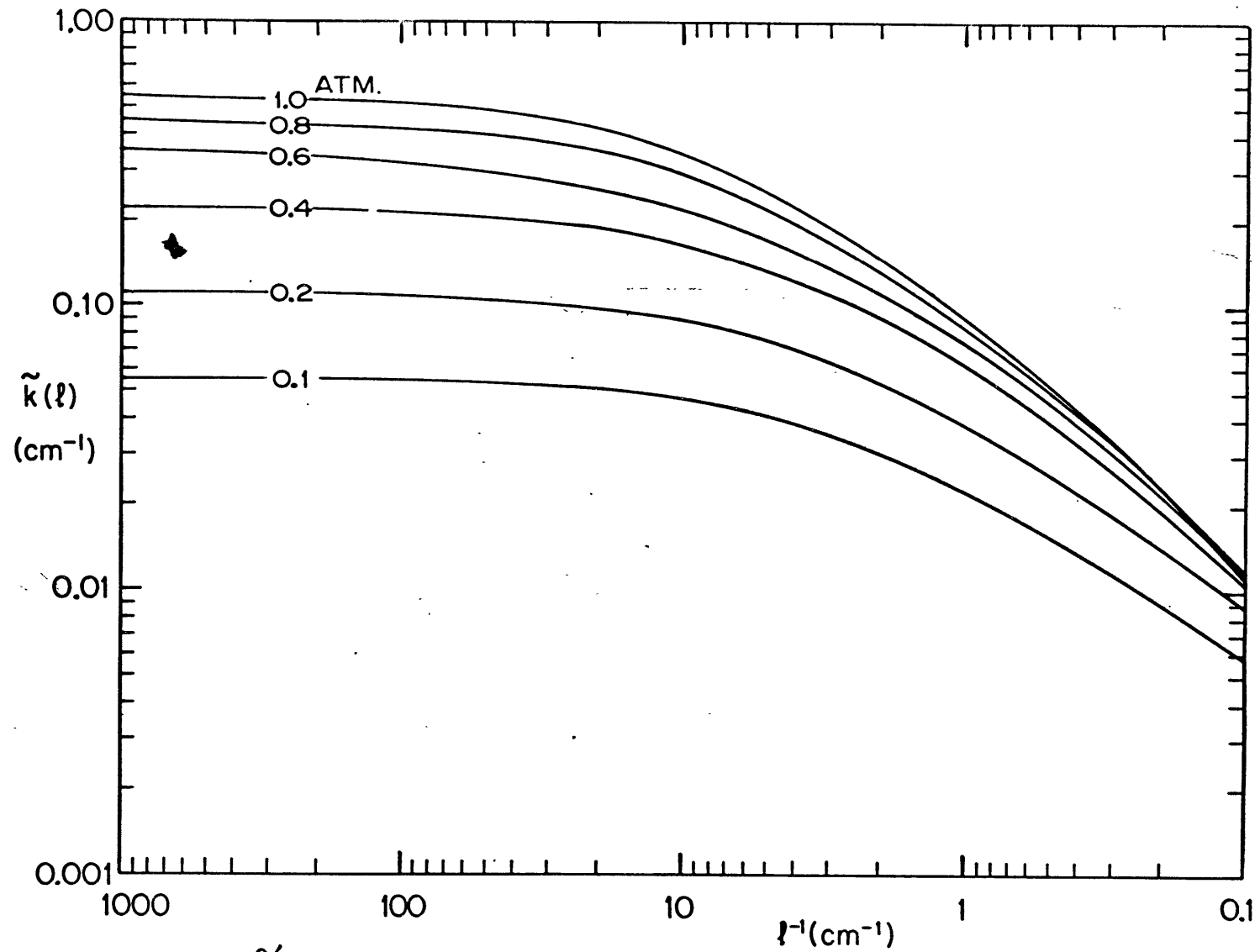


Fig. 6-2. $\tilde{k}(l)$ AS A FUNCTION OF $n = l^{-1}$
 Pressures are given on the curves.

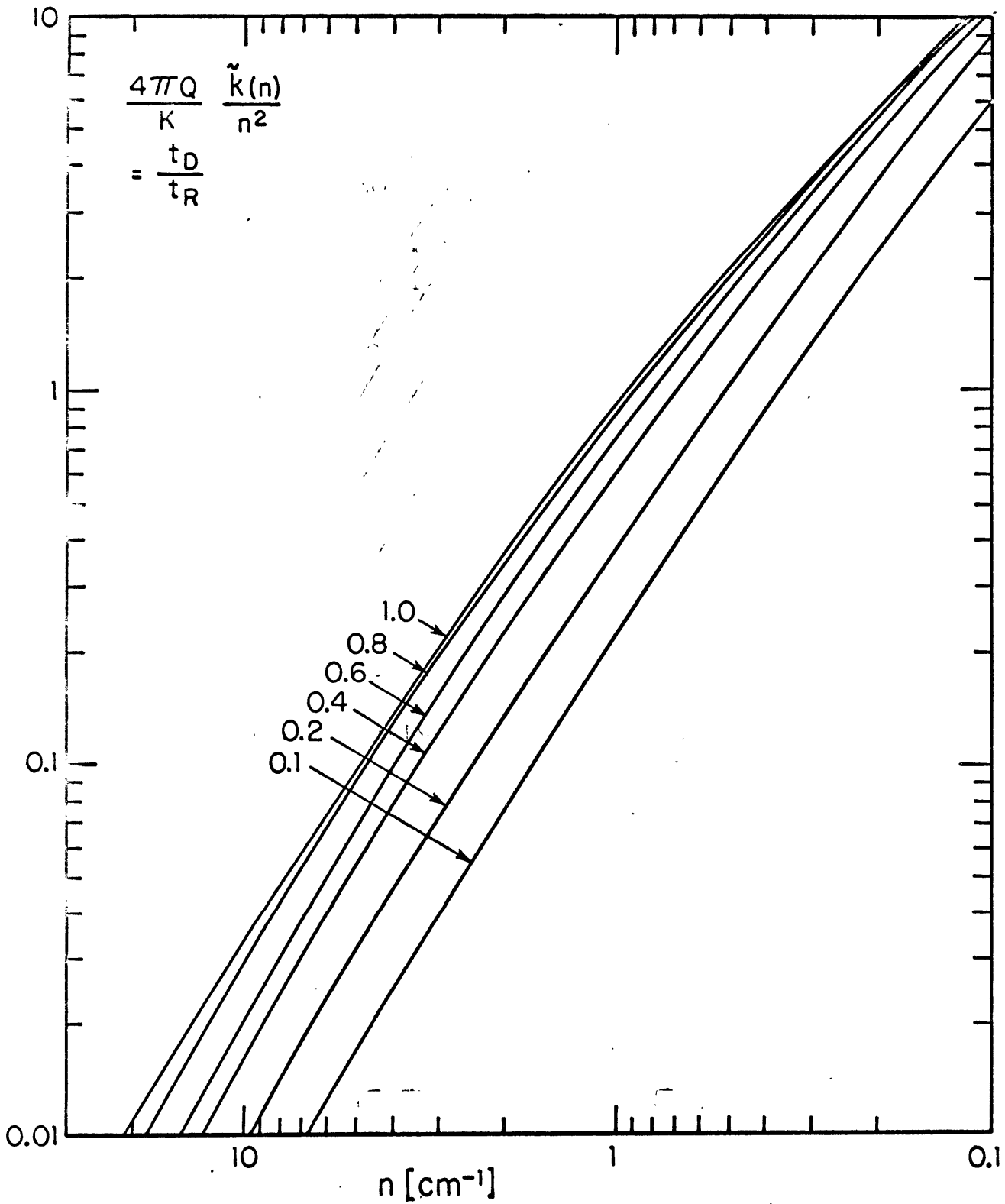


FIG. 6-3 $\frac{t_D}{t_R}(n)$ as a function of n .

Pressures in atmospheres are given on the curves.

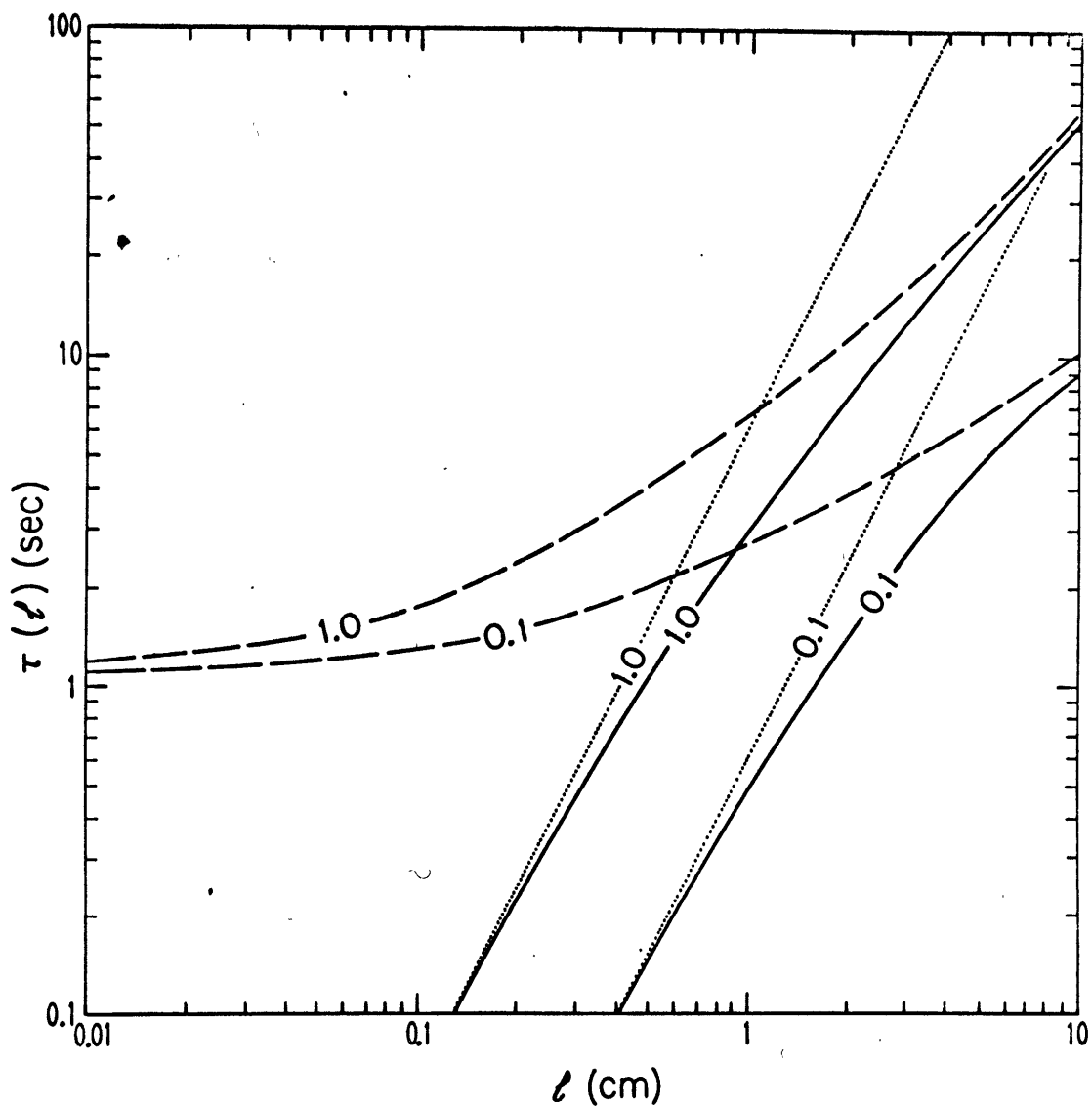


Fig. 6-4. CHARACTERISTIC TIME CONSTANTS IN AMMONIA

Pressures of ammonia in atmospheres are marked on the curves.

- τ (diff) (from 6.111)
- τ (rad) (from 6.113)
- τ (from 6.65)

6.5 Measurement of the Critical Rayleigh Number

6.5.1 The Method of Effective Conductivity

To date there have been three ways of measuring the onset of convection. They are (1) observations of motions of tracers in the fluid [Silveston, 1958; Bénard and Avsec, 1938; De Graaf and Van der Held, 1952], (2) observations of changes in refractive index [Schmidt and Milverton, 1935; Schmidt and Saunders, 1938; De Graaf and Van der Held, 1952], and (3) measurements of the change of heat transported across the layer when motions begin or end within it [Schmidt and Milverton, 1935; De Graaf and Van der Held, 1952; Malkus, 1954a; Silveston, 1958].

A variant of the last method has been used in this investigation, in that the effective conductivity of the fluid layer as a function of Rayleigh number was measured. When convection begins, more heat is transported across the fluid, and the apparent conductivity increases.

In Chapter 2 the quantity

$$S = \frac{0.85 \Delta \theta_{II} + \Delta \theta_I}{\Delta \theta} \quad (6.120)$$

was defined, where

$\Delta \theta_I$ is the temperature drop across the lower insulating disc,

$\Delta \theta_{II}$ is the temperature drop across the upper insulating disc,

$\Delta \theta$ is the temperature drop across the gas-filled gap.

As noted previously, this is not proportional to the Nusselt number because an appreciable portion of the heat flux is direct radiation between the two plates. The power of the method lies in the fact that we do not need to know the exact division between conductive and radiative

fluxes or the absolute conductivities. It is a null-type experiment, in which the effective conductivity for a series of Rayleigh numbers is measured and the Rayleigh number found at which the effective conductivity changes from its preconvective value.

6.5.2 Determination of the Rayleigh Number

The Rayleigh number is given by

$$Ra = \frac{g \alpha}{K \nu} \rho c_p h^3 \Delta \theta \quad (6.121)$$

where the symbols are (to recapitulate)

g = acceleration of gravity

$\alpha = \frac{1}{v} \frac{dv}{d\theta} = - \frac{1}{\rho} \frac{d\rho}{d\theta}$ = the coefficient of thermal expansion

ρ = density

c_p = specific heat at constant pressure

K = thermal conductivity

ν = kinematic viscosity

h = separation of plates between which convection occurs

$\Delta \theta$ = temperature difference applied across the fluid.

Equation (6.121) may be written

$$Ra = \frac{g \alpha}{K \eta} \rho^2 c_p \left(\frac{\rho_0}{\rho} \right)^2 \left(\frac{\rho}{\rho_0} \right)^2 h^3 \Delta \theta \quad (6.122)$$

which illustrates the effect of the four distinct factors.

The quantity

$$A = \frac{gd}{K\eta} \rho^2 c_p \left(\frac{p_0}{\rho} \right)^2 \quad (6.123)$$

does not depend on the particular experimental details, but only on the mean temperature and the fluid used. It was calculated in Chapter 4 for air and ammonia over a temperature range about room temperature.

The pressure ratio p/p_0 can be set independently of the other factors by admitting air or ammonia to the containing vessel or evacuating it with a vacuum pump. The value of p is read from a manometer.

The cube of the height, h^3 , is one of the parameters specified before an experiment is begun by inserting spacers of height h . These were described in Chapter 2. This was the most difficult factor in the Rayleigh number to change, since the pressure vessel had to be opened and the convection cell mechanically manipulated.

The temperature difference $\Delta\theta$ is set by adjusting the temperature baths and allowing the whole apparatus to come to equilibrium.

In the work of previous authors on gases, the factors A and h were set, the experiments run at atmospheric pressure putting $p/p_0 = 1$, and the temperature altered to sweep a range of Rayleigh numbers, as is done in the case of liquids.

The long time necessary for this apparatus to accommodate thermal change and the inconvenience of changing bath regulators often led to the procedure of setting $\Delta\theta$ at convenient values and regulating p/p_0 . The possibility of changing Rayleigh numbers by changing densities does not seem to have been previously noted or exploited.

Changing Rayleigh numbers by changing temperature would also have changed the radiative flux, since the coefficient multiplying $\Delta\theta$ varies

as $\bar{\theta}_0^3$, a 2°C change in $\bar{\theta}$ would only be a two percent change of radiative flux, but at $h = 5.048 \text{ cm.}$, that would be an appreciable part of the total change of heat transfer, necessitating another correction.

6.5.3 Taking of Data

When making a run, the temperature difference between the plates and the plate separation were set. The Rayleigh number was then altered by changing the pressure. A small quantity of gas was admitted, two or three hours were allowed for equilibrium to be reached, the temperatures in the four thermocouples were read, and the pressure was noted. Two or three more readings one-half hour apart were made at the same pressure; then more gas was admitted and the same procedure followed. Measurements were not taken above what was approximately twice the critical Rayleigh number.

Table 6-4 indicates the situations under which runs were made and the number of runs made. In this table, B refers to a convective situation in which heating is applied below, A refers to a conductive situation in which heating was applied above, and H refers to runs in which the Rayleigh number was lowered from about $2 Ra_c$ to zero to look for hysteresis effects in this type of measurement.

6.6 Reduction of Data to Get Critical Rayleigh Numbers

The data finally obtained consisted of 28 runs, each a group of paired values S_j, Ra_j . Subsequently one run was rejected because of experimental difficulties when it was taken.

Table 6-4

EXPERIMENTAL CONDITIONS FOR HEAT FLUX MEASUREMENTS

<u>Height[cm.]</u>	<u>$\Delta \theta$</u>	<u>Air</u>	<u>Ammonia</u>
5.048	$\sim 6^\circ$	2B A	2B A
	$\sim 2^\circ$	2B A	2B A
1.987	$\sim 2^\circ$	2B A	3B A
	$\sim 6^\circ$	2B A H	3B A H

It has been described in Chapters 2 and 5 how the eight conductive runs (i.e., heating above) and the preconvective portions of the 19 convective (heating below) runs were combined to give the description of the steady state in terms of \bar{S}_h vs. pressure for the four situations of two fluids and two separations. From these calculations the values of the standard deviations of a single point were also obtained.

6.6.1 Critical Rayleigh Number for Air

Denoting the standard deviation of \bar{S}_h as σ_g , all points with $\bar{S}_j < \bar{S}_h + 2 \sigma_g$ were discarded to reduce the possibility of including a nonconvecting point among the convecting ones.

Since values of \bar{S}_j are being used to find Ra , a regression should be performed of Ra on \bar{S} [Wilkes, 1949]. The data suggest primarily a linear relationship. The experimental data of Silveston and others and the theoretical work of Kuo indicate some curvature toward the

Ra axis. The data was fit to an ascending power series of the form

$$Ra = a + b\bar{S} + c\bar{S}^2$$

To reduce the amount of work necessary to get the Ra_c 's, use is made of the fact that $Ra = Ra_c$ when $\bar{S} = \bar{S}_h$, the value in the static state. The equation

$$Ra = Ra_c + b(\bar{S} - \bar{S}_h) + c(\bar{S} - \bar{S}_h)^2 \quad (6.124)$$

was fit on the Harvard I.B.M. 7094 for two cases:

1. $c = 0$. The program gave Ra_c , σ_{Ra} , b , σ_b , c , σ_c and the sums of the squares of the residuals.
2. c varied for best fit. The same quantities were found as in 1 above.

The values of c calculated from 2 varied considerably in similar circumstances, although most of them were less than σ_c . The standard deviation of Ra_c , σ_{Ra_c} , was larger in 2, indicating sensitivity to the value of c .

In addition, the restriction that the curve of \bar{S} vs. Ra should be concave to the Ra axis requires $c > 0$. Not all c 's measured individually fit this criterion. Therefore \bar{c} 's, the weighted means of the c 's from the runs, were taken, with the number of remaining degrees of freedom as the weighting factors. (The number of degrees of freedom is the number of data points minus three, the number of coefficients.) The standard deviation of \bar{c} was also found.

The calculations were then made, fitting

$$Ra = Ra_c + b(\bar{S} - \bar{S}_0) + \bar{c}(\bar{S} - \bar{S}_0)^2$$

$$Ra^+ = Ra_c^+ + b(\bar{S} - \bar{S}_0) + (\bar{c} + \sigma_{\bar{c}})(\bar{S} - \bar{S}_0)^2$$

$$Ra^- = Ra_c^- + b(\bar{S} - \bar{S}_0) + (\bar{c} - \sigma_{\bar{c}})(\bar{S} - \bar{S}_0)^2$$

and obtaining σ_{Ra_c} , $\sigma_{Ra_c^+}$, and $\sigma_{Ra_c^-}$.

The final figure for the standard deviation was then calculated as the result of two parts:

1. σ_{Ra_c} , due to the scatter of the data, denoted $\sigma_{Ra_c}^{(d)}$.
2. $|Ra_c^+ - Ra_c^-|$, due to uncertainty in the value of \bar{c} , which might be denoted as $\sigma_{Ra_c \bar{c}}$. (This differs negligibly from $|Ra_c^+ - Ra_c^-|$.)

The complete standard deviation was then given by

$$\sigma_{Ra_c}^2 = \sigma_{Ra_c}^{2(d)} + \sigma_{Ra_c \bar{c}}^2 \quad (6.125)$$

In Fig. 6-5 the experimental points and fitted curve are shown for Run 8. The results for all the air runs are given in Table 6-5, along with the experimental conditions.

The weighted mean value for all the air determinations is 1786 ± 16 , which is 4.5 percent higher than the theoretical value of 1708, calculated by Pellew and Southwell [1940] and Reid and Harris [1958], and observed in liquids by Silveston [1958] and many others. The deviations could be due to two effects;

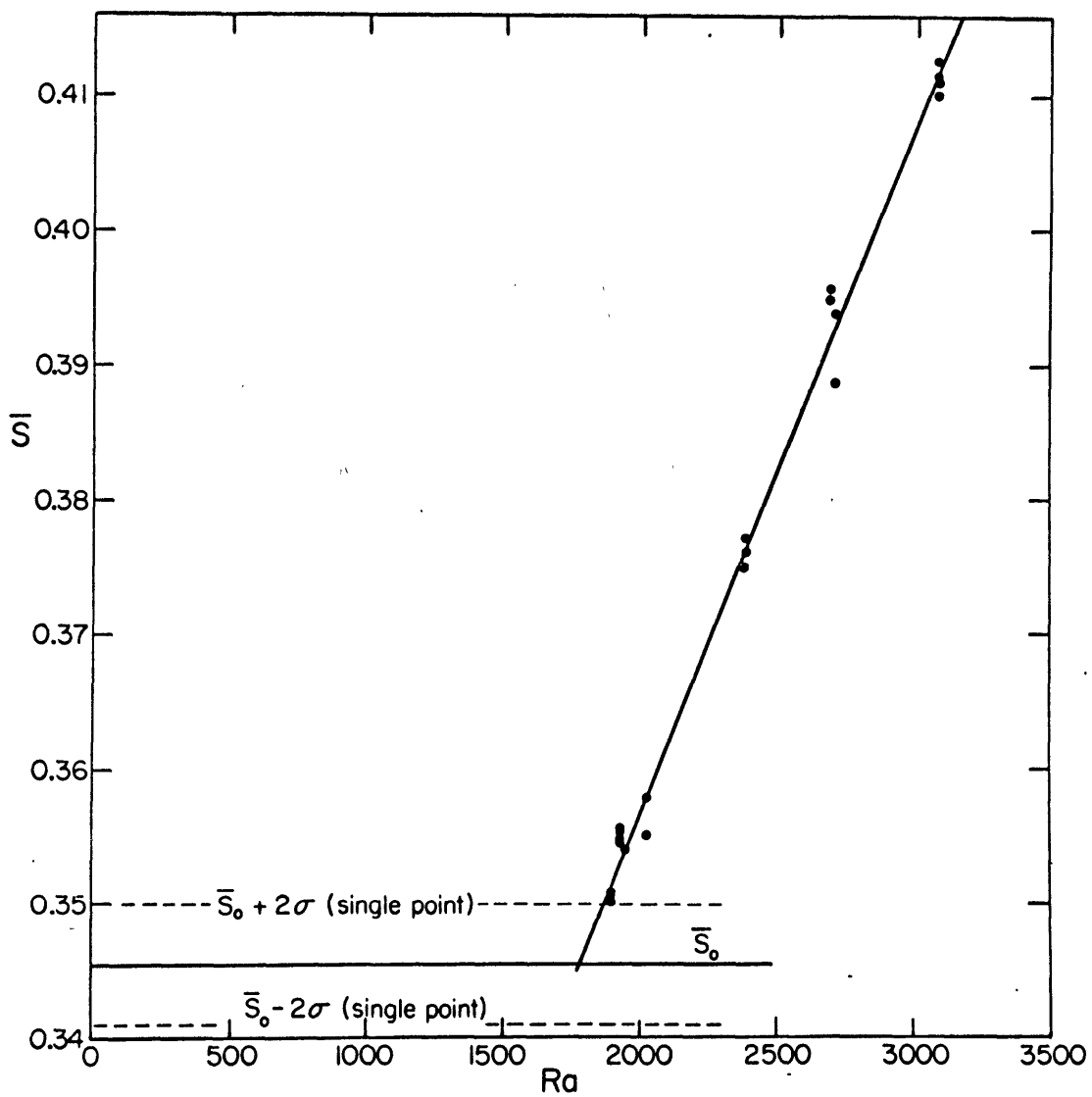


Fig. 6-5. \bar{S} AS A FUNCTION OF RAYLEIGH NUMBER FOR DRY AIR

$h = 1.987$ cm.

$\Delta \theta = -5.9^\circ$ K.

Points are observed during one run.

Intersection of the two solid lines gives Ra_0 .

Table 6-5
MEASURED CRITICAL RAYLEIGH NUMBERS IN AIR

Run (1)	h [cm.] (2)	$\Delta \theta$ [° C] (3)	p_c [cm. Hg.] (4)	σRa_c [data] (5)	$\sigma Ra_c (\bar{c})$ (6)	Ra_c (7)
1	5.048	5.7	11.9	83	140	1738 ± 162
<u>2</u>	<u>5.048</u>	<u>6.1</u>	<u>11.3</u>	<u>72</u>	<u>140</u>	<u>1755 ± 157</u>
Mean	5.048	5.9	11.6			1747 ± 112
3	5.048	1.75	21.8	119	148	2042 ± 189
<u>4</u>	<u>5.048</u>	<u>1.75</u>	<u>21.3</u>	<u>538</u>	<u>122</u>	<u>1568 ± 552</u>
Mean	5.048	1.75	21.7			1991 ± 179
5	1.987	2.85	68.8	32	3	1810 ± 32
<u>6</u>	<u>1.987</u>	<u>2.80</u>	<u>68.3</u>	<u>33</u>	<u>5</u>	<u>1761 ± 34</u>
Mean	1.987	2.80	68.6			1786 ± 23
7	1.987	6.2	48.1	60	48	1828 ± 77
<u>8</u>	<u>1.987</u>	<u>5.9</u>	<u>47.8</u>	<u>16</u>	<u>18</u>	<u>1781 ± 24</u>
Mean	1.987	6.0	47.8			1785 ± 23

1. The constants are not as accurate as would be desirable. Slight increases of K and η , within the range of different determinations, or a decrease in ρ could easily cover this difference.
2. We do not have an infinite horizontal plane upon which our cells can form. The walls exist and may force a periodicity on the cells which is not optimum. Recent work in England [Hide, 1962] indicates the importance of wall regions. Recent demonstrations by Koschmieder [1963] indicate that the walls influence cell development even with a diameter/height ratio of 20.

Since it is expected that these wall effects operate on ammonia in nearly the same way, they would have very little effect on the ratios of critical Rayleigh numbers.

Run 8 was made by decreasing the Rayleigh numbers from about $2 Ra_c$, and if it is plotted with Run 7, the points mingle together with no significant differences. These experiments give no indication of hysteresis effects. None is predicted by theory.

6.6.2 Critical Rayleigh Numbers for Ammonia

In getting the critical Rayleigh numbers for ammonia, the same sort of procedure was followed, with the exception that allowance had to be made for the fact that the static state curve of \bar{S} , which may be denoted $S_h(p)$, is a function of p and not parallel to the Ra axis.

From the curves of $\bar{S}_h(p)$ vs. p for the two h 's (see Chapter 5), and using the same $\bar{\theta}_m$ and $\Delta\theta$ that pertained to the runs in question, curves of $\bar{S}_h(p)$ vs. Ra were constructed for the static state. On these graphs the post-convective points were plotted and an approximate Ra_c found. At this point a tangent to the static state curve was drawn, its slope measured, and its intercept with the \bar{S} axis, \bar{S}_h' , found. The origin was then shifted analytically to \bar{S}_h' , and the coordinates rotated until the Ra axis coincided with the tangent. The rotated Ra axis was called the Ra' axis. The intersection of the curve passed through the convecting points with the Ra' axis is Ra'_c , which, when found, was rotated back into the Ra frame to be Ra_c .

The fitting was done with gratifying rapidity on the I.B.M. 7094 for the form:

$$Ra' = Ra'_c + b(\bar{s}' - \bar{s}'_h) + c(\bar{s}' - \bar{s}'_b)^2$$

for the cases:

1. $c \equiv 0$
2. c found by best fit.

As in the case of air, the values of c calculated under 2 varied considerably, with more values greater than σ_c than less. This is probably due to greater complexity of the radiative flux phenomena, i.e., a continuation of the curvature of the static portion of the $\bar{S}_h(p)$ vs. Ra curve. The occurrence of several negative values makes one chary of asserting too strongly that these measurements show this curvature. Intuitively one would expect that finite amplitude calculations for convective motions with radiation would have more curvature when, as here, the optical depth and Rayleigh number are changed simultaneously.

The points and fitted curve for Run 9 are shown in Fig. 6-6.

Since the c 's calculated for NH_3 showed evidence of not being from the same population, the values of Ra_c for the three-parameter fit were used. In the data given in Table 6-6, σ_{Ra_c} includes both the effects of data scatter and uncertainty of c . A run lowering Ra found no evidence of hysteresis in ammonia either.

6.7 Radiative Stabilization

The measured stabilization is defined as the ratio of measured ammonia Rayleigh numbers to the weighted mean of the measured air Rayleigh numbers, 1786. Recalling previous results

$h = 1.987 \text{ cm.}$
 $\Delta \theta = -6.3^\circ \text{ K.}$

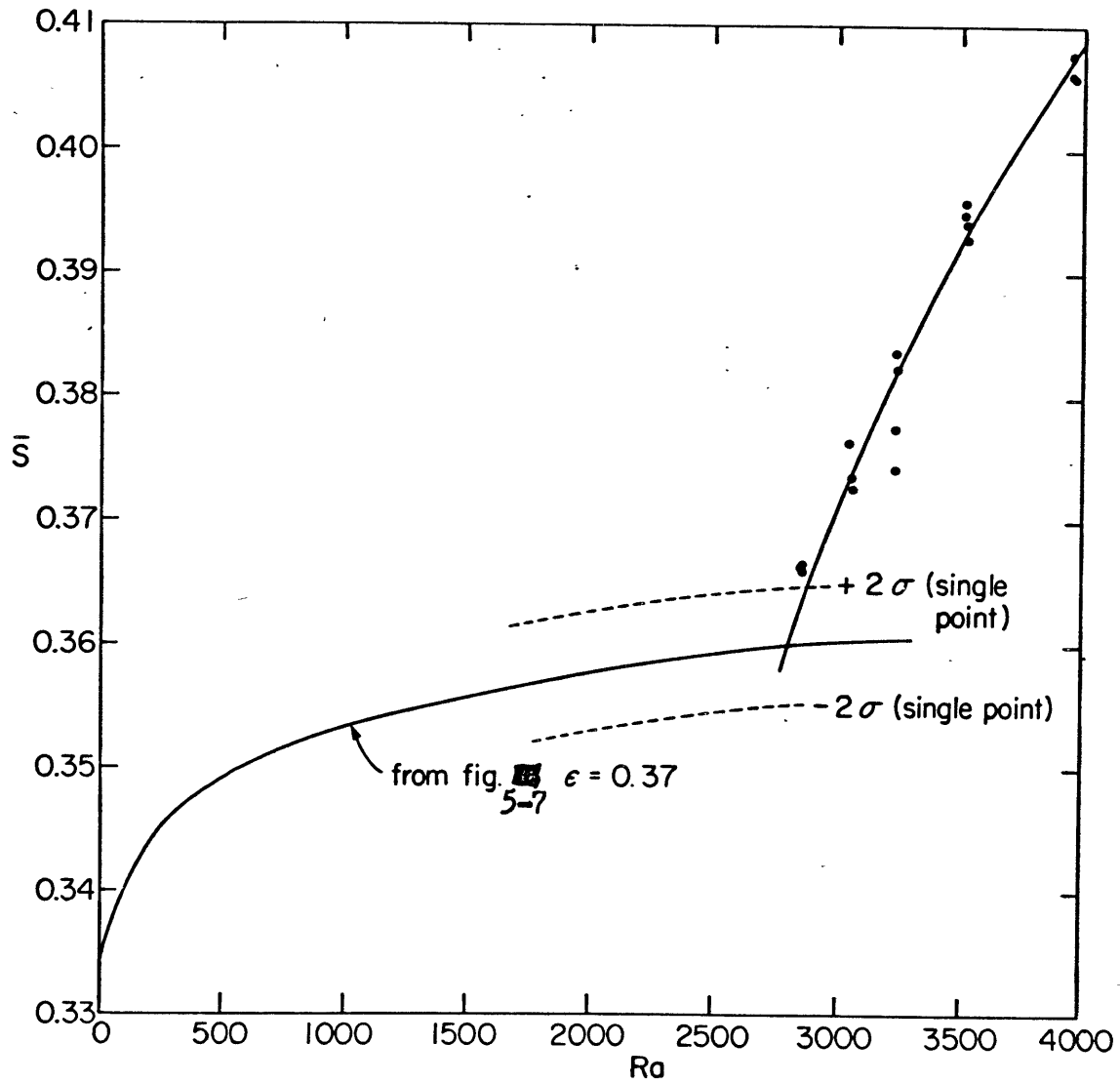


Fig. 6-6. \bar{S} AS A FUNCTION OF RAYLEIGH NUMBER FOR AMMONIA'

Table 6-6

MEASURED CRITICAL RAYLEIGH NUMBERS IN AMMONIA

Run (1)	h [cm.] (2)	$\Delta \theta$ [° C] (3)	Pc [cm.Hg.] (4)	Ra _c (5)
1	5.048	5.8	11.9	2515 ± 572
2	5.048	5.8	13.5	2999 ± 206
Mean	5.048	5.8	13.0	2943 ± 194
3	5.048	1.8	30.13	4947 ± 1604
4	5.048	1.8	29.73	4759 ± 712
Mean	5.048	1.8	29.80	4790 ± 651
5	1.987	2.8	59.9	1955 ± 123
6	1.987	2.8	67.4	2454 ± 199
7	1.987	2.8	64.3	2251 ± 208
Mean	1.987	2.8	62.4	2125 ± 93
8	1.987	6.4	46.4	2464 ± 62
9	1.987	6.3	49.6	2793 ± 69
10	1.987	6.4	47.5	2546 ± 104
11	1.987	6.3	44.8	2241 ± 266
Mean	1.987	6.35	47.7	2591 ± 42

$$S_{\beta} = A^{-1} \quad (6.44)$$

$$S_{\mu} = 1 + \frac{t_D}{t_R} \left(p, \frac{5.0}{h} \right) \quad (6.77)$$

the values in Table 6-7 are collected.

In Table 6-7 the errors of S_{β} allow for a four percent change of A. This was the change in A between the three- and four-coefficient calculation of the temperature gradient reported in Chapter 5. The error

attributed to S_H is the uncertainty in reading t_D/t_R from the graph. It is about the same as the accuracy of the radiative data. The errors in the observed stabilizations do not include uncertainties in the physical properties; the probable error due to that cause is 6-1/2 percent.

Table 6-7

STABILIZATION IN AMMONIA

h [cm.]	$\Delta \theta$ [° C]	$\frac{Ra_c}{1785}$	S_β	S_H	$S_\beta \cdot S_H$	τ_c
5.048	5.8	1.65 ± 0.11	1.22 ± 0.05	1.33 ± 0.03	1.63 ± 0.09	.065
5.048	1.8	2.68 ± 0.37	1.29 ± 0.05	1.59 ± 0.02	2.05 ± 0.10	.094
1.987	2.8	1.19 ± 0.05	1.13 ± 0.04	1.25 ± 0.02	1.41 ± 0.08	.104
1.987	6.4	1.45 ± 0.03	1.12 ± 0.04	1.21 ± 0.02	1.36 ± 0.07	.094

The quantity τ_c in the last column is presented to give an idea of the optical depth in these experiments. It is based on the somewhat arbitrary definition

$$\tau_c = h \tilde{k} \left(\rho_c, \frac{1}{h} \right)$$

This indicates that $\tau_c \approx 0.1$ for all the experiments reported here.

The fact that the values of $Ra_c/1786$ differ considerably is an indication that a different process is occurring than in the standard problem, and not merely an error in the physical constants for NH_3 .

That would give a constant ratio $\neq 1$ (but hardly 2.7). The fact that they are larger at large plate spacings is an indication that we have the right sort of mechanism, as is the pressure variation at the larger spacing.

The agreement with theory is good in two cases, close to the limits of error in a third, and very poor in the fourth. The mean of the ratios of experimentally observed to theoretically calculated stabilizations is 1.04 ± 0.18 . This is a rather strong indication that the theory does account for the phenomenon.

The cause of the discrepancy at $h = 1.987$ cm., $\Delta \theta = 2.8^\circ$ C , is not clear. The theoretical calculations of S_β and S_H indicate that Ra_c should be higher and slightly above the results at $\Delta \theta = 6.35^\circ$ C. (Since the results at $h = 5.048$ cm. tend to be higher than the theoretical values, the values at $h = 1.987$ cm. may be expected to be not less than the theoretical values.) The closeness of physical situation in geometry, \tilde{k} , and p suggests that little difference should be expected, even from a more refined theory based on this physical mechanism.

The air results taken just preceding this ammonia run are not unusual, nor are the $\Delta \theta = 6.35^\circ$ C ammonia results taken just afterward. It does not seem then that we can introduce a systematic leakage of air into the chamber diluting the NH_3 in these measurements and not the next series. Pressure is a straightforward measurement, though it is possible that leakage to the manometer could make it read too low. Since it was checked every few days, this need only have affected one series of measurements. No evidence for or against this can be found in the lab notebooks.

6.8 Conclusions

All things considered, the effortless dimensional argument and the gradient stabilization calculation have provided answers that agree rather well with the experimental results in three of four cases. In the fourth another effect is plausible. The mean ratio of observed to theoretical results of 1.04 ± 0.18 does not differ significantly from 1.00, especially if the uncertainties in physical properties are considered. The dimensional argument is never worse than saying no effect exists, and usually it is much better.

The mean value of Ra_c for air is 1786 ± 16 , which is $4\frac{1}{2}$ percent above the accepted value. As mentioned above, the difference could be due to uncertainties in the physical properties necessary to calculate the Rayleigh number and also to the effects of the walls in imposing a non-optimum cell spacing on the convective motions.

A search for hysteresis effects has indicated that none are present, in accord with physical theory.

In planning a convection experiment, one is brought to the realization that there is a limited range of layer thicknesses for gases within which one can work. At large plate separation, the temperature differences and pressures must be accurately maintained and measured. In addition, leakage through the walls becomes more serious and radiative flux becomes relatively larger than the conductive flux. The latter makes it difficult to observe the onset of convection by change of heat transport.

If the study of convective onset is the object, at small separations one must use reasonable $\Delta\theta$'s to remain within the limits of the use of constant coefficients in the dynamic and temperature equations. This forces one to high pressures and care in the design of a vessel and manometer to keep gas at higher pressure in. Measurement by heat flux change is rather sensitive in this region.

On the other hand, if one wishes to study radiative effects, he is constrained to layer thicknesses that are large enough to avoid the "conductive limit" mentioned in Chapter 5 and large enough to lead to motion scales in which radiative dissipation becomes important. The heights $h = 5.048$ and $h = 1.987$ seem to be close to the limiting values set by the present state of the art for air and ammonia, especially under the restriction of p not much greater than one atmosphere.

From this chapter, the following statements can be made:

1. A determination has been made of the absolute Ra_c in air giving full consideration to the various problems. This has yielded the result 1786 ± 16 , within $4\frac{1}{2}$ percent of the theoretical value of 1708, indicating a possible effect of the walls as well as the lack of accuracy of the quantities used to compute Rayleigh numbers. This appears to be the most thorough and accurate determination for air yet made.
2. Under the same conditions as above, the Ra_c in ammonia, a gas very active in the infra-red, has been measured. Large and significant deviations from the theoretical value of 1708, and the values for air, have been measured. The difference is not constant

with change of parameters h and $\Delta\theta$, and varies in such a way as to make clear that we have measured a radiative stabilization.

3. From the physical principles underlying the problem, and with the insight of several accurate calculations, a simple theory has been constructed which predicts the results of these experiments. For the first time a solution to a dynamical problem with radiation has been verified.
4. More exactly and importantly for problems of planetary atmospheres' dynamics (as well as laboratory problems), the gray solution has been extended by the dimensional argument and time constant calculation to the realizable and occurring case of dynamic effects in non-gray media. The verification of this extension opens the way to its confident application, not only in laboratory problems but in large-scale atmospheric problems, where radiation certainly is important [Goody, 1964].
5. The dependence of Rayleigh number in a gas on pressure through the density dependence of $K/\rho c_p$ and ν has been noted here for the first time and discovered to have the same critical characteristics as those observed previously by varying $\Delta\theta$ or h . This dependence has proved a most useful and convenient technique in these researches.

CHAPTER 7
CONCLUSIONS

7.1 Introduction

The results of this work are reviewed. The theoretical and experimental problems that suggest themselves are briefly discussed.

7.2 Results of This Work

7.2.1 Calculation of Radiative Properties of Ammonia

Beginning with the spectral data, line width, and total band intensities, it has been proven possible to calculate the integrated emissivity as a function of distance for ammonia broadened by nitrogen. The agreement of the calculated with the measured emissivity lends credence to a calculation of the perturbation emissivity \mathcal{E} and its distance derivative \mathcal{E}' . The subsequent use of these quantities in several calculations that predict the results of measurements successfully is an indication that they are probably accurate to a few percent.

These calculations were a time-consuming though necessary adjunct to the problem of measuring and predicting radiative stabilization in convection. Now available, they may prove to be some of the most seminal results of this work. For the first time, the properties of a rather strong radiating fluid are presented in a form convenient for use over a range of laboratory pressures and distances. Since the fluid is common and inexpensive, this may make possible experiments on radiative effects that had been prevented previously by lack of such data.

7.2.2 Accurate Interferometer Measurements

The previous semiquantitative use of the interferometer to measure temperature has been remarked upon. In this work the interferometric technique has been applied with an accuracy of 0.02° C, five times that previously reported. It has been shown to be capable of measuring a one-dimensional temperature distribution within a fluid with great precision if the length over which the temperature distribution is applied is accurately known, or equivalently, if the temperature and fringe interference number are accurately known at two places. This restriction puts some limitation on the uses of this technique, but with more geometric and temperature control over the end regions and the use of a known profile (i.e., conductive) to calibrate the instrument, the restriction should not be severe.

7.2.3 Extension of the Gray Solution to General Boundary Conditions

The closed form solution obtained by Goody [1956] for black boundaries was extended by allowing boundaries of any emissivity. This exercise is mainly illustrative, indicating that the two shiny boundaries will distort the gradient more than two black ones, and that asymmetric boundaries will produce an asymmetric temperature profile.

7.2.4 Solution to the Problem of Temperature Distribution for a Mixed Diffusive-Non-Gray-Radiative Medium with General Boundary Conditions

Temperature profiles have been calculated for the atmosphere, where large differences of pressure and temperature exist between regions and the geometry is semi-infinite.

Although the problem of the temperature distribution between parallel plates is complicated by thermal diffusivity and non-black boundaries that allow multiple reflections, it must be regarded as simpler than the atmospheric problem. As such, it is not surprising that a solution can be obtained by careful application of existing principles and techniques.

7.2.5 Experimental Measurement of a State of Radiative-Diffusive Equilibrium and Verification of the Calculations

The use of the interferometer to measure temperature accurately within a fluid without introducing a material probe has allowed the first experimental study of a radiative-diffusive equilibrium. This shows, as expected, that diffusion wipes out the temperature discontinuity at the boundary predicted by radiative transfer alone. Instead, a boundary layer of steep temperature gradient is observed.

The experimental determination goes beyond merely demonstrating the general quality of the solution, however, in that it verifies the calculational procedures used to get temperature profiles within the fluid. It is a distinct triumph for the computational method to predict profiles that agree so strikingly with the measured results.

As remarked earlier, since apparently nowhere in the atmosphere is there radiative equilibrium, this provides a first experimental verification of the type of calculations often used in meteorology.

7.2.6 Calculation of Heat Flux Changes with Optical Depth

The curious effects of changes of optical depth on heat flux have been shown for a full range of optical depths with the gray model. Detailed

calculations for a non-gray model have been presented over a limited range. These predict an initial increase in effective conductivity with pressure. As with temperature profiles, the techniques are similar to meteorological ones, while the boundary conditions are not.

7.2.7 Verification of Heat Flux Change

Because the calculated and observed heat flux changes do not agree as well as the similar quantities for temperature distribution, this is not as complete a verification of the calculational techniques as the other. However, changes of the right size are obtained. In the thin-layer case, both experimentally and computationally more accurate, the results could be explained very well by a slight change of ammonia conductivity, much less than its standard deviation. Inaccuracies in absolute heat flux measurements in the thicker layer case could explain the discrepancy there.

This again constitutes some underpinning for the techniques used in flux calculations in the atmosphere.

7.2.8 Establishment of a Dimensional Argument Predicting Convective Instability

The technique of splitting the stabilization into the gradient portion and the perturbation-damping portion has been demonstrated. The gradient stabilization has been accurately calculated and the difference between different formulations shown to be only a few percent for gradients typical of this experiment. The perturbation stabilization is only a slight extension of Spiegel's [1960] argument, with the discovery by Goody [1963] that a \hat{q} could be found that was independent of optical depth.

7.2.9 Calculation of Effective Absorption Coefficients and Ratios of Diffusive to Radiative Time Constants for a Non-Gray Gas

Like the results mentioned in 7.2.1, these data have uses beyond those for which they are employed here. In this work they were substituted in the general formulation to predict dissipative stabilization. In any formulation in which an effective absorption coefficient or time constant is of interest, these should find use.

7.2.10 Variation of Rayleigh Number by Pressure Change

The possibility of varying the Rayleigh number in a gas by varying the density through its pressure dependence does not appear to have been previously noted. This proved to give results like those obtained by other investigators who varied h or $\Delta\theta$, and provides (hardly needed) justification for the formulation of the Rayleigh problem. This was a very convenient way of changing the Rayleigh number.

7.2.11 Measurement of the Rayleigh Number in Air

Although other rough checks on the validity of Rayleigh's theory of convection in gases had been made, there had not been a systematic attempt to make a precise measure of the Rayleigh number at convective onset. The determination reported here is $Ra_c = 1786 \pm 16$, a value $4\frac{1}{2}$ percent above the accepted theoretical value of 1708. This discrepancy can be explained by inaccuracies in the data used for the physical properties and by the possibility that wall effects had a stabilizing influence.

7.2.12 Measurement of Radiative Stabilization in Ammonia

For four situations the stabilization in ammonia, defined as $Ra_c/1786$, has been measured. Since interferometer measurements have verified the calculations of $\beta/\bar{\beta}$ and the gradient stabilization can be calculated, it can be divided from the observed stabilization. The variation of the residual stabilization with p and h strongly suggests that it is due to radiative transfer.

7.2.13 Comparison of Observed and Calculated Stabilizations

As mentioned in 7.2.5, the interferometer measurements indicate that the technique of calculating gradients is highly accurate. The use of Chandrasekhar's technique (in the first approximation) provides a way of estimating the stabilization due to the gradients.

A dimensional argument that agrees very closely with the exact solution for diffusion and gray radiation can be devised. The radiative time constants can be inserted to give the heating rate stabilization. When this is multiplied by the gradient stabilization, a total stabilization is predicted.

The agreement between the measured (7.2.12) and calculated stabilizations is good for three of four cases and differs rather a lot for the fourth. A plausible explanation is that some systematic error may have been present for this series of runs, or the measurement of convection in our apparatus is not as accurate as other factors indicate.

7.3 Suggestions for Future Research

7.3.1 Theoretical and Numerical Problems

7.3.1.1 More Detailed Calculations of Ammonia Radiative Properties

The many simplifications introduced in Chapter 3 have been described. The excellent spectroscopic data make possible a more exact treatment of the spectrum, line by line, with individual line intensities and widths, by either integrating over narrow regions (e.g., 25 cm.^{-1}) or setting up a band for every 10 lines, and calculating a more realistic emissivity. With a general computer program, it would also be possible to make a systematic quantitative study of the effects of errors in the values used for total band intensities. Mixing with other gases and changes of conditions that might be useful in predicting laboratory effects could be easily explored with such a program.

The changes necessary in the calculations of α_L and the effects of possible line shifts at pressures greater than 1.6 atmospheres should also be considered. The emissivity calculations might then be extended to the moderately higher pressures that could be used advantageously in the laboratory.

7.3.1.2 Calculations of Emissivities of Other Gases

From data of the sort used here and from transmission data taken at long path lengths at various pressures and temperatures, one could calculate the emissivities of the gases believed to exist on planets of the solar system -- notably the oxides of nitrogen and methane. (Water vapor and carbon dioxide seem to have a great deal of available data

already.) Long path length data for NH_3 would also be useful. These could be valuable to the earthbound theoretician devising meteorologies for much different physical systems and designers contemplating planetary probe experiments.

7.3.1.3 Extension of Numerical Methods to Convection

As noted above, it was necessary to employ a dimensional argument to enable the expression for the heating rate stabilization to be expressed as a function of dissipation times. The integration over frequency was then done in quantities that appeared in the dissipation time. Although the dimensional argument seems capable of explaining the results obtained in this work, a more rigorous treatment is desirable.

These might take one of two forms; analytical or numerical. In the former, one could try to take Spiegel's gray heating rate as a function of wave number, integrate over frequency, and express the result in terms of known emissivities. Conceivably what would be necessary would be the numerical construction of a new integral over frequency from the spectral data.

The second approach would replace the integral over depth in Spiegel's formulation with a sum over n layers in the fluid. The weighting factors multiplying the perturbation temperatures would have either an explicit a^2 dependence or provision would have to be made to evaluate them at a series of values of a^2 .

Alternatively, the kernel of the integral could be expanded in terms of known functions with numerically determined coefficients. This must have an a^2 dependence also, of course. These should all be in

such a form that when $a \rightarrow 0$ (no horizontal variation), the heating equation will be that for the static state.

If one had perturbation heating as a function of a^2 , one could solve for the static state $(\beta/\bar{\beta})$ and find Ra vs. a^2 for families of \mathcal{X} and τ using the complete expression. On minimization, this would yield

$$Ra_c = Ra_c(\mathcal{X}, \tau)$$
$$a_c = a_c(\mathcal{X}, \tau).$$

These complete solutions to the convective instability problem with radiation and diffusion should be scrutinized to find any features missed by the dimensional argument or worthy of experimental study.

7.3.1.4 Further Applications of the Dissipation Time Argument

Many of the dynamical and transport properties of the atmosphere are considered in terms of dimensional arguments. It would seem that for any in which diffusion has entered, the radiative case might well be included with this sort of dissipation time comparison.

Further, the importance of radiation in dynamical situations might be assessed through the comparison of radiative dissipation times and time scales of the motion.

7.3.2 Problems Involving Experiment

7.3.2.1 Improved and Extended Calculations of the Heat Flux and Temperature Distribution and Their Verification

While the calculation of temperature distribution gave good results, the computation of heat flux showed some scatter which was attributed to

the calculated gas emissivities ϵ and $\tilde{\epsilon}$. A more detailed calculation of $\tilde{\epsilon}$ (7.3.1.1) coupled with a more detailed integration to get $\tilde{\epsilon}$ would be expected to remove at least part of this and would hopefully agree better with the measurements. Another technique which might reduce this scatter somewhat would be obtaining both $\beta/\bar{\beta}$ and F_T from the same equation (i.e., (5.103)).

To verify and extend the knowledge of this phenomenon, the numerical techniques should be extended to predict profiles and fluxes in the situation where the emissivities of the upper and lower plates are not equal, and if possible, the theory should be extended to the case where emission and absorption by the plates is not isotropic. The emissivities and their angular dependences could then be measured by conventional means for use in the calculations.

The numerical calculations could then be performed and extended to greater pressures to predict situations where an increase in pressure will cause a decrease in heat flux and to follow the temperature profile as it becomes linear with pressure.

The results of these calculations for $\beta/\bar{\beta}$ and F_T should then be experimentally verified. There are four independent parameters to vary: h , ϵ_U , ϵ_L , and pressure, all of whose effects can be predicted. (Comparison with air and a vacuum high enough that $K = 0$ could serve as useful checks.)

The possibility that extensive runs of this sort might be inverted to give data on emissivities over a useful range should be explored.

7.3.2.2 Temperature Measurements in Convection

A use that immediately comes to mind for the interferometric temperature-measuring apparatus is the measurement of temperature profiles after convection has begun, preferably from the laminar region all the way to turbulent convection. These data would provide another solid point of comparison (the first is heat flux) between theories of finite amplitude convection and measurement. In fully turbulent convection, several implementations of Malkus' [1954b] approach have been worked out to predict profiles. Provided high enough Rayleigh numbers can be reached, these should be capable of being tested.

These measurements could be done not only for air, but also for a radiating fluid like ammonia. Presumably until the air measurements are explained, there is not much point in trying to explain the radiating-convecting profiles. The two might be expected to become more similar as Ra is increased and convective transports dominate.

7.3.2.3 Heat Fluxes in Finite Amplitude Convection and Convective Turbulence for Radiating and Non-Radiating Fluid

The results of De Graaf and Van der Held [1952] should be corroborated and more points taken. Theories to account for heat transports have been proposed, but with little success to date. These non-radiating transports should be compared with results in a radiating fluid when the radiative transport has been removed to see if there is a common dependence on Ra/Ra_c . If not, a single rule might be sought to relate convective heat transports in fluids having different modes of perturbation dissipation.

7.3.2.4 Other Radiative Processes in Ammonia

The knowledge of the radiative properties of ammonia now may make possible the demonstration of radiative processes which can occur in laboratory fluid dynamics and modeling those which occur in the atmosphere. Of the many that come to mind, the propagation and properties of temperature waves as a function of frequency might be investigated.

BIBLIOGRAPHY

- Anderson, P. W. 1940, Phys. Rev. 76, 647.
- Bénard, H. 1901, Ann. Chim. Phys. 23, 62.
- Bénard, H. and Avsec, D. 1938, J. Phys. Radium (7) 9, 486.
- Benedict, W. S., Plyler, E. K., and Tidwell, E. D. 1958, J. Res. N.B.S. 61, 123.
- Bisshopp, F. E. 1960, Notes on the 1960 Summer Study Program in Geophysical Fluid Dynamics at the Woods Hole Oceanographic Institution. Vol. III, p. 127.
- Bleaney, B., and Penrose, R. P. 1948, Proc. Phys. Soc. 60, 540.
- Chandra, K. 1938, Proc. Roy. Soc. A 164, 231.
- Chandrasekhar, S. 1960, Radiative Transfer. Dover Publications, Inc., N. Y.
- Chandrasekhar, S. 1961, Hydrodynamic and Hydromagnetic Stability. Clarendon Press, Oxford.
- Chapman, S., and Cowling, T. G. 1952, The Mathematical Theory of Non-Uniform Gases. Cambridge University Press.
- Croft, J. F. 1958, Quart. J. Roy. Met. Soc. 84, 418.
- Cuthbertson, C. and M. 1913, Phil. Trans. Roy. Soc. London A 213, 1.
- De Graaf, J. G. A., and Van der Held, E.F.M. 1952, Appl. Sci. Research A 3, 393.
- Dowding, L. F. 1939, Heat Transmission by Radiation from Non-Luminous Gases; Experimental Study of Ammonia. S.M. Thesis. Course XA, M.I.T.
- Elsasser, W. M. 1942, Heat Transfer by Infrared Radiation in the Atmosphere. Harvard Meteorological Studies No. 6. Harvard University Press.
- Finch, D. I. 1962, Temperature, its Measurement and Control in Science and Industry. Vol. III Part 2. Page 3. Reinhold Publishing Co., New York.
- Foley, H. M. and Randall, H. M. 1941, Phys. Rev. 59, 171.
- Franck, E. U. 1951, Z. Electrochemie 55, 636.

- Friberg, S. 1927, Z. Physik 41, 378.
- Frivold, O. E., Hassal, O., and Rustand, S. 1937, Physikal. Z. 38, 191.
- Garing, J. S., Nielson, H. H., and Rao, K. N. 1959, J. Mol. Spectroscopy 3, 496.
- Gerhard, S. L. and Dennison, D. M. 1933, Phys. Rev. 43, 197.
- Godson, W. L. 1955, J. Meteorology 12, 272 and 533.
- Goody, R. M. 1956, J. Fluid Mechanics 1, 424.
- _____ 1963, Memorandum.
- _____ 1964, Atmospheric Radiation. I. Theoretical Basis. Clarendon Press, London.
- Hadni, A. 1953, Compt. Rend. 237, 317.
- Handbook of Chemistry and Physics, 38th Ed. (1956) Chemical Rubber Publishing Company, Cleveland, Ohio.
- Hansler, R. L. and Oetjen, R. A. 1952, J. Chem. Phys. 21, 1340.
- Herzberg, G. 1952, (Should read 1945) Molecular Spectra and Molecular Structure II. Infrared and Raman Spectra of Polyatomic Molecules. D. van Nostrand Co., Inc., Princeton, New Jersey.
- Hide, R. 1963, Conversation.
- Hirschfelder, J. O., Curtiss, C. F., and Bird, R. B. 1954, Molecular Theory of Gases and Liquids. John Wiley and Sons, Inc., New York
- Hottel, H. C. 1954, Chapter IV in Heat Transmission by W. H. McAdams. McGraw Hill, New York.
- Ince, E. 1944, Ordinary Differential Equations. Dover Publications, Inc., N. Y.
- Kaplan, L. D. and Eggers, D. F. 1956, J. Chem. Phys. 25, 876.
- Kaye and Laby 1956, Tables of Physical and Chemical Constants and some Mathematical Functions. 11th Ed. Longmans, Green and Co., New York
- Klemm, W. and Henkel, P. 1933, Z. anorg. allg. Chem. 213, 115.
- Kennard, R. B. 1941, Temperature, its Measurement and Control in Science and Industry. Vol. II, page 625. Reinhold Publishing Co., New York
- Koşçmieder, L. 1963, Unpublished work.

- Krieger, F. J. 1951, Research Memorandum RM646. The Rand Corporation, Santa Monica, California. (The computations in this report have since been Proven incorrect.)
- Landholt and Bornstein 1960, Zahlenwerte und Functionen. 6th Ed. Springer-Verlag, Berlin.
- Malkus, W. V. R. 1954a, Proc. Roy. Soc. A 225, 185.
- _____ 1954b, Proc. Roy. Soc. A 225, 196.
- Mason, E. A., and Monchick, L. 1962, J. Chem. Phys. 36, 1622.
- McKean, D. C. and Schatz, P. N. 1956, J. Chem. Phys. 24, 316.
- National Bureau of Standards 1955a, Circular 561. Reference Tables for Thermocouples. U. S. Dept. of Commerce, Washington 25, D. C.
- National Bureau of Standards 1955b, Circular 564. Tables of Thermal Properties of Gases. U. S. Dept. of Commerce, Washington 25, D. C.
- Osborne, N. S., Stimson, J. F., Sligh, T. S. Jr., and Crague, C. S. 1924, Sci. Papers. National Bureau of Standards 20, 65. (Number 501).
- Pellew, Anne and Southwell, R. V. 1940, Proc. Roy. Soc. A 176, 312.
- Penner, S. S. 1961. Quantitative Molecular Spectroscopy and Gas Emissivities. Addison-Wesley, Reading, Mass.
- Pierson, R. H., Fletcher, A. N. and Gantz, E. St.C., 1956, Analytical Chemistry 28, 1218.
- Port, F. J., 1940, Heat Transmission by Radiation from Gases. Sc.D. Thesis Course, X, M.I.T.
- Rayleigh, Lord. 1916, Phil. Mag. (6) 32, 529. Also Collected Papers 6, 432.
- Reid, W. H. and Harris, D. L. 1958, Phys. of Fluids 1, 102.
- Schmidt, R. J. and Milverton, S. W. 1935, Proc. Roy. Soc. A 152, 586.
- Schmidt, R. J. and Saunders, O. A. 1938, Proc. Roy. Soc. A 165, 216.
- Silverston, P. L. 1958, Forsch. Ing. Wes. 24, 29 and 59.
- Slawsky, Z. I. and Dennison, D. M. 1939, J. Chem. Phys. 7, 509.
- Spencer, H. M. and Flannagan, G. N. 1942, J. Am. Chem. Soc. 64, 2511.

Spiegel, E. A. 1957, Ap. J. 126, 202.

_____ 1958, The Onset of Thermal Convection in a Radiating Atmosphere.
Un. of Michigan Ph.D. Dissertation.

_____ 1960, Ap. J. 132, 716.

_____ 1962, Conversation.

Sutton, O. G. 1951, Proc. Roy. Soc. A 204, 297.

Thompson, H. W. 1941, Trans. Faraday Soc. 37, 344.

Townsend, A. A. 1958, J. Fluid Mech. 4, 361.

Van Cleave, A. B. and Maass O. 1935, Can. J. Research 13, 140.

Wilkes, S. S. 1949. Elementary Statistical Analysis. Princeton University
Press.

Wright, N. and Randall, H. M. 1933, Phys. Rev. 44, 391.

BIOGRAPHY

John Charles Gille was born in Akron, Ohio on October 12, 1934. He attended schools in Akron, Washington D. C. and Teaneck, New Jersey. In June 1952 he was graduated from Teaneck High School.

He held scholarships for his four years at Yale, where he was elected to Phi Beta Kappa and an associate of Sigma Xi. He was graduated Magna Cum Laude in June 1956, with a B.S. in Physics.

He was awarded a Mellon Fellowship to travel and study for two years at Clare College of Cambridge University (England). He received a B.A. from Cambridge in June 1958.

The following September he entered M.I.T.'s Department of Geology and Geophysics. He was elected to full membership in Sigma Xi, and held a National Science Foundation Predoctoral Fellowship for two years. The award of a Summer Fellowship by Woods Hole Oceanographic Institution led to an interest in the problems of Geophysical Fluid Dynamics. Most of his research was carried out at Harvard's Division of Engineering and Applied Physics, where he was a half time research assistant from 1960-64.

He served as a resident tutor in physics in an M.I.T. undergraduate dormitory for three years.

He is married to the former Ellen Cole Fetter of Winnetka, Illinois.

He is a member of the American Geophysical Union.